STELLINGEN

behorende bij

Elastic Impact with Friction

door

J. Jaeger

Stelling 1

Raoof & Hobbs (1989) calculated the load-displacement relation of the Cattaneo-problem, in a coordinate system with rotated axes. In that article an assumption about the contact law is made, in which one coordinate axis points into the direction of the force. It can be proved that their assumption is correct. Furthermore their transformation law can easily be generalized for any rotation of the axes and for finite slip.

Stelling 2

Szalwinsky (1985) calculated the flexibilities for the contact of elastic bodies, with elliptical contact areas, on the base of Cattaneo's solution, where $\beta = dF_x/|dF_t|$ and either F_x of F_y is held constant. Szalwinsky's formulae are only correct for uni-directional tangential forces with varying absolute values, because Cattaneo assumes constant slip directions in the slip area. In the general case, where an arbitrary traction distribution (σ_x, σ_y) is overlaid by a new stress increment $(\Delta\sigma_{zx}, \Delta\sigma_{zy})$, the slip direction varies in the elliptical, annular slip area. Consequently, the displacements in the slip area must also be considered. Numerical experience shows, that the slip directions in the contact area are almost constant on elliptical rings. For a circular contact area, the corresponding boundary value problem can be described by an integral equation system. These integral equations are so difficult, that analytical solutions are difficult to find.

Stelling 3

It can be shown that the contact problem of a rigid punch with known base form, indenting a simply supported rectangular plate, is very similar to the normal half-space problem. Using the Fourier solution for a constant pressure distribution on a small rectangle (Timoshenko & Woinowsky-Krieger, 1959), the discrete load-displacement relation can be deduced. This relation is very similar to equ. (4.13) of my thesis, with the displacement w_{ij} as the product of the influene matrix A_{ijkl} and the pressure p_{kl}. The contact area can be found with Kalker's module Norm and the proof of convergence is equal to Kalker (1990).

Stelling 4

Recently a Fourier-solution was developed (Axelrad, 1983), which uses Fourier-matrices to multiplicate Fourier series. This method is very easy to program and to verify. It can favourably be used to solve the problem of a flange at the end of a tube, loaded by two singular forces, acting symmetrically on the flange. It is assumed that the flange is a circular beam, supported by the tube, which is a cylindrical shell. The simplifications of the half-momentless theory of shells, where the stress is split into the main-solution and the boundary part, are introduced. The moments M_ϕ, acting on an axial section, are much smaller than M_ξ, acting on a section perpendicular to the axis. The solution of the problem is

obtained by matrix-invertion. We also wrote a small program for this problem.

Stelling 5

The heat expansion of tubes in industrial plants can be compensated by expansion bellows, which are flexible tubes with circumferential corrugations. Their behaviour is described by the differential equations of shell theory, which in former times where solved by analytical methods and FEM-techniques. Similar to Stelling 4, the Fourier-Matrix-Method allows a real simplification. It can also be used to solve nonlinear differential equations, which occur e. g. for large deformations, where the pressure-loading acts on the deformed geometry. We will demonstrate this method for a simple bellows under pressure and dilatation. We also wrote a small program for this problem.

Stelling 6

The Fast Fourier Transformation Method (FFT) can be used to calculate the normal displacement of a half-space, using a 'generalized' convolution theorem. The number of multiplications is $O(8N \log (4N))$, where N denotes the number of points in the area where the displacment is measured. The Fourier-series for p_z and $1/r$ are calculated and the integral is obtained by the backward transformation of the product of the coefficients. The period of the Fourier-series in one dimension must be two times the period of the region, where the displacements are determined, because the 'generalized' convolution is taken over the periodical supplement. Available FFT-programs solve this problem very fast, but it turns out that a large number of points is necessary for a good result, because the singular function $1/r$ is difficult to model with Fourier-series. An analytical expansion of the function $1/r$ is possible, which allows analytical expressions for the displacement. It should be noted that convergence is certain for this problem, even for large series.

Stelling 7

Deresiewicz (1954) published the solution of the contact of elastic spheres under an oscillating torsional couple on the base of Lubkin's solution (Lubkin, 1951). This solution is limited to small torsional couples acting on a constant contact area and the superposition of only two Lubkin-functions. It can be generalized for the elastic contact of spheres under a varying torsional couple and a varying normal force. Different load-histories can generate the same pressure distribution, but for every pressure distribution exists only one load-history with the smallest number of Lubkin-functions. Load-histories with pure torsion are also characterized by points of instantaneous adhesion and periods of decreasing stick area, as described in chapter 6 for varying oblique forces.

Stelling 8

Although the computation velocity of Personal Computers increased considerably

in the last years, software improvements for incremental load-histories can be faster. A new Intel 80586/50 MHz processor is about 200 times faster than a five year old 80286/12 MHz processor and modern PC's may even be 200 times faster in five years. Lubrecht & Ioannidis (1991) developed a Multi-Level-Method, which performs the matrix-vector product of the load-displacement equations with $N \log N$ multiplications. The possible velocity increase of a combination of the Gauss-Seidel and the Multi-Level-Method compared with the standard Gauss-Elimination is of the order $N^3/(N \log N)$, which amounts to a value of 333 000 for $N = 1000$ points in the contat area. Other Multi-Grid methods and the Fast-Fourier-Transformation method are also promising. If special vector computers or parallel computers are used, much work must be done to develop special software for these machines. It follows that the development of fast software on standard computers is the most promising way for incremental load-histories, and even if personal computers are really 200 times faster in five years, this factor can be multiplied with the factor due to software improvements.

Literature

E. Axelrad, 1987, Theory of flexible shells, Elsevier science publishing company, Amsterdam, ISBN 0-444-87954-4.

E. Axelrad, 1983, Schalentheorie, Teubner Stuttgart, ISBN 3-519-02360-1.

C. Cattaneo, 1938, Sul contatto di due corpi elastici: distributione locale degli sforzi, Academia Nazionale dei Lincei, Rendiconti, Serie 6, Vol 27, 342-348, 434-436, 474-478. 623-624.

H. J. Deresiewicz, 1954, J. Appl. Mech., Contact of elastic spheres under an oscillating torsional couple, Vol 21, 52-56.

H. J. Deresiewicz, 1957, J. Appl. Mech., Oblique contact of nonspherical elastic bodies, Vol. 24, 623-624.

J. J. Kalker, 1990, Three-dimensional bodies in rolling contact, Kluwer Academic Publishers, ISBN 0-7923-0712-7.

J. L. Lubkin, 1951, The torsion of elastic spheres in contact, Journal of Applied Mechanics, Vol. 18, 183-187.

A. A. Lubrecht, E. Ioannidis, 1991, A fast solution of the dry contact problem and the associated sub-surface stress field, using multilevel techniques, Journal of Tribology, Vol. 113, 128-133.

M. Raoof, R. E. Hobbs, 1989, Tangential compliance of rough elastic bodies in contact, Journal of Tribology, Vol. 111, 726-729.

C. M. Szalwinsky, 1985, Flexibility of a contact area of an isotropic elastic body, J. Appl. Mech., Vol. 52, 62-66.

S. P. Timoshenko & S. Woinowsky-Krieger, 1959, Theory of plates and shells, McGraw-Hill Book Company, Library of Congress # 58-59675.

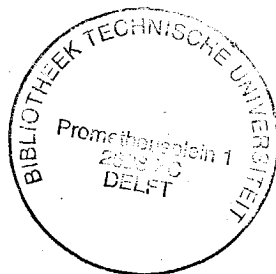# Elastic Impact with Friction

PROEFSCHRIFT

ter verkrijging van de graad van doctor aan de
Technische Universiteit Delft, op gezag van de
Rector Magnificus, prof. drs. P. A. Schenck, in
het openbaar te verdedigen ten overstaan van
een commissie aangewezen door het College van
Dekanen op vrijdag 30 oktober 1992 te 14 uur

door

Juergen Jaeger,

geboren te Laufenburg,

Dipl. Ing. Maschinenbau.

Contents

Samenvatting

De klassieke botsingstheorieën beschouwen hetzij wrijvingsloze oppervlakken dan wel volledig doorglijden in het gehele contactvlak. En realistischere theorie moet ook de verdeling van het contactvlak in glijd- en hechtgebieden beschouwen. Drie restitutiecoëfficiënten bepalen de rotaties en de snelheden van de twee lichamen na de botsing.

Dit werk is gebaseerd op de grondvergelijkingen van de drie-dimensionale elasticiteitsleer. H. Hertz (1882) loste deze vergelijkingen op voor de normaal gerichte botsing van twee lichamen. Hij gebruikte de halfruimteoplossingen voor puntlasten van Boussinesq (1885) en Cerruti (1882) om het spanningsveld in de buurt van het contactvlak te bepalen. Dit geldt voor compacte lichamen, waarin de afmetingen van het contactvlak klein zijn vergeleken met de globale kromtestralen en afmetingen van de lichamen. Wij generaliseren de Hertz oplossing op basis van deze vereenvoudiging. Dit werk is outsluitend beperkt tot de halfruimtebenadering en tot elastische materialen.

Hoofdstuk 3 is de inleiding tot dit werk. De contactprocessen gedurende de botsing vereisen de analyse van enige fundamentele belastingsgeschiedenissen. Hoofdstuk 4 vat de fundamentele formules van halfruimteproblemen samen. Enkele bekende belastingsgeschiedenissen voor lichamen van gelijke materialen worden in hoofdstuk 5 besproken. Hoofdstuk 6 geeft de theorie van Mindlin en Deresiewicz voor veranderlijke normale en scheve krachten weer van een nieuw gezichtspunt uit. We voeren de zogenaamde Cattaneo-Mindlin functies in, en we komen tot een formule voor de krachten die alleen afhangen van de zg. punten van ogenblikkelijke hechting, waarin het gehele contactvlak gedurende één ogenblik hecht en van de momentane verplaatsing, maar niet van de specifieke vorm van de voorafgaande belastingsgeschiedenis. In hoofdstuk 7 generaliseren we deze theorie voor elliptische contactvlakken onder scheve belasting met variabele richting. Als gevolg van deze theorie zijn verschillende belastingsgeschiedenissen mogelijk die leiden tot dezelfde spanningsverdeling. Elliptische contactvlaken onderworpen an veranderlijke momenten kunnen worden benaderd door een eenvoudige formule, die wij hebben vergeleken met enige numerieke berekeningen in sectie 7.6.

De grondvergelijkingen voor de botsing van twee lichamen worden uitgesproken in hoofdstuk 8. De drie verschillende contacttoestanden van volledige hechting, gedeeltelijke slip en volledig doorglijden worden ingevoerd en de bewegingsvergelijkingen worden afgeleid. Enkele analytische oplossingen worden in hoofdstuk 9 bepaald. Tenslotte bespreken wij torsiebotsing in hoofdstuk 10. Het resulterend moment is veel kleiner dan de momenten voortgebracht door de tangentiële krachten, doordat in het kader van de Hertztheorie de afmeting van het contactvlak minder dan 10% van de afmeting van het lichaam moet zijn. Dus is de arm van de torsiebelasting vewaarloosbaar vergeleken met de arm van de tangentiële spanning, en kunnen het torsiemoment en de momenten binnen het contactvlak vewaarloosd worden in een eerste-orde botsingstheorie.

Hoofdstuk 11 is gewijd aan de numerieke oplossingen van J. J. Kalker, aangezien onze numerieke procedures gebaseerd zijn op zijn methodes. De toepassing van de Gauss-Seidel procedure, uitgelegd in hoofdstuk 12, verbeterd de rekentijd en het geheugenbeslag aanzienlijk. In hoofdstuk 13 bewijzen wij de convergentie van onze gemodificeerde Gauss-Seidelmethode voor enige bijzondere belastingsgeschiedenissen. De convergentie van de gelineariseerde wrijvingswet is niet onderzocht, aangezien de convergentie zeker is voor oneindig kleine aangroiïngen van een belastingsgeschiedenis met Hertz'se oppervlakken, waarbij de richting van de spanningen nauwelijks verandert. In dit geval verandert het hechtgebied ook in slechts weinige punten, en de hechtgebiedlus convegeert zeer goed. Het probleem van een vlakke stempel die op een elastische halfruimte drukt is moeilijker, omdat bij de aanvang van het contact het hechtgebied sterk verandert. Voorts kan de richting van de spanning slechts worden berekend, als de eerste schatting van het hechtgebied redelijk goed is. Wij hebben een aantal stuurvariabelen ingevoerd, die de convergentie van het programma beheersen, zoals het maximum van het aantal iteraties in elke lus, de nauwkeurigheid en de aafmeting vaan de aangroeiïngen. Empirische ervaring leert, dat een juiste instelling van de parameters convergentie van het programma oplevert, zelfs voor grote contactvlakken van 1000 punten. De convergentiesnelheid is ook belangrijk voor grote contactvlakken, omdat rekentijden van 1 of 2 dagen op een 80386/33MHz computer normaal zijn voor 1000 punten. De rekentijd is ongeveer evenredig met n^2, terwijl het geheugenbeslag evenredig is met n, waarbij n het aantal punten in het potentieël contactvlak is.

In hoofdstuk 14 vergelijken wij de vereenvoudigde oplossingen van hoofdstuk 7 met de numerieke resultaten. Het blijkt dat in afwijking van de theorie van hoofdstuk 7 de richting van de spanning in het glijdgebied nogal variëert. De overeenkomst tussen de numerieke en de analytische theorie aangaande de afmeting van het hechtgebied en de absolute waarde van de tangentiële spanning is veel beter. Een nieuw gefolg van de numerieke resultaten is dat voor elliptische conatctvlakken met $\nu_1 = \nu_2 = 0$ de spanningen σ_{zx}, σ_{zy} constant zijn op ellipsen homothetisch met de contactellips, althans zolang er geen torsie is. Zelfs wanneer de Poissongetallen van nul verschillen, zijn de spanningen nog steeds vrijwel constant op zulke ellipsen, zolang althans de materialen van de lichamen gelijk zijn. Kleine wrijvingscoëfficiënten bij ongelijke materialen leveren de meest onvoorspelbare spanningsverdelingen op. Een voorbeeld van de superpositie van torsie en tangentiële verplatsing word ook gegeven in sectie 14.4. In sectie 14.5 geven wij enige (niet-Hertz'se) resultaten voor vlakke stempels.

De tangentiële restitutiecoëfficiënt is de verhouding van de tangentiële snelheid in het contactpunt voor de botsing tot de tangentiële snelheid na de botsing. Hoofdstuk 15 toont aan dat de overeenstemming tussen de Cattaneo-Mindlintheorie en het numerieke resultaat zeer goed is. Verder worden de restitutiecoëfficiënten voor lichamen van verschillende materialen en voor torsie van lichamen in de vorm van ellipsoïden gegeven.

Verdere informatie over de bovengenoemde onderwerpen wordt in de Inleiding gegeven.

1 Summary

The classical impact theories consider either frictionless surfaces or gross slip of the whole contact area. A more realistic theory must consider the partition of the contact area into stick and slip areas. Three coefficients of restitution determine the rotations and velocities of the two bodies after the impact. These coefficients will be calculated for some examples.

This work is based on the fundamental equations of the three dimensional theory of linear elasticity. H. Hertz (1882) solved these equations for the normal impact of two bodies. He used the half-space solutions for single forces of Boussinesq (1885) and Cerruti (1882) to determine the stress field in the vicinity of the contact area. This holds for compact bodies, where the dimensions of the contact area are small compared to the global curvatures and dimensions of the bodies. We generalize the Hertz solution on the basis of this simplification. This work is exclusively confined to the half-space approximation and elastic materials.

Chapter 3 is the introduction to this work. The contact processes during impact require the analysis of some basic load-histories. Chapter 4 summarizes the basic formulae for half-space problems. Some well-known load-histories for similar material are discussed in chapter 5. Chapter 6 presents the theory of Mindlin and Deresiewicz for varying normal and oblique forces under a new point of view and generalizes their result. We introduce the so-called Cattaneo-Mindlin functions and we will arrive at a formula for the forces, which depends only on so-called points of instantaneous adhesion, where the entire contact area is stuck for a moment, and on the current displacements, but not on the specific form of the previous load history. In Chapter 7 we generalize this theory for elliptical contact areas under oblique forces with varying directions. This theory is based on the simplifying assumption that the stress direction in the entire slip area is constant between two points of instantaneous adhesion. In consequence of this theory different load histories with the same stress distribution are possible. Elliptical contact areas under varying torques can be approximated by a simple formula, which we compare with some numerical calculations in chapter 7.6.

The basic equations for the impact of two bodies are stated in chapter 8. The three different contact regimes of full adhesion, partial slip and complete sliding are introduced and the equations of motion are deduced. Some analytical solutions are presented in chapter 9. Finally we discuss the torsional impact in chapter 10. The

resulting torque is much smaller than the moments produced by the tangential forces, because the dimensions of the contact area should be less than 10% of the the dimensions of the body, in the frame of the Hertz theory. Consequently the lever-arm of the torsional stress is almost negligible compared with the lever-arm of the tangential stress, and the torsional torque and the moments inside of the contact area can be neglected in a first order impact theory.

Chapter 11 is dedicated to the numerical solutions by J.J. Kalker, because our numerical procedures are based on his methods. The application of the Gauss-Seidel procedure, explained in chapter 12, improves the calculation time and the storage requirements considerably. In chapter 13 we prove convergence of our modified Gauss-Seidel method for a few special load histories. The convergence of the linearized frictional law is not investigated, because convergence is certain for infinitely small increments of a load history with Hertzian surfaces, where the stress directions hardly change. In this case the adhesive area also varies in a few points only, and the stick area loop converges very well. The problem of a flat punch pressing on an elastic half space is more difficult, because at the beginning of contact the stick area changes very much. Furthermore the stress directions can only be calculated, if the first estimation of the stick area is not too wrong. We introduced a number of control parameters, which control the convergence of the program, like the maximal number of iterations for each loop, the precision and the size of the increments. Empirical experience shows, that a correct parameter setting yields convergence of the program, even for large contact areas of 1000 poins. The velocity of convergence is also very important for large contact areas, because calculation times of one or two days on an 80386/33MHz computer are normal for 1000 points. The calculation time increases with n^2 approximately, while the storage requirements increase with n, where n denotes the number of points in the area of integration.

In chapter 14 we compare the simplified solutions of chapter 7 with some numerical results. It turns out that in contrast to our theory the stress directions in the slip area vary considerably. The correspondence between numerics and theory for the size of the stick area and the absolute value of the tangential stress is much better. A new conclusion of the numerical results is that for elliptical contact areas with $\nu_1 = \nu_2 = 0$ the stresses σ_{zx}, σ_{zy} are constant on ellipses, as long as torsion is absent. Even if the Poisson numbers are different from zero, the stresses are still almost constant on ellipses as long as the materials are similar. Small frictional coefficients with different materials yield the most unpredictable stress distributions. An example for the superposition of torsion and tangential shift is also presented in section 14.4. In

section 14.5 we present some results for non-Hertzian contact areas in form of flat punches.

The tangential coefficient of restitution is the ratio of the tangential velocity in the contact point before impact to the velocity after impact. Chapter 15 shows that the correspondence between the Cattaneo-Mindlin theory and the numerical result is very good. Furthermore the coefficients of restitution for dissimilar materials, superposition of torsion and ellipsoid bodies are presented. Additional information about the above mentioned topics can be found in the introduction.

2 Symbols and notation

All variables, except general constants like e.g. Young's modulus E, are defined in the section where they first appear. We list only the variables, which are frequently used in more than one chapter. The reference denotes the equation where the variable is mentioned first. Bold capital letters denote matrices and bold small letters signify vectors.

Indices:

x, y, z	Cartesian coordinates.
1, 2, ...	1.) numbers of body 1 or 2;
	2.) part of a load history;
	3.) functions of a similar type.
A	index for the beginning of impact.
E	index for the end of impact.
old	index for the 'frozen' stress distribution in the area of adhesion.
[ ]	brackets enclose indices of an array, following the notation of the programming language Pascal.

Symbol	Definition	Reference
A	combined curvature in x-direction $(A \geq B)$	(3.4),(5.3)
A_i	elliptical area	(6.1a),(7.1a)
A	load displacement matrix	(12.10)
a	semiaxis of the contact ellipse $(a \leq b)$	(3.7),(5.9)
$a^{\cdot}$	semiaxis of the elliptical area of adhesion	(5.22)
B	combined curvature in y-direction $(A \geq B)$	(3.4),(5.3)
B(k)	elliptical integral	(5.33)
b	semiaxis of the contact ellipse $(a \leq b)$	(3.7),(5.9)
$b^{\cdot}$	semiaxis of the area of adhesion	(3.10),(5.22)

Symbol	Definition	Reference
C	contact area	(3.7)
C(k)	elliptical integral	(5.33)
c_x, c_y, c_z	stiffness coefficients	(5.25)
D(k)	elliptical integral	(5.13)
D	matrix of the equation of motion	(8.33)
E	Young's modulus	(3.2)
E(k)	elliptical integral	(5.13)
E_x, E_z	kinetic energy in x- and z-direction	(9.58)
e,e_1,e_2	adapted displacement vector	(7.2c)
e_x, e_y, e_z	base of the cartesian coordinate system x,y,z	(8.2)
e_a, e_b, e_c	base of the inertial coordinate system a,b,c	(8.2)
F_x, F_y, F_z	force in x-, y-, z-direction	(5.11),(5.27)
F(a,b;c;S)	hypergeometric function	(9.9)
f	frictional coefficient $(f=f_{kin}=f_{stat})$	(5.23)
f_{stat}	static frictional coefficient	(12.4)
f_{kin}	kinetic coefficient of friction	(12.4)
G	combined modulus of rigidity	(4.7)
H	area of adhesion	(5.22)
k_x, k_y	curvature	(8.11)
K(k)	elliptical integral	(5.13)
M_z	torque around the common normal	(5.35)
m	index in y-direction	(4.10)
m_1, m_2	mass of body 1 resp. 2	(8.25)

Symbol	Definition	Reference
n	index in x-direction	(4.10)
p	direction parameter	(5.26)
p_z	normal contact pressure	(5.10)
P_i	i-th point of instantaneous adhesion	chap. 6
q	direction parameter	(5.26)
R	radius of the sphere	(6.1)
R_1, R_2	curvature in x-direction of body 1 resp. 2	(5.1)
R'_1, R'_2	curvature in y-direction of body 1 resp. 2	(5.1)
R_{ik}	Horak's coefficient of restitution	(3.3)
R_x	coefficient of restitution in x-direction	(9.33)
R_i	vector from center of inertia to contact point	(8.25)
r	1.) distance from the origin	(3.6)
	2.) distance between two points	(4.4)
S	$=(\zeta/\zeta_{MAX})^{5/2}$	(9.4)
S_i	slip area	(6.1a),(7.1a)
s_x, s_y	slip	(12.5)
t	time	(8.25)
t_N	dimensionless time	(9.4)
U	Array of displacements	(4.12)
u	displacement in x-direction	(4.1)
u_i	displacement vectorof body i	(8.27)
v	1.) displacement in y-direction	(4.1)
	2.) $d\xi/dt_N$	(9.12)
v_{abs}	absolute velocity	(8.27)
v_{rig}	rigid velocity	(8.27)

Symbol	Definition	Reference
w	displacement in z-direction	(4.1)
x	Cartesian coordinate	(3.4)
x'	Cartesian coordinate where the stress acts	(4.4)
x_{iM}	coordinates of the center of gravity of body i	(8.25)
y	Cartesian coordinate	(3.4)
y'	Cartesian coordinate of the stress	(4.4)
z	1.) distance of the two surfaces at x,y	(3.4)
	2.) Cartesian coordinate	(4.4)
z'	Cartesian coordinate of the stress, z'=z	(4.4)
α	Hertzian parameter	(5.12)
β	1.) Hertzian parameter	(5.12)
	2.) torsional angle	(5.31)
$\Gamma(x)$	Gamma function	(9.18)
γ	1.) hertzian parameter	(5.12)
	2.) dimensionless material parameter	(13.5)
Δx	mesh size in x-direction	(4.16)
Δy	mesh size in y-direction	(4.16)
δ	parameter of Cattaneo's solution	(5.25)
ε	Difference parameter	(5.20)
ε_1	dimensionless difference parameter	(13.40)

Symbol	Definition	Reference
ζ	displacement in z-direction	(5.4)
$\zeta^{\bullet}$	normal penetration corresponding to $a^{\bullet}$	(5.26)
η	displacement in y-direction	(5.19)
θ_i	tensor of inertia	(8.25)
θ	polar coordinate	(3.17)
ϑ_i	material parameter of body i	(5.14)
κ	1.) material parameter	(6.1c)
	2.) combined material parameter	(15.1)
λ	impact parameter	(15.1)
μ	material parameter	(6.1c)
ν	combined Poisson's ratio	(4.7)
ξ	displacement in x-direction	(5.18)
ξ	shift vector	(8.45)
Π	transformation matrix	(8.2)
ρ	polar coordinate	(3.17)
σ_{zx}, σ_{zy}, σ_{zz}	stress on the surface	(4.2),(4.3)
σ_{zo}	maximal Hertzian normal stress	(3.9)
σ_1, σ_2	ellipsoid functions	(3.12)
σ_{CM}	Cattaneo-Mindlin function	(6.1),(7.1)
σ_H	Hertzian pressure distribution	(5.10)
σ	pressure distribution	(4.13),(12.10)
σ_t	tangential stress	(7.2a)
ω_i	vector of rotation of body i	(8.25)

3 Introduction

3.1 Brief historical outline

E. Mach wrote in his book (1912, english translation: 1960): 'The laws of impact were the occasion of the enunciation of the most important principles of mechanics, and furnished also the first examples of the application of such principles'. Galileo (1638) performed several experiments to determine the concept of impact. Newton (1686) developed his laws of motion and introduced a coefficient of restitution, which is still widely in use. Further general theorems were added by Marci (1639) and Huygens (1669). Euler (Szabo 1979) proved in an article (1745), that the principles of mechanics together with a material law suffice to determine all important values during the impact process. This theory was further developed in two directions, which differ with the consideration of the elastic waves (free vibrations).

Franz Neumann (1885) and Barré de St. Venant (1883) calculated the longitudinal impact of thin cylinders of similar material with constant diameters, which collide with their front faces. The solution of the one-dimensional wave equation yields the plane longitudinal waves, which penetrate from the contact surfaces into the bodies and are reflected at the free ends. Heinrich Hertz (1882), on the other side, established a quasistatic theory for the normal impact by neglection of the elastic waves, on the base of his solution for the static compression of two bodies in normal contact.

Eason (1966) and Hunter (1957) proved the validity of this solution for half-space problems. Eason calculated the displacements produced in an elastic half space by a suddenly applied surface force, in the form of a spherical or constant pressure distribution, acting on a circular area of diameter 2a. He found, that the displacement of the surface in the center of the loaded region reaches its statical equivalent value after the time t:

$$t = 2a/\sqrt{(\lambda+2\mu)/\rho} \, , \; \lambda, \; \mu \; = \; \text{Lamé's constants,} \; \rho \; = \; \text{density.} \quad (3.1)$$

The time t corresponds to the time, which compressive waves in an elastic half space need, to run through the diameter of 2a of the circular area. It barely

changes with the form of the stress distribution.

Hunter (1957) calculated the energy loss produced by elastic waves during the impact of a sphere on an elastic half space. The fraction of the energy loss in the half space and the initial kinetic energy of the sphere has the value:

$$1.04 \ (v_A/\sqrt{E/\rho})^{3/5}, \quad E : \text{Young's modulus.} \tag{3.2}$$

This energy loss is negligible, as long as the value of the impact velocity v_A at the beginning of the impact of the sphere amounts only to a few percent of the velocity of compressive waves in thin elastic rods.

From these results follows that only bodies which are able to vibrate, like rods, plates, etc., loose a negligible amount of energy by the propagation of elastic waves. During the impact of massive bodies, whose dimensions are huge compared to the dimensions of the loaded region, the elastic waves can be neglected as long as the duration of impact is short compared with the time t, which elastic waves need to run through the contact area. The reflected waves can also be neglected in the frame of this theory, because the energy of spherical waves decreases with the distance traveled through the body.

In the year 1938 appeared a work of Cattaneo with the solution of the boundary value problem for the statical displacement of a half-space in tangential direction. He introduced the notion of *partial slip*, i.e. slip takes place on a part of the contact area. Mindlin calculated in 1949 the fraction of a differential displacement dξ and the necessary differential force dF_x for the tangential and torsional problem of bodies with Hertzian surfaces under complete adhesion, which he called *elastic compliance*. Later, Mindlin & Deresiewicz (1953) investigated the influence of varying oblique forces on the contact of rough spheres. This was the first approach to *load-histories*, where the stress distribution depends on the complete previous history of the contact process. We generalized the Mindlin/Deresiewicz theory for elliptical contact areas and two-directional load-histories in x- and y-direction. Up to this day, many papers were published which study special types of contact problems.

More complicated problems, such as load-histories for dissimilar materials, or the calculation of the stresses inside of the two bodies (Kalker 1986b), can only be solved by numerical methods. Frictional, numerical contact-elastostatics starts with a work of Kalker (1967), where he developed a variational approach to the problem of rolling. In that work a polynomial series was used for the solution of the

quasistatic contact problem, which worked well for rolling. In the following years he developed several improvements to reduce the computation time (1986a, 1988). One method was the simplified theory which approximates the real stress distribution by simplified functions. Another method of the type of the Gauss-Seidel Block Iteration Method, called the Panagiotopoulos-Johnson process, accelerates the matrix inversion considerably. Furthermore Kalker published several papers to prove the convergence of contact algorithms (1985). The basic problems of the numerical treatment are the computer storage requirements for the large load-displacement matrix, the computation time to determine the location and the form of the stick area, and the slip direction in the slip area. We developed a new method on the base of Kalker's work, which applies the Gauss-Seidel procedure to the contact problem. This method is fast enough to solve impact processes and involved load- histories, but improvements are still necessary for large contact areas which consist of more than 1000 points.

The group N. Maw, J.R.Barber and J.N.Fawcett published in the year 1975 a numerical solution for the oblique impact of elastic spheres on the base of analytical series. They also performed experiments (1976) to test the theoretical predictions. Later (1979), Barber published another paper with an analytical solution in the form of hypergeometric series for a period of complete adhesion in the compressive period of the impact of two spheres. We generalized this solution for the period of partial slip with infinitely small forces and for elliptical contact areas.

Horák (1948) and his coworker Machalicky (1973) published some numerical results for the tangential and torsional impact, but it appears that they did not consider the dependence of the tangential force and the torsional moment on the variation of the contact radius. Horák (1931) established a general theory of impact by the introduction of additional coefficients of restitution, defined by three equations of the form:

$$v_{iE} = - \sum_{k=1}^{3} R_{ik} v_{kA} , \qquad (3.3)$$

where the indices 1,2,3 denote the x, y, z-directions; the indices E resp. A signify the end resp. beginning of the impact. Our work shows, that the coefficients of restitution depend on several parameters: Young's modulus E, Poisson's number v, the special form of the surface (Hertzian, non-Hertzian etc.), the inertial properties, the initial velocities and rotations etc. If the equations of motion in x-, y- and z-

direction are independent, the coefficients of restitution form a diagonal tensor, whose entries we will calculate for some special cases.

3.2 Thesis outline

The subject of this work is the oblique impact of two elastic bodies of arbitrary geometry under the influence of stick and slip stresses in the contact area. We solve this problem on the base of the fundamental equations of the three-dimensional theory of linear elasticity with appropriate simplifications. The contact surfaces shall be *non-conforming*, so that the surfaces do not 'fit' together without deformation. At the time $t_A = 0$ the bodies shall be brought together and touch first at one point, the *contact point O*. An orthogonal coordinate system is introduced with its origin in the contact point O. The z-axis points normally into body 1 and the x- and y-axis lie in the common tangent plane. Figure 3.1 shows a part of the surfaces of the two bodies in the vicinity of the contact point. The coordinate system shall be fixed in space, while the contact point moves with the bodies.

The distance of point P_1 on the surface of body 1 to P_2 on the surface of body 2 is quadratic in x and y near the contact point. We have

$$z(x,y) = z_1 + z_2 = Ax^2 + Cxy + By^2. \tag{3.4}$$

By a suitable choice of the axis we can make C zero and $A \geq B$, hence:

$$z(x,y) = Ax^2 + By^2, A \geq B. \tag{3.5}$$

The constants A and B may be expressed in the local radii of curvature of the bodies, and in the angle, which the planes of principal curvature take to one another, in the manner of the Hertz theory (Love, 1927).

Under the influence of a normal force the two bodies will be compressed and a contact area forms. The dimensions of this contact area shall be small compared to the dimensions of the two bodies. The physical behaviour of the two bodies near the contact point can be approximated by two half spaces. For that purpose, we decompose the stress distribution into infinitely small forces acting on infinitely small areas.
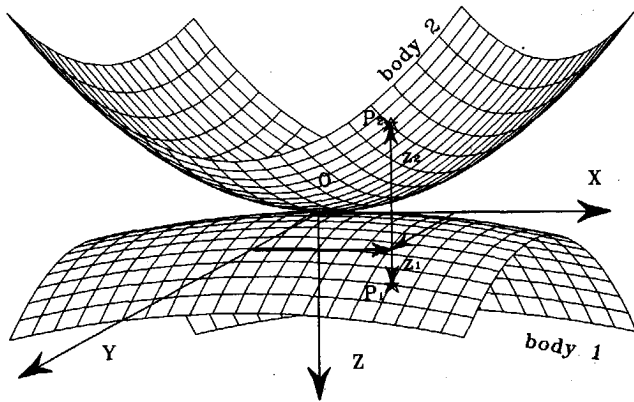
Fig. 3.1 The surfaces of the two bodies near the contact point

The deformation field, produced by a singular force F_z in normal direction, acting on a half-space, is known as the Flammant solution (Flammant 1892). The deformations u, v, w of body 1 in x-, y- and z-directoin of the coordinate system of figure 3.1 are:

$$u = \frac{F_z}{4\pi G}\left[\frac{xz}{r^3} - \frac{(1-2\nu)x}{(r^2+rz)}\right],\ v = \frac{F_z}{4\pi G}\left[\frac{yz}{r^3} - \frac{(1-2\nu)y}{(r^2+rz)}\right],\ w = \frac{F_z}{4\pi G}\left[\frac{z^2}{r^3} + \frac{2(1-\nu)}{r}\right], \quad (3.6)$$

$$r = \sqrt{x^2+y^2+z^2},$$

with the modulus of rigidity G and the force F_z in z-direction. ν is Poisson's number and x, y, z are the coordinates where the displacement is measured. Figure 3.2 shows the displacements along the x-axis for y=0 and z=0 with $F_z=0.08\pi G$.

The displacements of the surface are hyperbolas with a singularity at the origin. This singularity disappears for a distribution of infinitely small forces. The deformation u in x-direction becomes zero for $\nu=0.5$. In this case the normal and tangential solutions are independent. The displacements of an arbitrary stress distribution can now be calculated by decomposing the area into small intervals; the action of the stress on an interval is equivalent to a small singular force in its center. We get the solution as a sum of singular forces acting on each interval. The limit of infinitely small intervals yields an integral. The corresponding integral equations and the tangential solution will be explained in chapter 4.

According to the theory of H. Hertz (1882), the contact area C is an ellipse

with the semi-axes a and b:

$$C = \{ (x,y) \mid (x/a)^2 + (y/b)^2 \leq 1 \}. \tag{3.7}$$

The normal contact stress has the form of a semi-ellipsoid acting on the contact area:

$$p_z(x,y) = \begin{cases} \sigma_{z0} \sqrt{1-(x/a)^2-(y/b)^2}, & \text{if } (x,y) \in C, \\ 0, & \text{if } (x,y) \notin C, \end{cases} \tag{3.8}$$

where $p_z(x,y)$ is positive for compression. The factor σ_{z0} is determined by the normal force F_z:
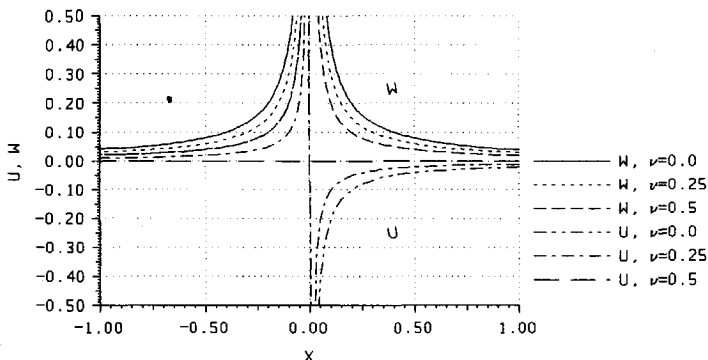
$$\sigma_{z0} = 3F_z/(2\pi ab). \tag{3.9}$$

Fig. 3.2: Deformations u, w for $F_z = 0.08\pi G$.

Application of an additional force in tangential direction and a balanced moment defines the tangential problem. A kinematic boundary condition for the additional boundary value problem is obtained from the consideration, that contacting points in the contact area displace equally, except a constant, which is determined by the relative displacement in tangential direction of far points of both bodies. Coulomb's law is taken as base with equal static and kinetic coefficients of friction. The solution was found by Cattaneo (1938) and Mindlin (1949). Cattaneo found, that the stick area H is also an ellipse, similar to the contact area with the semi-axes a*, b*:

$$H = \{ (x,y) \mid (x/a^*)^2 + (y/b^*)^2 \leq 1 \}, \ a^*/a = b^*/b. \tag{3.10}$$

Slip appears locally in the slip area outside of the stick area. We call this effect *partial slip* or *local slip*. Other authors use the expression *microslip*, which we will not use here, because it suggests microscopic movements, whereas the slip can be large if the displacements are large. We distinguish between the three processes of *complete adhesion, partial slip* and *complete sliding*. Similar to the Hertzian stress distribution (3.8), the Cattaneo-Mindlin stress distribution consists of two concentric semi-ellipsoids σ_1 and σ_2. σ_1 extends over the complete contact area and σ_2 over the stick area, pointing into the opposite direction:

$$\sigma_1 = \begin{cases} f\sigma_{z0}\sqrt{1-(x/a)^2-(y/b)^2} \ , & \text{for } \{ x,y \in C \} \ , \\[2mm] 0 \ , & \text{for } \{ x,y \notin C \} \ , \end{cases} \tag{3.11a}$$

$$\sigma_2 = \begin{cases} f\sigma_{z0}(a^*/a)\sqrt{1-(x/a^*)^2-(y/b^*)^2} \ , & \text{for } \{ x,y \in H \} \ , \\[2mm] 0 \ , & \text{for } \{ x,y \notin H \} \ , \end{cases} \tag{3.11b}$$

with σ_{z0} from equ. (3.9). The pressure distribution has the form:

$$\sigma_{zx} = p \ (\sigma_1 - \sigma_2), \quad \sigma_{zy} = q \ (\sigma_1 - \sigma_2), \quad \text{in } H, \tag{3.12}$$
$$\sigma_{zx} = p \ \sigma_1, \quad \sigma_{zy} = q \ \sigma_1, \quad \text{in the slip area } S.$$

The stiffness coefficients c_x, c_y, c_z define the stiffnesses of the force-displacement relation in x-, y- and z-direction:

$$\frac{c_x}{c_z} = \frac{(1-\nu)/G}{1/G - \delta \cdot \nu/G} \ , \quad \frac{c_y}{c_z} = \frac{(1-\nu)/G}{(1-\nu)/G + \delta \cdot \nu/G}, \quad \delta = \frac{D(k)}{K(k)},$$
$$c_z = \frac{2\pi\sqrt{D(k)}}{\sqrt{B}\,K^{3/2}(k) \, (1-\nu)/G} \ . \tag{3.13}$$

Equations (3.13) hold for $a<b$. The constant B is the combined curvature of both bodies in y-direction, while K(k) and E(k) are the complete elliptic integrals of the first and second kind, defined by (5.13). The material properties G and ν are combined values:

$$k = \sqrt{1-a^2/b^2}, \; D(k) = (K(k)-E(k))/k^2,$$

$$1/G = 1/G_1+1/G_2, \; \nu/G = \nu_1/G_1+\nu_2/G_2, \; G_i = E_i/(2+2\nu_i). \tag{3.14}$$
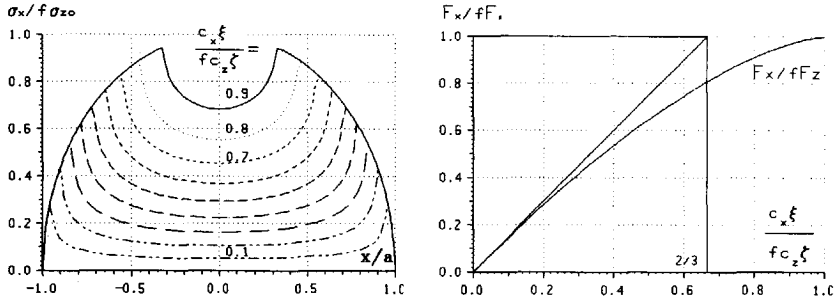

Fig. 3.3: Stress distributions of Cattaneo and Mindlin for $F_y=0$ and $\eta=0$.

The parameters p and q and the radius of the stick area a^* are defined as follows:

$$p = c_x\xi/\sqrt{(c_x\xi)^2+(c_y\eta)^2}, \; q = c_y\eta/\sqrt{(c_x\xi)^2+(c_y\eta)^2}, \; p^2+q^2 = 1,$$

$$\zeta^*/\zeta = (a^*/a)^2 = 1 - \sqrt{(c_x\xi)^2+(c_y\eta)^2}/(fc_z\zeta). \tag{3.15}$$

ξ, η and ζ are the displacements of the contact point in x-, y- and z-direction and ζ^* is the normal penetration which produces a contact area of the radius a^*. The formulae for the forces F_x, F_y, F_z are:

$$F_x = p \, f \, F_z \, (1-a^{*3}/a^3), \quad F_y = q \, f \, F_z \, (1-a^{*3}/a^3), \quad F_z = 2 \, c_z \sqrt{\zeta^3}/3. \tag{3.16}$$

Figure 3.3 shows the stress distribution σ_x at y=0 for different values of the tangential displacement ξ. The letter f denotes the coefficient of friction and F_x the tangential force.

The solutions of Hertz and Cattaneo-Mindlin are one step solutions, because the tangential deformation is applied in one step after the bodies are compressed in normal direction. If the normal and tangential compressions are applied simultaneously, the deformation must be decomposed into small increments, and each increment can be approximated by a one step solution. The general oblique impact for instance consists of a sequence of normal and tangential increments.
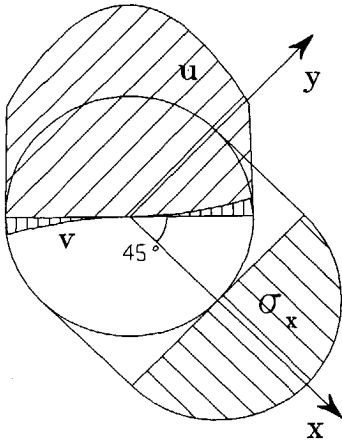
Fig. 3.4: u,v from (3.17) for $\nu = 0.5$.

Cattaneo's solution is based on the two simplifications that the direction of the stress is constant in the entire slip area and the direction of the force is constant during the complete load-history. The value of the tangential stress perpendicular to the shift is smaller than 5% of the tangential stress, for spheres (K. L. Johnson 1985). The displacements u, v in x- and y-direction for a semispherical pressure distribution σ_x are:

$$\sigma_x = C \sqrt{1-\rho^2/a^2}, \quad \rho = \sqrt{x^2+y^2}, \quad (3.17)$$

$$u = \frac{\pi C}{16Ga} [2(2-\nu)(2a^2-\rho^2)+\nu\rho^2\cos(2\theta)],$$

$$v = \frac{\pi C}{16Ga} \nu \rho^2 \sin(2\theta), \quad \text{for } 0 \leq \rho \leq a.$$

The polar coordinate θ is measured from the positive x-axis and ν is Poisson's module. The displacement v becomes maximal at an angle of $\theta = 45°$ to the stress direction (see Fig. 3.4). This effect is a result of the coupling between the tangential deformations and dissappears for $\nu = 0$.

The direction of the force changes during the load-history, in which the displacement direction is constant, when the stiffness coefficients c_x and c_y are unlike. In this case the pressure direction for complete adhesion is different from the direction for *rigid sliding*. The term *rigid sliding* denotes the sliding of perfectly rigid bodies. In the course of the load-history the direction of the force varies between complete adhesion and rigid sliding. This effect appears clearly for slender contact ellipses with Poisson's number $\nu = 0.5$. Several numerical calculations showed, that the error remains below 5% as long as an area of adhesion exists. The larger the area of adhesion, the smaller the error. The direction changes much, when *gross slip* or *complete sliding* starts, where the complete contact area slides. Equations (3.13) and (3.16) yield the following inequalities:

$$0.5 \leq c_x/c_y \leq 1.0, \quad 0.5 \leq P_x/P_y \leq 1.0, \quad \text{for } a > b \text{ and } \xi = \eta. \quad (3.18)$$

Figure 3.5 shows the numerical results for a load-history with equal displacements in x- and y-direction: $\xi = \eta$, $\nu = 0.5$ and $a/b = 20$. Equations (3.13), (3.15) yield the displacement, which is necessary to produce complete sliding: $\xi = \eta \approx \zeta$. During the sliding process the direction of the force adjusts to the slip direction of rigid bodies. This result suggest to distinguish between four contact regimes: The term *full adhesion* or *complete adhesion* is used when no relative motion in the whole contact area takes place; *partial slip* signifies the occurence of slip on a part of the contact area; *full sliding* or *gross slip* denote sliding of the whole contact area; *rigid sliding* or *rigid slip* signify the sliding of perfectly rigid bodies. Kalker (1990) uses the term rigid slip for the relative motion in tangential direction of two corresponding points of the undeformed surfaces.
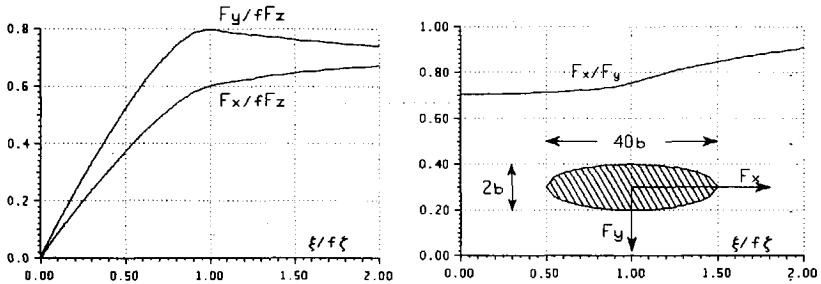

Fig. 3.5: The tangential force for a load-history with $\xi = \eta$, $\nu = 0.5$.

In impact theories the transition from full sliding to rigid slip can be ignored, because it happens in a very short time. Depending on the start velocities either full adhesion or rigid slip dominates. Thus the stress direction can be approximated by Cattaneo's formulae.

Lubkin solved the problem of the torsion of elastic spheres with partial slip. In section 5.4 we propose an approximation for the relation between the torque and the twisting angle, which we generalized for elliptical contact areas under varying torques in section 14.4. This approximation is based on the fact, that Lubkin's formulae can be generalized for the torsion of elastic spheres under varying torques. The first approach to load-histories was published by Mindlin & Deresiewicz (1953) in an article about varying normal and oblique forces. In chapter 6 we will introduce the so-called *Cattaneo-Mindlin functions*, in order to deduce a new formula for general load-histories under partial slip. This formula

depends only on the *points of instantaneous adhesion*, in which the entire contact area is stuck for a moment in the course of the load-history, but not on the specific form of the load-history. In chapter 7 this formula is generalized for elastic bodies with elliptical contact areas under oblique forces in varying directions. This generalization is restricted to bodies of similar material without torsion and load-histories under partial slip. Only numerical methods render better results for special cases.

In the next chapters we investigate impact problems, on the base of the contact laws mentioned above. We call the velocity of body 1 relative to body 2 the *relative velocity*. It can be decomposed into a component parallel to the z-axis: The normal component v_z, and two components lying in the tangential plane: The tangential components v_x and v_y. At the time t_A, when contact is first made, v_z is negative, because the bodies approach each other. This approach compresses the two bodies and a contact area forms between them. Normal and tangential stresses are transmitted in the contact area. The contact area will shift relative to the fixed coordinate system, but the impact duration T shall be so short, that the rotation of the bodies is very small, and the material contact point remains in the center of the contact areas. This condition is satisfied, if the impact duration T is much smaller than the reciprocal value of the angular velocity ω: $T \ll 1/\omega$, i.e. the impact duration is very small compared to the time for one rotation of the bodies.

The global effect of the stresses on the two bodies can be described by the statically equivalent forces and moments in tangential and normal direction. Depending on the forces we distinguish between three types of impact: Normal, tangential and torsional. The normal impact was calculated by H. Hertz (1882) and consists of the two special types: Central impact of bodies of similar material and frictionless impact, where only the normal force acts. Tangential impact denotes the oblique impact with friction, where also a tangential force acts. Torsional impact includes a rotation of both bodies around the common normal, i.e. the normal force is accompanied by a torque. The torsional velocity around the common normal is also called *spin*. An asymmetric normal stress distribution in the contact area also produces torques around the x- and y- axis. We neglect these moments in our theory, because the contact area is so small, that the lever-arm of the torsional stresses is much smaller than the lever-arm of the tangential forces.

In chapter 10 we discuss an approximation for the torsional impact, which shows, that the angular velocity of two spheres changes proportional to $(a/R)^2 = (\zeta_{MAX}/R)$, with the contact radius a, the radius R of the spheres and the
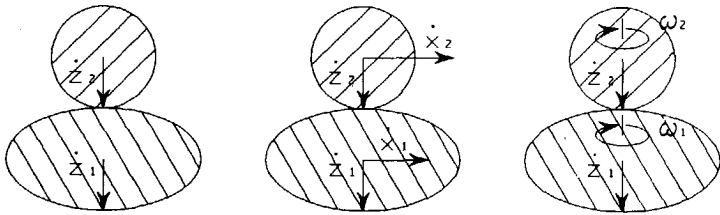
Fig 3.6: Normal, tangential and torsional impact.

maximal compression ζ_{MAX}. Hertz presupposes, that the contact radius should be smaller than $R/10$ for his theory. It follows, that the change of the torsional moment should be neglected, within the frame of the Hertz theory. More important is the effect of the rotation on the location of the stick area. Furthermore the spin changes the slip directions and this reduces the tangential forces. These effects are very important for small normal velocities.

The normal impact consists of a period of compression and a period of restitution. The impact of similar materials is completely reversible, because no frictional forces are transmitted, provided both bodies consist of elastic material. During the tangential impact the three contact regimes of full adhesion, partial slip and rigid sliding must be distinguished. For small tangential relative velocities at the beginning of impact the contact points stick and complete adhesion arrives as the contact area increases. During the initial stage of the impact process the increase of the tangential stresses is smaller than the increase of the normal stresses and complete adhesion persists first. The frictional force accelerates the two bodies opposite to the tangential relative velocity of the centers and generates an increasing opposite stress distribution, until the increase of the tangential stresses is no longer compensated by the normal stresses. At this point partial slip starts. For high tangential velocities at the beginning of impact the stick condition of Coulomb's law is violated and both surfaces slide upon each other, until all points stick together at the same time. At the end of impact the normal stresses become zero while the tangential stresses produce complete sliding. The torsional impact proceeds quite similarly to the tangential impact as just described.

We assume, that the bodies shall be massive, such that the elastic waves propagate unhindered and without reflexion into and throughout the body. The amplitude of these waves decreases with the depth of penetration into the body and the surface deformation reaches the quasistatic value, as long as the normal velocity

is small compared to the velocity $v = \sqrt{E/\rho}$ of compressive waves in thin elastic rods (E denotes Young's modulus and ρ the density of the bodies). This result was elaborated by Hunter (1957), who published another paper (1960), where the experimental energy-loss of steel spheres etc. was explained by viscous (dissipative) forces in the material.

We presuppose, that the bodies do not vibrate and that the contact area is small compared to their dimensions and curvatures, so that they can be regarded as rigid bodies with a small elastically deformed region. Now we apply the impuls and momentum equations, with singular forces in the contact area, which are statically equivalent to the stresses. The forces can be described by the contact law, which we adopt from the solutions of the static boundary value problem mentioned above.

In chapter 8 the transformation matrix between the coordinate system of the principal curvatures in the contact point, which we call the *contact base*, and the *inertial base* of the principal axes of inertia is deduced, which is necessary to formulate the equations of motion. We show in section 8.2 that the equations of motion consist of a system of ordinary differential equations. The contact law of chapter 7 is inserted in the equations of motion. Some analytical solutions in form of hypergeometric functions are presented in chapter 9. Complete solutions are possible for full adhesion and full sliding, while the equations for partial slip must be solved numerically. The ratio of the tangential velocities after impact to the values before impact is called the tangential coefficient of restitution. The impact of spheres can perfectly be described by this coefficient.

If a torsional rotation is superposed or if the materials are dissimilar, the numerical methods discussed in chapter 11 are necessary. Much work was done by J. J. Kalker to develop algorithms for the normal and frictional contact, especially for rolling problems. He solves the integral equations by discretization rather than using polynomials or splines. Kalker showed, that the nonlinear frictional problem can be solved by recursive algorithms. The form of the contact area and the slip area can be determined by a successive correction. Furthermore he developed several algorithms to accelerate the calculation. In an article (1971) he introduced a variational principle for the frictional contact problem.

In chapter 12 we show, how these methods can be improved by the Gauss-Seidel algorithm. In the area of adhesion the deformation is prescribed and a matrix inversion is necessary to determine the stress. This matrix inversion was performed with the Gauss-Seidel method. During the Gauss-Seidel iteration the slip

direction is held constant and the new values of the frictional stress are continuously inserted in the linear equation system for the stresses. Numerical experience and a restricted proof of convergence in chapter 13 show, that this modification of the Gauss-Seidel procedure converges also. The linearization of the frictional law yields large matrices again and the Gauss-Seidel method can not be applied here, but the linearized equation system can be solved blockwize i.e. by the Gauss-Seidel Block Iteration Method. A proof of convergence for the linearization was not elaborated, because convergence problems can be avoided, using small increments. For infinitely small increments the slip directions change infinitely, i.e. the correction of the slip direction becomes zero, and convergence is certain. Numerical expirience shows, that the variation of the stress direction is maximal at the border of the contact area. The Gauss-Seidel method reduces the execution time and the memory requirements. Compared with the Gauss elimination, the required computer memory increases with n instead of n^2, and the computation time with n^2 instead of n^3, where n denotes the number of elements. For 400 elements the memory and the execution time can be reduced by the factor 400. As a typical example a contact problem with dissimilar materials, 400 points and a load-history of 20 increments was calculated in 1 hour on an 80486/33 MHz processor. It follows that contact problems with many points must be solved with this method.

Chapter 14 presents some numerical results for incremental load-histories for Hertzian surfaces and flat punches. The stress distribution for spheres of similar material is discussed in section 14.1 and compared with the theory of chapter 7. In contradiction to the theory the tangential stress direction is not constant in the slip area, but the absolute value of the tangential stress, the size of the stick area and the tangential forces are very correct. A large number of calculations for elliptical contact areas proved, that the stresses σ_{zx} and σ_{zy} are constant on ellipses, which are similar to the contact area, for bodies of similar material with $\nu_1 = \nu_2 = 0$. A load-history for elliptical contact areas with bodies of dissimilar material is discussed in chapter 14.3. The numerical and theoretical stress distribution differ considerably in this case. It turned out, that in the period of compression of dissimilar materials the stress direction is constant on radial lines. In section 14.4 the approximation for elastic bodies under varying torque is compared with the numerical results. Furthermore the combination of shift and torsion is investigated for two examples. Section 14.5 presents a contact problem for a flat punch with 1000 points in the area of integration.

In chapter 15 some numerical results for the coefficient of restitution R_x are presented; R_x is the ratio of the tangential velocities in the contact point before and after impact. The influence of torsional rotation and dissimilar materials on the impact of bodies with elliptical contact areas was emphasized in this chapter. Fig. 3.7 shows an example for a tangential impact with different values of R_x. A book is held over a table and a rubber ball is thrown under the book, such that the ball will be reflected by the table and the book. People expect, that the ball travels forward, but it comes back. The only classical approach to this phenomen is the model of full sliding, which is not adequate here. In contrast to classical impact theories the angle of incidence is not equal to the angle of reflexion and the ball rotates after the first reflexion. Fig. 3.7 shows the behaviour of the ball for a value of $R_x = 0.6$, which corresponds to the theoretical value of $\lambda \approx 3$ in fig. 15.1, for similar materials with $\kappa \approx 3/2$, $f \approx 0.3$, and an angle of incidence of $45°$. The value of R_x varies between -1.0 for an impact without friction, zero for a plastic impact and $+1.0$ for a fully elastic reflexion. The determination of the coefficient of friction is the most difficult part of this experiment, because this value depends on many parameters like the material, the normal force and the tangential velocity etc.
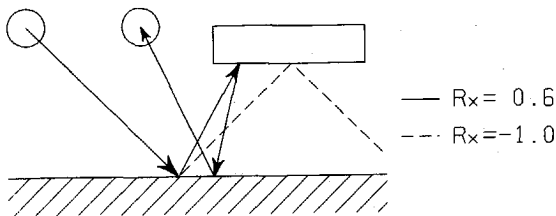

Fig. 3.7: Example for the influence of frictional forces on the oblique impact.

Another example for the oblique impact is the landing process of an airplane, where the wheels strike the runway. In billard games the frictional forces cause the rotation of the balls. Impact happens on every type writer, when the letters or pins impact on the platen. The tangential impact is also important for the pneumatic transport of solid particles in a pipeline, where the flow resistance increases by such impacts between the particles and the wall. Many impact phenomena involve plastic deformations, especially in military research. Such problems are not in the frame of this thesis.

4 Summary of the basic formulae for half-space problems

4.1 The equations of Boussinesq and Cerruti

Boussinesq (1885) and Cerruti (1882) calculated the elastic displacement of an infinite half-space loaded by a singular force. The displacement produced by an arbitrary stress distribution can be found by dividing the loaded area into a mesh of small rectangles and replacing the stress distribution on each rectangle by a statically equivalent force. We obtain the displacement by superposition of the forces on each rectangle. It is convenient in mathematics to reduce the size of these rectangles to an infinitely small value and to describe the correct displacements in form of an integral. The force on such a small rectangle is called *point load*, because the loaded area dwindles to a point. The displacements produced by a point load are given by the solution of Boussinesq and Cerruti. The derivation of this solution can be found in Love (1927). Then if F_x, F_y, F_z denote the forces on the surface, the displacements u, v, w are given by (Gladwell 1980):

$$4\pi Gu = \frac{2(1-\nu)F_x}{z+r} + \frac{2\nu Tx}{(z+r)^2} - \frac{(1-2\nu)F_z x}{r(z+r)} + \frac{z}{r}\left\{ \frac{F_x}{z+r} + \frac{Tx(z+2r)}{r(z+r)^2} + \frac{F_z x}{r^2}\right\} ,$$

$$4\pi Gu = \frac{2(1-\nu)F_y}{z+r} + \frac{2\nu Ty}{(z+r)^2} - \frac{(1-2\nu)F_z y}{r(z+r)} + \frac{z}{r}\left\{ \frac{F_y}{z+r} + \frac{Ty(z+2r)}{r(z+r)^2} + \frac{F_z y}{r^2}\right\} ,$$

$$4\pi Gw = \frac{2(1-\nu)F_z}{r} + \frac{(1-2\nu)T}{(z+r)} + \frac{z}{r}\left\{ \frac{zF_z}{r^2} + \frac{T}{r}\right\} , \qquad (4.1)$$

$$r = \sqrt{x^2+y^2+z^2} , \quad T = (xF_x + yF_y) ,$$

where the z-coordinate points into the body. The stresses inside the half space produced by a tangential force F_x are defined by (Johnson, 1985):

$$2\pi\sigma_{xx} = -3F_x \frac{x^3}{r^5} + xF_x(1-2\nu)\left\{ \frac{1}{r^3} - \frac{3}{r(r+z)^2} + x^2 \frac{3r+z}{r^3(r+z)^3}\right\} ,$$

$$2\pi\sigma_{xy} = -3F_x \frac{x^2 y}{r^5} + y F_x(1-2\nu)\left\{ \frac{-1}{r(r+z)^2} + x^2 \frac{3r+z}{r^3(r+z)^3}\right\} , \qquad (4.2a)$$

$$2\pi\sigma_{yy} = -3F_x\frac{xy^2}{r^5} + xF_x(1-2\nu)\left\{\frac{1}{r^3} - \frac{1}{r(r+z)^2} + y^2\frac{3r+z}{r^3(r+z)^3}\right\},\quad (4.2b)$$

$$2\pi\sigma_{zx} = -3F_x zx^2/r^5,\quad 2\pi\sigma_{zy} = -3F_x zxy/r^5,\quad 2\pi\sigma_{zz} = -3F_x xz^2/r^5.$$

The displacements u,w of the surface z=0 produced by the normal force F_z are shown in fig 3.2. The stresses inside of the half space produced by a normal force F_z are:

$$2\pi\sigma_{xx} = -F_z\frac{3zx^2}{r^5} - \frac{F_z}{r^3}(1-2\nu)\left\{\frac{r^2-rz-z^2}{r+z} - \frac{2r+z}{(r+z)^2}x^2\right\},$$

$$2\pi\sigma_{xy} = -\frac{F_z}{r^3}\left\{\frac{3xyz}{r^2} - (1-2\nu)\frac{xy(2r+z)}{(r+z)^2}\right\}\quad (4.3)$$

$$2\pi\sigma_{yy} = -F_z\frac{3zy^2}{r^5} - \frac{F_z}{r^3}(1-2\nu)\left\{\frac{r^2-rz-z^2}{r+z} - \frac{2r+z}{(r+z)^2}y^2\right\},$$

$$2\pi\sigma_{zx} = -3F_z z^2x/r^5,\quad 2\pi\sigma_{zy} = -3F_z z^2y/r^5,\quad 2\pi\sigma_{zz} = -3F_z z^3/r^5.$$

4.2 The displacements for an arbitrary load distribution

The displacements u,v,w of a point x,y,z produced by a pressure distribution σ_{zx}, σ_{zy}, σ_{zz} applied at the point x', y' on the surface z'=0 can now be calculated by replacing the letters x,y in (4.1) with x-x', y-y'. We introduce the normal contact pressure p_z, which is positive for compression, because the normal force F_z from (4.1) is mostly compressive in contact mechanics, and obtain (Love, 1927):

$$p_z(x,y) = -\sigma_{zz}(x,y,0),$$

$$r = \sqrt{(x-x')^2+(y-y')^2+z^2},\qquad L = \int\sigma_{zx}[z\cdot\ln(z+r)-r]dx'dy',$$

$$M = \int\sigma_{zy}[z\cdot\ln(z+r)-r]dx'dy',\qquad N = \int p_z[z\cdot\ln(z+r)-r]dx'dy', \quad (4.4a)$$

$$\psi = \partial L/\partial x + \partial M/\partial y + \partial N/\partial z,$$

$$4\pi Gu = 2\nu \frac{\partial \psi}{\partial x} - z \frac{\partial^2 \psi}{\partial z \partial x} + 2 \frac{\partial^2 L}{\partial z^2} - \frac{\partial^2 N}{\partial z \partial x} \,,$$

$$4\pi Gv = 2\nu \frac{\partial \psi}{\partial y} - z \frac{\partial^2 \psi}{\partial z \partial y} + 2 \frac{\partial^2 M}{\partial z^2} - \frac{\partial^2 N}{\partial z \partial y} \,, \qquad (4.4b)$$

$$4\pi Gw = (1-2\nu) \frac{\partial \psi}{\partial z} - z \frac{\partial^2 \psi}{\partial z^2} - \frac{\partial^2 N}{\partial z^2} \,.$$

The formulae may be proved by performing the differentiations and comparing these with (4.1). The displacements of the surface $z = 0$ are easily evaluated from (4.4):

$$4\pi u = \frac{2}{G} \int \frac{\sigma_{zx}}{r} dS - \frac{2\nu}{G} \left\{ \int \sigma_{zx} \frac{\partial^2 r}{\partial x^2} \, dS + \int \sigma_{zy} \frac{\partial^2 r}{\partial x \partial y} \, dS \right\} - \frac{1-2\nu}{G} \int p_z \frac{\partial}{\partial x} \ln r \, dS \,, \quad (4.5a)$$

$$4\pi v = \frac{2}{G} \int \frac{\sigma_{zy}}{r} dS - \frac{2\nu}{G} \left\{ \int \sigma_{zy} \frac{\partial^2 r}{\partial y^2} \, dS + \int \sigma_{zx} \frac{\partial^2 r}{\partial x \partial y} \, dS \right\} - \frac{1-2\nu}{G} \int p_z \frac{\partial}{\partial y} \ln r \, dS \,, \quad (4.5b)$$

$$4\pi w = \frac{1-2\nu}{G} \int \sigma_{zx} \frac{\partial}{\partial x} \ln r \, dS + \frac{1-2\nu}{G} \int \sigma_{zy} \frac{\partial}{\partial y} \ln r \, dS + \frac{2-2\nu}{G} \int \frac{p_z}{r} \, dS \,. \qquad (4.5c)$$

For $\nu = 0.5$ the normal and tangential displacement systems are uncoupled, i.e. a normal traction σ_{zz} produces no tangential displacements and vice versa. In this case the solution of the integral equations for prescribed displacements can be simplified. On the other hand for $\nu = 0$ the tangential stress distributions are uncoupled, because a traction σ_{zx} produces no displacement v in y-direction and vice versa.

4.3 The load-displacement equations in discrete form

In this chapter we will determine the load-displacement equations for two bodies in contact. First the two bodies are compressed in normal direction and a contact area forms. We assume, that in the contact area *corresponding points* come into contact. Different points of the two surfaces are said to correspond given their undeformed location in x- and y-direction coincides. The displacements of the surfaces of the two bodies can be calculated by equations (4.5). We have to take into consideration, that

the normal coordinate of the upper body 2 points opposite to the normal coordinate of body 1. Newton's law states that the stresses at two points in contact are opposite. We introduce the stress variables σ_{zx}, σ_{zy}, σ_{zz} and the difference of the displacements u, v, w:

$$\sigma_{zx} = \sigma_{zx1} = -\sigma_{zx2} \ , \quad \sigma_{zy} = \sigma_{zy1} = -\sigma_{zy2} \ , \quad \sigma_{zz} = \sigma_{zz1} = \sigma_{zz2} \ ,$$

$$u = u_1 - u_2 \ , \ v = v_1 - v_2 \ , \ w = w_1 + w_2 \ , \tag{4.6}$$

and the combined material parameters:

$$\frac{1}{G} = \frac{1}{G_1} + \frac{1}{G_2}, \quad \frac{\nu}{G} = \frac{\nu_1}{G_1} + \frac{\nu_2}{G_2} \ . \tag{4.7}$$

We obtain the displacements by inserting (4.6), (4.7) in (4.5) :

$$4\pi u = \frac{2}{G} \int \frac{\sigma_{zx}}{r} dS - \frac{2\nu}{G} \int \sigma_{zx} \frac{\partial^2 r}{\partial x^2} dS - \frac{2\nu}{G} \int \sigma_{zy} \frac{\partial^2 r}{\partial x \partial y} dS - \left(\frac{1-2\nu_1}{G_1} - \frac{1-2\nu_2}{G_2} \right) \int p_z \frac{\partial}{\partial x} \ln r \, dS \ ,$$

$$4\pi v = \frac{2}{G} \int \frac{\sigma_{zy}}{r} dS - \frac{2\nu}{G} \int \sigma_{zy} \frac{\partial^2 r}{\partial y^2} dS - \frac{2\nu}{G} \int \sigma_{zx} \frac{\partial^2 r}{\partial x \partial y} dS - \left(\frac{1-2\nu_1}{G_1} - \frac{1-2\nu_2}{G_2} \right) \int p_z \frac{\partial}{\partial y} \ln r \, dS \ ,$$

$$4\pi w = \left(\frac{1-2\nu_1}{G_1} - \frac{1-2\nu_2}{G_2} \right) \left(\int \sigma_{zx} \frac{\partial}{\partial x} \ln r \, dS + \int \sigma_{zy} \frac{\partial}{\partial y} \ln r \, dS \right) + \frac{2-2\nu}{G} \int \frac{p_z}{r} dS \ .$$

$$r = \sqrt{(x-x')^2 + (y-y')^2} \ , \quad dS = dx' dy', \tag{4.8}$$

Evaluation of the derivatives in (4.8) yields :

$$\frac{\partial r}{\partial x} = \frac{-x'+x}{r} \ , \quad \frac{\partial^2 r}{\partial x^2} = -\frac{(x'-x)^2}{r^3} + \frac{1}{r} \ , \quad \frac{\partial}{\partial x} \ln r = \frac{-x'+x}{r^2} \ ,$$

$$\frac{\partial^2 r}{\partial x \partial y} = \frac{-1}{r^3} (x'-x)(y'-y) \ . \tag{4.9}$$

We calculate the integrals in equations (4.8) by dividing the contact area into a uniform mesh of rectangles with a constant pressure distribution inside of each rectangle. We direct the rows of this mesh parallel to the x-axis and the columns parallel to the y-axis. The centers of these rectangles have the coordinates x_n and y_m, with:

$$0 \leq n \leq \text{cols} - 1, \quad 0 \leq m \leq \text{rows} - 1, \tag{4.10}$$

where cols denotes the total number of columns and rows the total number of rows. The pressure distribution σ_{zx} can be held in a two-dimensional array of variables:

$$\sigma_{zx}(y_m, x_n) = \sigma_{zx}[m,n] \tag{4.11}$$

To simplify notation, we replace the displacements u,v,w and the surface pressure $\sigma_{zx}, \sigma_{zy}, p_z$ by two arrays U and σ :

$$U[1,j,k] = u(y_j, x_k), \quad U[2,j,k] = v(y_j, x_k), \quad U[3,j,k] = w(y_j, x_k),$$

$$\sigma[1,m,n] = \sigma_{zx}(y_m, x_n), \quad \sigma[2,m,n] = \sigma_{zy}(y_m, x_n), \quad \sigma[3,m,n] = p_z(y_m, x_n) \ . \tag{4.12}$$

The load-displacement equations (4.8) thus may be denoted:

$$U[i,j,k] = \sum_{l=1}^{3} \sum_{m=0}^{rows-1} \sum_{n=0}^{cols-1} A[i,j,k;l,m,n] \ \sigma[l,m,n] \ ,$$

$$i, l = 1,2,3; \quad 0 \leq j, m \leq rows-1, \quad 0 \leq k, n \leq cols-1 \ . \tag{4.13}$$

Figure 4.1 shows a contact area for 4 rows and 9 columns. The length of one element is $2\Delta x$ in x-direction and $2\Delta y$ in y-direction.
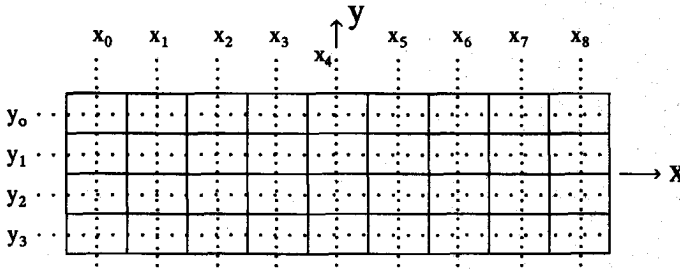

Fig. 4.1: contact area.

We calculate the elements $A[i,j,k;l,m,n]$ by integration of equ. (4.8) over one rectangle with the center y_m, x_n and obtain:

$$A[1,j,k;1,m,n] = \frac{1}{2\pi} \left(\frac{1}{G_1} + \frac{1}{G_2} \right) \int \frac{dS}{r} - \frac{1}{2\pi} \left(\frac{\nu_1}{G_1} + \frac{\nu_2}{G_2} \right) \int \frac{\partial^2 r}{\partial x_k^2} \, dS \,,$$

$$A[1,j,k;2,m,n] = -\frac{1}{2\pi} \left(\frac{\nu_1}{G_1} + \frac{\nu_2}{G_2} \right) \int \frac{\partial^2 r}{\partial x_k \partial y_j} \, dS \,,$$

$$A[1,j,k;3,m,n] = -\frac{1}{4\pi} \left(\frac{1-2\nu_1}{G_1} - \frac{1-2\nu_2}{G_2} \right) \int \frac{\partial}{\partial x_k} \ln r \, dS \,,$$

$$A[2,j,k;1,m,n] = A[1,j,k;2,m,n] \,,$$

$$A[2,j,k;2,m,n] = \frac{1}{2\pi} \left(\frac{1}{G_1} + \frac{1}{G_2} \right) \int \frac{dS}{r} - \frac{1}{2\pi} \left(\frac{\nu_1}{G_1} + \frac{\nu_2}{G_2} \right) \int \frac{\partial^2 r}{\partial y_j^2} \, dS \,, \qquad (4.14)$$

$$A[2,j,k;3,m,n] = -\frac{1}{4\pi} \left(\frac{1-2\nu_1}{G_1} - \frac{1-2\nu_2}{G_2} \right) \int \frac{\partial}{\partial y_j} \ln r \, dS \,,$$

$$A[3,j,k;1,m,n] = -A[1,j,k;3,m,n],$$

$$A[3,j,k;2,m,n] = -A[2,j,k;3,m,n],$$

$$A[3,j,k;3,m,n] = \frac{1}{2\pi} \left(\frac{1-\nu_1}{G_1} + \frac{1-\nu_2}{G_2} \right) \int \frac{dS}{r} \,,$$

where we used the abbreviations:

$$r = \sqrt{(x'-x_k)^2 + (y'-y_k)^2} \,, \quad dS = dx'dy' \,. \qquad (4.15)$$

The integrals in equations (4.14) extend over one rectangle with the center y_m, x_n :

$$A[i,j,k;l,m,n] = \int f(y_j,x_k,y',x') \, dS = \int_{x_n-\Delta x}^{x_n+\Delta x} \int_{y_m-\Delta y}^{y_m+\Delta y} f(y'-y_j, x'-x_k) \, dy' \, dx' \,, \quad (4.16)$$

Substitution of :

$$\theta - y_0 = y' - y_j \,, \quad \phi - x_0 = x' - x_k \,, \qquad (4.17)$$

in equations (4.16) yields:

$$A[i,j,k;l,m,n] = \int_{x_n-x_k+x_0-\Delta x}^{x_n-x_k+x_0+\Delta x} \int_{y_m-y_j+y_0-\Delta y}^{y_m-y_j+y_0+\Delta y} f(\theta-y_0, \phi-x_0) \, d\theta \, d\phi \,. \qquad (4.18)$$

The value of $A[i,j,k;l,m,n]$ in (4.16) represents the displacements $u[i,j,k]$ at the point

x_k, y_j due to a constant pressure distribution $\sigma[l,m,n]$ over the rectagle with the center in x_n, y_m. The comparison between (4.16) and (4.18) shows that the integral in (4.18) represents the displacement at the point x_0, y_0 due to a constant pressure distribution over a new rectangle with its center in x_{n^*}, y_{m^*} :

$$x_{n^*} = x_n - x_k + x_0 , \quad y_{m^*} = y_m - y_j + y_0 \tag{4.19}$$

Fig. 4.1 shows the definition of our coordinates:

$$x_{n^*} = x_0 + 2 \Delta x\, n^*, \quad y_{m^*} = y_0 - 2 \Delta y\, m^*, \quad 2\Delta x = x_2 - x_1 , \quad 2\Delta y = y_2 - y_1 , \tag{4.20}$$

Comparison of equations (4.19) and (4.20) yields:

$$x_{n^*} = x_{n-k} , \quad y_{m^*} = y_{m-j} , \quad \text{for } n-k > 0 \quad \text{and} \quad m-j > 0 . \tag{4.21}$$

Since the displacements $U[i,j,k]$ in (4.13) are defined for $j \geq 0$ and $k \geq 0$, (4.21) holds for $m-j \geq 0$, $n-k \geq 0$ only. Inserting (4.20) and (4.21) in (4.18) and comparison with (4.16) yields:

$$A[i,j,k;l,m,n] = A[i,0,0;l,m-j,n-k], \text{ for } m > j \text{ and } n > k . \tag{4.22}$$

The definition of $A[i,j,k;l,m,n]$ in (4.14) shows, that the integrals for $i=l$ do not depend on the sign of $x'-x_k$ and $y'-y_j$ and we can take the absolute values of $m-j$ and $n-k$ in this case. For the other integrals we have to consider the change of sign for negative $x'-x_k$ or $y'-y_k$, with the result:

$$A[1,j,k;1,m,n] = A[1,0,0;1,|m-j|,|n-k|] ,$$

$$A[1,j,k;2,m,n] = \text{sign}(m-j)\, \text{sign}(n-k)\, A[1,0,0;2,|m-j|,|n-k|] ,$$

$$A[1,j,k;3,m,n] = \text{sign}(n-k)\, A[1,0,0;3,|m-j|,|n-k|] ,$$

$$A[2,j,k;1,m,n] = A[1,j,k;2,m,n] ,$$

$$A[2,j,k;2,m,n] = A[2,0,0;2,|m-j|,|n-k|] , \tag{4.23}$$

$$A[2,j,k;3,m,n] = \text{sign}(m-j)\, A[2,0,0;3,|m-j|,|n-k|] ,$$

$$A[3,j,k;1,m,n] = -A[1,j,k;3,m,n] ,$$

$$A[3,j,k;2,m,n] = -A[2,j,k;3,m,n] ,$$

$$A[3,j,k;3,m,n] = A[3,0,0;3,|m-j|,|n-k|] ,$$

The value of $\text{sign}(0)$ for $m=j$ or $n=k$ is arbitrary, because all expressions in (4.23)

containing the factor sign(0) vanish beforehand. J.J. Kalker implemented the relation $|A(i,x,j,y)| = |A(i,0,j,y-x)|$ in his program CONTACT (1990), where x, y are the vectors to the rectangles where the stress and displacements are determined. Furthermore he pointed out to me, that the symmetry relation $A[i,j,k;l,m,n] = A[l,m,n;i,j,k]$, which we will use later, follows from equs. (4.23).

Equation (4.23) shows that we have to save the values of $A[i,j,k;l,m,n]$ for $j=k=0$ only. A contact area with 20 rows and 20 columns requires $3 \cdot 20 \cdot 3 \cdot 20 \cdot 8 = 28$ kilobytes, while the whole set of elements occupies 400 times more space, which is 11.5 megabytes.

The integrals in (4.14) can be evaluated over a right angle triangle, and two such triangles can be composed to a rectangle. We outline the procedure for $A[1,j,k;3,m,n]$ in (4.14):

$$\int \frac{\partial}{\partial y_j} \ln r \, dS = \int_{x_n - \Delta x}^{x_n + \Delta x} \int_{y_m - \Delta y}^{y_m + \Delta y} \frac{(-x' + x_k)}{(x' - x_k)^2 + (y' - y_j)^2} \, dy' \, dx'. \tag{4.24}$$

We substitute:

$$x = x' - x_k, \quad y = y' - y_j , \tag{4.25}$$

and obtain for the integral (4.24) :

$$\int \frac{\partial}{\partial y_j} \ln r \, dS = \int_{x_n - x_k - \Delta x}^{x_n - x_k + \Delta x} \int_{y_m - y_j - \Delta y}^{y_m - y_j + \Delta y} \frac{-x}{x^2 + y^2} \, dx \, dy, \tag{4.26}$$
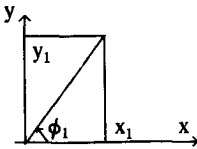
Fig. 4.2: Rectangle

First we evaluate (4.26) over one rectangle with one corner in the origin, by dividing it into two triangles. We use the cylindrical coordinates:

$$x = s \cdot \cos\phi, \quad y = s \cdot \sin\phi, \quad \phi_1 = \tan^{-1}(y_1/x_1), \tag{4.27}$$

and obtain for the integral (4.26) :

$$\int_{x=0}^{x_1} \int_{y=0}^{y_1} \frac{-x}{x^2+y^2} \, dx \, dy = \int_{\phi=0}^{\phi_1} \int_{s=0}^{x_1/\cos\phi} \frac{-s\cos\phi}{s^2} s \, ds \, d\phi + \int_{\phi_1}^{\pi/2} \int_{s=0}^{y_1/\sin\phi} \frac{-s\cos\phi}{s^2} s \, ds \, d\phi$$

$$= \int_0^{\phi_1} -x_1 \, d\phi + \int_{\phi_1}^{\pi/2} -y_1 \frac{\cos\phi}{\sin\phi} \, d\phi = -x_1 \tan^{-1}\frac{y_1}{x_1} + y_1 \ln \frac{y_1}{\sqrt{x_1^2 + y_1^2}} \tag{4.28}$$

Every rectangle in our mesh can be composed of four rectangles with one corner in the origin. The calculation of the other integrals in (4.14) is straightforward, with the result:

$$\int \frac{\partial^2 r}{\partial x\, \partial y}\, dS = \sqrt{a_1^2+b_1^2} - \sqrt{a_2^2+b_1^2} - \sqrt{a_1^2+b_2^2} + \sqrt{a_2^2+b_2^2} \ ,$$

$$\int \frac{\partial^2 r}{\partial x^2}\, dS = a_1 \ln \frac{b_1+\sqrt{a_1^2+b_1^2}}{b_2+\sqrt{a_1^2+b_2^2}} - a_2 \ln \frac{b_1+\sqrt{a_2^2+b_1^2}}{b_2+\sqrt{a_2^2+b_2^2}} \ ,$$

$$\int \frac{\partial^2 r}{\partial y^2}\, dS = b_1 \ln \frac{a_1+\sqrt{a_1^2+b_1^2}}{a_2+\sqrt{a_2^2+b_1^2}} - b_2 \ln \frac{a_1+\sqrt{a_1^2+b_2^2}}{a_2+\sqrt{a_2^2+b_2^2}} \ ,$$

$$\int \frac{dS}{r} = \int \frac{\partial^2 r}{\partial x^2}\, dS + \int \frac{\partial^2 r}{\partial y^2}\, dS \ , \tag{4.29}$$

$$-\int \frac{\partial}{\partial x} \ln r\, dS = \frac{b_1}{2} \ln \frac{a_1^2+b_1^2}{a_2^2+b_1^2} + \frac{b_2}{2} \ln \frac{a_2^2+b_2^2}{a_1^2+b_2^2}$$
$$+ a_1 \left(\tan^{-1} \frac{b_1}{a_1} - \tan^{-1} \frac{b_2}{a_1} \right) + a_2 \left(\tan^{-1} \frac{b_2}{a_2} - \tan^{-1} \frac{b_1}{a_2} \right) ,$$

$$-\int \frac{\partial}{\partial y} \ln r\, dS = \frac{a_1}{2} \ln \frac{a_1^2+b_1^2}{a_1^2+b_2^2} + \frac{a_2}{2} \ln \frac{a_2^2+b_2^2}{a_2^2+b_1^2}$$
$$+ b_1 \left(\tan^{-1} \frac{a_1}{b_1} - \tan^{-1} \frac{a_2}{b_1} \right) + b_2 \left(\tan^{-1} \frac{a_2}{b_2} - \tan^{-1} \frac{a_1}{b_2} \right) ,$$

$$a_1 = x_n - x_k + \Delta x, \quad a_2 = a_1 - 2\Delta x, \quad b_1 = y_m - y_j + \Delta y, \quad b_2 = b_1 - 2\Delta y \ .$$

Replacing the terms a_1, a_2 with b_1, b_2 and vice versa in the derivations of x, y yields the corresponding derivations of y. The area of integration is defined by (4.16) and r by (4.15).

5 Some basic load-histories for bodies of similar material

5.1 Hertz's theory of contact

The Hertz theory of contact was already mentioned in section 3.2. In this chapter we will introduce some more details. We suppose that, in the unstressed state, the surfaces of the two bodies near the contact point O (Fig. 3.1) can be approximated by two paraboloids :

Fig. 5.1: The local coordinate systems.

$$z_1 = \frac{x_A^2}{2R_1} + \frac{y_A^2}{2R_1'} \ ,$$

$$z_2 = \frac{x_B^2}{2R_2} + \frac{y_B^2}{2R_2'} \ ,$$

$$(5.1)$$
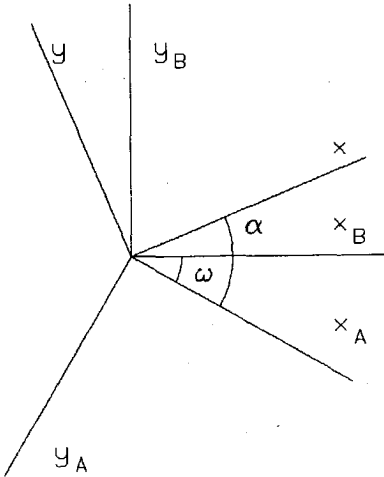
The indices 1 resp. 2 denote body 1 resp. 2 with the radii of the principal curvatures R_1, R_1' resp. R_2, R_2'. The axis z_1, z_2 are directed into the bodies and the axis x_A, x_B form the angle ω. We choose a common coordinate system x, y, z so, that the mixed terms in x and y vanish :

$$z = z_1 + z_2 = Ax^2 + By^2. \quad (5.2)$$

The variables A, B and the angle α between the x_A- and the x-axis are defined as follows (fig. 5.1):

$$2(A+B) = \frac{1}{R_1} + \frac{1}{R_1'} + \frac{1}{R_2} + \frac{1}{R_2'} \ , \quad (5.3a)$$

$$4(A-B)^2 = \left(\frac{1}{R_1} - \frac{1}{R_1'} \right)^2 + \left(\frac{1}{R_2} - \frac{1}{R_2'} \right)^2 + 2\left(\frac{1}{R_1} - \frac{1}{R_1'} \right) \left(\frac{1}{R_2} - \frac{1}{R_2'} \right) \cos 2\omega \ ,$$

$$\left(\cos 2\omega - \frac{1/R_1 - 1/R_1'}{1/R_2 - 1/R_2'}\right) \tan 2\alpha = -\sin 2\omega , \tag{5.3b}$$

When the bodies are pressed together they approach each other by the value ζ, and the point x_1, y_1 of the surface of body 1 and x_2, y_2 of surface 2 will come into contact. The deformations must satisfy the following equations :

$$x_1 + u_1 = x_2 + u_2 , \quad y_1 + v_1 = y_2 + v_2 , \quad z_1 + w_1 = -(z_2 + w_2) + \zeta . \tag{5.4}$$

The equations (5.1) can be formulated in the common coordinate system (5.2) with the result :

$$z_1 = A_1 x_1{}^2 + B_1 y_1{}^2 + 2H_1 x_1 y_1 , \quad z_2 = A_2 x_2{}^2 + B_2 y_2{}^2 + 2H_2 x_2 y_2 , \quad H_1 = -H_2 , \tag{5.5}$$

where the constants A_i, B_i, H_i are easily evaluated. Equation (5.5) inserted in (5.4) yields :

$$\begin{aligned} w_1 + w_2 = {}&\zeta - A x_1{}^2 - B y_1{}^2 - A_2(x_1 + x_2)(u_1 - u_2) - B_2(y_1 + y_2)(v_1 - v_2) \\ &- 2H_2\{x_1(v_1 - v_2) + y_1(u_1 - u_2)\} , \end{aligned} \tag{5.6}$$

with $A = A_1 + A_2$, $B = B_1 + B_2$. Equation (5.6) is due to Love (1927). In the case of incremental load histories this formula must be replaced by an incremental formulation. When the bodies consist of similar material, corresponding points come into contact, and we have: $u_1 = u_2$, $v_1 = v_2$, $x_1 = x_2$, $y_1 = y_2$. Otherwise, the last three terms in equation (5.6) are high order terms, which can be neglected, with the result :

$$\zeta = z_1 + w_1 + w_2 + z_2 , \text{ in } C . \tag{5.7}$$

In the case of similar materials equation (4.8) and (5.2), (5.7) define the basic integral equation:

$$w_1 + w_2 = \frac{1-\nu}{2\pi G} \int \frac{p_z}{r} \, dS = \zeta - A x^2 - B y^2, \tag{5.8}$$

with the combined material parameters $1/G$ and ν/G, defined by (4.7). The solution of this equation is known from potential theory. The contact area C is an ellipse with the semiaxis a and b :

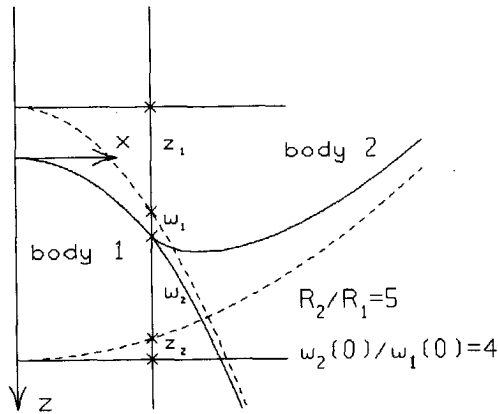$$C = \{ (x,y) \mid (x/a)^2 + (y/b)^2 \le 1 \} . \tag{5.9}$$

Fig. 5.2: The deformed state of the bodies.

The normal pressure p_z is a semi-ellipsoid:

$$p_z(x,y) = \sigma_H(a) = \begin{cases} \sigma_{z0}\sqrt{1-(x/a)^2-(y/b)^2}, & \text{if } (x,y) \in C, \\ 0, & \text{if } (x,y) \notin C. \end{cases} \tag{5.10}$$

The function $\sigma_H(a)$ in (5.10) denotes the Hertzian pressure distribution, which we will use in the next chapter. The semiaxes a, b in (5.10) are defined by the geometry of the bodies. The coefficient σ_{z0} is determined by the total normal force F_z:

$$\sigma_{z0} = \frac{3F_z}{2\pi ab}. \tag{5.11}$$

The problem is determined by three dimensionless constants α, β, γ (Kalker, 1990) :

$$\alpha = \frac{3}{2\pi}\sqrt{1-k^2}\,E(k)\,,\ \beta = \frac{E(k)}{K(k)}\,,\ \gamma = \frac{K(k)-D(k)}{E(k)}\,,\ k = \sqrt{1-a^2/b^2}\,,\ \text{for } a<b, \tag{5.12}$$

where the expression E(k), K(k) and D(k) denote the complete elliptical integrals of first and second kind (Abramowitz & Stegun, 1964):

$$E(k) = \int_0^{\pi/2}\sqrt{1-k^2\sin^2\phi}\,d\phi\,,\ \ K(k) = \int_0^{\pi/2}\frac{d\phi}{\sqrt{1-k^2\sin^2\phi}}\,d\phi\,,\ \ D(k) = \frac{K(k)-E(k)}{k^2}\,. \tag{5.13}$$

If either the surface geometry or the contact semiaxis and the Force F_z or the approach ζ are given, the unknown expressions may be determined by :

$$\alpha = \frac{a^3(A+B)}{F_z(\vartheta_1+\vartheta_2)} \ , \ \vartheta_i = \frac{(1-\nu_i^2)}{E_i} \ ,$$

$$\beta = \frac{a^2(A+B)}{\zeta} \ , \tag{5.14}$$

$$\gamma = \frac{A}{A+B} \ .$$

The equation for z of the contact area can be read from Fig. 5.2, with the result:

$$z = z_1 + w_1 = \zeta - z_2 - w_2 \ , \tag{5.15}$$

Equation (5.8) yields :

$$w_1 = \frac{1}{\pi} \vartheta_1 F(x,y), \quad w_2 = \frac{1}{\pi} \vartheta_2 F(x,y), \tag{5.16}$$

with ϑ_i defined by (5.14). The deformation w_1, w_2 can be eliminated from (5.15), (5.16) :

$$(\vartheta_1+\vartheta_2) z = \vartheta_2 z_1 - \vartheta_1 z_2 + \vartheta_2 \zeta \ . \tag{5.17}$$

The functions z_1 and z_2 defined by (5.1) are quadratic functions. The bigger the constant ϑ_1, i.e. the softer body 1, the more the contact area adapts to the surface of body 2. The contact area approaches to the contour of the harder body and becomes a plane for similar bodies.
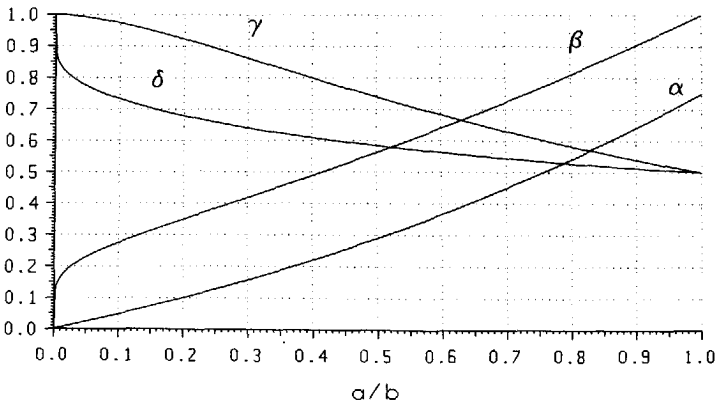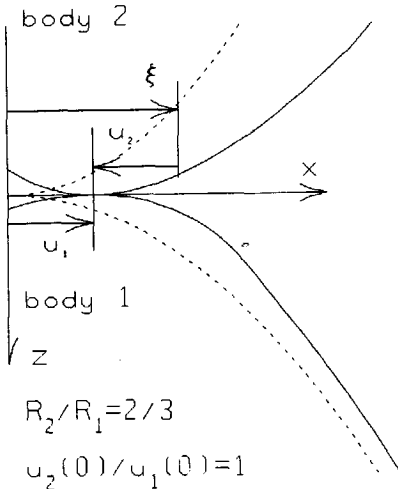

Fig. 5.3: The dimensionless parameters α, β, γ, δ.

5.2 The solutions of Cattaneo and Mindlin for tangential shift

This theory is confined to bodies of similar materials with elliptical contact areas. They are pressed together and shifted in tangential direction. The tangential shift may have the components ξ, η in x- and y-direction. We suppose that the point x_1, y_1 will be displaced by the values u_1, v_1 in x- and y-directions, before it comes into contact with the point x_2, y_2. We use the two coordinate systems x,y,z_1 and x,y,z_2, where the z-coordinates point inside of the corresponding body. The kinematic relations are:

$$\left. \begin{array}{l} x_1 + u_1(x_1,y_1) = x_2 + u_2(x_2,y_2) + \xi \ , \\ y_1 + v_1(x_1,y_1) = y_2 + v_2(x_2,y_2) + \eta \ , \end{array} \right\} \text{ in H,} \qquad (5.18)$$

$$z_1 + w_1(x_1,y_1) = -z_2 - w_2(x_2,y_2) + \zeta \ , \ \text{ in C,}$$

body 2

ξ

u_2

$\times$

u_1

body 1

z

$R_2/R_1 = 2/3$

$u_2(0)/u_1(0) = 1$

Fig. 5.4: A sectional view for $y=0$ of the deformed bodies; $\xi_1 = 0$.

with the contact area C and the area of adhesion H. We assume, that corresponding points will come into contact and obtain from (5.18):

$$x_1 = x_2 \ , \ \ y_1 = y_2 \ ,$$
$$u_1 = u_2 + \xi, \ \ v_1 = v_2 + \eta, \ \text{ in H,}$$
$$w_1 = -w_2 + \zeta - Ax^2 - By^2, \text{ in C ,} \qquad (5.19)$$
$$\xi = \xi_2 - \xi_1 \ , \ \ \eta = \eta_2 - \eta_1 \ .$$

The deformed bodies are plotted in fig. 5.4. Equation (4.8) shows, that the normal and tangential displacements are independent, when the difference parameter ε becomes zero:

$$\varepsilon = \left(\frac{1-2\nu_1}{2G_1} - \frac{1-2\nu_2}{2G_2} \right) . \qquad (5.20)$$

Substitution of (5.20) in (4.8) yields:

$$2\pi u = \frac{1}{G} \int \frac{\sigma_{zx}}{r} dS - \frac{\nu}{G} \int \sigma_{zx} \frac{\partial^2 r}{\partial x^2} dS - \frac{\nu}{G} \int \sigma_{zy} \frac{\partial^2 r}{\partial x \partial y} dS - \varepsilon \int p_z \frac{\partial}{\partial x} \ln r \, dS \, ,$$

$$2\pi v = \frac{1}{G} \int \frac{\sigma_{zy}}{r} dS - \frac{\nu}{G} \int \sigma_{zy} \frac{\partial^2 r}{\partial y^2} dS - \frac{\nu}{G} \int \sigma_{zx} \frac{\partial^2 r}{\partial x \partial y} dS - \varepsilon \int p_z \frac{\partial}{\partial y} \ln r \, dS \, ,$$

$$2\pi w = \varepsilon \int \sigma_{zx} \frac{\partial}{\partial x} \ln r \, dS + \varepsilon \int \sigma_{zy} \frac{\partial}{\partial y} \ln r \, dS + \frac{1-\nu}{G} \int \frac{p_z}{r} dS \, . \qquad (5.21)$$

$$r = \sqrt{(x-x')^2 + (y-y')^2} \, , \quad dS = dx'dy',$$

$$u = u_1 - u_2 \, , \quad v = v_1 - v_2 \, , \quad w = w_1 + w_2 \, .$$

The parameter ε from (5.20) becomes zero for similar or for incompressible materials. In this case the Hertz solution can be used for the normal pressure and the tangential problem can be solved independently. Cattaneo (1938) found, that the stick area H is also an ellipse, homothetic to the contact area with the semi-axes a^*, b^*:

$$H = \{ \, (x,y) \mid (x/a^*)^2 + (y/b^*)^2 \le 1 \, \}, \quad a^*/a = b^*/b \le 1. \qquad (5.22)$$

The stress distribution consists of two concentric ellipsoids σ_1 and σ_2, similar to the Hertzian distribution σ_H. σ_1 extends over the complete contact area C and σ_2 over the stick area H, pointing in opposite direction:

$$\sigma_1 = f\sigma_{z0}\sqrt{1-(x/a)^2-(y/b)^2} \, , \quad \text{in C,}$$
$$\sigma_2 = f\sigma_{z0}(a^*/a)\sqrt{1-(x/a^*)^2-(y/b^*)^2} \, , \quad \text{in H,} \qquad (5.23)$$

with σ_{z0} from eq. (5.11) and the frictional coefficient f. The pressure distribution has now the form:

$$\sigma_{zx} = p \, (\, \sigma_1 - \sigma_2 \,), \quad \sigma_{zy} = q \, (\, \sigma_1 - \sigma_2 \,), \quad \text{in H,}$$
$$\sigma_{zx} = p \, \sigma_1, \quad \sigma_{zy} = q \, \sigma_1, \quad \text{in the slip area S,} \qquad (5.24)$$
$$S = \{ \, x,y \in C \setminus H \, \}.$$

The slip area S has the form of an elliptical ring and contains all points of the contact area which are outside of the stick area. The displacements ξ, η can be calculated by insertion of (5.24) in (5.21). To simplify matters we introduce the stiffness coefficients c_x, c_y, c_z in x-, y- and z-direction:

$$\frac{c_x}{c_z} = \frac{(1-\nu)/G}{1/G - \delta \cdot \nu/G} \, , \quad \frac{c_y}{c_z} = \frac{(1-\nu)/G}{(1-\nu)/G + \delta \cdot \nu/G}, \quad \delta = \frac{D(k)}{K(k)}, \qquad (5.25a)$$

$$c_z = \frac{2\pi\sqrt{D(k)}}{\sqrt{B}\,K^{3/2}(k)\,(1-\nu)/G} = \frac{3\beta^{3/2}}{2(\vartheta_1+\vartheta_2)\alpha\sqrt{A+B}} \quad , \quad k = \sqrt{1-a^2/b^2}\ . \qquad (5.25b)$$

Equations (5.25) hold for $a<b$. The constants c_x, c_y, c_z are the stiffness coefficients of the force-displacement relation. c_x and c_y are equal for $\nu=0$, for circular contact areas with $a/b=1$ and for similar materials. $K(k)$ and $E(k)$ are the complete elliptic integrals of the first and second kind defined by (5.13). The material properties G and ν are combined values (4.7). The parameter δ is plotted in fig. 5.3. The parameters p and q and the semiaxis of the stickarea a^*, b^* are defined as follows:

$$p = c_x\xi/\sqrt{(c_x\xi)^2+(c_y\eta)^2}\,, \quad q = c_y\eta/\sqrt{(c_x\xi)^2+(c_y\eta)^2}\,, \quad p^2+q^2 = 1,$$
$$\zeta^*/\zeta = (a^*/a)^2 = (b^*/b)^2 = 1 - \sqrt{(c_x\xi)^2+(c_y\eta)^2}/(fc_z\zeta). \qquad (5.26)$$

ζ^* is the normal penetration which produces a contact area with the semiaxis a^*. The formulas for the forces F_x, F_y, F_z are:

$$F_x = p\,f\,F_z\,(1-a^{*3}/a^3), \quad F_y = q\,f\,F_z\,(1-a^{*3}/a^3), \quad F_z = 2c_z\sqrt{\zeta^3}/3\ . \qquad (5.27)$$

Figure 3.3 of chapter 3 shows the stress distribution σ_x at $y=0$ for different values of the tangential displacement ξ. Equations (5.26), (5.27) describe the forces as a function of the displacement. The equations for the displacement as a function of the forces are:

$$\xi = F_x\,\frac{1}{c_x}\,\frac{3fF_z}{2T\sqrt{\zeta}}\left[\,1 - (1-\frac{T}{fF_z})^{2/3}\,\right] = p\,\frac{f\,c_z}{c_x}\,(\zeta-\zeta^*),$$

$$\eta = F_y\,\frac{1}{c_y}\,\frac{3fF_z}{2T\sqrt{\zeta}}\left[\,1 - (1-\frac{T}{fF_z})^{2/3}\,\right] = q\,\frac{f\,c_z}{c_y}\,(\zeta-\zeta^*), \qquad (5.28)$$

$$T = \sqrt{F_x^2+F_y^2}\ ,$$

The force displacement relation (5.28) is nonlinear and a rotation of the coordinate system follows the transformation laws of second order tensors (see also Raoof & Hobbs 1989). Substitution of c_x, c_y, c_z with (5.25) and insertion of (5.14), (5.26) yields:

$$\xi = p\,\frac{3fF_z}{4\pi b}\left[\,\frac{1}{G}\,K(k) - \frac{\nu}{G}\,D(k)\,\right]\left[1-\left(1-\frac{T}{fF_z}\right)^{2/3}\right]\,, \quad \left.\begin{array}{l} \text{for } a\leq b \\[2ex] \text{and } T\leq f\,F_z \end{array}\right\} \qquad (5.29)$$

$$\eta = q\,\frac{3fF_z}{4\pi b}\left[\,\frac{1-\nu}{G}\,K(k) + \frac{\nu}{G}\,D(k)\,\right]\left[1-\left(1-\frac{T}{fF_z}\right)^{2/3}\right]\,.$$

When the tangential force acts parallel to one of the semiaxis, we have $p=1$ resp. $q=1$

and formula (5.29) is identical to the result obtained by Deresiewicz (1957). We obtain the displacement of body i by replacing $1/G$ and ν/G with $1/G_i$ and ν_i/G_i. The limit $T\rightarrow 0$ for small forces in (5.29) yields:

$$\lim_{T\rightarrow 0} \frac{\xi}{F_x} = \frac{d\xi}{dF_x} = \frac{1}{c_x\sqrt{\zeta}}$$

$$\lim_{T\rightarrow 0} \frac{\eta}{F_y} = \frac{d\eta}{dF_y} = \frac{1}{c_y\sqrt{\zeta}} \ . \tag{5.30}$$

Cattaneo presupposes that the stress-directions are constant in the whole contact area, which is correct for similar materials with a Poisson number of zero. In chapter 14 we present some numerical solutions for the tangential deformation of materials with different Poisson numbers. It follows that Cattaneo's theory is correct for similar materials.

5.3 Torsion under complete adhesion

After a normal compression both bodies will be twisted by the angle β around the common normal of the tangential plane. Similar to the chapter before, the materials are equal. We calculate only the additional stresses and displacements which must be added to the results of the normal problem. Adhesion in the contact area signifies, that the displacements of both bodies are equal except from a constant rotation, similar to equation (5.19).

$$u_1-u_2 = \beta y \ , \quad v_1-v_2 = -\beta x \ , \quad \text{in the stick are H} \ ,$$

$$w_1 + w_2 = 0, \ \sigma_{zz} = 0 \ , \quad \text{in the contact area C} \ ,$$

$$\sigma_{zx} = \sigma_{zy} = \sigma_{zz} = 0 \ , \quad \text{outside the contact area C} \ , \tag{5.31}$$

$$\lim_{x,y,z\rightarrow\infty}(u,v,w) \ = \ 0 \ .$$

Mindlin satisfies these boundary conditions using a solution of Neuber (1937) for the stress concentration in a hyperbolic notch, with the result :

$$\sigma_{zx} = T'y/\sqrt{1-x^2/a^2-y^2/b^2}, \ \ \sigma_{zy} = T''x/\sqrt{1-x^2/a^2-y^2/b^2}, \ \ \sigma_{zz} = 0, \text{ in H,}$$

$$\sigma_{zx} = \sigma_{zy} = \sigma_{zz} = 0 \ , \quad \text{outside H} \ . \tag{5.32}$$

Equation (5.32) satifies all boundary conditions. The value of T', T" can be calculated by insertion of (5.32) in (4.8), (5.31). We introduce the abbreviations :

$$B(k) = K(k) - D(k) , \quad C(k) = (2D(k) - K(k)) / k^2 ,$$

$$B(0) = \pi/4, \; C(0) = \pi/16, \; D(0) = \pi/4, \; E(0) = K(0) = \pi/2, \qquad (5.33)$$

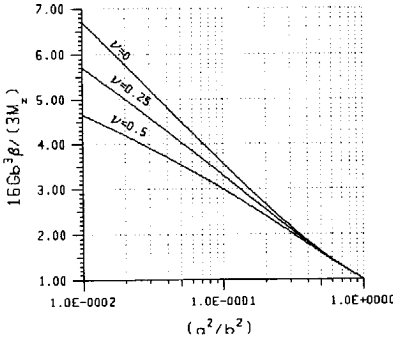$$B(1) = 1, \; C(1) = \infty, \; D(1) = \infty, \; E(1) = 1, \; K(1) = \infty ,$$

Fig. 5.5: The torsional compliance for complete adhesion.

where the elliptical integrals K(k) and D(k) are defined by (5.13), and get the result :

$$T' = \frac{G\beta}{a} \; \frac{B(k)/G - 2(1-k^2)C(k)\nu/G}{B(k)D(k)/G - C(k)E(k)\nu/G} \; ,$$
$$(5.34)$$
$$T'' = \frac{G\beta}{a} \; \frac{D(k)/G - 2C(k)\nu/G}{B(k)D(k)/G - C(k)E(k)\nu/G} \; ,$$

Integration of the stresses yields the torque M_z :

$$\frac{\beta}{M_z} = \frac{3 \cdot 8 \, [\, B(k)D(k)/G - C(k)E(k)\nu/G \,]}{16Gb^3\pi \, [\, E(k)/G - 4C(k)(1-k^2)\nu/G \,]} \, ,$$
$$(5.35)$$

5.4 Lubkin's solution for the torsion of elastic spheres in contact.

Equations (5.32) show, that the stresses become infinite at the border of the stick area. Thus slip must be expected, starting at the boundary and progressing inward of the stick area. In the case of spheres the problem is axially symmetric and the boundary conditions become :

$$u_\theta = -\beta\rho \, , \; u_\rho = \sigma_{zz} = 0 \, , \text{ for } \; \rho \leq a^* \text{ in H,}$$

$$\left. \begin{array}{l} \sigma_{z\theta} = 3fF_z\sqrt{a^2-\rho^2} / (2\pi a^3) \, , \\[4pt] \sigma_{z\rho} = \sigma_{zz} = 0 \, , \text{ for } \; a^* \leq \rho \leq a, \end{array} \right\} \text{ in the slip area ,} \qquad (5.36)$$

$$\sigma_{z\rho} = \sigma_{z\theta} = \sigma_{zz} = 0 \, , \text{ for } \; \rho > a,$$

$$\lim (u_\rho, u_\theta, u_z) = 0 \, , \text{ for } \sqrt{\rho^2+z^2} \to \infty \, .$$

Lubkin (1951) found the following formula for the stress :

$$\sigma_{z\theta} = \frac{3fF_z}{\pi^2 a^2} \sqrt{1 - r^2/a^2} \left[\frac{\pi}{2} + k^2 D(k)F(k',\theta_1) - K(k)E(k',\theta_1) \right], \qquad (5.37)$$

with the inclomplete elliptic integrals $F(k,\phi)$, $E(k,\phi)$ and the modular angle θ_1 :

$$\sin \theta_1 = \frac{a}{a^*} \sqrt{\frac{a^{*2} - \rho^2}{a^2 - \rho^2}} \ , \quad k = \sqrt{1 - a^{*2}/a^2}, \quad k' = \sqrt{1 - k^2},$$

$$F(k,\phi) = \int_0^\phi \frac{d\phi}{\sqrt{1 - k^2\sin^2\phi}} \ , \quad E(k,\phi) = \int_0^\phi \sqrt{1 - k^2\sin^2\phi} \ d\phi \ . \qquad (5.38)$$

The relation between the angle of twist and the radius of the stick area a^* is :

$$\frac{Ga^2}{fF_z} \beta = \frac{3}{4\pi} \{ K(k) - E(k) \} ,$$

$$\lim_{k \to 0} (K(k) - E(k)) = \frac{\pi}{2} \left\{ \frac{1}{4} k^2 + \frac{1}{4} k^2 \ ..... \right\} = \frac{\pi}{4} (1 - \frac{a^{*2}}{a^2}), \qquad (5.39)$$

where $K(k)$ and $E(k)$ are defined by (5.13). Lubkin found the following result for the twisting moment M_z :

$$\frac{M_z}{fF_z a} = \frac{1}{4\pi} \left\{ \frac{3\pi^2}{4} + k'k^2 \left[6K(k) + (4k'^2 - 3)D(k) \right] - 3kK(k)\sin^{-1}k' \right.$$

$$\left. - 3k^2 \left[K(k) \int_0^{\pi/2} \frac{\sin^{-1}(k'\sin\alpha)}{(1 - k'^2\sin^2\alpha)^{3/2}} \ d\alpha - D(k) \int_0^{\pi/2} \frac{\sin^{-1}(k'\sin\alpha)}{\sqrt{1 - k'^2\sin^2\alpha}} \ d\alpha \right] \right\} . \qquad (5.40)$$

Formula (5.40) can be reduced, by direct integration of $\sigma_{z\theta}$ in form of the complete elliptic integral of the third kind in his work, with the result :

$$\frac{M_z}{fF_z a} = \frac{k'k^2}{4\pi} \left[D(k)(1 + 2k^2) + 6E(k) \right] + \frac{3}{4\pi} \int_0^{\cos^{-1}(k')} \cos^{-1}(k'/\cos\beta)d\beta . \qquad (5.41)$$

The values of (5.41) are plotted in fig. 5.6. They agree completely with Lubkin's results. Equation (5.41) can be approximated by the function :

$$\frac{M_z}{f\,F_z\,a} = \frac{3\pi}{16}\left[\,1 - \exp\left(\frac{-16^2}{3^2\pi}\,\frac{Ga^2\beta}{f\,F_z}\right)\,\right],\tag{5.42}$$

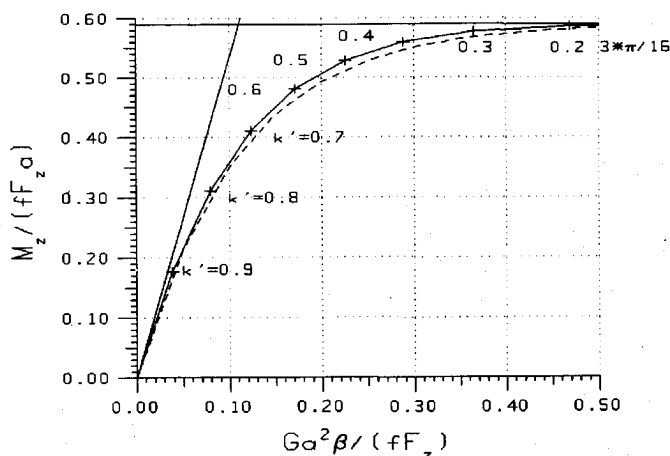with a maximal error of 3%. Formula (5.42) is plotted with a broken line in fig. (5.6).

Fig. 5.6 : The twisting moment (5.41) and (5.42).

6 Elastic contact of spheres under varying oblique

forces

Two elastic spheres of similar material and geometry are pressed together in normal direction and subjected to tangential forces. We consider load-histories, for oblique forces with varying normal component and varying, uni-directional, tangential component with changing sign. The load-history starts at the time t_0, when the undeformed surfaces of both bodies touch at one point, the contact point. Afterwards the centres of gravity of both bodies are shifted in normal and tangential direction. We distinguish between *periods of compression* and *periods of restitution,* in which the centres of gravity approach resp. separate from each other in normal direction. Another distinction is made regarding the slip direction in the slip area, which can be positive or negative in the work of Mindlin & Deresiewicz (1953). Their paper shows, that each reversion of the slip direction causes either a point of instantaneous adhesion P_N at the beginning, in which the entire contact area sticks, followed by a *period of decreasing stick area,* in which the size of the stick area shrinks monotonously, or a *period of complete adhesion* over a space of time. After the (N-1)-th point of instantaneous adhesion P_{N-1} follows the N-th period of decreasing stick area. This period continues, until either the slip direction reverses again and the N-th point of instantaneous adhesion P_N takes place, or the old stick area is overlaid by the new one. In the latter follows the period of (N-2)-th decrease of the stick area, because the additional stress distribution of the (N-1)-th decrease of the stick area is completely overlaid.

We will show, that the tangential stress distribution depends only on the points P_N and the current positions of the centres of gravity, while the solution of Mindlin & Deresiewicz depends on the entire previous load-history and the current variation of the normal and tangential forces. We will deduce a criterion to decide, whether a point of instantaneous adhesion or a period of decreasing stick area resp. a period of complete adhesion takes place.

The solution of the tangential boundary value problem is unique, if the load-history can be presented as a series of infinite, successive, incremental equilibrium

positions (Klarbring, 1990). In this case exists a unique solution for each increment and the incremental method of Mindlin & Deresiewicz seems appropriate. We will arrive at a non-incremental formula, however, because the slip direction of load-histories with uni-directional tangential component is constant between P_N and P_{N+1} and opposite to the slip direction between the two beforegoing points P_{N-1} and P_N. The two most important boundary conditions are: Coulomb's law for sliding friction must be satisfied in the slip area and the stick area must undergo a constant rigid body displacement in tangential direction. We will show, that the stress distribution between two points of instantaneous adhesion can always be presented as a Cattaneo-Mindlin function, such that the load-history consists of a sum of Cattaneo-Mindlin functions, as long as no period of complete adhesion takes place. In the case of a period of complete adhesion the tangential displacement $\xi(\zeta)$ must be known as function of the normal displacement ζ. A similar method was used by Barber (1979) for the tangential impact. The resulting, non-incremental formula for the force can be understood as a sequence of incremental equilibrium positions, after differentiation. The advantage of this method is, that a criterion for points of instantaneous adhesion can be deduced from the formula for the displacement.

For several load-histories, Mindlin & Deresiewicz calculated the compliance, which is the derivative of the displacement with respect to the force. We will calculate the force as a function of the displacement, because the force can directly be inserted in the equations of motion for two bodies, while the displacement appears in the acceleration term, and must be derived two times with respect to the time. Mindlin & Deresiewicz arrived at 7 basic load cases by differentiation between decreasing and increasing normal and tangential forces on the loading or unloading curve. They also found points of instantaneous adhesion and periods of decreasing stick area, but they did not use these characteristics for the arrangement of the load cases.

The so-called Cattaeno-Mindlin functions are introduced in section 6.1 and some basic mathematical relations are stated. Furthermore the boundary value problem of the Cattaneo-Mindlin theory is discussed. The load-histories of sections 6.2, 6.3, 6.4, correspond basically with the load-cases 4, 7, 8 of Mindlin-Deresiewicz (1953). In sections 6.2-6.4 the non-incremental formulae for the forces and displacements are deduced, using the law of superposition (6.9). Differentiation yields the tangential stiffness $dF_x/d\xi$, which is the reciprocal of Mindlin & Deresiewicz's compliance. In section 6.5 the first point of instantaneous adhesion P_1 is discussed, and it is shown that the load-cases for increasing and decreasing normal compression ζ_2 yield the same formulae for the force F_x and the displacement ξ. Section 6.5 corresponds with

Mindlin & Deresiewicz's load cases for increasing or decreasing N and decreasing T, at $T = T^*$, where T^* of Mindlin & Deresiewicz denotes the first point of instantaneous adhesion. In section 6.6 the period of the second decrease of the stick area is analysed and the conditions for periods of the 1-st decrease, the 2-nd decrease and complete adhesion are deduced. The result corresponds with Mindlin & Deresiewicz's sections 10 and 11. The first point of instantaneous adhesion P_1 occurs at the beginning of the 2-nd decrease, for infinitely small variations $\Delta \xi_N = \xi_N - \xi_{N-1}$, $\Delta \zeta_N = \zeta_N - \zeta_{N-1}$, and it is shown that the formulae for sections 6.5 and 6.6 are identical. The stress distribution for the 2-nd decrease has 2 breaks. Finally, in section 6.7, the formulae and the conditions for further points of instantaneous adhesion P_{N-1} and N-th decrease of the stick area are stated. The tangential traction distribution for the period of the N-th decrease of the stick area has N breaks at $a_1^* < a_2^* < ... < a_N^*$. Each break represents a point of instantaneous adhesion P_i, with $1 \le i \le N-1$. It should be noticed, that the sections 12a), 13a) of Mindlin & Deresiewicz treat the problem of the 3-rd decrease of the stick area, recognizable by three breaks of the resulting stress distribution.

The displacements ξ and ζ in this chapter are the displacements of the centers of gravity of one sphere alone. The indices 1, 2, ... denote either points of instantaneous adhesion or the current values. The boundary condition of non-penetration in normal direction resp. adhesion of the contact point in tangential direction requires that the relative elastic displacements of the contact point $w_{body,1} - w_{body,2}$ resp. $u_{body,1} - u_{body,2}$ must be equal to the motion of the centers of gravity $\zeta_{body,2} - \zeta_{body,1}$ resp. $\xi_{body,2} - \xi_{body,1}$:

$$\left. \begin{array}{l} 2\xi = \xi_{body,2} - \xi_{body,1} = u_{body,1} - u_{body,2} \, , \\ 2\zeta = \zeta_{body,2} - \zeta_{body,1} = w_{body,1} - w_{body,2} \, , \end{array} \right\} \text{ in the contact point.} \qquad (6.1)$$

6.1 The Cattaneo-Mindlin theory

In the next sections we will use the so-called spherical *Cattaneo-Mindlin functions*, which are defined on the circles A_i, A_k (fig.6.1):
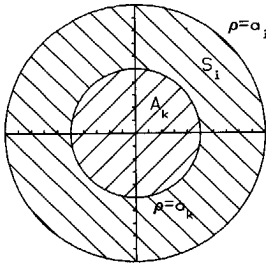
Fig. 6.1: The regions A_k and S_i.

$$A_i = \{\rho \leq a_i\}, \quad A_k = \{\rho \leq a_k\}, \quad a_i > a_k \,, \tag{6.2}$$

$$S_i = \{\rho \in A_i \setminus A_k\}, \quad \rho = \sqrt{x^2 + y^2} \,,$$

$$\sigma_{CM}(a_i, a_k) = \begin{cases} \mu\sqrt{a_i^2 - \rho^2} \,, & \text{in } S_i \,, \\ \mu(\sqrt{a_i^2 - \rho^2} - \sqrt{a_k^2 - \rho^2}) \,, & \text{in } A_k \,, \\ 0 \,, & \text{outside } A_i \,, \end{cases} \tag{6.3}$$

$$\mu = \frac{4fG}{\pi R(1-\nu)} \,, \quad \kappa = \frac{2-\nu}{2(1-\nu)} \,, \tag{6.4}$$

where we introduced the variables μ and κ. We determine the force by integration of (6.3) over A_k and the displacements from the load displacement equations (5.21) :

$$F_x = 2\pi \int_0^{a_i} \sigma_{CM}(a_i, a_k)\rho \, d\rho = \frac{2\pi\mu}{3}(a_i^3 - a_k^3) \,, \tag{6.5}$$

$$\xi = f\kappa(\zeta_i - \zeta_k) \,, \quad \text{in } A_k \,,$$

where ζ_i denotes the normal penetration (6.1) of the contact point, produced by a Hertzian traction on a circle of the radius a_i, and ξ the tangential displacement of one body in A_k. The displacements outside A_k can be calculated from the solution of K. L. Johnson (1985), for a traction distribution of the form $\sqrt{a^2 - \rho^2}$:

$$\sigma_{zx} = \sqrt{a^2 - \rho^2} \,,$$

$$u = \frac{\pi}{16G}\left[2(2-\nu)(2a^2 - \rho^2) + \nu\rho^2\cos 2\theta \right] \,, \quad \text{for } 0 \leq \rho \leq a \,,$$

$$u = \frac{1}{8G}\left[2(2-\nu)\left\{(2a^2 - \rho^2)\sin^{-1}\left(\frac{a}{\rho}\right) + a\sqrt{\rho^2 - a^2}\right\} + \nu\left\{\rho^2\sin^{-1}\left(\frac{a}{\rho}\right) + a\left(2\frac{a^2}{\rho^2} - 1\right)\sqrt{\rho^2 - a^2}\right\}\cos 2\theta \right] \,,$$
$$\text{for } \rho > a \,,$$

$$v = \frac{\pi}{16G}\nu\rho^2\sin 2\theta \,, \quad \text{for } 0 \leq \rho \leq a \,, \tag{6.6}$$

$$v = \frac{1}{8G}\left[\rho^2\sin^{-1}\left(\frac{a}{\rho}\right) + a\left(2\frac{a^2}{\rho^2} - 1\right)\sqrt{\rho^2 - a^2}\right]\sin 2\theta \,, \quad \text{for } \rho > a \,.$$

We derive three relations from (6.3), which simplify the calculations:

$$\sigma_{CM}(a_i, a_k) = f\sigma_H(a_i) \,, \quad \text{in } S_i \,, \tag{6.7}$$

$$\sigma_{CM}(a_i, 0) = f\sigma_H(a_i) \,, \quad \text{for all } x, y \,, \tag{6.8}$$

$$\sigma_{CM}(a_1, a_2) + \sigma_{CM}(a_2, a_3) = \sigma_{CM}(a_1, a_3) \,, \quad a_1 \geq a_2 \geq a_3 \,, \tag{6.9}$$

with the Hertzian stress distribution σ_H from (5.10). Equation (6.7) satisfies Coulomb's

law in the slip area S_i and (6.8) shows, that the Hertzian stress distribution is a special case of the Cattaneo-Mindlin function. The law of superpostition (6.9) is the base of our simplifications. For the case $a_3 = 0$ in (6.9), the Cattaneo-Mindlin function $\sigma_{CM}(a_1, a_2)$ is a combination of two Hertzian stress distributions.

We basically distinguish between three types of contact regimes: Complete adhesion, partial slip and full sliding. In the case of partial slip the previous load-history of the system only influences the current behaviour in so far as it determines the locked-in tangential stresses in those regions of the contact area which are stuck. If the stick area continues to decrease, it undergoes and additional rigid body displacement, and the additional stress distribution must satisfy the following boundary conditions:

1.) The load-displacement relation is given by the half-space theory;

2.) The stick area undergoes a rigid body displacement in tangential direction;

3.) We assume Coulomb's law, which states that the tangential traction in the slip area is equal to the product of a constant coefficient of friction and the normal traction. The tangential traction in the slip area acting on one body has the opposite sense of the velocity of that body relative to the other body, in the corresponding points.

4.) The tangential stress in the stick area must be smaller than the product of the coefficient of friction and the corresponding normal stress.
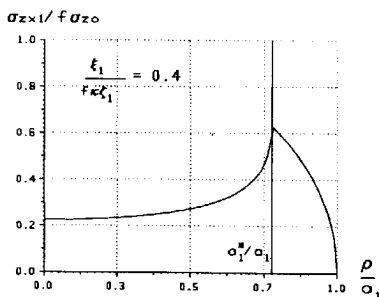
Fig. 6.2: The stress distribution (12).

Suppose, now, that one sphere is compressed by he value ζ_1 and subsequently shifted by the value ξ_1 in tangential direction. The following Cattaneo-Mindlin function satisfies the boundary conditions:

$$\sigma_{zx1} = \sigma_{CM}(a_1, a_1^*), \quad a_1^* \le a_1, \qquad (6.10)$$

in which a_1 denotes the radius of the contact area and a_1^* the radius of the stick area. The velocity s_x of body 1 relative to body 2 in the slip area can be calculated from (6.6) :

$$s_x = \frac{\pi(2-\upsilon)}{8G} \left[\left(2a_1^{*2} - \rho^2\right)\left(1 - \frac{2}{\pi}\sin^{-1}\left(\frac{a_1^*}{\rho}\right)\right) - \frac{2}{\pi} a_1^* \sqrt{\rho^2 - a_1^{*2}} \right], \text{ for } a_1^* \le \rho \le a_1, \quad (6.11)$$

where we neglected the $\cos(2\theta)$ and $\sin(2\theta)$ terms. These terms are smaller than 5%

of the displacement in the stick area (K. L. Johnson, 1985). From (6.11) follows that the sign of the slip s_x is negative, while the stress σ_{zx1} on body 1 is positive, such that, with (6.7), the 3-rd boundary condition is satisfied. Fig. 6.2 shows, that the 4-th boundary condition is also satisfied. Equation (6.5) yields the tangential force:

$$|F_{x1}| = \frac{2\pi\mu}{3} (a_1^3 - a_1^{*3}). \qquad (6.12)$$

Equations (6.10), (6.5) yield the tangential displacement ξ_1, in the stick area, which must be constant :

$$\xi_1 = \text{f}\kappa(\zeta_1 - \zeta_1^*), \text{ for } \rho \leq a_1^*, \qquad (6.13)$$

Fig. 6.3: The force (6.16).

Equations (5.12), (5.14), (6.12) and (6.13) can be reformulated to:

$$a_1^* = \sqrt{R\zeta_1^*} = a_1\sqrt{1 - \frac{|\xi_1|}{f\kappa\zeta_1}},$$

$$\qquad (6.14)$$

$$F_{x1} = fF_{z1}\left[1 - \left(1 - \frac{|\xi_1|}{f\kappa\zeta_1}\right)^{3/2}\right].$$

The stress distribution and the relation between force and displacement are shown in Figs. 6.2, 6.3. From (6.14) follows, that the radius a_1^* of the stick area decreases monotonously with increasing ξ_1 and fig.6.2 shows, that σ_{zx1} has a break at a_1^*. For $|F_{x1}| = fF_{z1}$ resp. $|\xi_1| = f\kappa\zeta_1$ the radius of the adhesive area a_1^* becomes zero and the displacement in fig. 6.3 is undefined. The variation of F_{x1} for an infinitesimal variation of ξ_1 can be obtained by partial differentiation of equation (6.14) :

$$\frac{dF_{x1}}{d\xi_1} = \frac{8Ga_1^*}{2-\nu} = \frac{8G\sqrt{R}}{2-\nu}\sqrt{\zeta_1 - \frac{|\xi_1|}{f\kappa}}. \qquad (6.15)$$

The tangential stiffness $dF_{x1}/d\xi_1$ is the reciprocal value of the tangential compliance defined by Mindlin and Deresiewicz.

6.2 Constant ζ , decreasing ξ .

Suppose, that the tangential displacement ξ is reduced, after it has reached the value ξ_1, while the normal compression remains constant: $\zeta = \zeta_1$. In the following the index is omitted for the current values of ξ, ζ etc. The reduction of the tangential displacement reduces the tangential stress in the entire contact area and causes a first point of instantaneous adhesion P_1 at the beginning. Since for complete adhesion the tangential stress becomes infinite at the border of the contact area (Mindlin, 1949), a new slip area forms with opposite slip directions, i.e. the period of the 2-nd decrease of the stick area follows. Similar to the section before, the stress σ_{zx} in the slip area $a^* \leq \rho \leq a$ is proportional to $f\sigma_{zz}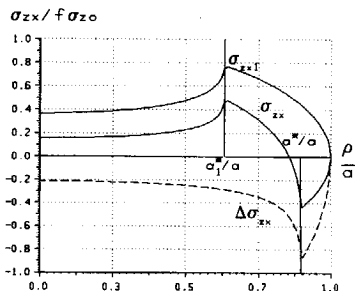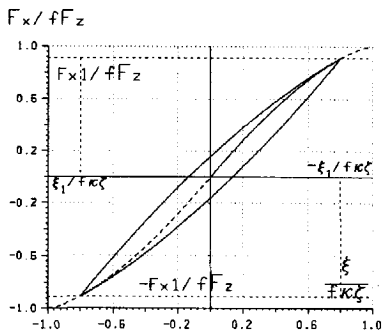$, but it has the opposite sense. Thus the tangential stress changes by the amount $-2f\sigma_{zz}$ in the slip area and the stick area $\rho \leq a^*$ undergoes a pure rigid body displacement. This boundary value problem is similar to section 1 with the following solution for the additional tangential stress $\Delta\sigma_{zx}$:

$$\Delta\sigma_{zx} = -2\sigma_{CM}(a,a^*) . \qquad (6.16)$$

The resulting stress distribution σ_{zx} is the sum of the equations (6.10), (6.16) :

$$\sigma_{zx} = \sigma_{CM}(a,a_1^*) - 2\sigma_{CM}(a,a^*) , \qquad (6.17)$$

with the current contact radius $a = a_1$. The stress σ_{zx}, plotted in fig. 6.4, has two breaks, with the inner break at the radius a_1^* of the old stick area, for P_1. The outer break occurs at the border of the new stick area $\rho = a^*$. Integration of the stress distribution (6.16) over the complete contact area yields, similar to (6.12), the tangential force ΔF_x:

Fig. 6.4: The stress distribution (6.17).

Fig. 6.5: The force F_x from (6.18).

$$|\Delta F_x| = |F_{x1} - F_x| = \frac{-4\pi\mu}{3} (a^3 - a^{*3}) , \quad F_x = \frac{2\pi\mu}{3} (2a^{*3} - a^3 - a_1^{*3}) . \qquad (6.18)$$

We obtain the new displacement ξ from (6.5) by superposition of (6.10), (6.16) :

$$\xi = \xi_1 + \Delta\xi = f\kappa(\zeta - \zeta_1^*) - 2f\kappa(\zeta - \zeta^*). \qquad (6.19)$$

Substitution of ζ_1^* from (6.13) for $\zeta = \zeta_1$ yields the radius a^* of the stick area:

$$a^* = \sqrt{R\zeta} \sqrt{1 - \frac{|\xi_1 - \xi|}{2f\kappa\zeta}} . \qquad (6.20)$$

This equation is finally inserted in (6.18) and partially differentiated, with the result:

$$\frac{dF_x}{d\xi} = \frac{-8Ga^*}{2-\nu} , \quad \text{for } \zeta = \text{const.} \qquad (6.21)$$

The slope of the load-deformation curve (6.21), resp. the tangential stiffness, at the beginning of the unloading process ($\xi = \xi_1$) is the same as the initial stiffness on loading ($\xi_1 = 0$ in eq. (6.15)). When the tangential force becomes zero, there is a permanent set ξ (fig. 6.5), the magnitude of which is obtained by setting $F_x = 0$ in eq. (6.18). The accompanying self-equilibrating stress distribution is obtained by inserting (6.20) in (6.17). When the force has been reduced to $F_x = -F_{x1}$, the unloading curve has the same slope as the loading curve at the point ξ_1. Hence the unloading curve is tangent to the loading curve for negative displacements $\xi_1 < 0$.

6.3 Increasing ζ, increasing ξ.

Suppose, that after application of the normal displacement ζ_1 and the tangential displacement ξ_1, the normal displacement ζ_1 is increased by the value $\Delta\zeta$ to ζ, while the tangential displacement ξ_1 remains constant :

$$\zeta = \zeta_1 + \Delta\zeta , \quad a = \sqrt{R(\zeta_1 + \Delta\zeta)} . \qquad (6.22)$$

In the following the current variables do not carry any index. With the normal compression ζ held constant, increase the tangential displacement by an increment $\Delta\xi < f\kappa\Delta\zeta$. Partial slip starts at the radius $\rho = a$ and progresses inward to a radius a^*.

The additional stress distribution $\Delta\sigma_{zx}$ in Fig. 6.6 is the Cattaneo-Mindlin function $\sigma_{CM}(a,a^*)$ and the radius of the stick area a^* is defined by (6.14):

$$a^* = \sqrt{R}\,\sqrt{\zeta - \Delta\xi/(f\kappa)}\,. \qquad (6.23)$$

Insertion in eq. (6.15) yields for $\Delta\xi\to 0$, $\Delta\zeta\to 0$:

$$\frac{dF_x}{d\xi} = \frac{8Ga^*}{2-\nu} = \frac{8Ga}{2-\nu}, \text{ for } d\xi < f\kappa d\zeta. \qquad (6.24)$$

Fig. 6.6: Stress distribution for $\Delta\xi < f\kappa\Delta\zeta$.

This is the slope of the load-displacement curve between the points 1 and 2 in fig. 6.8. For an infinitesimal change of F_x and F_z the radius of the stick area becomes equal to the radius of the old contact area $a^* \to a$, and the change of the stress distribution is obtained from (6.10), (6.12):

$$\lim_{\Delta F_x\to 0} \frac{\Delta\sigma_{zx}}{\Delta F_x} = \frac{d_{zx}}{dF_x} = \frac{1}{2\pi a\sqrt{a^2-\rho^2}}. \qquad (6.25)$$

Multiplication of (6.24), (6.25) yields :

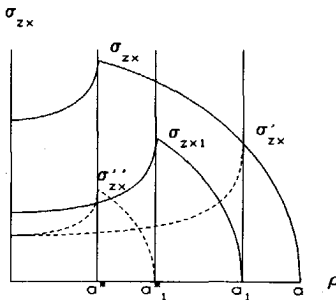$$\frac{d\sigma_{zx}}{d\xi} = \frac{4G}{\pi(2-\nu)\sqrt{a^2-\rho^2}}. \qquad (6.26)$$

The summation of n such displacements $d\xi_i$, da_i and substitution of an integral for the summation symbol yields the stress σ_{zx} at the point ρ for the time $t(a)$, when the contact radius has reached the value a:

$$\sigma_{zx} = \frac{4G}{\pi(2-\nu)} \int_\rho^a \frac{1}{\sqrt{a^2-\rho^2}} \frac{d\xi}{da}\, da\,, \qquad (6.27)$$

for $|d\xi| < f\kappa d\zeta$.

If the function $\xi(a)$ is known equation (6.27) can be evaluated.

Fig. 6.7: Stress distribution for $\Delta\xi > f\kappa\Delta\zeta$.

If the displacement is increased by the

increment $\Delta\xi = f\kappa\Delta\zeta$, the radius a^* of the stick area, in fig. 6.6, reduces to the value a_1^*, i.e. the radius of the stick area shrinks to its original value. The additional stress σ_{zx}' in fig. 6.7 is the Cattaneo-Mindlin function:

$$\sigma_{zx}' = \sigma_{CM}(a,a_1) , \qquad (6.28)$$

Superposition of (6.28) and the initial stress distribution (6.10) yields with (6.9) :

$$\sigma_{zx1} + \sigma_{zx}' = \sigma_{CM}(a_1,a_1^*) + \sigma_{CM}(a,a_1) = \sigma_{CM}(a,a_1^*) , \qquad (6.29)$$

We obtain the same stress distribution if we first apply the normal compression $\zeta_1 + \Delta\zeta$ in the origin 0 and subsequently increase the tangential displacement to the value $\xi_1 + f\kappa\Delta\zeta$. A further increase of ξ follows the curve 2-3 in fig. 6.8. Then we obtain the total stress increment $\Delta\sigma_{zx}$ by addition of σ_{zx}' and a second Cattaneo-Mindlin function σ_{zx}'' :
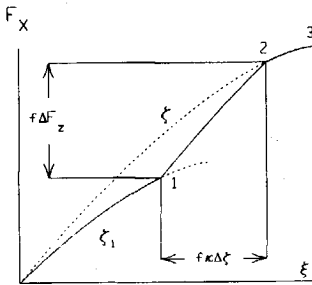

Fig. 6.8: The force F_x.

$$\sigma_{zx}'' = \sigma_{CM}(a_1^*,a^*) , $$
$$\sigma_{zx} = \sigma_{zx1} + \sigma_{zx}' + \sigma_{zx}'' = \sigma_{CM}(a,a^*), \qquad (6.30)$$

where we used (6.9). Equations (6.5), (6.30) yield the force and the displacement:

$$F_x = \frac{2\pi\mu}{3}(a^3 - a^{*3}), \qquad (6.31)$$
$$\xi = f\kappa(\zeta - \zeta^*).$$

Insertion of (6.22), (6.23) in (6.31) with $\Delta\zeta \to 0$, $\Delta\xi \to 0$ and partial differentiation yields with (6.24:

$$\frac{dF_x}{d\xi} = \frac{\partial F_x}{\partial\zeta}\frac{d\zeta}{d\xi} + \frac{\partial F_x}{\partial\zeta^*}\frac{d\zeta^*}{d\xi}, \qquad (6.32)$$

$$\frac{dF_x}{d\xi} = \begin{cases} \dfrac{8Ga}{2-\nu} , & \text{for } d\xi < f\kappa d\zeta , \\[2mm] \dfrac{8G}{2-\nu}\left\{ f\kappa a\dfrac{d\zeta}{d\xi} + a^*\left(1 - f\kappa\dfrac{d\zeta}{d\xi}\right)\right\}, & \text{for } d\xi \geq f\kappa d\zeta. \end{cases} \qquad (6.33)$$

When a number of n incremental displacements $d\xi_i$, $d\zeta_i$ is superposed, equation (6.31), yields:

$$\left(\frac{dF_x}{d\xi}\right)_n = \frac{8Ga_n}{2-\nu} \ , \quad F_x = \frac{8G}{2-\nu} \int_{a_0}^{a_n} a \frac{d\xi}{da} \, da \ , \quad \text{for} \ \left(\frac{d\xi}{d\zeta}\right)_i = \left(\frac{d\xi}{da} \frac{\sqrt{R}}{2a}\right)_i < f\kappa \ ,$$

$$F_x = \frac{8fG}{3(1-\nu)R} \, (a_n{}^3 - a_n{}^{*3}) \ , \quad a_n{}^* = a_n \sqrt{1 - \frac{|\xi_n|}{f\kappa\zeta_n}} \ , \quad \text{for} \ \left(\frac{d\xi}{d\zeta}\right)_i \geq f\kappa \ , \quad 1 \leq i \leq n \ .$$

$$(6.34)$$

The stress distribution is obtained from (6.27) resp. (6.30) by substitution of a_n for a and $a_n{}^*$ for a^*. In the case $d\xi_i \leq f\kappa d\zeta_i$ we have *complete adhesion*, because the increase of the contact area compensates the increase of the slip area for each increment, such that the new slip area always lies outside of the old contact area. Otherwise the stick area decreases for the first time.

6.4 Decreasing ζ, increasing ξ.

In contrast to section 6.3 it is desired to decrease the normal compression from ζ_1 to ζ. For that purpose it is necessary, to remove the tangential traction from the annular region between a and a_1 (fig. 6.9) using the stress distribution σ'_{zx}. Another stress distribution σ''_{zx} is necessary to compensate the reduction of σ_{zx1} due to σ'_{zx} and the increase of ξ. The necessary stress distribution can be read from fig. (6.9)

Fig. 6.9: The stress distribution (6.31).
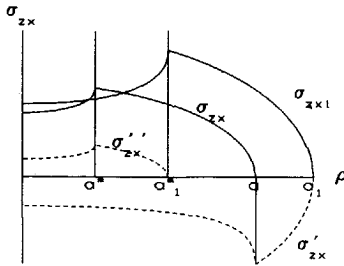
$$\sigma'_{zx} = -\sigma_{CM}(a_1,a) \ , \quad \sigma''_{zx} = \sigma_{CM}(a_1^*,a^*) \ ,$$
$$\sigma_{zx} = \sigma_{zx1} + \sigma'_{zx} + \sigma''_{zx} = \sigma_{CM}(a,a^*) \ , \quad (6.35)$$

where we used (6.9). The formula (6.35), which is identical with (6.30), is independent of the function $\xi(a)$ and of the variation $d\zeta$ as long as partial slip continues. This justifies the non-incremental formulation. Again we obtain the force F_x and the displacement ξ from (6.7):

$$F_x = \frac{2\pi\mu}{3} \, (a^3 - a^{*3}) \ , \quad \xi = f\kappa(\zeta - \zeta^*) \ . \quad (6.36)$$
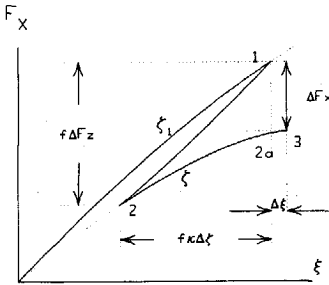
Fig. 6.10: The Force F_x (6.30).

Differentiation of (6.36) yields the tangential stiffness, similar to (6.33):

$$\frac{dF_x}{d\xi} = \frac{8G}{2-\nu}\left\{ f\kappa a\,\frac{d\zeta}{d\xi} + a^*\left(1 - f\kappa\,\frac{d\zeta}{d\xi}\right)\right\}. \quad (6.37)$$

The first term in curved brackets in (6.37) is the decrease of F_x due to σ'_{zx} (path 1-2 in fig. 6.10). The second term is the increase of F_x due to σ''_{zx} and corresponds to path 2-3. In contrast to (6.36) the tangential stiffness (6.37) depends on the function $d\zeta/d\xi$.

6.5 The first point of instantaneous adhesion

The first point of instantaneous adhesion for constant normal penetration was discussed in section 6.2. Section 6.3 and 6.4 studied the contact processes of the first decrease of the stick area resp. complete adhesion for varying contact areas. In order to arrive at a point of instantaneous adhesion P_1, the stress distribution must be reduced. Mathematically a Cattaneo-Mindlin function with the opposite sense as the old stress distribution σ_{zx1} must be added in the new slip area. If the contact area varies, there is a first stress distribution σ'_{zx} necessary to compensate this variation, which has the same sense as the old stress σ_{zx1} for $\Delta\zeta > 0$ resp. the opposite sense for $\Delta\zeta < 0$. Note that the increments $\Delta\xi$, $\Delta\zeta$ must be infinitely small, in order to arrive at a point of instantaneous adhesion. In the next step another stress distribution σ''_{zx} is superposed in the new slip area $a_2^* \leq \rho \leq a_2$, pointing into the opposite direction of σ_{zx1}. Both stress distributions are selected such that the law of superposition (6.9) of Cattaneo-Mindlin functions is applicable. They are plotted in fig. 6.11a) for $\Delta\zeta > 0$ and 6.11b) for $\Delta\zeta < 0$, where the index 1 denotes the old values and 2 the new values. The traction σ'_{zx} is different in the case a) and b), while the formula for σ''_{zx} is identical:

$$\sigma'_{zx} = \begin{cases} \sigma_{CM}(a_2,a_1)\,, & \text{for } \Delta\zeta > 0\,, \\ -\sigma_{CM}(a_1,a_2)\,, & \text{for } \Delta\zeta < 0\,, \end{cases} \quad (6.38a)$$

$$\sigma''_{zx} = -2\sigma_{CM}(a_2, a_2^*) , \tag{6.38b}$$

$$\sigma_{zx2} = \sigma_{zx1} + \sigma'_{zx} + \sigma''_{zx} = \sigma_{CM}(a_2, a_1^*) - 2\sigma_{CM}(a_2, a_2^*) , \quad \text{for } |\Delta\xi| > \text{fic}|\Delta\zeta| , \tag{6.38c}$$

where we used the law of superposition (6.9). The last equation proves, that the resulting stress distribution σ_{zx2} depends only on the contact radius a_1^* at the first point of instantaneous adhesion P_1, and the current values a_2, a_2^*, i.e. the formula is independent of the function $\xi(a)$. The resulting stress distribution has two breaks again, the inner one at $\rho = a_1^*$ for P_1, and the outer one at $\rho = a_2^*$, the border of the new, decreasing stick area.
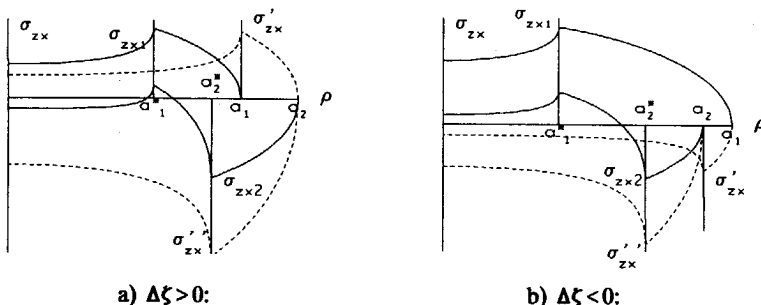

a) $\Delta\zeta > 0$:   b) $\Delta\zeta < 0$:

Fig. 6.11: Stress distribution a) for $\Delta\zeta_2 > 0$ and b) for $\Delta\zeta_2 < 0$.

Application of equation (6.5) on the additional stress distributions yields the force and the displacement:

$$\left.\begin{array}{l} F_{x2} = F_{x1} + \dfrac{2\pi\mu}{3} (a_2^3 - a_1^3 - 2a_2^3 + 2a_2^{*3}) , \\[2mm] \xi_2 = \xi_1 + \text{fic} (\zeta_2 - \zeta_1 - 2\zeta_2 + 2\zeta_2^*) , \end{array}\right\} \quad \text{for } |\Delta\xi| > \text{fic}|\Delta\zeta| , \tag{6.39}$$

The result (6.39) is independent of the sign of $\Delta\zeta_2$. Reformulation of (6.39) and partial differentiation yields the tangential stiffness $dF_{x2}/d\xi_2$:

$$\zeta_2^* = \zeta_2 + \frac{1}{2}\left(\frac{\xi_2 - \xi_1}{\text{fic}} - \zeta_2 + \zeta_1 \right) , \quad \frac{d\zeta_2^*}{d\xi_2} = \frac{1}{2}\left(\frac{d\zeta_2}{d\xi_2} + \frac{1}{\text{fic}} \right) ,$$

$$\frac{dF_{x2}}{d\xi_2} = \frac{8G}{2-\nu}\left\{ -\text{fic}a_2 \frac{d\zeta_2}{d\xi_2} + a_2^*\left(1 + \text{fic}\frac{d\zeta_2}{d\xi_2} \right) \right\}. \tag{6.40}$$

We prefer equation (6.39) to (6.40), because the former depends only on the first point of instantaneous adhesion P_1 and on the current values ξ_2, η_2. The value of a_2^* resp. the corresponding penetration ζ_2^* is defined by the second equation in (6.39).

6.6 Second decrease of the stick area

Suppose, that after a first point of instantaneous adhesion, as described in section 6.5, the displacement is continously decreased. The mathematical procedure is identical to the previous section and we list only the results. The necessary stress distributions σ'_{zx}, σ''_{zx} are plotted in fig. 6.12 and have the form:

a) $\Delta\zeta > 0$ b) $\Delta\zeta < 0$:
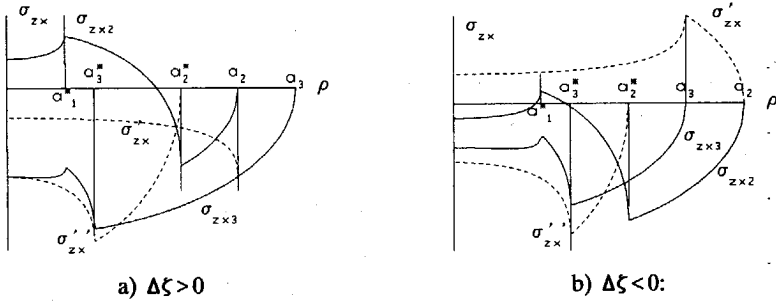
Fig. 6.12: Stress distribution for a) $\Delta\zeta > 0$ and b) $\Delta\zeta < 0$.

$$\sigma'_{zx} = \begin{cases} -\sigma_{CM}(a_3,a_2) \text{ , for } \Delta\zeta > 0 \text{ ,} \\ \sigma_{CM}(a_2,a_3) \text{ , for } \Delta\zeta < 0 \text{ ,} \end{cases} \tag{6.41a}$$

$$\sigma''_{zx} = -2\sigma_{CM}(a_2^*,a_3^*) \text{ ,} \tag{6.41b}$$

$$F_{x3} = F_{x2} + \frac{2\pi\mu}{3} \left(-a_3^3 + a_2^3 - 2a_2^{*3} + 2a_3^{*3} \right) \text{ ,} \tag{6.41c}$$

$$\xi_3 = \xi_2 + \text{fic} \left(-\zeta_3 + \zeta_2 - 2\zeta_2^* + 2\zeta_3^* \right) \text{ ,}$$

$$\frac{dF_{x3}}{d\xi_3} = \frac{8G}{2-\nu} \left\{ -\text{fica}_3 \frac{d\zeta_3}{d\xi_3} + a_3^* \left(1 + \text{fic} \frac{d\zeta_3}{d\xi_3} \right) \right\}. \tag{6.41d}$$

The equation (6.39) for the first point of instantaneous adhesion P_1, where the stick area begins to decrease for the second time, can be found by setting $a_2^* = a_2$ and substituting the index 2 for 3 and 1 for 2 in the formulae (6.41c). Since both equations are identical, we will use the former one, because it is simpler. We introduce the variables ΔF_2, $\Delta\xi_2$:

$$\Delta F_2 = F_2 - F_1 \text{ , } \quad \Delta\xi_2 = \xi_2 - \xi_1 \text{ ,} \tag{6.42}$$

were the index 1 denotes P_1 and 2 the current values. The necessary condition for the 2-nd decrease, in the case of $\Delta\zeta_2 > 0$, is that the radius a_2^* of the new stick area, in fig. 6.11, is smaller than the radius a_1 of the old contact area; for $\Delta\zeta_2 < 0$ the radius a_2^* must be smaller than the radius a_2 of the new contact area :

$$\zeta_2^* < \zeta_1 , \quad \text{for } \Delta\zeta_2 > 0 ; \quad \zeta_2^* < \zeta_2 , \quad \text{for } \Delta\zeta_2 < 0 . \tag{6.43}$$

Insertion of (6.40) into this condition yields:

$$\Delta\xi_2 < -\text{fic}|\Delta\zeta_2| , \text{ necessary for } P_1 \text{ and the 2-nd decrease,} \tag{6.44}$$

with P_1 for $\Delta\xi_2 \to 0$, $\Delta\zeta_2 \to 0$, resp. the period of the 2-nd decrease for finite values of $\Delta\xi_2$, $\Delta\zeta_2$. Complete adhesion without partial slip, where the new stick area lies outside of the old contact area ($\zeta_2^* > \zeta_1$), occurs only for $\Delta\zeta_2 > 0$ and infinitely small values of $\Delta\xi_2$, $\Delta\zeta_2$:

$$|d\xi_2| < \text{ficd}\zeta_2 , \text{ necessary for complete adhesion.} \tag{6.45}$$

Formula (6.45) is identical with the condition (6.24) for complete adhesion. The last condition for a period of the 2-nd decrease is, that the new stick area does not eliminate the old stick area:

$$\zeta_2^* > \zeta_1^* , \tag{6.46}$$

Insertion of (6.40) yields:

$$\xi_2 > -\xi_1 - \text{fic}\Delta\zeta_2 , \text{ necessary for the 2-nd decrease.} \tag{6.47}$$
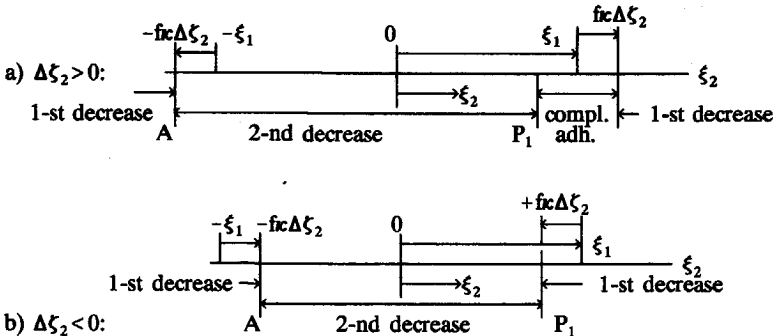

Fig. 6.13: The contact regimes for different ξ_2.

The conditions (6.44), (6.45), (6.47) for ξ_2 are plotted in fig. 6.13a) and b). A period of complete adhesion from (6.45) exists only for $\Delta\zeta_2 > 0$. If ξ_2 lies on the right side of the period of complete adhesion in fig. 6.13a) resp. on the right side of P_1 in 12b) the period of the first decrease continues. If ξ_2 lies on the left side of A the slip direction is opposite to the old slip direction and another period of the 1-st decrease occurs.

6.7 Further of points instantaneous adhesion and decreasing stick area

We introduce the sign s_N of the slip direction after the N-th point of instantaneous adhesion P_N. The resulting formulae hold for $N > 2$, with the points P_N and P_{N-1}. The derivation of the equations for the pressure distribution is similar to (6.38) :

$$s_N = -\text{sign}(\Delta\xi_N), \quad s_{N-1} = -\text{sign}(\Delta\xi_{N-1}) = -s_N, \quad \Delta\xi_N = \xi_N - \xi_{N-1}, \quad (6.48a)$$

$$\sigma'_{zx} = \begin{cases} -s_{N-1}\,\sigma_{CM}(a_N, a_{N-1}), & \text{for } \Delta\zeta_N > 0, \\ s_{N-1}\,\sigma_{CM}(a_{N-1}, a_N), & \text{for } \Delta\zeta_N < 0, \end{cases} \quad (6.48b)$$

$$\sigma''_{zx} = -2\,s_N\,\sigma_{CM}(a_N, a_N^\bullet), \quad (6.48c)$$

$$F_{xN} = F_{xN-1} + \frac{2\pi\mu}{3}\left(-s_{N-1}\,a_N^3 + s_{N-1}\,a_{N-1}^3 - 2s_N\,a_N^3 + 2s_N\,a_N^{\bullet 3}\right),$$

$$= F_{xN-1} + \frac{2\pi\mu}{3}\,s_N\left(2a_N^{\bullet 3} - a_N^3 - a_{N-1}^3\right), \quad (6.48d)$$

$$\xi_N = \xi_{N-1} + f\kappa s_N(2\zeta_N^\bullet - \zeta_N - \zeta_{N-1}), \quad (6.48e)$$

$$\frac{dF_{xN}}{d\xi_N} = \frac{8G}{2-\nu}\left\{-f\kappa s_N a_N \frac{d\zeta_N}{d\xi_N} + a_N^\bullet\left(1 + f\kappa s_N \frac{d\zeta_N}{d\xi_N}\right)\right\}. \quad (6.48f)$$

The resulting pressure distribution σ_{zxN} has N breaks. The force F_{xN} in (6.48d) depends only on the force F_{xN-1}, the contact radius a_{N-1} at the previous point of instantaneous adhesion P_{N-1}, and on the current values a_N, $a_N^\bullet$. Equation (6.48f) for the tangential compliance depends on $d\xi_N/d\zeta_N$. Similar to formula (6.43) the necessary condition for the N-th decrease of the stick area is:

$$\zeta_N^\bullet < \zeta_{N-1}, \quad \text{for } \Delta\zeta_N > 0, \quad \text{and} \quad \zeta_N^\bullet < \zeta_N, \quad \text{for } \Delta\zeta_N < 0. \quad (6.49)$$

The necessary condition that the new stick area does not overlay the old stick area is

$$\zeta_N^* > \zeta_{N-1}^*. \tag{6.50}$$

Equation (6.48c) in (6.49), (6.50) yields the condition for the process of the N-th decrease of the slip area, which follows the N-th point of instantaneous adhesion. This condition together with the condition for complete adhesion (6.50) yields :

$$\boxed{\begin{array}{l} |fic\Delta\zeta_N| \leq |\Delta\xi_N| \leq |\Delta\xi_{N-1}| + fic(\Delta\zeta_{N-1}+\Delta\zeta_N)\,,\ \text{for}\ N > 2\,,\quad \text{necessary for the}\\ \hspace{10cm} \text{N-th decrease,}\\ |\Delta\xi_N| < fic\Delta\zeta_N\,,\ \text{with}\ \Delta\xi_N{\to}0,\ \Delta\zeta_N{\to}0,\ \text{for complete adhesion.} \end{array}} \tag{6.51}$$

The conditions (6.51) are plotted in fig. 6.14 for $\Delta\xi_N > 0$. We obtain the condition for $\Delta\xi_N < 0$ by mirroring fig. 6.14 at a vertical axis. It should be noticed, that for $\Delta\xi_N$ on the right hand side of the point A a period of the (N-2)-th decrease takes place, because the N-th decrease overlays the (N-1)-th decrease and the slip direction has the sense of the (N-2)-th decrease.
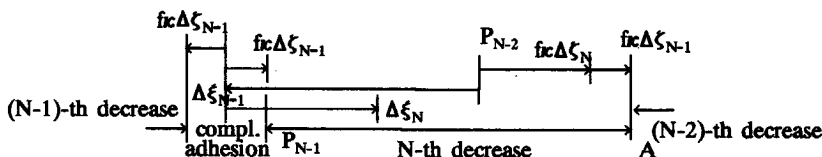

Fig. 6.14a) : The contact regimes for $\Delta\zeta_N > 0$, $\Delta\zeta_{N-1} > 0$, $\Delta\xi_N > 0$.
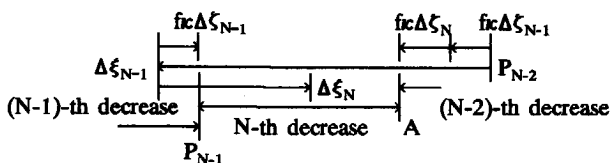

Fig. 6.14b) : The contact regimes for $\Delta\zeta_N < 0$, $\Delta\zeta_{N-1} < 0$, $\Delta\xi_N > 0$.

7 Load-histories with elliptical contact areas

Only bodies with similar stiffnesses c_x, c_y from (5.25) and similar inertial properties in x- and y-direction, like e. g. spheres, keep their initial displacement direction throughout the entire impact. Otherwise the tangential displacement $\boldsymbol{\xi} = (\xi, \eta)^T$ changes its direction. In the following bold letters, like e.g. $\boldsymbol{\xi}$, denote vectors, and the superscript T signifies transposition. In Fig. 7.1 the normal and tangential displacements ζ and ξ are plotted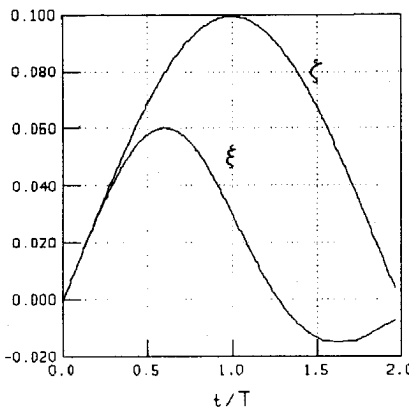 for the impact of two spheres with initial adhesion. This example will be analysed in detail in chapter 9. In the period of adhesion, which ends shortly after ξ reached its maximum, equation (6.24) for complete adhesion is valid. Subsequently partial slip starts, similar to section 6.1, under consideration of the old stress distribution in the stick area. After ξ has reached its minimum, the differential $\dot{\xi}$ and the slip direction change again. This change of direction reduces the tangential stress, which can produce a point of instantaneous adhesion, if the condition for adhesion: $|d\sigma_{zx}| < f d\sigma_{zz}$ is satisfied. Since for complete adhesion the stress becomes infinite at the border of the contact area, a new slip area forms, which starts at the border and progresses inward, superposing the original stress distribution. In chapter 6 this contact phenomenon was studied for the case of spheres and we found that, in the case of partial slip, the system depends only on the so-called points of instantaneous adhesion P_N and the current displacements. The boundary value problem for the tangential shift of elliptical contact areas has a very similar solution. Similar to chapter 6 we define a point of instantaneous adhesion P_{N-1}, where the entire contact area sticks for an infinitely short moment, followed by the N-th period of decreasing stick area, during which the size of the stick area decreases monotonically. The stress distribution has to satisfy the

Fig. 7.1: ξ, η as function of the time for the oblique impact.

following boundary conditions:

1.) The load-displacement relation is given with (5.21).

2.) Constant displacement ξ, η in the stick area.

3.) We assume partial slip with Coulomb's law in the slip area, which states that the tangential traction is equal to the product of a constant coefficient of friction and the normal traction. The tangential traction in the slip area acting on one body has the opposite sense of the velocity of that body relative to the other body, in the corresponding points.

4.) The tangential stress in the stick area must be smaller than the product of the coefficient of friction and the corresponding normal stress.

If the slip direction varies, the third boundary condition for the slip direction yields a system of two nonlinear integral equations, which can not be solved by analytical methods. Therefore we assume constant stress directions in the slip area and compare this theory with numerical results in chapter 14. The values for the force and the size of the slip area are in good accordance with the numerical solution as long as the slip area is small enough. We also found that the slip direction is constant on elliptical rings, but its value depends on the previous load-history. Thus this theory is usefull for approximations, as long as the limits are kept in mind.

Our solution is *non-incremental*, because the slip direction is constant during a period of decreasing stick area and changes only at points of instantaneous adhesion. If follows that the displacement must have a constant direction between the actual value ξ_N and the value ξ_{N-1} at P_{N-1}. Otherwise, if the tangential displacement changes its direction continously while the stick area decreases, an incremental method must be used to calculate the correct stress directions in the slip area, and our theory is only a first approximation.

In section 7.1 we start with the boundary value problem of Cattaneo. He solved the problem of the two-dimensional shift of two bodies in x- and y-direction with a tangential pressure distribution of constant direction in the whole contact area. The displacement direction is also constant and the stick area decreases continuously with increasing displacement, until gross slip occurs.

In section 7.2 we discuss the case, where the tangential displacement is reduced, after Cattaneo's stress distribution was applied. At the beginning of the reduction a first point of instantaneous adhesion P_1 occurs, followed by a period of the 2-nd decrease of the stick area, where a new slip area forms at the border of the contact area, progressing inward with increasing ξ. This behaviour is similar to the theory of Mindlin & Deresiewicz in chapter 6, but the tangential displacement must not be

directed parallel to one of the semiaxis of the contact ellipse, as Deresiewicz (1957) presupposed. If another displacement in a different direction is superposed, a point P_3 may occur, which is the topic of section 7.3. Furthermore the size of the contact area may change also, which is discussed in section 7.4 for P_1 and in 7.5 for P_N. In section 7.6 pure torsion of elliptical contact areas is discussed. We compare the numerical and theoretical solutions in chapter 7.7.

In all sections of this chapter we will use the so-called *Cattaneo-Mindlin functions* $\sigma_{CM}(a_i, a_k)$, which are defined on similar ellipses A_i, A_k :

$$\left. \begin{array}{c} A_i = \left\{ \dfrac{x^2}{a_i^2} - \dfrac{y^2}{b_i^2} < 1 \right\} , \quad A_k = \left\{ \dfrac{x^2}{a_k^2} - \dfrac{y^2}{b_k^2} < 1 \right\} , \\[2mm] a_i > a_k , \quad a_i/b_i = a_k/b_k, \\[2mm] S_i = \{ x, y \in A_i \setminus A_k \}, \end{array} \right\} \quad (7.1a)$$

$$\sigma_{CM}(a_i, a_k) = \left\{ \begin{array}{l} \mu a_i \sqrt{ 1 - \dfrac{x^2}{a_i^2} - \dfrac{y^2}{b_i^2} } \ , \ \text{in } S_i , \\[4mm] \mu \left[a_i \sqrt{ 1 - \dfrac{x^2}{a_i^2} - \dfrac{y^2}{b_i^2} } - a_k \sqrt{ 1 - \dfrac{x^2}{a_k^2} - \dfrac{y^2}{b_k^2} } \right] , \ \text{in } A_k , \\[4mm] 0 , \quad \text{outside } A_i \end{array} \right\} \quad (7.1b)$$

$$\mu = \frac{f\sigma_{z0}}{a_i} = \frac{3fF_{zi}}{2\pi a_i^2 b_i} = \frac{3f(A+B)\sqrt{1-k^2}}{2\pi\alpha(\vartheta_1+\vartheta_2)} , \quad (7.1c)$$

where we used (5.14) for the variable μ, which depends on the fraction a_i/b_i and on the materials, but not on the penetration ζ. Integration of (7.1b) yields the force and equation (5.21) the displacements. We introduce the normalized displacement vector e, the force F, the stress direction p, the displacement vector ξ and the tangential stress vector σ_t. We obtain the force F by integration of (7.1b) over the loaded area A_i, and the displacement e by integration of (5.21) :

$$\sigma_t = \begin{pmatrix} \sigma_{zx} \\ \sigma_{zy} \end{pmatrix} = p \, \sigma_{CM}(a_i, a_k) , \quad (7.2a)$$

$$p = \begin{pmatrix} p \\ q \end{pmatrix} , \quad |p| = 1 , \quad (7.2b)$$

$$e = \frac{1}{fc_z} \begin{pmatrix} c_x \xi \\ c_y \eta \end{pmatrix} = p \, (\zeta_i - \zeta_k) , \quad \text{in } A_i \quad (7.2c)$$

$$F = p \, \frac{2fc_z}{3} (\zeta_i^{3/2} - \zeta_k^{3/2}) . \quad (7.2d)$$

In (7.2) we replaced the semiaxis a_k (a_i) with the corresponding normal penetration ζ_k (ζ_i) produced by a Hertzian pressure distribution (5.10) over the ellipse A_k (A_i). The displacement vector e was obtained by integration of (5.21), neglecting the asymmetric terms, similar to chapter 6. From (7.1) three relations, which simplify the calculations, can be derived:

$$\sigma_{CM}(a_i, a_k) = f\sigma_H(a_i), \text{ in } S_i, \tag{7.3a}$$

$$\sigma_{CM}(a_i, 0) = f\sigma_H(a_i), \text{ for all } x,y, \tag{7.3b}$$

$$\sigma_{CM}(a_1, a_2) + \sigma_{CM}(a_2, a_3) = \sigma_{CM}(a_1, a_3), \text{ for } a_1 \geq a_2 \geq a_3. \tag{7.3c}$$

The first equation (7.3a) satisfies Coulomb's law in the slip area S_i. Equation (7.3b) shows, that the Hertzian stress distribution σ_H is a special Cattaneo-Mindlin function. (7.3c) shows, that two Cattaneo-Mindlin functions can be linearly superposed. The case $a_3 = 0$ in (7.3c) shows, that the Cattaneo-Mindlin function is a superposition of two Hertzian stress distributions. Equation (7.2c) proves, that the Cattaneo-Mindlin function satisfies the boundary condition of constant displacement in the stick area A_i.

7.1 Tangential shift with decreasing stick area

Suppose, that two bodies of similar material are compressed by the value ζ_1 in normal direction. The normal stress distribution is defined by the Hertzian theory of section 5.1. Now we apply a tangential displacement with the components ξ_1, η_1 and increase its value in a constant direction. Introduction of the relative velocity s of body 1 relative to body 2 and the tangential stress σ_{t1} on body 1 yields the following equation for the third boundary condition :

$$\sigma_{t1} = -f_{kin} \frac{s}{|s|} \sigma_{zz1}, \text{ in the slip area }. \tag{7.4}$$

The following Cattaneo-Mindlin function (7.2a) satisfies the boundary conditions:

$$\sigma_{t1} = p_1 \sigma_{CM}(a_1, a_1^*), \quad |p_1| = \sqrt{p_1^2 + q_1^2} = 1, \tag{7.5}$$

The area of adhesion $H = A_1^*(a_1^*, b_1^*)$ and the contact area $C = A_1(a_1, b_1)$, with $A_1(a_1, b_1)$ defined by (7.1a), are similar ellipses with the semiaxis a_1^*, b_1^* resp. a_1, b_1. The slip

area S_1 occupies an annular region inside of the contact area, but outside of the area of adhesion. The values of the stress are constant on similar ellipses. Equation (7.2c), (7.5) yield:

$$e_1 = p_1(\zeta_1 - \zeta_1^\cdot) , \quad \zeta_1^\cdot = \zeta_1 - |e_1| , \tag{7.6}$$

The penetration ζ_1^*, which produces a contact area with the semiaxis a_1^*, decreases proportional to the scalar value of $|e_1|$. The force is defined by (7.2d) :

$$F_1 = p_1 \frac{2fc_z}{3} (\zeta_1^{3/2} - \zeta_1^{*3/2}) , \tag{7.7}$$

From (7.6), (7.7) follows, that the direction of the force differs from the direction of the displacement, if c_x and c_y are unlike. The stress distribution (7.5) and the force F_x for $F_y = \eta_1 = 0$ are shown in fig. 3.3. The relation between ζ_1 and a_1 resp. $\zeta_1^\cdot$ and $a_1^\cdot$ can be deduced from (5.14) :

$$\zeta_1 = Bb_1^2 K(k)/D(k), \quad b_1^*/b_1 = a_1^*/a_1 = \sqrt{\zeta_1^*/\zeta_1} . \tag{7.8}$$

If the displacements ξ_1, η_1 are given, the parameters p_1, q_1 can be calculated by (7.6). Otherwise, if the force F_x, F_y is given, equations (7.2b), (7.7) define the unknown parameters.

Equations (7.5)–(7.8) hold for a load-history, where the displacements ξ_1 and η_1 are applied in one step. Other load histories are possible, e.g. the displacement ξ_1 can be applied first followed by the displacement η_1. In this case the slip directions in the slip area differ considerably from the slip directions defined by equation (7.2). Numerical calculations proved that the force displacement relation (7.5) is a good approximation, as long as the stick area is large enough to prevent gross slip, where the whole contact area slides. In the case of gross slip, Coulomb's law (7.3) holds in the entire contact area, and the slip direction is defined by the relative velocity of the two bodies. In chapter 14 some elementary load-histories are investigated, using the numerical method.

The displacements in the contact area due to a traction distribution of the form :

$$\sigma_{zx} = \sigma_{z0}\sqrt{1-x^2/a^2-y^2/b^2} , \tag{7.9}$$

were calculated by P. J. Vermeulen and K. L. Johnson in 1964, with the result :

$$u = u_0 \left[\Gamma - \Phi \frac{x^2}{a^2} - \Psi \frac{y^2}{b^2} \right] , \quad v = u_0 \Theta \frac{xy}{ab}, \quad u_0 = \begin{cases} \sigma_{z0}b/(2G) , & a<b \\ \sigma_{z0}a/(2G) , & a>b \end{cases} \tag{7.10}$$
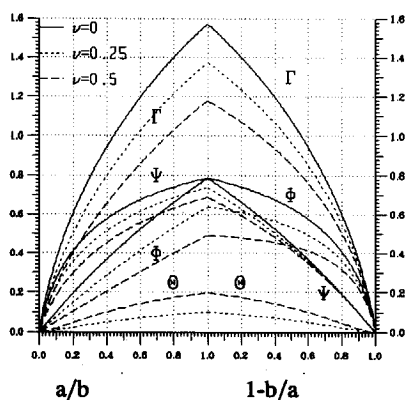
$$\Gamma = \begin{cases} \dfrac{a}{b}\,(K-\nu D)\,, & a<b, \\[2mm] \pi(2-\nu)/4\,, & a=b, \qquad (7.11) \\[2mm] \dfrac{b}{a}\,[K-\nu B]\,, & a>b, \end{cases}$$

$$\Phi = \begin{cases} \dfrac{a}{b}\,[B-\nu(D-C)]\,, & a<b, \\[2mm] \pi(4-3\nu)/16\,, & a=b, \qquad (7.12) \\[2mm] \dfrac{b}{a}\,[D-\nu(D-C)]\,, & a>b, \end{cases}$$

$$\Psi = \begin{cases} \dfrac{a}{b}\,(D-\nu C)\,, & a<b, \\[2mm] \pi(4-\nu)/16\,, & a=b, \qquad (7.13) \\[2mm] \dfrac{b}{a}\,\Big[B-\nu\,\dfrac{b^2}{a^2}\,C\Big]\,, & a>b, \end{cases}$$

Fig. 7.2: The functions (7.11)-(7.14).

$$\Theta = \begin{cases} 2\nu\,\dfrac{a^2}{b^2}\,C\,, & a<b, \\[2mm] \pi\nu/8\,, & a=b, \qquad (7.14) \\[2mm] 2\nu\,\dfrac{b^2}{a^2}\,C\,, & a>b, \end{cases}$$

The functions K, E and D are defined by (5.13). B and C are defined as:

$$B = K-D\,,\ C = (2D-K)/k^2. \qquad (7.15)$$

They are tabulated by Jahnke and Emde (1945) in terms of the modulus $k=\sqrt{1-a^2/b^2}$ for $a<b$ and $k=\sqrt{1-b^2/a^2}$ for $a>b$. Fig. 7.1 shows the functions (7.11)-(7.14) for different Poisson's ratios.

7.2 First point of instantaneous adhesion

First we apply the pressure distribution of section 7.1, defined by (7.4)-(7.8). In the next step we superpose an additional displacement, such that the initial stress distribution decreases. At the beginning of the reduction a first point of instantaneous adhesion P_1 takes place, followed by a period of the second decrease of the stick area. The new slip direction has two components, one parallel and the other perpendicular to the old slip direction. We will show that the parallel component must be opposite to the old slip direction to cause instantaneous adhesion of the entire contact area.

We satisfy the 3-rd boundary condition only in so far, that the absolute value of

the stress in the slip area follows Coulomb's law :

$$\sigma_{zx2}^2 + \sigma_{zy2}^2 = (f\sigma_{zz2})^2, \text{ in the slip area,} \qquad (7.16)$$

where the index 2 denotes the new stress distribution. The boundary conditions can be satisfied by a superposition of Cattaneo-Mindlin functions:

$$\sigma_t = p_1 \sigma_{CM}(a,a_1^*) + p_2 \sigma_{CM}(a,a_2^*) , \quad |p_1 + p_2| = 1 , \quad p_k = (p_k, q_k)^T, \qquad (7.17)$$

where the term $p_1 \sigma_{CM}(a,a_1^*)$ is the old stress distribution and $p_2 \sigma_{CM}(a,a_2^*)$ the additional stress. Insertion of (7.5) in (7.17) yields:

Fig. 7.3: Stress distribution.

Fig. 7.4: Condition (7.23).

$$p_2 (p_2 + 2p_1) = 0 . \qquad (7.18)$$

The additional displacements $\Delta\xi_2$, $\Delta\eta_2$ are defined by (7.2c) resp. (5.28) :

$$\Delta e_2 = e_2 - e_1 = p_2(\zeta_2 - \zeta_2^*) ,$$

$$\Delta e_2 = \frac{1}{fc_z} (c_x \Delta\xi_2, c_y \Delta\eta_2)^T. \qquad (7.19)$$

Insertion of (7.7), (7.18) in (7.19) yields the compression ζ_2^*:

$$\zeta_2^* = \zeta_2 + \frac{|e_1||\Delta e_2|^2}{(e_1 \Delta e_2)} . \qquad (7.20)$$

The normal compression ζ_2^* of the corresponding semiaxis a_2^* must be smaller than ζ_2. It follows, that the numerator of (7.20) must be less than zero. This condition is necessary but not sufficient for the existence of a new slip area. The sufficient condition is, that the semiaxis a_2^* of the new stick area must be larger than the semiaxis of the old stick area a_1^*. The same holds for the corresponding compressions:
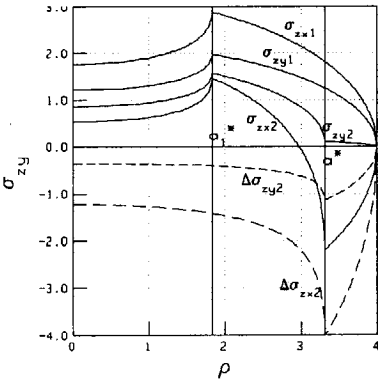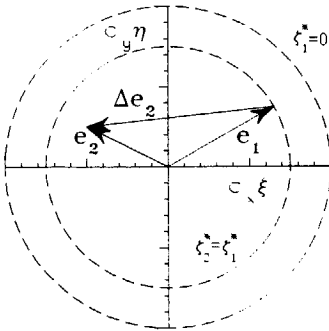
$$\zeta_2^* - \zeta_1^* > 0 . \qquad (7.21)$$

Insertion of (7.6) and (7.20) in (7.21) yields for constant ζ:

$$(\Delta e_2)^2 + 2(e_1 \Delta e_2) < 0. \tag{7.22}$$

Insertion of (7.19) in (7.22) yields:

$$e_2^2 < e_1^2 . \tag{7.23}$$

If the vector e_2 lies inside of the circle with the radius $|e_1|$ in Fig. 7.4, a new slip area forms and solution (7.17) is valid. Outside of the circle the stress distribution can be approximated by equation (7.5), independent of the foregoing load-history. If the current displacement exceeds the circle $|e_1|$, the new slip area overlays the old slip area completely. If the new slip directions are much different from the foregoing directions, the angle of the slip directions varies considerably. Some load-histories of this type are calculated in chapter 14 and compared with the simplified solution of this chapter. Mindlin and Deresiewicz's theory is a special case, where e_1 and Δe_2 have opposite directions and the contact area is circular. Equation (7.2d) yields for the force:

$$F = \frac{2fc_z}{3}[p_1(\zeta_1^{3/2} - \zeta_1^{*3/2}) + p_2(\zeta_1^{3/2} - \zeta_2^{*3/2})]. \tag{7.24}$$
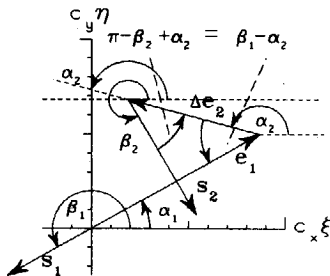
Introduction of the slip-direction in the slip area :

$$s_1 = -p_1 , \quad s_2 = -p_1 - p_2 , \tag{7.25}$$

insertion of (7.19) :

$$s_2 \Delta e_2 = -(p_1 + p_2)\Delta e_2 = -(p_1 + p_2)p_2(\zeta_2 - \zeta_2^*) , \tag{7.26}$$

and insertion of (7.18), (7.19), (7.25) yields:

$$s_2 \Delta e_2 = -s_1 \Delta e_2 , \tag{7.27}$$

We introduce the angles α_k, β_k :

$$\Delta e_k = (\cos \alpha_k, \sin \alpha_k)^T,$$

$$s_k = (\cos \beta_k, \sin \beta_k)^T, \tag{7.28}$$

$$\Delta e_1 = e_1 ,$$

and obtain from (7.26) :

$$\beta_1 - \alpha_2 = \pi - \beta_2 + \alpha_2 . \tag{7.29}$$

Fig.. 7.5: Condition (7.30).

Equation (7.29) states that the angle between the old slip direction s_1 and e_2 is equal to the angle between the new slip direction s_2 and $-\Delta e_2$ (Fig. 7.5). It is a consequence of our assumptions, that the angle β_2 of the new slip direction depends only on the angle α_2 of the additional displacement and on the old slip direction β_1, but not on the value of Δe_2.

7.3 Further points of instantaneous adhesion

Suppose, now, that $N-1$ points of instantaneous adhesion P_i occured, followed by N periods of decreasing stick area. The additional stress distributions $\Delta\sigma_{ti}$ of step i have the form :

$$\Delta\sigma_{ti} = p_i \sigma_{CM}(a_N, a_i^*), \quad \sigma_t = \sum_{i=1}^{N} p_i \sigma_{CM}(a_N, a_i^*). \tag{7.30}$$

In the slip area S_N the two surfaces slide partially upon each other and Coulomb's law must be satisfied:

$$\sigma_{zx}^2 + \sigma_{zy}^2 = (f\sigma_{zz})^2 , \quad \text{in } S_N . \tag{7.31}$$

Insertion of (7.31) in (7.32) and (7.3a) yields :

$$\left(\sum_{i=1}^{N} p_i\right)^2 = 1 . \tag{7.32}$$

Equation (7.2c) and (7.30) yield:

$$\Delta e_N = p_N(\zeta_N - \zeta_N^*) . \tag{7.33}$$

The slip direction s_k is opposite to the stress direction (7.30) :

$$s_k = - \sum_{i=1}^{k} p_i , \quad |s_k| = 1 . \tag{7.34}$$

Insertion of (7.34) in (7.32) :

$$p_N(p_N - 2s_{N-1}) = 0 , \tag{7.35}$$

and the definition of s_N (7.34) yields with (7.35) :

$$s_N \, \Delta e_N = (s_{N-1} - p_N) \Delta e_N = (s_{N-1} - p_N) p_N (\zeta_N - \zeta_N^{\cdot}) \, . \tag{7.36}$$

The last two equations can be reformulated with (7.33) :

$$s_N \, \Delta e_N = - \, s_{N-1} \, \Delta e_N \, . \tag{7.37}$$

We obtain the compression $\zeta_N^{\cdot}$ from (7.33), (7.35) :

$$\zeta_N^{\cdot} = \zeta_N - \frac{(\Delta e_N)^2}{2(\Delta e_N s_{N-1})} = \zeta_N + \frac{(\Delta e_N)^2}{2(\Delta e_N s_N)} \, , \tag{7.38}$$

Introduction of α_N, β_N from (7.28) in (7.37) yields an equation for the angle of the new slip direction β_N, similar to (7.29):

$$\beta_N - \alpha_N = \alpha_N - \beta_{N-1} + \pi \, . \tag{7.39}$$

The angle between the new slip directions_N and Δe_N is equal to the angle between $-\Delta e_N$ and the old slip direction s_{N-1}. Similar to section 7.2 $\zeta_N^{\cdot}$ must be greater than $\zeta_{N-1}^{\cdot}$ for a point of instantaneous adhesion. From equation (7.38) we obtain the condition :

$$|\Delta e_N| < |\Delta e_{N-1}| \, \frac{\cos(\gamma_N)}{\cos(\gamma_{N-1})} \, , \tag{7.40}$$

where we introduced the angle γ_i :

$$\gamma_i = \beta_{i-1} - \alpha_i, \quad i = 1..N. \tag{7.41}$$

Condition (7.40) is satisfied, if $|\Delta e_N|$ lies inside of the large circle in fig. 7.6. It has the diameter $|\Delta e_{N-1}|/\cos(\gamma_{N-1})$ and the center lies on the line BC which forms the angle γ_{N-1} with Δe_{N-1}. This circle can be constructed as follows:

1.) Draw Δe_{N-1} and s_{N-2} defined by (7.34), through A.

2.) Draw the line s_{N-1} at an angle γ_{N-1} to $-\Delta e_{N-1}$ through B.

3.) The center of the circle lies on the intersection of s_{N-1} and s_{N-2} in Fig. 7.6.
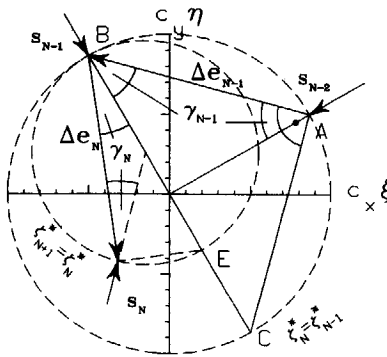
$$\frac{|\Delta e_N|}{\cos \gamma_N} = BE \, , \quad \frac{|\Delta e_{N-1}|}{\cos \gamma_{N-1}} = BC \, ,$$

Fig. 7.6: Condition (7.40)

From the construction of this circle follows, that the centers of two succeeding circles lie on the same line s_{N-1}. The vector Δe_N, which defines a segment of the succeeding circle, must lie completely inside of the foregoing circle. It follows that each circle is completely inside of all preceeding circles.

7.4 The first point of instantaneous adhesion for varying contact areas

Suppose, a stress distribution of section 7.2 is applied with the additional displacements $\Delta\xi_2$ from (7.19), such that the contact area sticks instantaneously at P_1. In the next step the normal displacement is increased by $\Delta\zeta_2$. The resulting stress σ_t is a sum of Cattaneo-Mindlin functions, similar to sections 6.5, 6.6 :

$$\sigma_t = p_1\sigma_{CM}(a_1,a_1^{\bullet}) + p_1\sigma_{CM}(a_2,a_1) + p_2\sigma_{CM}(a_2,a_2^{\bullet}) . \tag{7.42}$$

We obtain the same stress distribution for a decreasing $\Delta\zeta_2$, similar to section 6.5. The first term on the right hand side of (7.42) is the old stress distribution, the second term compensates the variation of the stick area and the third term satisfies the boundary conditions. Equation (7.3c) inserted in (7.42) yields:

$$\sigma_t = \sum_{i=1}^{2} p_i \, \sigma_{CM}(a_2,a_i^{\bullet}) . \tag{7.43}$$

The stress distribution (7.43) depends only on the points of instantaneous adhesion and on the current values of a_N, $a_N^{\bullet}$, such that it is unimportant how the stress distribution was established and if the normal compression increases or decreases, as long as partial slip continues. Equation (7.19) holds again :

$$p_2(p_2+2p_1) = 0 . \tag{7.44}$$

Again, we obtain the displacements from (7.2c), (7.45) :

$$e_2 = p_1(\zeta_2-\zeta_1^{\bullet}) + p_2(\zeta_2-\zeta_2^{\bullet}) , \tag{7.45}$$

The semiaxis $a_1^{\bullet}$ resp. the corresponding compression $\zeta_1^{\bullet}$ was produced by the initial displacement ξ_1, when the contact area had the semiaxis a_1. Equation (7.6) yields :

$$p_1 \zeta_1^* = p_1 \zeta_1 - e_1 , \; s_1 = -p_1. \tag{7.46}$$

Insertion of equations (7.46) in (7.45) yields :

$$(\Delta e_2 + s_1 \Delta \zeta_2) = p_2 (\zeta_2 - \zeta_2^*). \tag{7.47}$$

We obtain the compression ζ_2^* by insertion of (7.46), (7.47) in (7.44) :

$$\zeta_2^* = \zeta_2 - \frac{(\Delta e_2')^2}{2s_1 \Delta e_2'}, \;\; \Delta e_2' = \Delta e_2 + s_1 \Delta \zeta_2 . \tag{7.48}$$

The condition (7.21) is necessary for the first point of instantaneous adhesion. Insertion of (7.6), (7.46) :

$$s_1 = -p_1 = -e_1/|e_1| , \tag{7.49}$$

and (7.6) in (7.21) yields :

$$e_2^2 < (e_1 - s_1 \Delta \zeta_2)^2 , \;\; \text{for instantaneous adhesion.} \tag{7.50}$$

Equations (7.49), (7.50) can be reformulated :

$$|e_2| = |e_1 + \Delta e_2| < |e_1| + \Delta \zeta_2 . \tag{7.51}$$

If the displacement e_2 is a function of the time t, we can divide (7.51) by the small time intervall Δt and get for the limit $\Delta t \rightarrow 0$:

$$c_x^2 \xi_1 \dot{\xi}_1 + c_y^2 \eta_1 \dot{\eta}_1 - f c_z \dot{\xi}_1 \sqrt{(c_x \xi_1)^2 + (c_y \eta_1)^2} < 0, \tag{7.52}$$

where the dot denotes the differentiation by the time. This condition is always necessary for instantaneous adhesion. Suppose, now, that condition (7.52) is valid and the contact area increases ($\dot{\zeta}_1 > 0$). After compressing the bodies, complete adhesion in the entire contact area takes place. Only if the semiaxis a_2^* of the stick area resp. the corresponding compression ζ_2^* is smaller than the semiaxis a_1 of the old contact area resp. ζ_1, the new slip area lies inside of the old slip area. If the new slip area lies outside of the old contact area, we have a first decrease of the stick area on the new part of the contact area, and (7.6) yields :

$$\Delta \zeta^* = (\zeta_2 - \zeta_2^*) = \sqrt{(c_x \Delta \xi)^2 + (c_y \Delta \eta)^2} / f c_z < \Delta \zeta = \zeta_2 - \zeta_1 . \tag{7.53}$$

Division by the time increment Δt and the limit $\Delta t \rightarrow 0$ yields :

$$\sqrt{(c_x \dot{\xi}_1)^2 + (c_y \dot{\eta}_1)^2} < f c_z \dot{\zeta}_1, \; \text{for complete adhesion,} \tag{7.54}$$

as a necessary condition that the new slip area does not overlay the old slip area. In the case of infinitely small increments occurs permanent, complete adhesion. Thus we can identify three different contact regimes :

1.) Condition (7.51) or (7.52) is satisfied and instantaneous adhesion occurs.

2.) Condition (7.53) or (7.54) is satisfied and permanent, complete adhesion takes place.

3.) Condition (7.51) or (7.52) is violated and the process of the first decrease of the stick area continues.

In case 3.) the new stick area superposes and eliminates the old stick area completely and the size of the stick area decreases. In Fig. 7.7 the conditions (7.51) and (7.53) are plotted for increasing and decreasing contact areas.
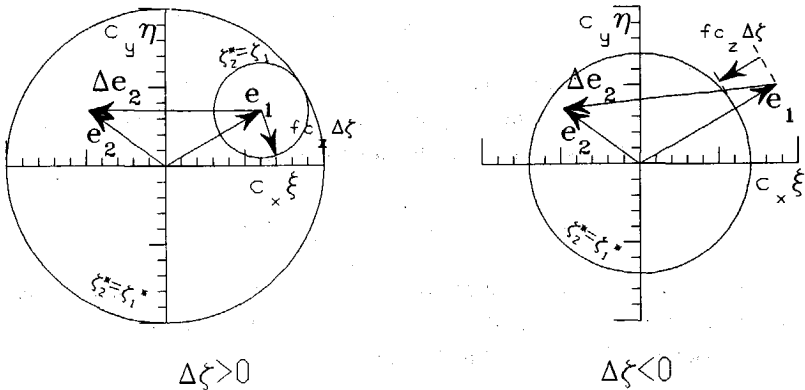

Fig. 7.7 : Equations (7.52) and (7.54) for varying contact areas.

This suggest a general procedure for load-histories, where the displacements are continuous functions of the time. At the beginning a small normal compression $\Delta\zeta$ and a tangential deformation $\Delta\xi$, $\Delta\eta$ is applied. Equation (7.54) defines, whether complete adhesion or partial slip takes place. If complete adhesion takes place, an incremental formulation defines the stresses and displacements, until partial slip occurs. An example for complete adhesion during impact will be calculated in section 9.3. In the case of partial slip, the old stress distribution in the stick area must be considered. As long as the direction of the displacement changes, all three contact regimes area possible. If the contact area decreases, instantaneous adhesion followed by a period of decreasing stick area is possible, but permanent complete adhesion over

a long period cannot take place, because equation (7.54) is always violated.

7.5 Further points of instantaneous adhesion for varying contact areas

We start with a stress distribution of section 7.4 and apply the additional displacements $\Delta\xi_N$, $\Delta\eta_N$, $\Delta\zeta_N$. The new stress distribution in the case of instantaneous adhesion is similar to (7.42) :

$$\sigma_t = \sum_{i=1}^{N-1} p_i \sigma_{CM}(a_{N-1}, a_i^*) + \sum_{i=1}^{N-1} p_i \sigma_{CM}(a_{N-1}, a_N) + p_N \sigma_{CM}(a_N, a_N^*) . \qquad (7.55)$$

Similar to section 7.4 the first term on the right hand side is the old stress distribution and the second and third term compensate the variation of the contact area and satisfy the boundary conditions. Equation (7.3c) inserted yields again:

$$\sigma_t = \sum_{i=1}^{N} p_i \sigma_{CM}(a_N, a_i^*) , \quad \left(\sum_{i=1}^{N} p_i\right)^2 = 1 . \qquad (7.56)$$

The stress distribution (7.56) depends only on the points of instantaneous adhesion and on the current values a_N, a_N^*, and is independent of the functions $\xi(a)$, $\eta(a)$. The total displacements e_N is defined by (7.2c) :

$$e_N = \sum_{i=1}^{N} p_i (\zeta_N - \zeta_i^*) , \quad e_N = e_{N-1} + \Delta e_N . \qquad (7.57)$$

The old displacement Δe_{N-1} was applied at the semiaxis a_{N-1} resp. ζ_{N-1}. The additional displacement Δe_N becomes :

$$\Delta e_N = e_N - e_{N-1} = \sum_{i=1}^{N-1} p_i \Delta\zeta_N + p_N(\zeta_N - \zeta_N^*) = -s_N \Delta\zeta_N + p_N(\zeta_{N-1} - \zeta_N^*). \qquad (7.58)$$

The slip direction s_N (7.34) inserted in (7.56) yields:

$$p_N(p_N - 2s_{N-1}) = 0 . \qquad (7.59)$$

We obtain the compression ζ_N^* by insertion of (7.58) in (7.59) :

$$\zeta_N^* = \zeta_{N-1} - \frac{(\Delta e_N^*)^2}{2(\Delta e_N^* s_N)} , \quad \Delta e_N^* = \Delta e_N + s_N \Delta\zeta_N , \quad \text{for } N > 2. \qquad (7.60)$$

Equations (7.58), (7.59) yield similar to (7.27) :

$$s_N \Delta e_N' = -s_{N-1} \Delta e_N' .$$ (7.61)

Introduction of the angles α_N', β_N similar to (7.28) in (7.61) yields :

$$\beta_N - \alpha_N' = \alpha_N' - \beta_{N-1} + \pi .$$ (7.62)

The angle α_N' is the angle of the vector $(\Delta e_N + \Delta \zeta_N \sigma_N)$. Relation (7.62) is drawn in figure 7.8. The condition for an increasing stick area is :

$$\zeta_N^* > \zeta_{N-1}^* .$$ (7.63)

Equation (7.60) in (7.63) yields :

$$\left. \begin{array}{l} |\Delta e_N'| < (2 \Delta \zeta_{N-1} + |\Delta e_{N-1}'| / \cos \gamma_{N-1}') \cos \gamma_N' , \\ \Delta e_N' = \Delta e_N + \Delta \zeta_N s_N , \quad \gamma_N' = \beta_{N-1} - \alpha_N' , \end{array} \right\} \text{ for } N > 2.$$ (7.64)
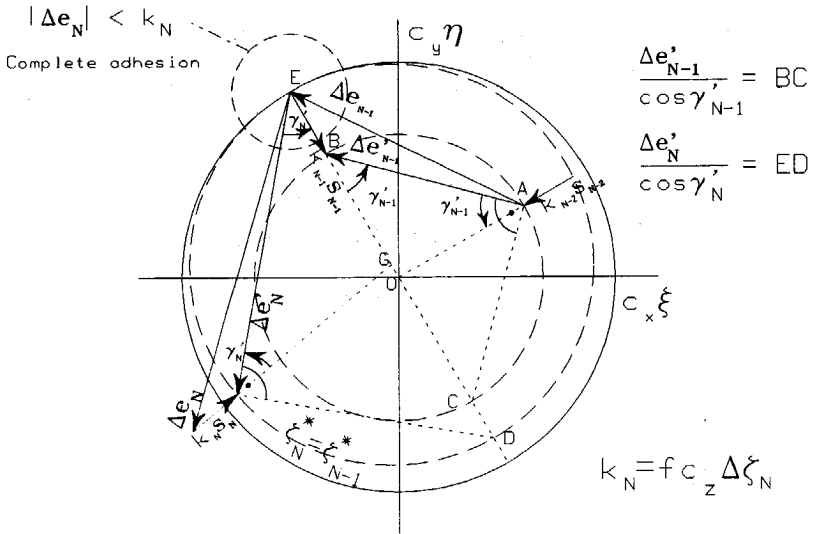

Fig. 7.8: The circle $\zeta_N^* = \zeta_{N-1}^*$ for e_N' in the case $\Delta \zeta_N > 0$.

Equation (7.64) defines the circles, which are plottet in figure 7.8 for positive $\Delta \zeta_{N-1}$, $\Delta \zeta_N$. The geometrical construction of these circles is similar to section 7.3 and can easily be seen in figure 7.8. The vector $\Delta e_N'$ must lie inside of the circle drawn with a

full line, in order to produce a further point of adhesion. The circle for complete adhesion is also plotted. The limits for the displacement ξ_2 in fig. 6.12a of section 6.6 are a special case of fig. 7.8 for $\gamma_N' = 180$.

7.6 Torsion

The stress distribution for pure torsion of spherical bodies was calculated by Lubkin (chapter 5.4). Formula (5.42) approximates Lubkin's formula for the torque. A similar approximation can be found for elliptical areas:

$$\frac{M_z}{M_{ZS}} = 1 - \exp\left(\frac{-M_{ZA}'}{M_{ZS}} \beta \right) ,$$

$$M_{ZS} = \lim_{\beta \to \infty} M_z = \frac{3}{8} f_{STAT} F_Z b E(k) ,$$

$$M_{ZA}' = \lim_{\beta \to \emptyset} \left(\frac{dM_z}{d\beta} \right) = \frac{3}{8} G b^3 E(k) \delta_T , \qquad (7.65)$$

$$\delta_T = \frac{16}{9E(k)} \quad \frac{\pi\left(E(k) \frac{1}{G} - 4C(k)(1-k^2) \frac{\nu}{G} \right)}{\left(B(k)D(k) \frac{1}{G} - C(k)E(k) \frac{\nu}{G} \right)}$$
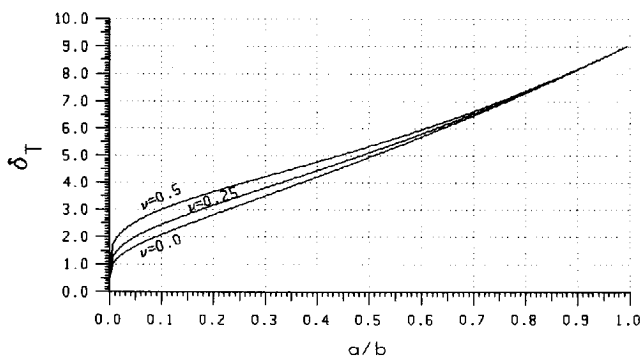
Fig. 7.9: The variable δ_T of formula (7.65).

with the elliptical integrals B(k), C(k), D(k) and E(k) defined by (5.13), (5.33); M_{ZS}, is the torque for complete sliding and M_{ZA}' from (5.35) the slope for $\beta = 0$ (β dimensionless). The stiffness δ_T is plotted in figure 7.9, similar to the compliance in fig. 5.4, defined by formula (5.35). Fig. 7.10 shows the torque of the numerical (marker) and the theoretical solution (full line), for a/b = 1 and a/b = 10. The approximation (7.65) corresponds very well with the numerical solution, even in the case of dissimilar materials. Furthermore it turns out, that the numerical results for an area of integration with 50 points differ only slightly from the results with 400 points.
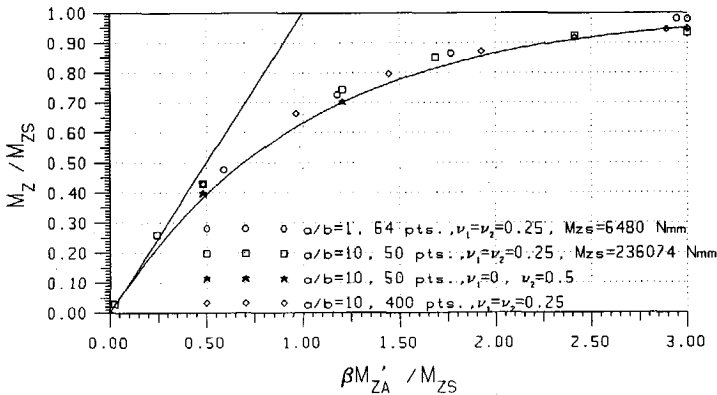

Fig. 7.10: The torque M_z as function of the twisting angle β (dimensionless).

Equation (7.65) can be generalized for load-histories with varying torque. The basic idea is, that similar to Mindlin & Deresiewicz's theory for varying forces (chap. 6) a opposite stress distribution overlays the old stick area, when the angle β is reduced after having reached the value β_1. Since the stiffness at the beginning of the reduction must be equal to the initial stiffness, and the torque at $\beta = -\beta_1$ must be opposite to the value for $\beta = \beta_1$, the formula for the torque can be deduced similarly to equation of section 6.2:
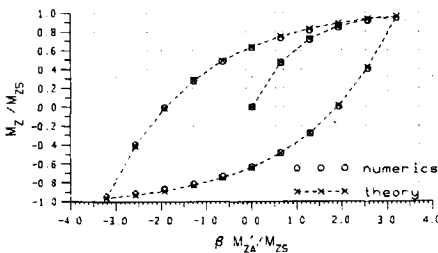

Fig. 7.11: Varying torque with a/b = 1/10, $\nu_1 = \nu_2 = 0$.

$$\frac{M_{Z1}-M_Z}{2M_{ZS}} = 1 - \exp\left[\frac{-M'_{ZA}}{2M_{ZS}}(\beta-\beta_1)\right].\qquad(7.66)$$

This method is only an approximation, because the exact stress distribution and the form of the stick area are unknown, but the results agree very well with the empirical results. A correct analytical solution is very difficult, because the influence of different materials and the elliptical contact area make this problem unsolvable.
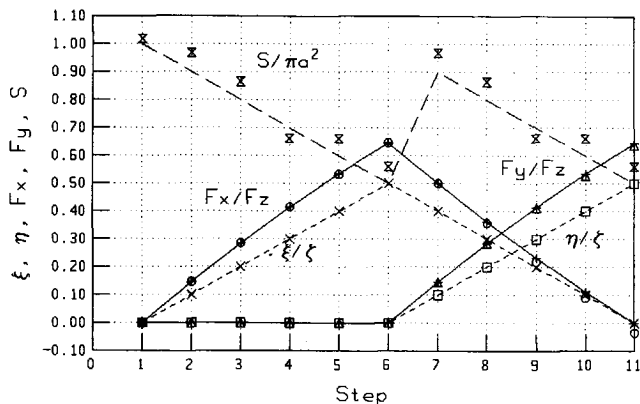
7.7 Examples

Fig. 7.12: Theoretical (lines) and numerical (markers) forces and displacements for example 1.

In the first step of example 1 (fig. 7.12) we compress two similar spheres by the value ζ_1. Subsequently we apply a tangential deformation ξ_1, consisting of 5 increments, in x-direction. Poisson's number was taken zero, the modulus of rigidity was equal for both materials, the coefficient of friction was taken one and the area of integration consisted of 100 points. The value of ξ_1 was half the value of the corresponding normal compression, which is necessary to generate total slip ($\zeta_1^* = \zeta_1/2$). In the next step we superpose the additional displacement $\Delta\xi_2$ at an angle of 135° to the positive x-axis in 5 increments, such that the old stick area is overlaid by the new one in the last step. The forces F_x, F_y, the displacements ξ, η and the stick area S are

plottet in figure 7.13 It is obvius, that the simplified solution for the force does not differ much from the numerical solution. The first point of instantaneous adhesion occurs in step 7, where the size of the stick area S becomes maximal.
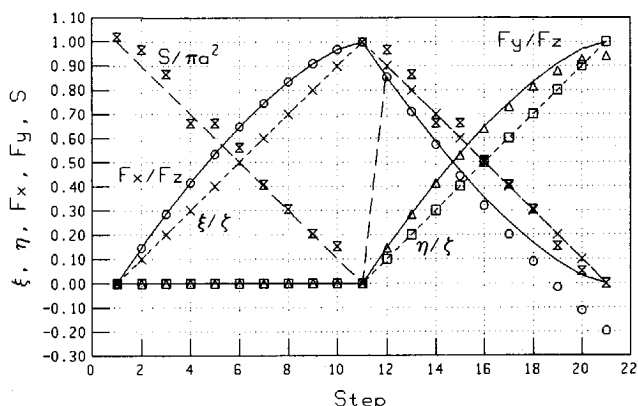

Fig. 7.13: Theoretical (lines) and numerical results for example 2.

The next example is similar to example 1, except that it consists of 21 steps and ξ_1 was increased to the value, which is necessary to produce total slip ($\zeta_1^* = 0$). The displacement ξ_1 was applied in 10 steps. In the following step we superpose the additional displacement ξ_2, in the same direction as in the example before, until complete sliding takes place ($\zeta_2^* = \zeta_1^* = 0$), in 10 steps. Figure 7.14 shows the force and displacements. The difference between the simplified and the numerical solution is larger than in the example before, because the slip area is larger. In all three examples the theory predicted the point of instantaneous adhesion correctly.

In the last example 3 the additional displacement ξ_2 is applied at an angle of 165° to the x-axis, after application of the same displacement ξ_1 as in the example before. The load-history was applied in 21 steps again. The difference between the numerical and the theoretical force is shown in fig. 7.15. The slip and stress-directions of the numerical solution for the last step are plottet in fig. 7.15 (the stress points to the left, crosses mark the centers of the elements). The slip angle varies between -15° at the border and -35° in the center of the contact area. The constant angle of the theory amounts to -30°. It turns out that the simplified solution is a good approximation for $\alpha_2 \approx 180°$, even for large slip areas.
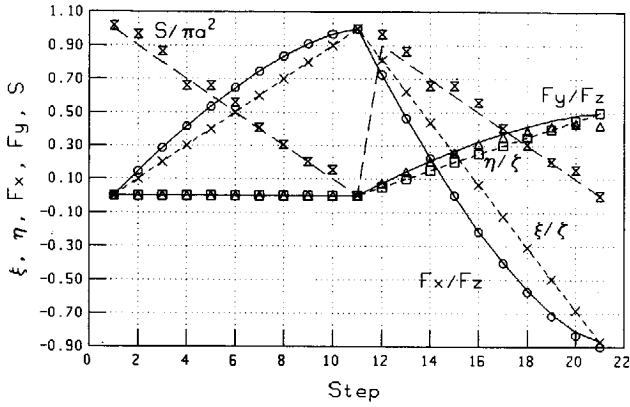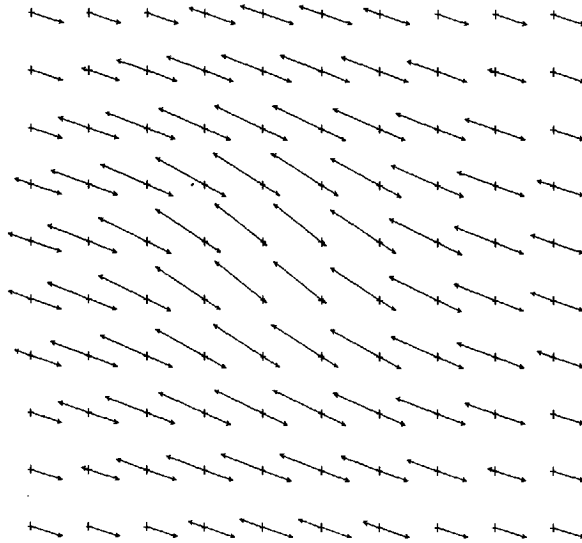
Fig. 7.14: Theoretical (lines) and numerical (markers) results for example 3.

Step= 21, Slip and stress directions

Fig 7.15: Slip and stress directions of the numerical solution for step 21 of example 3.

8 The basic equations for the impact of two bodies

The basic equations for the impact of two bodies are the equations of motion and the contact law for the forces and displacements in the contact point. We presuppose that the surfaces of the two bodies are given analytically in the coordinate system of the principal axes of inertia, which we will call the *inertial base*. This is the case for geometrically simple bodies like cylinders, spheres, ellipsoids etc. The principle curvatures in the initial contact point O, where the bodies touch first, must be known, in order to describe the contact law in the manner of the Hertz and the Cattaneo-Mindlin theory. We develop the surface equation as a Taylor-series at the contact point, and obtain the principal curvatures and the orientation of the local coordinate system of the curvatures in the initial contact point, which we will call the *contact base*. Therefore the first order resp. second order derivatives of the surfaces are necessary. If the surfaces are given in form of a set of discrete points, the differentiations must be performed numerically and the tensor of inertia must be calculated by numerical integration.

In section 8.1 we will derive the formulae for the orientation of the contact base and the principal curvatures, for the case that the coordinate c of the surface is given as a function of a,b: c(a,b). The equations of motion are presented in section 8.2 in form of a system of ordinary diffential equations. Finally, in section 8.3-8.5, the contact law is deduced for the contact regimes of full adhesion, partial slip and rigid body sliding.

8.1 The principal axes of inertia and the principal curvatures

Suppose that the surfaces of the two bodies are prescribed in the inertial base. Any vector $(x,y,z)^T$ given in the contact base can be transformed to the inertial base of the corresponding body:

$$t''' = (a,b,c)^T = \Pi\, t \,, \quad t = (x,y,z)^T = \Pi^{-1}\, t''' \,, \quad \Pi^{-1} = \Pi^T \,, \qquad (8.1)$$

where a,b,c denote the coordinates of t''' in the inertial base and x,y,z the components of t in the contact base. The transformation matrix has the components :

$$\Pi = \begin{vmatrix} e_a e_x & e_a e_y & e_a e_z \\ e_b e_x & e_b e_y & e_b e_z \\ e_c e_x & e_c e_y & e_c e_z \end{vmatrix} = \begin{vmatrix} \Pi_{ax} & \Pi_{ay} & \Pi_{az} \\ \Pi_{bx} & \Pi_{by} & \Pi_{bz} \\ \Pi_{cx} & \Pi_{cy} & \Pi_{cz} \end{vmatrix} . \tag{8.2}$$

The coordinate system e_a, e_b, e_c is thought to be the result of three successive rotations. Before the first rotation both coordinate systems coincide. The first rotation is carried out about the e_z-axis at an angle of γ whereby e_y turns into e_y' (Fig. 8.1). The second rotation is carried out about the new axis e_y' at an angle β. The final orientation is produced by a rotation about the new axis e_a at an angle α. The equations of the transformations for each rotation are :

$$t' = \Pi_\gamma t \;,\; t'' = \Pi_\beta t' \;,\; t''' = \Pi_\alpha t'' \;,\; \tag{8.3}$$

with :

$$\Pi_\gamma = \begin{vmatrix} \cos\gamma & \sin\gamma & 0 \\ -\sin\gamma & \cos\gamma & 0 \\ 0 & 0 & 1 \end{vmatrix} \;,\; \Pi_\beta = \begin{vmatrix} \cos\beta & 0 & -\sin\beta \\ 0 & 1 & 0 \\ \sin\beta & 0 & \cos\beta \end{vmatrix} \;,\; \Pi_\alpha = \begin{vmatrix} 1 & 0 & 0 \\ 0 & \cos\alpha & \sin\alpha \\ 0 & -\sin\alpha & \cos\alpha \end{vmatrix} . \tag{8.4}$$
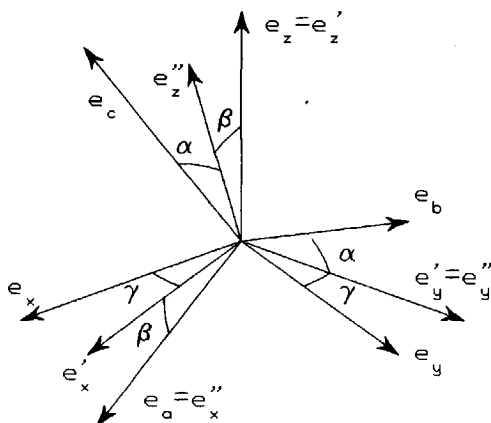

Fig. 8.1: The rotations of the coordinate base.

The transformation matrix Π follows from equations (8.3) and (8.4) :

$$\Pi = \Pi_\alpha \Pi_\beta \Pi_\gamma \;,\; \tag{8.5a}$$

$$\Pi = \begin{vmatrix} \cos\beta\cos\gamma & \cos\beta\sin\gamma & -\sin\beta \\ \sin\alpha\sin\beta\cos\gamma - \cos\alpha\sin\gamma & \sin\alpha\sin\beta\sin\gamma + \cos\alpha\cos\gamma & \sin\alpha\cos\beta \\ \cos\alpha\sin\beta\cos\gamma - \sin\alpha\sin\gamma & \cos\alpha\sin\beta\sin\gamma - \sin\alpha\cos\gamma & \cos\alpha\cos\beta \end{vmatrix} . \tag{8.5b}$$

This coordinate system can be transformed into a system with the Euler angles (ψ,θ,ϕ), with ψ as the first rotation and θ the second (Wittenburg, 1977), by replacing (ψ,θ,ϕ) with $(\gamma+\pi/2,\beta+\pi/2,\alpha)$ and the resulting vector base (e_a,e_b,e_c) with (e_b,e_c,e_a) in equation (8.2).

Suppose that the surfaces of the bodies are given implicitly in the base of the principal axes :

$$f(a,b,c) = 0 . \tag{8.6}$$

Taylor's formula at the contact point (a_0,b_0,c_0) yields :

$$f_{,i}(i-i_0) + \frac{1}{2} f_{,ij}(i-i_0)(j-j_0) + ... = 0, \quad i,j = a,b,c, \quad i_0,j_0 = a_0,b_0,c_0. \tag{8.7}$$

with the abbreviations:

$$\frac{\partial f}{\partial i}\bigg|_{i=i_0} = f_{,i}\ , \quad \frac{\partial^2 f}{\partial i \partial j}\bigg|_{i=i_0,\ j=j_0} = f_{,ij}\ , \quad ... \tag{8.8}$$

The third order terms $(a-a_0)^3$, $(a-a_0)^2(b-b_0)$, etc. in (8.7) are neglected. In (8.7)-(8.10) Einstein's summation convention is used and the indices i,j are summarized over a,b,c. We insert the transformation :

$$i-i_o = \Pi_{ik}k\ , \quad k = x,y,z\ , \tag{8.9}$$

in equation (8.7). The origin of the contact base (x,y,z) is the initial contact point (a_0,b_0,c_0). Reorganization of the formula with respect to k yields :

$$k\,f_{,i}\,\Pi_{ik} + \frac{1}{2}\,k\,l\,f_{,ij}\,\Pi_{ik}\,\Pi_{jl} = 0\ , \quad i,j = a,b,c, \quad k,l = x,y,z. \tag{8.10}$$

Remembering that the distance z between the two surfaces is quadratic in x and y, we neglect the third order terms zx, zy, z^2. Hence all factors with z dissapear in the second term of (8.10). The transformation angles (α,β,γ) must be selected such that formula (8.10) has the form:

$$z = \frac{1}{2}\,k_x x^2 + \frac{1}{2}\,k_y y^2 . \tag{8.11}$$

To eliminate the factors $f_{,i}\,\Pi_{ix}$ of x and $f_{,i}\,\Pi_{iy}$ of y in equation (8.10), we choose α, β
with (8.5) such that $f_{,i}$ is parallel to the third column of Π_{ik} in (8.5) :

$$\frac{\Pi_{bz}}{\Pi_{cz}} = \frac{f_b}{f_c} = \tan\alpha\ , \quad \frac{\Pi_{az}}{\Pi_{cz}} = \frac{f_a}{f_c} = \frac{-\tan\beta}{\cos\alpha}\ . \tag{8.12}$$

With equation (8.12) and definition (8.2) the two factors of x and y in equation (8.10) represent the scalar products $(e_x e_z)$ and $(e_y e_z)$, which disappear. To eliminate the factor of xy in (8.10) also, we insert equation (8.5) in (8.10) and get a quadratic equation for $\sin\gamma$. To simplify the procedure we set $c = c(a,b)$, i.e. the surface is given explicitely :

$$f(a,b,c) = -c + c(a,b) = 0 \ . \tag{8.13}$$

Insertion of (8.13) in (8.12) yields :

$$\tan\alpha = -\frac{\partial c}{\partial b}, \quad \tan\beta = \cos\alpha\frac{\partial c}{\partial a} = \frac{\dfrac{\partial c}{\partial a}}{\sqrt{1+\left(\dfrac{\partial c}{\partial b}\right)^2}} \ . \tag{8.14}$$

Equation (8.3) shows, that the base $(e_x' e_y' e_z')$ lies in the tangential plane and has to be rotated at the angle $-\gamma$ to point into the direction of the principal curvatures. Equation (8.10) yields after insertion of (8.13) :

$$\frac{z}{\Pi_{cz}} = \frac{1}{2} x'^2(c_{aa}\Pi_{ax}^2 + c_{bb}\Pi_{bx}^2 + 2c_{ab}\Pi_{ax}\Pi_{bx}) + \frac{1}{2} y'^2(c_{aa}\Pi_{ay}^2 + c_{bb}\Pi_{by}^2 + 2c_{ab}\Pi_{ay}\Pi_{by}) +$$
$$+ x'y'[c_{aa}\Pi_{ax}\Pi_{ay} + c_{bb}\Pi_{bx}\Pi_{by} + c_{ab}(\Pi_{ax}\Pi_{by} + \Pi_{ay}\Pi_{bx})] \ . \tag{8.15}$$

Equations (8.5) with $\gamma = 0$ are inserted in (8.15) :

$$z = \frac{1}{2} x'^2 \cos\alpha \cos\beta \ (c_{aa}\cos^2\beta + c_{bb}\sin^2\alpha \cos^2\beta + 2c_{ab}\sin\alpha \sin\beta \cos\beta) +$$
$$+ \frac{1}{2} y'^2 c_{bb} \cos^3\alpha \cos\beta + x'y' \cos^2\alpha \cos\beta \ (c_{bb}\sin\alpha \sin\beta + c_{ab}\cos\beta) \ , \tag{8.16}$$

and abbreviated to :

$$z = \frac{1}{2} k_x' x'^2 + \frac{1}{2} k_y' y'^2 + k_{xy}' x'y'. \tag{8.17}$$

The first equation in (8.3) is inserted in (8.17), with the result :

$$z = \frac{1}{2} x^2(k_x'\cos^2\gamma + k_y'\sin^2\gamma - 2k_{xy}'\sin\gamma \cos\gamma) + \frac{1}{2} y^2(k_x'\sin^2\gamma + k_y'\cos^2\gamma + 2k_{xy}'\sin\gamma \cos\gamma)$$
$$+ xy[(k_x' - k_y')\sin\gamma \cos\gamma + k_{xy}'(\cos^2\gamma - \sin^2\gamma)] \ . \tag{8.18}$$

Setting the last term in square brackets zero, we obtain :

$$\tan\gamma = \frac{k_x' - k_y'}{2k_{xy}'} \pm \sqrt{\frac{k_x' - k_y'}{2k_{xy}'} + 1} \ . \tag{8.19}$$

Elimination of k_{xy}' from the other two brackets in (8.18) yields with (8.11) :

$$k_x = \frac{k_x' \cos^2\gamma - k_y' \sin^2\gamma}{\cos^2\gamma - \sin^2\gamma \cos^2\gamma - \sin^2\gamma} \qquad k_y = \frac{-k_x' \sin^2\gamma + k_y' \cos^2\gamma}{} .$$ (8.20)

We write :

$$D = \frac{k_x' - k_y'}{2k_{xy}'} ,$$ (8.21)

and simplify equations (8.20) with the formula :

$$\tan^2\gamma = 1 + 2D^2 \pm 2D\sqrt{D^2 + 1} .$$ (8.22)

We insert (8.14) and (8.16) in (8.17) and summarize all results :

$$\sin \alpha = \frac{-c_b}{\sqrt{1+c_b^2}} , \quad \cos \alpha = \frac{1}{\sqrt{1+c_b^2}} ,$$

$$\sin \beta = \frac{c_a}{\sqrt{1+c_a^2+c_b^2}} , \quad \cos \beta = \frac{\sqrt{1+c_b^2}}{\sqrt{1+c_a^2+c_b^2}} ,$$ (8.23a)

$$k_x' = \frac{1}{(1+c_a^2+c_b^2)^{3/2}} \left\{ c_{aa}(1+c_b^2) + \frac{c_{bb}c_a^2c_b^2}{1+c_b^2} - 2c_{ab}c_ac_b \right\} ,$$

$$k_y' = \frac{c_{bb}}{(1+c_b^2)\sqrt{1+c_a^2+c_b^2}} , \quad k_{xy}' = \frac{c_{ab}(1+c_b^2)-c_{bb}c_ac_b}{(1+c_b^2)(1+c_a^2+c_b^2)} ,$$

$$\tan \gamma = \frac{k_x'-k_y'}{2k_{xy}'} (\bar{+}) \sqrt{\frac{k_x'-k_y'}{2k_{xy}'} + 1} ,$$ (8.23b)

$$\gamma_y = \pi/2 + \gamma_x , \quad \text{because } \gamma_x < 0 ,$$

$$k_{x(y)} = \frac{1}{2} (k_x'+k_y') (\pm) \sqrt{\frac{1}{4} (k_x'+k_y')^2 + k_{xy}'^2 - k_x'k_y'} .$$

We selected the sign of the root such that, for $k_{xy}' = 0$:

$$\gamma_{x(y)} = 0 \ (\pi/2) , \quad k_{x(y)} = k_x' \ (k_y') , \quad \text{for } k_{xy}' = 0.$$ (8.24)

8.2 The equations of motion

The local base, introduced in section 8.1, will be used for the dynamic equations, because the nonlinear contact law is difficult to transform into another coordinate system. It shall be fixed in space with its origin at the initial contact point O of the

two bodies. The contact area will shift relative to this coordinate system, but we assume that the impact duration T is infinitesimally short, such that the rotation is much smaller than the dimensions of the bodies and the material contact point remains in the center of the contact areas.

For infinitesimally small impact durations the gravitational forces, springs, dampers and similar elements in the hinges of a system do not play any role, since they exert forces and torques of finite magnitude, whose integrals over the infinitesimal short time interval T are zero. In classical mechanics it is assumed that T tends toward zero: $T \rightarrow 0$, and the magnitude of the impulsive force F_i tends toward infinity during T (Wittenburg, 1977). It was proved by Hunter (1957), that the energy loss for bulky bodies is negligible, as long as the impact velocity is smaller than the velocity of compressive waves in thin elastic rods. Eason (1966) found, that the displacement produced by a suddenly applied, constant pressure distribution on a circular area, reaches its statically equivalent value after the time, which elastic waves need, to run through the diameter of the loaded area. Hence, the bodies can be idealized as rigid bodies in their global behaviour, while elastic deformations take place locally, in a small volume surrounding the contact point. We obtain the equations of motion, which are necessary to study the phenomena during impact, by differentiation of the linear and angular impulse- and momentum laws (Wittenburg, 1977):

$$m_i \, \ddot{x}_{iM} = F_i \, , \quad \frac{d}{dt} \, (\theta_i \omega_i) = \theta_i \dot{\omega}_i + \omega_i \times (\theta_i \omega_i) = R_i \times F_i \, , \quad i = 1, 2, \qquad (8.25)$$

where m_i denotes the mass and θ_i the tensor of gyroscopic inertia of body i; R_i signifies the vector from the initial center of gravity to the initial contact point of the two bodies, neglecting the small elastic deformations (see fig. 8.2); ω_i denotes the vetor of rotation of body i; x_{iM} is the coordinate of the center of gravity of body i in the local base; t is the time.

In (8.25) we neglect the internal moments in the contact area, because for Hertzian contact problems the contact radius is always very small compared to the dimension R_i of the bodies, and thus the stress inside of the contact area has a very small lever-arm compared to the forces F_i. For the same reason we neglect the small dislocation of the resulting forces F_i in the case of different materials and assume, that they act in the contact point. The influence of the spin around the z-axis on the tangential stress distribution and the location of the stick area will be analysed in chapter 14. In the case of non-Hertzian contact areas the numerical theory of chapters 11 or 12 must be used for the contact law and the equations of motion must be integrated numerically. In this case we also perform the coordinate transformations numerically.
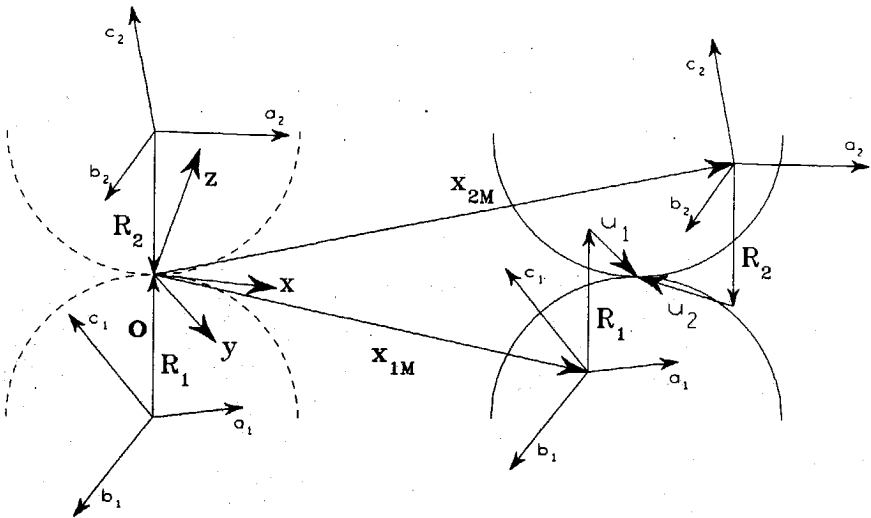
Fig. 8.2: The bodies at the beginning of contact (left) and during impact (right).

If the reciprocal value of the impact duration is large compared to the absolute value of the rotational velocity ω_i, it can be shown that the term $d\omega_i/dt$ is large compared to the square of the angular velocity ω_i^2. In other words the impact duration is assumed to be very small compared to the time $2\pi/|\omega_i|$ for one rotation around the axis of ω_i, i.e. the rotational motion is infinitesimal. Then we can neglect the cross product on the left side of the angular momentum equation, which is important for slow dynamical effects only. Thus we obtain from (8.25):

$$\theta_i \dot{\omega}_i = R_i \times F_i , \quad i = 1, 2, \tag{8.26}$$

Keller (1986) developed an impact theory for complete sliding with reversing slip directions, based on a very similar mathematical formulation. Our theory, however, predicts a period of adhesion with partial slip in the case of reversing slip directions. Now we introduce the 'Rigid body velocities' v_{rig} and the 'Absolute velocities' v_{abs} of the two bodies in the contact point:

$$v_{rig,i} = \dot{x}_{iM} + \omega_i \times R_i , \quad v_{abs,i} = v_{rig,i} + \dot{u}_i , \tag{8.27}$$

with the elastic displacement vectors u_i. We differentiate (8.27) and neglect the coriolis and gyroscopic terms analogously to the neglection in equ. (8.26):

$$\dot{v}_{rig,i} = \ddot{x}_{iM} + \dot{\omega}_i \times R_i \ , \ \dot{v}_{abs,i} = \dot{v}_{rig,i} + \ddot{u}_i \ . \tag{8.28}$$

We insert equations (8.25), (8.26) in (8.28) and get after a second differentiation:

$$\ddot{v} = \ddot{v}_{rig,2} - \ddot{v}_{rig,1} = -D \cdot \dot{F}_1 , \tag{8.29a}$$

$$D\dot{F}_1 = \sum_{i=1}^{2} \left\{ D_i \dot{F}_1 + \frac{1}{m_i} \cdot \dot{F}_1 \right\} , \tag{8.29b}$$

$$D_i \dot{F}_1 = \left[\theta_i^{-1}(R_i \times \dot{F}_1) \right] \times R_i , \tag{8.29c}$$

where we introduced the symbols D_i, which we will use later, and the *relative rigid body velocity* $v = (\dot{x}, \dot{y}, \dot{z})$, i.e. the velocity of body 2 relative to body 1. The first equation in (8.29) is the basic differential equation of our impact theory. In equations (8.29) we used Newton's principle of actio and reactio which states, that the contact force F_1 on body 1 is equal and opposite to the force F_2 on body 2. The components of the matrix D_i can be determined by transformation into the diagonal system of θ_i and back transformation. We show this for the first term D_1 in (8.29c). In the next three equations (8.30), (8.31), (8.32) we will omit the index 1 to simplify notation. In the diagonal system the tensor θ and the vector R have the form:

$$\theta_{DS} = \begin{bmatrix} \theta_a & 0 & 0 \\ 0 & \theta_b & 0 \\ 0 & 0 & \theta_c \end{bmatrix} , \ R_{DS} = \begin{bmatrix} a \\ b \\ c \end{bmatrix} , \tag{8.30}$$

where the indices DS denote the Diagonal Coordinate System of θ. Matrix D_1 has now the form:

$$D_{DS} = \left[\theta^{-1}(R \times \dot{F}) \right] \times R \Big|_{DS} = \begin{bmatrix} \dfrac{c^2}{\theta_b} + \dfrac{b^2}{\theta_c} & \dfrac{-ab}{\theta_c} & \dfrac{-ac}{\theta_b} \\ \dfrac{-ab}{\theta_c} & \dfrac{c^2}{\theta_a} + \dfrac{a^2}{\theta_c} & \dfrac{-bc}{\theta_a} \\ \dfrac{-ac}{\theta_b} & \dfrac{-bc}{\theta_a} & \dfrac{b^2}{\theta_a} + \dfrac{a^2}{\theta_b} \end{bmatrix} \begin{bmatrix} \dot{F}_a \\ \dot{F}_b \\ \dot{F}_c \end{bmatrix} . \tag{8.31}$$

We transform the matrix back into the coordinate system of chapter 3 using the transformation matrix Π, which transforms a vector into the diagonal system:

$$D = \Pi^{-1} D_{DS} \Pi , \quad F_{DS} = \Pi F. \tag{8.32}$$

We perform the same procedure for the matrix D_2, with a different transformation matrix Π. Now we introduce the indices 1 and 2 again. The following formula for D

can be proved by a componentwise evaluation :

$$D_{ik} = \left\{ (R_1 \times e_i)^T [\theta_1^{-1}(R_1 \times e_k)] \right\} \Big|_{DS1} + \left\{ (R_2 \times e_i)^T [\theta_2^{-1}(R_2 \times e_k)] \right\} \Big|_{DS2} + \delta_{ik}\left(\frac{1}{m_1} + \frac{1}{m_1}\right),$$

$$
\begin{aligned}
(e_i^T)_{DS} &= (\, \Pi_{ai}, \, \Pi_{bi}, \, \Pi_{ci} \,), \\
i, \, k &= x, \, y, \, z,
\end{aligned}
\qquad
\delta_{ik} = \begin{cases} +1, & \text{for } i=k, \\ 0, & \text{for } i \neq k. \end{cases}
\tag{8.33}
$$

We reformulate the equations (8.25), (8.26) :

$$\dot{\omega}_i = \theta_i^{-1} (R_i \times F_i) = \theta_i^{-1} \left[R_i \times \ddot{x}_{iM} \right] m_i, \tag{8.34}$$

and integrate (8.34) :

$$\omega_i - \omega_{iA} = m_i \theta_i^{-1} \left[R_i \times (\dot{x}_{iM} - \dot{x}_{iMA}) \right]. \tag{8.35}$$

where the index A denotes the values at the beginning of impact. Insertion of (8.35) in (8.27), (8.29a) yields :

$$
\begin{aligned}
\dot{x}_{1M} + \omega_{1A} \times R_1 + m_1 \left\{ \theta_1^{-1} [R_1 \times (\dot{x}_{1M} - \dot{x}_{1MA})] \right\} \times R_1 = \\
\dot{x}_{2M} + \omega_{2A} \times R_2 + m_2 \left\{ \theta_2^{-1} [R_2 \times (\dot{x}_{2M} - \dot{x}_{2MA})] \right\} \times R_2 - v.
\end{aligned}
\tag{8.36}
$$

We integrate the first equation of (8.25) :

$$m_1(\dot{x}_{1M} - \dot{x}_{1MA}) = -m_2(\dot{x}_{2M} - \dot{x}_{2MA}), \tag{8.37}$$

and get after insertion in (8.36) :

$$m_1 D(\dot{x}_{1M} - \dot{x}_{1MA}) = \dot{x}_{2MA} - \dot{x}_{1MA} + \omega_{2A} \times R_2 - \omega_{1A} \times R_1 - v. \tag{8.38}$$

Equation (8.35) can be transformed to the diagonal system of body i :

$$(\omega_i - \omega_{iA})_{DSi} = m_i \theta_{iDSi}^{-1} \left\{ R_{iDSi} \times \left[\Pi(\dot{x}_{iM} - \dot{x}_{iMA}) \right] \right\}. \tag{8.39}$$

Retransformation to the coordinate system of principal curvatures yields with (8.32) :

$$\omega_i - \omega_{iA} = m_i \Pi_i^T \theta_{iDS}^{-1} \left\{ R_{iDS} \times \left[\Pi_i (\dot{x}_{iM} - \dot{x}_{iMA}) \right] \right\} = E_i(\dot{x}_{iM} - \dot{x}_{iMA}). \tag{8.40}$$

The components of E_i are :

$$[E_{ik}]_N = m_N \left\{ (\theta^{-1}e_i)^T (R \times e_k) \right\} DS \text{ of body } N. \tag{8.41}$$

If v is known, all the other unknown variables $\dot{x}_1$, $\dot{x}_2$, ω_1, ω_2 can be evaluated. Summarization of the formulae (8.29), (8.36), (8.37), (8.41) yields :

$$\ddot{\mathbf{v}} = -\mathbf{D}\dot{\mathbf{F}}_1 \, ,$$

$$m_1 \mathbf{D}(\dot{\mathbf{x}}_{1M} - \dot{\mathbf{x}}_{2M}) = \dot{\mathbf{x}}_{2MA} - \dot{\mathbf{x}}_{1MA} + \boldsymbol{\omega}_{2A} \times \mathbf{R}_2 - \boldsymbol{\omega}_{1A} \times \mathbf{R}_1 - \mathbf{v} \, ,$$

$$m_2(\dot{\mathbf{x}}_{2M} - \dot{\mathbf{x}}_{2MA}) = -m_1(\dot{\mathbf{x}}_{1M} - \dot{\mathbf{x}}_{1MA}) \, ,$$

$$\boldsymbol{\omega}_1 - \boldsymbol{\omega}_{1A} = m_1 \mathbf{E}_1(\dot{\mathbf{x}}_{1M} - \dot{\mathbf{x}}_{1MA}) \, , \quad \boldsymbol{\omega}_2 - \boldsymbol{\omega}_{2A} = m_2 \mathbf{E}_2(\dot{\mathbf{x}}_{2M} - \dot{\mathbf{x}}_{2MA}) \, .$$

(8.42)

The matrices **D** and **E** are defined by :

$$\mathbf{D} = \mathbf{G}_1^T \mathbf{D}_{1DS} \mathbf{G}_1 + \mathbf{G}_2^T \mathbf{D}_{2DS} \mathbf{G}_2 + \left(\frac{1}{m_1} + \frac{1}{m_1} \right) \mathbf{I} \, ,$$

$$\mathbf{E}_i = \mathbf{F}_i \mathbf{G}_i \, ,$$

(8.43)

$$\mathbf{G}_i = [\mathbf{R} \times \mathbf{e}_x, \ \mathbf{R} \times \mathbf{e}_y, \ \mathbf{R} \times \mathbf{e}_z]_{\text{body } i} \, , \quad \left. \begin{array}{l} \text{all components are} \\ \text{defined in the diagonal} \\ \text{system of body } i, \end{array} \right.$$

$$\mathbf{F}_i = [\boldsymbol{\theta}^{-1}\mathbf{e}_x, \ \boldsymbol{\theta}^{-1}\mathbf{e}_y, \ \boldsymbol{\theta}^{-1}\mathbf{e}_z]_{\text{body } i} \, ,$$

$$i = 1, \ 2, \ \text{no summation over } i.$$

Each vector in square brackets in (8.43) is thought to be a column of the matrices $\mathbf{F}_i$, $\mathbf{G}_i$. $\mathbf{I}$ is the identity matrix. The vector $\mathbf{R}_i$ has the components $(a,b,c)_i$ in the diagonal system of body i and the vectors $(\mathbf{e}_k)_i$, $(\mathbf{R} \times \mathbf{e}_k)_i$ in the corresponding diagonal system are:

$$(\mathbf{e}_k)_i = \begin{pmatrix} \Pi_{ak} \\ \Pi_{bk} \\ \Pi_{ck} \end{pmatrix}_{\text{body } i} \, , \quad (\mathbf{R} \times \mathbf{e}_k)_i = \begin{pmatrix} b\Pi_{ck} - c\Pi_{bk} \\ c\Pi_{ak} - a\Pi_{ck} \\ a\Pi_{bk} - b\Pi_{ak} \end{pmatrix}_{\text{body } i} \, . \quad (8.44)$$

Π_{ak} are the components of the matrix $\boldsymbol{\Pi}_i$ defined by (8.2), (8.32)

Equation (8.29) is the basic differential equation, with the unknown rigid body velocity $\mathbf{v}$ and the contact force $\mathbf{F}_1$. We have a contact law of the form:

$$\mathbf{F}_1 = \mathbf{F}_1(\boldsymbol{\xi}, \dot{\boldsymbol{\xi}}) \, , \quad \boldsymbol{\xi} = \mathbf{u}_1 - \mathbf{u}_2, \quad (8.45)$$

with $\boldsymbol{\xi}$ from (5.19). For complete adhesion the absolute velocity $\mathbf{v}_{abs,i}$ of eq. (8.27) in the contact point of body 1 and 2 will be equal. Thus we obtain :

$$\mathbf{v} = \dot{\boldsymbol{\xi}} \, , \quad \text{for complete adhesion.} \quad (8.46)$$

Equ. (8.46) is the kinematical law of adhesion. The equations (8.29), (8.45) and (8.46) represent a differential equation system for the nine components of the variables $\mathbf{v}$, $\mathbf{F}_1$ and $\boldsymbol{\xi}$ in the case of complete adhesion. Equations (8.29) and (8.46) hold for partial slip too, because the contact point will stick in this case and partial

slip is assumed to take place on an elliptical ring outside of the stick area.

In the case of complete sliding, equation (8.46) holds in normal direction only, because the two bodies do not move relative to each other in normal direction.

$$\dot{z} = \dot{\zeta}, \text{ no penetration in normal direction.} \tag{8.47}$$

The missing equations are defined by Coulomb's law for full sliding :

$$F_x = pf_{kin}F_z , F_y = qf_{kin}F_z , \text{ for full sliding,} \tag{8.48a}$$

$$\frac{p}{q} = \frac{\dot{x} - \dot{\xi}}{\dot{y} - \dot{\eta}} , \quad p^2 + q^2 = 1 , \quad \mathbf{v}^T = (\dot{x}, \dot{y}, \dot{z}), \tag{8.48b}$$

$$sign(p) = sign(\dot{x} - \dot{\xi}) , \tag{8.48c}$$

where the factors p and q depend on the absolute tangential veloctties of the bodies. Equation in (8.48c) assures, that the force F_1 on body 1 has the same sense as the velocity of body 2 relative to body 1. Thus for full sliding the equations (8.29), (8.45), (8.47) and (8.48) determine the problem completely.

8.3 The force-displacement relation for full adhesion

The dynamic equation (8.29a) is the basic equation for impact problems. For numerical purposes the derivative $\dot{\mathbf{v}}$ can be expressed by finite differences and stepwise integrated. The rigid body velocity $\mathbf{v}_n$ and the rotations $\boldsymbol{\omega}_n$ of step n determine the incremental shift and the spin of the stick area. The elastic deformations and stresses in the contact area can now be calculated using a contact law. We distinguish between two types of contact laws: the Cattaneo-Mindlin theory of chapter 6 and 7 and the numerical method of chapter 11 and 12. In this chapter we will use the Cattaneo-Mindlin theory, which is much faster than the numerical method, and we will present some analytical solutions for special cases.

Three different contact regimes must be distinguished: Complete adhesion, complete sliding and partial slip. During impact these regimes alternate with each other. The values for the rigid body shift x, its first two derivatives v, $\dot{v}$ and the elastic displacement must be adapted to the values of the foregoing phase. In the next sections we will summarize the entire set of equations.

In the case of complete adhesion the stress increment is so small, that the two bodies stick together in the whole contact area and equation (8.46) holds. We must use the contact law (5.30), where the normal compression ζ_n is held constant in step n. With equation (8.29) we get :

$$\dot{\xi} = v, \tag{8.49a}$$

$$\frac{dF_x}{d\xi} = c_x\sqrt{\zeta}, \quad \frac{dF_y}{d\eta} = c_y\sqrt{\zeta}, \quad F_z = \frac{2}{3} c_z \zeta^{3/2}, \tag{8.49b}$$

$$\ddot{v} = -D\dot{F}, \tag{8.49c}$$

with the force $F = F_1$. We use a common numerical procedure of integration and express all derivatives as finite differences. The initial values are either the rigid body velocities at the beginning of impact or the corresponding values of the foregoing phase. Equation (8.49a) yields the displacement increments $\Delta\xi_n$, $\Delta\eta_n$, $\Delta\zeta_n$ and (8.49b) the forces. Numerical integration of (8.49c) determines the rigid body shift x_{n+1}, y_{n+1}, z_{n+1} of the next step n+1. Now we return to equation (8.49a) and repeat this procedure until partial slip starts. Partial slip starts for all practical impact problems in the compressive phase, when :

$$\sqrt{\Delta F_x^2 + \Delta F_y^2} \geq f\, \Delta F_z . \tag{8.50}$$

8.4 Partial slip

Partial slip starts after a phase of adhesion or when complete sliding terminates in the period of restitution. The old stress distribution acting in the stick area is partially overlaid by a slip area. Thus the stress distribution can be split into the old stress distribution and an additional function, which produces rigid shift in the stick area following the Cattaneo-Mindlin law. Equations (5.26), (5.27), (5.28) must be reformulated, under consideration of the old stress distribution in the stick area. Equations (8.29) and (8.46) yield :

$$\dot{\xi} = v, \tag{8.51a}$$

$$F_z = \frac{2}{3} c_z \zeta^{3/2}, \tag{8.51b}$$

$$F_x = F_{x.old}(\zeta^*) + \frac{2}{3} p\, f\, c_z\, (\zeta^{3/2} - \zeta^{*3/2}), \tag{8.51c}$$

$$F_y = F_{y,old}(\zeta^*) + \frac{2}{3} q f c_z (\zeta^{3/2} - \zeta^{*3/2}) , \qquad (8.51d)$$

$$\dot{v} = -D \cdot F , \qquad (8.51e)$$

$$fc_z(\zeta - \zeta^*) = \sqrt{c_x^2(\xi - \xi_{old}(\zeta^*))^2 + c_y^2(\eta - \eta_{old}(\zeta^*))^2} , \qquad (8.51f)$$

$$\frac{p}{q} = \frac{\xi - \xi_{old}(\zeta^*)}{\eta - \eta_{old}(\zeta^*)} , \qquad p^2 + q^2 = 1 , \qquad (8.51g)$$

$$sign(p) = sign(\xi - \xi_{old}(\zeta^*)), \qquad (8.51h)$$

where (8.51h) assures, that the additional force has the same sense as the additinonal displacement. The numerical procedure of integration is straightforward. Once the values ξ_n, η_n, ζ_n are known, the new value ζ_{n+1}^* of the next step $n+1$ must be determined from (8.51f) by a Newton procedure :

$$fc_z(\zeta_n - \zeta_{n+1}^*) = \sqrt{c_x^2(\xi_n + \xi_{old}(\zeta_{n+1}^*))^2 + c_y^2(\eta_n + \eta_{old}(\zeta_{n+1}^*))^2} . \qquad (8.52)$$

At the moment, when partial slip starts, we have:

$$|\Delta\xi_n| = fc_z|\Delta\zeta_n|. \qquad (8.53)$$

This equation holds, approximately, in the next step also, so that the additional part of the contact area Δa_{n+1} is overlaid by the new slip area. The old slip area, in the period of complete adhesion, had the size $\Delta\zeta_n$ resp. Δa_n, so that the new slip area moves inward by the amount :

$$\Delta\zeta_{n+1}^* = -\Delta\zeta_n . \qquad (8.54)$$

The old values $F_{old}(\zeta^*)$ and $\xi_{old}(\zeta^*)$ are the values of the previous load history, where the contact radius had the value:

$$\zeta_{old} = \zeta^* . \qquad (8.55)$$

It follows that the discrete values F_i and ξ_i of the previous load history must be stored for the solution of equations (8.51). They can be linearly interpolated to improve the calculation.

8.5 Rigid body sliding

Rigid body sliding occurs, when the rigid shift increment is so large that the elastic deformation can be neglected and the two bodies slide relative to each other in the whole contact area. The basic equation is again equation (8.29a), which we will integrate here. Furthermore we need equation (8.47) and (8.48) and Cattaneo's contact law in the form of equation (5.26) and (5.27) with $a^* = \zeta^* = 0$. The values p and q determine the slip direction, which is identical to the absolute relative velocity v_{abs} of the two bodies in the contact point. In this case the contact law has no incremental form, because we have complete sliding for each increment. Thus the elastic displacement and the tangential force are known, once the contact radius and the slip direction are determined. We will summarize the entire set of equations to elucidate the problem:

$$\dot{\zeta} = \dot{z}, \tag{8.56a}$$

$$c_x \xi = p \, f \, c_z \, \zeta \,, \quad c_y \, \eta = q \, f \, c_z \, \zeta \,, \tag{8.56b}$$

$$F_z = \tfrac{2}{3} \, c_z \, \zeta^{3/2} \,, \quad F_x = f \, p \, F_z \,, \quad F_y = f \, q \, F_z \,, \tag{8.56c}$$

$$\dot{v} = -D \, F \,, \tag{8.56d}$$

$$\frac{p}{q} = \frac{\dot{x} - \dot{\xi}}{\dot{y} - \dot{\eta}} \,, \quad p^2 + q^2 = 1 \,, \tag{8.56e}$$

$$\mathrm{sign}(p) = \mathrm{sign}(\dot{x} - \dot{\xi}) \,, \tag{8.56g}$$

where the sign of the force is opposite to the relative velocity. Equation (8.29a) was integrated, because the tangential force is a function of F_z, p and q as a consequence of Coulomb's law for full sliding. Equation (8.56g) defines the sense of the tangential force F_1 on body 1 in the direction of the velocity of body 2 relative to body 1.

These are 11 scalar equations for the unkown ξ, v, F, p, q. At the beginning of the impact the force F does not change its direction, because the contact force is so small that the derivative $\dot{v}$ in (8.56e) is zero, and the rigid slip velocity v remains constant. Constant rigid slip increments produce constant elastic displacement increments. From (8.56b) follows a constant value for p and q. If we set :

$$p = \cos \phi_0 \,, \quad q = \sin \phi_0 \,, \tag{8.57}$$

equations (8.56b) and (8.56e) determine the angle ϕ_0 of the slip direction at the beginning of impact :

$$\dot{y}_0 \cos \phi_0 - \dot{x}_0 \sin \phi_0 + \dot{\zeta}_0 \sin \phi_0 \cos \phi_0 \; f \left(\frac{c_z}{c_y} - \frac{c_z}{c_x} \right) = 0 \;. \qquad (8.58)$$

Since the absolute value of the term in brackets is always smaller than one, it is not difficult to find some recursive formulas which solve this equation approximately. A numerical solution is not difficult either. For equal stiffness coefficients c_x and c_y the slip direction is equal to the rigid body velocity $\mathbf{v}$.

The system of differential equations (8.56) can again be integrated successively by replacing the derivatives with finite differences and using common numerical methods.

9 Analytical solutions for the tangential impact

Analytical solutions are possible when the matrix $\mathbf{D}$ of equation (8.29) has diagonal form. This is the case, when the diagonal systems of θ_i and the coordinate system of the principal curvateres defined in chapter 8.1 coincide, and the components a and b of $\mathbf{R}$ are zero. Now the tangential and the normal solutions are independent. We have a completely elastic reflection in normal direction, while frictional forces produce different coefficients of restitution in tangential direction.

The three different contact models were already presented in chapter 8.2. Impact starts either with complete adhesion or complete sliding. For complete adhesion the system (8.49) has the form:

$$\left.\begin{aligned}\ddot{\xi} &= -D_{xx}c_x/\sqrt{\zeta}\,\dot{\xi}\,, \\[2mm]\ddot{\eta} &= -D_{yy}c_y/\sqrt{\zeta}\,\dot{\eta}\,, \\[2mm]\ddot{\zeta} &= -D_{zz}c_z/\sqrt{\zeta}\,\dot{\zeta}\end{aligned}\right\} \text{ for complete adhesion },\qquad (9.1)$$

The letters D_{xx}, D_{yy}, D_{zz} denote the diagonal entries of the diagonal matrix $\mathbf{D}$. Equation (9.1) shows, that the physical behaviour is analogous to a nonlinear spring-mass system in normal and tangential direction. For all practical cases complete adhesion terminates in the period of compression, because the normal velocity becomes zero while the tangential velocities are nonzero and the increase of the contact radius can not prevent partial slip.

The tangential force need not be infinitesimal small, as the limit in equation (5.30) suggests. This equation holds for large tangential forces also, as long as the condition for partial slip (8.50) is violated.

9.1 Normal solution

The third equation of (9.1) holds for all three contact models presented in section 8.3. It can be integrated to:

$$\ddot{\zeta} = \frac{-2}{3}\,D_{zz}c_z\,\zeta^{3/2}\,, \qquad \dot{\zeta}^2 = \dot{\zeta}_A^2 - \frac{8}{15}\,D_{zz}c_z\,\zeta^{5/2}.\qquad (9.2)$$

From equation (9.2) follows the maximal penetration ζ_{MAX} for $\dot{\zeta} = 0$:

$$\zeta_{MAX}^{5/2} = \frac{15 \; \dot{\zeta}_A^2}{8 \; D_{zz} c_z} \; , \tag{9.3}$$

with the normal velocity $\dot{\zeta}_A$ at the beginning of impact. Introduction of the variable t_N:

$$t_N = t \dot{\zeta}_A/\zeta_{MAX} \; , \quad S = (\zeta/\zeta_{MAX})^{5/2} \tag{9.4}$$

and insertion in (9.2) yields:

$$\left(\frac{dS}{dt_N}\right)^2 = \frac{25}{4} S^{6/5} (1\text{-}S) \; . \tag{9.5}$$

With a few mathematical operations equation (9.5) can be transformed into the hypergeometrical differential equation:

$$S(1\text{-}S) \frac{d^2 t_N}{dS^2} + \frac{1}{10} (6\text{-}11S) \frac{dt_N}{dS} = 0. \tag{9.6}$$

The solution of this equation can be found in Abramowitz/Stegun (1972). We use the hypergeometric series in the neighbourhood of the singularities $S=0$ and $S=1$. The starting value:

$$t_N(0) = 0. \tag{9.7}$$

and equation (9.5) determine the solution for $t_N < T/2$:

$$t_N = T/2 - 0.8\sqrt{1\text{-}S} \; F(\; 1/2, \; 3/5, \; 3/2; \; 1\text{-}S \;), \quad \text{for } S>0.5,$$

$$t_N = S^{2/5} F(\; 1/2, \; 2/5, \; 7/5; \; S \;), \quad \text{for } S<0.5, \tag{9.8}$$

$$T/2 = t_N(1) = \frac{2 \sqrt{\pi} \; \Gamma(2/5)}{5 \; \Gamma(9/10)} \; .$$

The hypergeometric function is defined by:

$$F(a,b;c;S) = {}_2F_1(a,b;c;S) = \sum_{n=0}^{\infty} \frac{(a)_n (b)_n}{(c)_n} \frac{S^n}{n!} \; , \tag{9.9}$$

$$(a)_n = a(a+1)(a+2) \ldots (a+n\text{-}1), \; (a)_0 = 1.$$

In the case $t_N > T/2$ we have :

$$t_{N>} = T - t_N(S) \; , \tag{9.10}$$

where $t_N(S)$ is defined by (9.8). Hunter (1957) found a very good approximation for $\zeta(t)$:

$$\zeta = \zeta_{MAX} \sin(\pi t/T) = \zeta_{MAX} \sin(1.067380\, t\, \dot\zeta_A/\zeta_{MAX}) \;. \tag{9.11}$$
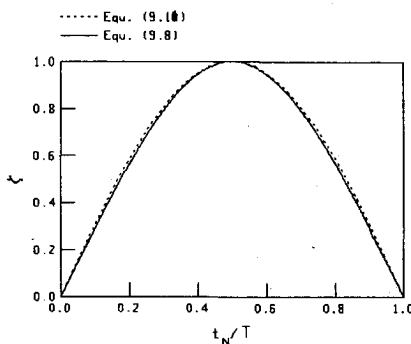

Fig. 9.1: Equations (9.8) and (9.10).

9.2 Tangential solution for complete adhesion

The displacements ξ and η are independent and the solution for η can be found by substitution of x for y in the solution for ξ. We introduce the new variable v:

$$v = d\xi/dt_N, \tag{9.12}$$

and rewrite the first of equations (9.1) using (9.3), (9.4):

$$\frac{d^2v}{dt_N^2} = -\frac{15\, D_{xx}c_x}{8\, D_{zz}c_z} S^{1/5}\, v. \tag{9.13}$$

Equation (9.5) inserted in (9.13) yields:

$$\frac{d^2v}{dt_N^2} = \frac{25}{4} S^{1/5} \left[\frac{d^2v}{dS^2} S(1-S) + \frac{dv}{dS} \frac{1}{10}(6-11S) \right], \tag{9.14}$$

The last two equations define the following differential equation:

$$S(1-S) \frac{d^2v}{dS^2} + \frac{1}{10}(6-11S)\frac{dv}{dS} + \frac{3}{10}\frac{D_{xx}c_x}{D_{zz}c_z} v = 0. \tag{9.15}$$

Equation (9.15) is a hypergeometric differential equation, which is identical to (9.6) in the case of $c_x = 0$. Again we use the two linearly independent solutions in the neighbourhood of the singular points (Abramowitz/Stegun 1972):

$$v = b_2 F\left(\frac{1-\phi}{20}, \frac{1+\phi}{20}; \frac{3}{5}; S\right) + 2b_4 S^{2/5} F\left(\frac{9-\phi}{20}, \frac{9+\phi}{20}; \frac{7}{5}; S\right)$$

$$= b_2' F\left(\frac{1-\phi}{20}, \frac{1+\phi}{20}; \frac{1}{2}; 1-S\right) + 2b_4' \sqrt{1-S}\, F\left(\frac{11-\phi}{20}, \frac{11+\phi}{20}; \frac{3}{2}; 1-S\right), \tag{9.16}$$

$$\phi = \sqrt{1 + 120 D_{xx}c_x/(D_{zz}c_z)}.$$

Barber (1975) found this result already for the special case of spheres. In equation (9.16) we used the transformation law (Abramowitz/Stegun 1972):

$$b_2 F(a, b; c; S) + 2b_4 S^{1-c} F(a-c+1, b-c+1; 2-c; S)$$

$$= b_2' F(a, b; a+b+1-c; 1-S) + 2b_4' (1-S)^{c-a-b} F(c-a, c-b, c-a-b+1; 1-S). \tag{9.17}$$

The constants b_2' and b_4' are functions of b_2 and b_4 :

$$b_2' = b_2 \frac{\Gamma(c)\Gamma(c-a-b)}{\Gamma(c-a)\Gamma(c-b)} + 2b_4 \frac{\Gamma(2-c)\Gamma(c-a-b)}{\Gamma(1-a)\Gamma(1-b)}, \tag{9.18}$$

$$2b_4' = b_2 \frac{\Gamma(c)\Gamma(a+b-c)}{\Gamma(a)\Gamma(b)} + 2b_4 \frac{\Gamma(2-c)\Gamma(a+b-c)}{\Gamma(a+1-c)\Gamma(b+1-c)},$$

and b_2, b_4 can be expressed as a function of b_2' and b_4' :

$$b_2 = -b_2' \frac{(c-a-b)\Gamma(2-c)\Gamma(a+b-c)}{(1-c)\Gamma(a+1-c)\Gamma(b+1-c)} + 2b_4' \frac{(c-a-b)\Gamma(c-a-b)\Gamma(2-c)}{(1-c)\Gamma(1-a)\Gamma(1-b)}, \tag{9.19}$$

$$2b_4 = b_2' \frac{(c-a-b)\Gamma(c)\Gamma(a+b-c)}{(1-c)\Gamma(a)\Gamma(b)} - 2b_4' \frac{(c-a-b)\Gamma(c-a-b)\Gamma(c)}{(1-c)\Gamma(c-a)\Gamma(c-b)},$$

where the symbol $\Gamma(x)$ denotes the Gamma function. The formulae:

$$\int S^n F(a, b; c; S)\, dS = \frac{S^{n+1}}{(n+1)}\, {}_3F_2(a, b, n+1; c, n+2; S), \quad \text{for } n \neq 0,$$

$$ {}_3F_2(a,b,c;d,e;S) = \sum_{n=0}^{\infty} \frac{(a)_n (b)_n (c)_n}{(d)_n (e)_n} \frac{S^n}{n!}, \tag{9.20}$$

can easily be proved. Insertion of (9.20) in (9.5), (9.12), (9.16) yields:

$$\xi = b_0 + b_2\, S^{2/5}\, {}_3F_2 \left(\frac{2}{5}, \frac{11-\phi}{20}, \frac{11+\phi}{20}; \frac{7}{5}, \frac{3}{5}; S \right) +$$

$$+ b_4\, S^{4/5}\, {}_3F_2 \left(\frac{4}{5}, \frac{19-\phi}{20}, \frac{19+\phi}{20}; \frac{9}{5}, \frac{7}{5}; S \right). \tag{9.21}$$

We need the solution ξ to determine ξ_{old} in the period of partial slip. Since formula (9.20) converges badly for $S=1$, it is necessary to develop another power series for the singularity $S=1$. For this purpose we insert equation (9.5) in the differential equation (9.15) with the result:

$$S^2(1-S)\xi''' + 3S\left(\frac{3}{5} - \frac{11}{10} S \right) \xi'' + \left[\frac{3}{10} \frac{D_{xx}c_x}{D_{zz}c_z} S + \frac{3}{25} (1-11S) \right] \xi' = 0, \tag{9.22}$$

where $'$ denotes the derivative d/dS. The solution for $S=1$ has the form:

$$\xi = \sum_{n=0}^{\infty} c_{n,0}\, (1-S)^n + \sum_{n=1}^{\infty} c_{n,-1/2}\, (1-S)^{n-1/2}, \tag{9.23}$$

with the start values:

$$c_{0,0} = \xi(1), \quad c_{1,0} = -\frac{4}{5}\, b_4', \quad c_{1,-1/2} = -4b_2'/5. \tag{9.24}$$

The constants b_2' and b_4' are defined by equation (9.16). The recursion formula for the coefficients $c_{n,x}$ has the form:

$$c_{n+2,x} = c_{n,x} \frac{\left(n+x\right)\left\{ \left(n+x-1\right)\left(-n-x-\frac{13}{10}\right) - \frac{33}{25} + \frac{3D_{xx}c_x}{10D_{zz}c_z} \right\}}{(n+x+2)(n+x+1)(n+x+3/2)} +$$

$$+ c_{n+1,x} \frac{\left(n+x\right)\left(2n+2x+\frac{28}{10}\right) + \frac{6}{5} - \frac{3D_{xx}c_x}{10D_{zz}c_z}}{(n+x+2)(n+x+3/2)}. \tag{9.25}$$

The start values (9.24) can alternatively be calculated by adapting the series (9.25) to the series (9.21) for $S=0.5$, once the values b_0, b_2, b_4 are known. The series converges relatively fast. 25 elements are the maximal number for a precision of 10^{-7}. We need the derivative of v for the determination of b_i:

$$\frac{d^2\xi}{dt_N^2} = -\frac{5}{4} \frac{D_{xx}c_x}{D_{zz}c_z}\, S^{3/5} b_2\, F\left(\frac{11-\phi}{20}, \frac{11+\phi}{20}; \frac{8}{5}; S \right) + 2b_4 F\left(\frac{-1-\phi}{20}, \frac{-1+\phi}{20}; \frac{2}{5}; S \right). \tag{9.26}$$

We get for complete adhesion at the beginning of impact :

$$b_0 = \xi(0) = 0, \quad b_2 = d\xi/dt_N(0), \quad 2b_4 = d^2\xi/dt_N^2(0) = 0. \tag{9.27}$$

For the special case $D_{xx}c_x = D_{zz}c_z$ equation (9.16) yields $\phi = 11$ and the solution (9.21) becomes :

$$\xi = b_2 S^{2/5} = \zeta \, \dot{\zeta}_0/\dot{\zeta}_0, \text{ for } D_{xx}c_x = D_{zz}c_z. \tag{9.28}$$

9.3 Rigid body sliding

A special solution of (8.58) for the slip direction at the start of impact holds for a rigid body velocity in x-direction :

$$\phi_0 = q = 0, \quad \text{for} \quad \dot{y}_0 = 0. \tag{9.29}$$

From (8.56d) follows $F_y(t_0)=0$ and there will be no accaleration in y-direction throughout the entire impact for diagonal matrices $\mathbf{D}$. We differentiate (8.56a) and rewrite (8.56d) :

$$\ddot{x} = D_{xx}F_x, \quad \ddot{z} = D_{zz}F_z = -\ddot{\zeta}, \tag{9.30}$$

Coulomb's law has the form:

$$F_x = -\text{sign}(\dot{x}_0) \, f \, F_z. \tag{9.31}$$

We insert equation (9.31) in (9.30) and get after integration:

$$\dot{x} = \dot{x}_0 + \text{sign}(\dot{x}_0) \, \frac{D_{xx}}{D_{zz}} \, f \, (\dot{\zeta} - \dot{\zeta}_0). \tag{9.32}$$

The normal velocity $\dot{\zeta}_1$ at the end of impact is equal and opposite to $\dot{\zeta}_0$ for an elastic reflection in normal direction. The tangential coefficient of restitution is defined as the ratio of the tangential velocities in the contact point before impact to the value after impact :

$$R_x = \frac{-\dot{x}_1}{\dot{x}_0} = -1 + 2 \, \frac{f \, \dot{\zeta}_0 D_{xx}}{|\dot{x}_0| \, D_{zz}}, \quad \text{for } |\dot{x}_0| > 2f\dot{\zeta}_0 D_{xx}/D_{zz}. \tag{9.33}$$

Equation (9.33) is valid for complete sliding in x-direction at the beginning of impact

and a diagonal matrix $\mathbf{D}$. The inequality in (9.33) assures, that R_x is less than zero, because otherwise the slip direction would reverse during impact and partial slip would occur.

9.4 Partial slip

An analytical solution is possible for small frictional forces T. In this case we have complete adhesion in the period of compression and the solution of chapter 9.2 can be applied. Before the period of restitution starts, partial slip occurs, because the increment of the normal force ΔF_z becomes negative and equation (8.50) will be satisfied. In this chapter we will discuss the case of infinitely small tangential forces. Now the radius of the stick area becomes as large as the contact area:

$$\lim_{T \to 0} a^* = a . \tag{9.34}$$

We proceed similarly to chapter 8.4 in consideration, that only the difference between the actual and the old stress distribution produces partial slip on an infinitely small elliptical ring on the border of the contact area. Again we use equations (5.29) :

$$F_x - F_{x,old} = c_x \sqrt{\zeta} \, (\, \xi - \xi_{old} \,) \, ,$$
$$F_y - F_{y,old} = c_y \sqrt{\zeta} \, (\, \eta - \eta_{old} \,) \, . \tag{9.35}$$

In contrast to the differential contact law (8.49b) for full adhesion, the contact law for partial slip depends on the actual displacements and not on the entire previous load history. We will calculate the solution for ξ only, because it is identical to the solution for η. The old and the actual solution satisfy the equation of motion (8.42) :

$$\ddot{\xi} = -D_{xx}F_x , \quad \ddot{\xi}_{old} = -D_{xx}F_{x,old} , \tag{9.36}$$

which we integrated here. Introduction of the variables :

$$F_x^* = F_x - F_{x,old} , \quad \xi^* = \xi - \xi_{old} , \tag{9.37}$$

and substitution in (9.36) yields :

$$\ddot{\xi}^* = - D_{xx}c_x\sqrt{\zeta}\,\xi^* . \tag{9.38}$$

The differential equation (9.38) is identical to the first equation of (9.1) for $\dot{\xi}$ and has the solution (9.16) of chapter 9.2 :

$$\xi = b_2 \, S^{2/5} \, {}_3F_2 \left(\frac{2}{5}, \frac{11-\phi}{20}, \frac{11+\phi}{20}; \frac{7}{5}, \frac{3}{5}; S \right) + d_2' \, F \left(\frac{1-\phi}{20}, \frac{1+\phi}{20}; \frac{1}{2}; 1-S \right) -$$

$$- 2d_4' \, \sqrt{1-S} \, F \left(\frac{11-\phi}{20}, \frac{11+\phi}{20}; \frac{3}{2}; 1-S \right) , \qquad (9.39a)$$

$$\frac{d\xi}{dt_N} = -b_2' \, F \left(\frac{1-\phi}{20}, \frac{1+\phi}{20}; \frac{1}{2}; 1-S \right) - 2b_4' \, \sqrt{1-S} \, F \left(\frac{11-\phi}{20}, \frac{11+\phi}{20}; \frac{3}{2}; 1-S \right) - \tag{9.39b}$$

$$- \frac{3}{2} \, C_{xx} c_x \, d_2' \, \sqrt{1-S} \, F \left(\frac{9-\phi}{20}, \frac{9+\phi}{20}; \frac{3}{2}; 1-S \right) + 2 \, d_4' \, \frac{5}{4} \, F \left(\frac{-1-\phi}{20}, \frac{-1+\phi}{20}; \frac{1}{2}; 1-S \right).$$

We used equation (9.5) for the derivative of ξ in (9.39), with a negative sign of dS/dt_N. The constants d_2', d_4' are determined by ξ_{old} for $S=1$:

$$\xi(1) = \xi_{old}(1), \tag{9.40}$$

yields :

$$d_2' = 0. \tag{9.41}$$

The derivative $d\xi/dt_N(1)$ must be identical to $v(1)$ in equation (9.16) :

$$d\xi/dt_N(1) = v(1) = b_2'. \tag{9.42}$$

Insertion in (9.39) yields :

$$2d_4' = \frac{8}{5} \, b_2'. \tag{9.43}$$

The constant b_2' is defined by (9.18) and (9.27). The transformation law (9.17) for equation (9.39) yields the velocity $d\xi/dt_N$ for the end of impact with $S=0$:

$$d\xi/dt_N(S=0) = -b_2 - 2d_4. \tag{9.44}$$

The relation between d_4 and d_4' follows from equation (9.18) and (9.19). Equation (9.44) and (9.27) define the coefficient of restitution (9.33):

$$R_x = (b_2 + 2d_4)/b_2. \tag{9.45}$$

Insertion of (9.18) and (9.19) in (9.45) yields:

$$R_x = 1 - 2\pi \left[\frac{\Gamma(0.6)}{\Gamma\left(\frac{11-\phi}{20}\right) \Gamma\left(\frac{11+\phi}{20}\right)} \right]^2 , \quad \phi = \sqrt{1 + 120 D_{xx} c_x/(D_{zz} c_z)}. \tag{9.46}$$
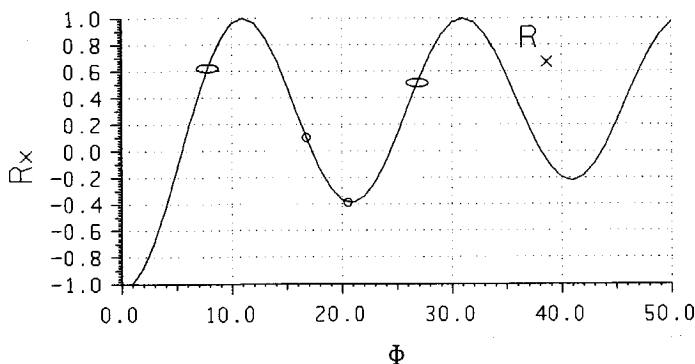
Fig 9.2: R_x for complete adhesion defined by equ. (9.46).
The circles mark the region of R_x for spheres.

Equation (9.46) holds for infinitely small tangential forces T only. Fig. 9.2 shows R_x, defined by equation (9.46), with the region for spheres marked by circles. The ellipses mark the region for ellipsoids.

9.5 Impact of spheres

Suppose, that the principal axes of inertia and the coordinate system of the principal curvatures of the two bodies have the same direction. Furthermore the vectors R_1, R_2 may point in e_z-direction. The matrices E_1, E_2, F_1, F_2, G_1, G_2 defined by (8.43) become :

$$e_x = \begin{bmatrix} 1 \\ 0 \\ 0 \end{bmatrix}, \quad e_y = \begin{bmatrix} 0 \\ 1 \\ 0 \end{bmatrix}, \quad e_z = \begin{bmatrix} 0 \\ 0 \\ 1 \end{bmatrix},$$

$$R_1 = \begin{bmatrix} 0 \\ 0 \\ -R_1 \end{bmatrix}, \quad R_2 = \begin{bmatrix} 0 \\ 0 \\ R_2 \end{bmatrix}, \tag{9.47a}$$

$$G_1 = \begin{bmatrix} 0 & R_1 & 0 \\ -R_1 & 0 & 0 \\ 0 & 0 & 0 \end{bmatrix}, G_2 = \begin{bmatrix} 0 & -R_2 & 0 \\ R_2 & 0 & 0 \\ 0 & 0 & 0 \end{bmatrix}, E_1 = \begin{bmatrix} \theta_{1X}^{-1} & 0 & 0 \\ 0 & \theta_{1Y}^{-1} & 0 \\ 0 & 0 & \theta_{1Z}^{-1} \end{bmatrix}, E_2 = \begin{bmatrix} \theta_{2X}^{-1} & 0 & 0 \\ 0 & \theta_{2Y}^{-1} & 0 \\ 0 & 0 & \theta_{2Z}^{-1} \end{bmatrix},$$

$$D_1 = \begin{bmatrix} 0 & R_1/\theta_{1X} & 0 \\ -R_1/\theta_{1Y} & 0 & 0 \\ 0 & 0 & 0 \end{bmatrix}, \quad D_2 = \begin{bmatrix} 0 & -R_2/\theta_{2X} & 0 \\ R_2/\theta_{2Y} & 0 & 0 \\ 0 & 0 & 0 \end{bmatrix}. \tag{9.47b}$$

For spheres every coordinate system is a system of principal axes of inertia, while in the case of rotational symmetric bodies the axis of symmetry is a principal axis. We calculated matrix D, defined by (8.33), (8.43), and the spring constants c_x, c_y, c_z, defined by (5.25), for the special cases of two spheres and two perpendicular crossed cylinders which contact in the middle :

Perpendicularly crossed cylinders :
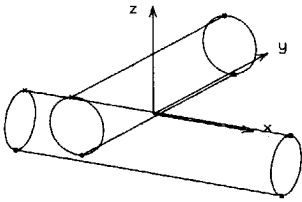
$$D_{xy} = D_{xz} = D_{yz} = 0 .$$

$$D_{xx} = \frac{R_1^2}{\theta_{1X}} + \frac{R_2^2}{\theta_{2X}} + \frac{1}{m_1} + \frac{1}{m_2},$$

$$D_{yy} = \frac{R_1^2}{\theta_{1Y}} + \frac{R_2^2}{\theta_{2Y}} + \frac{1}{m_1} + \frac{1}{m_2},$$

$$D_{zz} = \frac{1}{m_1} + \frac{1}{m_2}, \tag{9.48}$$

$$\left. \begin{aligned} c_x = c_y &= \frac{4\sqrt{2R_1}}{\frac{2-\nu_1}{G_1} + \frac{2-\nu_2}{G_2}}, \\ c_z &= \frac{2\sqrt{2R_1}}{\frac{1-\nu_1}{G_1} + \frac{1-\nu_2}{G_2}}, \end{aligned} \right\} \text{ for } R_1 = R_2 ,$$

Spheres :
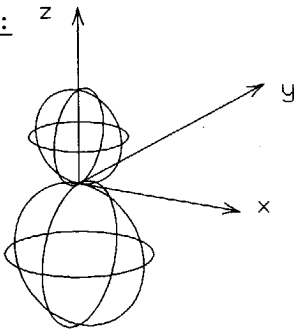
$$D_{xy} = D_{xz} = D_{yz} = 0 .$$

$$D_{xx} = D_{yy} = \frac{7}{2}\left(\frac{1}{m_1} + \frac{1}{m_2}\right) ,$$

$$D_{zz} = \frac{1}{m_1} + \frac{1}{m_2}, \tag{9.49}$$

$$c_x = c_y = \frac{8}{\sqrt{\frac{1}{R_1} + \frac{1}{R_2}}\left(\frac{2-\nu_1}{G_1} + \frac{2-\nu_2}{G_2}\right)},$$

$$c_z = \frac{4}{\sqrt{\frac{1}{R_1} + \frac{1}{R_2}}\left(\frac{1-\nu_1}{G_1} + \frac{1-\nu_2}{G_2}\right)},$$

The maximal compression ζ_{MAX} of both bodies and the duration of impact from (9.3), (9.8) are :

$$\zeta_{MAX} = \left(\frac{15}{8D_{zz}c_z}\right)^{2/5} \dot{\zeta}_A^{4/5} , \tag{9.50}$$

$$T = 2.943 \frac{\zeta_{MAX}}{\dot{\zeta}_A} = 2.943 \left(\frac{15}{8D_{zz}c_z}\right)^{2/5} \frac{1}{\dot{\zeta}_A^{1/5}} ,$$

The maximal compression for spheres becomes

$$\frac{\zeta_{MAX}}{R} = \left[\frac{5}{8} \sqrt{2}\,\pi\,(1-\nu)\right]^{2/5} \left[\frac{|\dot{\zeta}_2 - \dot{\zeta}_1|}{\sqrt{G/\rho}}\right]^{4/5} , \tag{9.51}$$

with the modulus of rigidity G and the specific density ρ. $\sqrt{G/\rho}$ is the velocity of torsional waves in the elastic space and has the value for steel :

$$\sqrt{G/\rho} \approx 3200 \text{ m/s} . \tag{9.52}$$

A steel sphere, which strikes a fixed sphere, falling from 1 m height, produces a maximal compression of :

$$\zeta_{MAX}/R \approx 6.8\ 10^{-3} , \tag{9.53}$$

and a maximal contact radius of :

$$a_{MAX}/R = \sqrt{a_{MAX}/2R} = 0.06 . \tag{9.54}$$

The duration of impact T is about three times the amount, which a sphere needs, to run through the distance ζ_{MAX} with the velocity $\dot{\zeta}_A$ of the beginning of impact. The impact duration becomes for our example :

$$T = 4.6\ 10^{-3} \frac{R[\text{meter}]}{\text{meter}} \text{ sec} . \tag{9.55}$$

Equations (8.42) yield for the impact of two spheres in x-direction :

$$\frac{7}{2}(1+\frac{m_1}{m_2})(\dot{x}_1-\dot{X}_2) = \dot{X}_2 - \dot{X}_1 + \Omega_{2y}R_2 + \Omega_{1y}R_1 + \dot{\xi} ,$$

$$\omega_{1y} - \Omega_{1y} = -\frac{5}{2R_1}(\dot{x}_1-\dot{X}_1) ,$$

$$\omega_{2y} - \Omega_{2y} = \frac{5}{2R_2}(\dot{x}_2-\dot{X}_2) , \tag{9.56}$$

$$m_2(\dot{x}_2-\dot{X}_2) = -m_1(\dot{x}_1-\dot{X}_1) .$$

Capital letters in (9.56) denote the velocities before impact. The deformations in y-direction are zero. Equation (9.56) can be transformed to :

$$\dot{x}_1 - R_1\omega_{1y} = \dot{x}_2 - R_2\omega_{2y} + \dot{\xi} \ . \tag{9.57}$$

Since the equation for ξ and ζ are decoupled, the energy-loss ΔE_x, ΔE_z in x- and z-direction can be calculated indepently. The result in x-direction is :

$$\Delta E_x = \frac{1}{2}m_1(\dot{x}_1^2 - \dot{X}_2^2) + \frac{1}{2}m_2(\dot{x}_2^2 - \dot{X}_2^2) + \frac{1}{5}m_1R_1^2(\omega_{1y}^2 - \Omega_{1y}^2) + \frac{1}{5}m_2R_2^2(\omega_{2y}^2 - \Omega_{2y}^2). \tag{9.58}$$

Again capitals denote the velocities before impact. With the coefficient of restitution from (9.33) and (9.56) we get :

$$\Delta E_x = -\frac{m_1m_2}{7(m_1+m_2)}\ (1+R_x)(1-R_x)\ \dot{\xi}_0^2 . \tag{9.59}$$

A similar calculation yields in z-direction :

$$\Delta E_z = -\frac{m_1m_2}{2(m_1+m_2)}\ (1+R_z)(1-R_z)\ \dot{\zeta}_0^2 . \tag{9.60}$$

The normal coefficient of restitution R_z is 1 for an elastic reflection, because the equations are decoupled and the frictional force acts in x-direction. For $R_x = \pm 1$ no energy is lost. The energy-loss is maximal for $R_x = 0$.

10 The torsional impact on a rigid plane

Suppose that a body with a rotational velocity $\dot{\beta}_A$ strikes a rigid plane. The absolute value of the rotational velocity after impact can not be greater than before impact, because the friction reduces the kinetic energy of the body. It follows that the change of the torsional angle $\Delta\beta$ has the magnitude :

$$|\Delta\beta| < 2|\dot{\beta}_A T| = 5.89 \, |\dot{\beta}_A| \, \frac{\zeta_{MAX}}{\dot{\zeta}_0} , \tag{10.1}$$

with the impact duration T from equation (9.8). Equation (10.1) yields for the tangential displacement at the border of the contact :

$$\Delta\beta \, a < 5.89 \, \frac{R\dot{\beta}_A}{\dot{\zeta}_A} \, \frac{a}{R} \, \zeta_{MAX} . \tag{10.2}$$

For large rotations $R\dot{\beta}_A \gg \dot{\zeta}_A$ the solution for complete sliding of chapter 10.4 can be applied. If the rotation $R\dot{\beta}_A$ has the same magnitude as the normal velocity $\dot{\zeta}_A$, the tangential displacements are by the factor a/R smaller than the normal compression. In this chapter we will show, that the change of the torsional velocity has the order of ζ_{MAX}/R, which is allways very small for Hertzian contact problems. It follows, that the change of the rotational velocity should be neglected in the frame of the Hertzian theory.

10.1 The period of compression with adhesion

We obtain the torque for complete sliding from equations (5.12), (5.14), (5.40) :

$$M_{ZR} = \frac{3\pi}{16} fF_z a = \frac{\pi Gf}{2(1-\nu)} R\zeta^2 , \tag{10.3}$$

In the case of complete adhesion equation (5.33) yields the torque :

$$M_{ZH} = \frac{16G}{3} a^3\beta , \tag{10.4}$$

where β denotes the torsional angle. For infinitely small variations of the normal compression $\Delta\zeta$ and the rotation $\Delta\beta$, equations (10.3) and (10.4) yield :

$$\Delta M_{ZR} = \frac{\pi G f}{(1-\nu)} R\zeta\Delta\zeta , \quad \Delta M_{ZH} = \frac{16G}{3} a^3\Delta\beta . \tag{10.5}$$

The increase of the contact radius by the infinitely small value Δa does not change the torque. Only the additional rotation $\Delta\beta$ alters the torque. Suppose, now, that the normal compression ζ and the torsional angle β are continuously changed. An increasing normal compression increases the contact area by a small annular region. Complete sliding occurs in this additional ring of the contact area, if the variation of the torque ΔM_{ZH} is larger than the necessary value for complete sliding ΔM_{ZR}:

$$\Delta M_{ZH} > \Delta M_{ZR} . \tag{10.6}$$

Insertion of (5.14), (10.3), (10.4) in (10.6) and division by the infinitely small value Δt yields:

$$R \frac{d\beta}{dt} > \frac{3\pi f R}{16(1-\nu) \sqrt{R\zeta}} \frac{d\zeta}{dt} , \quad \text{for partial slip.} \tag{10.7}$$

If (10.7) is violated, complete adhesion takes place. From (10.7) follows that at the beginning of impact always complete adhesion takes place, because ζ is very small. Since the normal velocity becomes zero at the end of the period of compression, partial slip starts always in the period of compression. Insertion of (10.9) in the equation of motion yields:

$$\theta_{ZZ} \frac{d^3\beta}{dt^3} = - \frac{16}{3} Ga^3 \frac{d\beta}{dt} . \tag{10.8}$$

θ_{ZZ} is the moment of inertia around the z-axis. We will use the dot for the derivation d/dt_N, with t_N defined by (9.4) :

$$\cdot = \frac{d}{dt_N} , \quad \frac{d}{dt} = \frac{\dot{\zeta}_A}{\zeta_{MAX}} \frac{d}{dt_N} . \tag{10.9}$$

Insertion of (10.9) in (10.8) yields:

$$\dddot{\beta} = - \varepsilon \, \zeta_N^{3/2} \, \dot{\beta} , \quad \varepsilon = \frac{25}{4} (1-\nu) \frac{\zeta_{MAX}}{R} . \tag{10.10}$$

Reformulation of (10.10) with $S=\zeta^{5/2}$ yields :

$$\frac{d^2\dot{\beta}}{dS^2} S(1-S) + \frac{d\dot{\beta}}{dS} \left(\frac{3}{5} - \frac{11}{10} S \right) - \frac{\zeta_{MAX}}{R} (1-\nu) S^{2/5} \dot{\beta} = 0 . \tag{10.11}$$

The last term in equation (10.11) is nonlinear and can not be solved by a power series with the variable S. Therefore we develop a power series in ε with the unknown functions $v_i(S)$:

$$\dot{\beta} = v_0 + \varepsilon v_1 + \varepsilon^2 v_2 \ldots . \tag{10.12}$$

and insert it in (10.10). The initial values for $t_N = 0$ are :

$$\dot{\beta}(0) = \dot{\beta}_A , \quad \theta_{zz}\ddot{\beta}(0) = M_z(0) = 0 . \tag{10.13}$$

Comparison of the factors of ε^i yields a set of differential equations which can be solved. The first order term ε^0 yields :

$$\ddot{v}_0 = 0 , \quad v_0 = \dot{\beta}_A + \ddot{\beta}(0) t_N = \dot{\beta}_A. \tag{10.14}$$

The initial conditions (10.13) are satisfied by v_0 alone. For the other functions v_i we have:

$$v_i(0) = \dot{v}_i(0) = 0 . \tag{10.15}$$

The factor of the second term ε^1 yields the differential equation :

$$\ddot{v}_1 = - S^{3/5} v_0 . \tag{10.16}$$

We insert (9.5) in (10.16) and obtain :

$$\dot{v}_1 = - \frac{2}{5} v_0 \int_0^S (1-S)^{-1/2} dS = - \frac{4}{5} v_0 (1-\sqrt{1-S}) . \tag{10.17}$$

A second integration and insertion of (9.8) yields the solution for v_1 :

$$v_1 = \frac{4}{5} v_0(S^{2/5} - t_N) = \frac{4}{5} S^{2/5} \left[1-F\left(\frac{2}{5},\frac{1}{2};\frac{7}{5};S\right) \right] v_0 . \tag{10.18}$$

The factor of ε^2 yields the equation :

$$\ddot{v}_2 = - \zeta_N^{3/2} v_1 = - \frac{4}{5} v_0 S \left[1- F\left(\frac{2}{5},\frac{1}{2};\frac{7}{5};S\right) \right] . \tag{10.19}$$

After insertion of (9.5) equation (10.19) can be integrated with respect to S :

$$\dot{v}_2 = -\frac{4}{5} v_0 \int_0^S \frac{2S\,dS}{5S^{3/5}\sqrt{1-S}} + \frac{4}{5} v_0 \int_0^S \frac{2S}{5S^{3/5}\sqrt{1-S}} F\left(\frac{2}{5},\frac{1}{2};\frac{7}{5};S\right) dS, \quad (10.20)$$

We reformulate (10.20) using the transformation law (9.17) :

$$\dot{v}_2 = -\frac{8}{25} v_0 \int_0^S S^{2/5} F\left(a,\frac{1}{2};a;S\right) dS + \frac{8}{25} v_0 \int_0^S S^{2/5} F\left(1,\frac{9}{10};\frac{7}{5};S\right) dS, \quad (10.21)$$

with the arbitrary constant a. Application of (9.20) yields the solution for $\dot{v}_2$ and v_2 :

$$\dot{v}_2 = -\frac{8}{35} v_0 S^{7/5} F\left(\frac{1}{2},\frac{7}{5};\frac{12}{5};S\right) + \frac{8}{35} v_0 S^{7/5} F\left(1,\frac{9}{10};\frac{12}{5};S\right). \quad (10.22)$$

$$v_2 = -\frac{16}{9\cdot 35} v_0 S^{9/5} \left\{ {}_3F_2\left(\frac{9}{5},\frac{7}{5},\frac{3}{2};\frac{12}{5},\frac{14}{5};S\right) - {}_3F_2\left(\frac{9}{5},\frac{19}{10},1;\frac{12}{5},\frac{14}{5};S\right) \right\}.$$

We use the power series (9.20) to develop (10.22) in the neighbourhood of $S=0$:

$$v_2 = -\frac{16}{9\cdot 35} v_0 S^{9/5} \left\{ 1 + \frac{9}{16} S + \frac{9\cdot 14\cdot 15}{16\cdot 17\cdot 19} S^2 + \ldots - 1 - \frac{3\cdot 19}{8\cdot 14} S - \frac{3\cdot 29}{32\cdot 17} S^2 \right\}.$$
$$(10.23)$$

We neglect $v_2(1)$ because it is much smaller than $v_1(1)$:

$$\frac{d\beta}{dt_N} = v_0 + \varepsilon v_1 = \frac{d\beta(0)}{dt}\left\{ 1 - 5(1-\nu)\frac{\zeta_{MAX}}{R}(t_N-\zeta_N) \right\}. \quad (10.24)$$

At the beginning of impact the condition for partial slip (10.7) is always satisfied, such that the impact starts with partial slip.

10.2 Partial slip

Equations (5.39), (5.41) describe the contact law for partial slip. They are still valid when the contact area decreases, as long as the rotation does not change its sign. During the previous load history a stress distribution was generated in the contact area. This stress distribution is conserved in the stick area and overlaid by a Cattaneo-Mindlin function (6.1), which satisfies the boundary conditions. Only the difference $M_{ZNEW}-M_{ZOLD}$ between the actual torque and the torque of the old stess distribution

in the stick area can produce partial slip, in the sense of the Cattaneo-Mindlin theory. Accordingly the displacement ξ_{NEW} consists of the old displacement $\xi_{OLD}(a^*)$ and a displacement ξ^*, which produces partial slip :

$$M_Z^* = M_{ZNEW} - M_{ZOLD}(a^*) \ , \quad \xi^* = \xi_{NEW} - \xi_{OLD}(a^*) \ . \tag{10.25}$$

With the equations of motion:

$$\theta_{ZZ} \frac{d^2 \beta_{NEW}}{dt^2} = - M_{ZNEW} \ , \quad \theta_{ZZ} \frac{d^2 \beta_{OLD}}{dt^2} = - M_{ZOLD} \ , \tag{10.26}$$

and (5.3), (5.41) we get the result :

$$\frac{\theta_{zz}}{fF_z a} \frac{d^2}{dt^2} (\beta_{NEW} - \beta_{OLD}(a^*)) = \frac{-k'k^2}{4} [D(k)(1+2k^2) + 6E(k)] - \frac{3}{4\pi} \int_0^{\cos^{-1}k} \cos^{-1}\left(\frac{k'}{\cos\gamma}\right) dk',$$

$$\beta_{NEW} - \beta_{OLD}(a^*) = \frac{2f}{\pi(1-\nu)} \frac{a}{R} (K(k) - E(k)) \ , \quad a = \sqrt{R\zeta} \ , \tag{10.27}$$

The differential equation (10.27) must be integrated numerically and the modul k of each increment is determined by the second equation of (10.27) :

$$k = \sqrt{1 - \frac{a^{*2}}{a^2}} = F(K(k) - E(k)) \ , \quad K(k) - E(k) = \frac{\pi(1-\nu)R}{2fa} (\beta_{NEW} - \beta_{OLD}) = F^{-1}(k) \ . \tag{10.28}$$

The function $k = F(K(k) - E(k))$ can be interpolated to simplify the procedure. Of course the second equation in (10.27) can be differentiated and inserted in the first equation, with the result :

$$\frac{1}{8}\left(\frac{-5}{2}\zeta_N - \frac{1}{\zeta_N} + \zeta_N^{3/2}\right)\left(K(k) - E(k)\right) (\pm) \frac{1}{2}\sqrt{\frac{1+\zeta^{5/2}}{\zeta_N}} \dot{k} + \sqrt{\zeta_N} E(k) \frac{k}{k'^2} \ddot{k} +$$

$$+ \sqrt{\zeta_N} \dot{k}^2 \left(\frac{2E(k)}{k'^2} - K(k)\right) = \tag{10.29}$$

$$= \frac{fF_z a}{\theta_{zz}} \frac{\pi(1-\nu)}{2f} \left(\frac{\zeta_{MAX}}{\dot\zeta_0}\right)^2 \left\{ -[D(k)(1+2k^2) + 6E(k)] \frac{k'k^2}{4} - \frac{3}{4\pi} \int_0^{\cos^{-1}k'} \cos^{-1}\left(\frac{k'}{\cos\gamma}\right) d\gamma \right\}.$$

10.3 Complete adhesion in the period of restitution

In the period of restitution a small annular slip area forms at the border of the contact area. For small rotations this slip area becomes very small and the limit $k' \to 1$ and $k \to 0$ in (5.41) yields :

$$\frac{\theta_{zz}}{fF_za} \frac{d^2}{dt^2}(\beta_{NEW} - \beta_{OLD}) = -k^2, \quad \beta_{NEW} - \beta_{OLD} = \frac{fak^2}{2(1-\nu)R}. \tag{10.30}$$

Substitution of t by t_N with (9.4) yields :

$$\frac{d^2}{dt_N^2}(\beta_{NEW} - \beta_{OLD}) = -\varepsilon \zeta_N^{3/2}(\beta_{NEW} - \beta_{OLD}), \quad \varepsilon = \frac{25}{4} \cdot \frac{\zeta_{MAX}}{R}(1-\nu). \tag{10.31}$$

We solve this nonlinear differential equation analogous to (10.10) :

$$\beta_{NEW} - \beta_{OLD} = v_0 + \varepsilon v_1 + \varepsilon^2 v_2 + \dots \tag{10.32}$$

The initial values for $t = T/2$ are :

$$\beta_{NEW} - \beta_{OLD} = 0, \quad \frac{d\beta_{NEW}}{dt_N} = \frac{d\beta(T/2)}{dt_N} = \dot{\beta}_1. \tag{10.33}$$
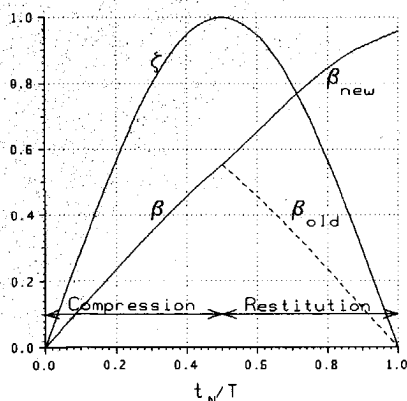

Fig. 10.1: The rotation β.

In the case of complete adhesion β_{OLD} is the mirror-image of β. The power series (10.32) is inserted in (10.31) and integrated similar to chapter (10.1). The solution for ε^0 becomes :

$$\ddot{v}_0 = 0, \quad v_0 = 2\dot{\beta}_1(t_N - \frac{T}{2}). \tag{10.34}$$

The solution for ε^1 is straightforward :

$$\ddot{v}_1 = -\zeta_N^{3/2} 2\dot{\beta}_1(t_N - \frac{T}{2}), \tag{10.35}$$

$$\ddot{v}_1 = -2\dot{\beta}_1 \left[SF\left(\frac{2}{5}, \frac{1}{2}; \frac{7}{5}; S\right) - \frac{T}{2}S^{3/5} \right],$$

$$\ddot{v}_1 = -2\dot{\beta}_1\left[\frac{2}{7}S^{7/5}F\left(1,\frac{9}{10};\frac{12}{5};S\right) - \frac{2}{7}F\left(1,\frac{9}{10};\frac{12}{5};1\right) + \frac{2}{5}T\sqrt{1-S}\right], \qquad (10.36)$$

Integration of (10.36) yields:

$$v_1 = -2\dot{\beta}_1\left\{\frac{4}{63}\left[S^{9/5}F\left(\frac{9}{5},\frac{7}{5},\frac{3}{2};\frac{14}{5},\frac{12}{5};S\right) - F\left(\frac{9}{5},\frac{7}{5},\frac{3}{2};\frac{14}{5},\frac{12}{5};1\right) - \frac{2}{7}F\left(1,\frac{9}{10};\frac{12}{5};1\right)\left(t_N - \frac{T}{2}\right) + \right. \right.$$

$$\left. \left. - \frac{2}{7}F\left(1,\frac{9}{10};\frac{12}{5};1\right)\left(t_N - \frac{T}{2}\right) + \frac{2}{5}T(S^{2/5}-1)\right]\right\}. \qquad (10.37)$$

Equations (10.24), (10.25) yield the angular velocity $\dot{\beta}_{NEW}$ (10.33) :

$$\dot{\beta}_{NEW} = 2\dot{\beta}_1\left\{\frac{1}{2} - \varepsilon\left[\frac{2}{7}S^{7/5}F\left(1,\frac{9}{10};\frac{12}{5};S\right) - \frac{2}{7}F\left(1,\frac{9}{10};\frac{12}{5};1\right) + \frac{2}{5}T\sqrt{1-S}\right]\right\}. \qquad (10.38)$$

With :

$$F\left(1,\frac{9}{10};\frac{12}{5};1\right) = \frac{14}{5}, \qquad (10.39)$$

equation (10.38) can be reformulated to :

$$\frac{d\beta_{NEW}(T)}{dt} = \frac{d\beta(0)}{dt}\left[1 - \frac{5}{2}\frac{\zeta_{MAX}}{R}(1-\nu)(T-2)\right]\left[1 - 5\frac{\zeta_{MAX}}{R}(1-\nu)(T-2)\right]. \qquad (10.40)$$

For a change of the sign of $\dot{\beta}$, the following condition is necessary :

$$\frac{\zeta_{MAX}}{R} > \frac{1}{5}, \quad \frac{a}{R} > \frac{1}{2}. \qquad (10.41)$$

H.Hertz (1882) calculated in his work the example of steel spheres, which are pressed on a rigid plane by their dead weight. The equation for the contact radius becomes :

$$a^3 = R^4\gamma(1-\nu^2)\frac{1}{E} = \frac{1}{1000}R^{4/3}, \quad (\text{ a, R in mm }), \qquad (10.42)$$

where γ denotes the specific gravity.

sphere radius R	1 mm	1 m	1 km	1000 km
contact radius a	10^{-3} mm	10 mm	100 m	1000 km
a/R	1/1000	1/100	1/10	1/1

A sphere with a radius of 1 km has already a contact radius of 100 m, i.e. $a/R = 1/10$. H. Hertz wrote in his work, that this deformation is to large for his theory. It follows that a reflection with a change of sign transcends the frame of the Hertzian theory. A small contact area can not produce a large torque around the normal axis. When the spheres slide partially upon each other, the torsional moment is smaller than for full adhesion and a change of sign of the torque is impossible also. In contrast to the torsional impact the force of the tangential impact has the large lever-arm R and a change of sign is possible.

10.4 Complete sliding

For complete sliding the limit $k \to 0$ in equation (5.39) yields :

$$\frac{Ga^2}{fF_z} \beta = \frac{3k^2}{4\pi} D(k) \to \infty, \tag{10.43}$$

The torsional angle β should theoretically become infinite when the radius of the stick area becomes zero. We can take a small value of the radius of the stick area, e.g. $k = 0.99$, for the beginning of complete sliding. The equation of motion :

$$\theta_{zz} \frac{d^2\beta}{dt^2} = -M_Z , \tag{10.44}$$

becomes with equation (10.3) :

$$\frac{d^2\beta}{dt^2} = -\frac{5}{2mR^2} \frac{fG\pi}{2(1-\nu)} \zeta^2 , \tag{10.45}$$

or after normalization with (9.4) :

$$\frac{d^2\beta}{dt_N^2} = -\frac{105}{128} \pi f \left(\frac{\zeta_{MAX}}{R}\right)^{3/2} S^{4/5} . \tag{10.46}$$

Equation (10.46) can be reformulated using (9.5) :

$$\frac{d\beta}{dt_N} = -\frac{21}{64} \pi f \left(\frac{\zeta_{MAX}}{R}\right)^{3/2} \int_{S_G}^{S} F(a, \frac{1}{2}, a; S) \, dS , \tag{10.47}$$

where the index G indicates the time, when the spheres begin to slide completely. The variable a is an arbitrary constant. Integration of (10.47) yields in the period of compression :

$$\frac{d\beta}{dt_N} = \frac{d\beta(S_G)}{dt_N} - \frac{35}{128}\,\pi f\left(\frac{\zeta_{MAX}}{R}\right)^{3/2}\left\{S^{6/5}F\left(\frac{6}{5},\frac{1}{2},\frac{11}{5};S\right) - S_G^{6/5}F\left(\frac{6}{5},\frac{1}{2},\frac{11}{5};S_G\right)\right\},$$

$$\beta = \beta_G + \dot{\beta}_G(t_N-t_G) - \frac{35\pi f}{8\cdot 64}\left(\frac{\zeta_{MAX}}{R}\right)^{3/2}\left\{S^{8/5}{}_3F_2\left(1,\frac{8}{5},\frac{17}{10};\frac{11}{5},\frac{13}{5};S\right) - \right. \tag{10.48}$$

$$\left. - S_G^{8/5}{}_3F_2\left(1,\frac{8}{5},\frac{17}{10};\frac{11}{5},\frac{13}{5};S_G\right) - S_G^{6/5}F\left(\frac{6}{5},\frac{1}{2},\frac{11}{5};S_G\right)\left(t_N-t_G\right)\right\}.$$

If complete sliding starts in the period of restitution, we obtain :

$$\frac{dS}{dt_N} = -\frac{5}{2}\,S^{3/5}\,\sqrt{1-S}, \tag{10.49a}$$

$$\frac{d\beta}{dt_N} = \frac{d\beta(S_G)}{dt_N} + \frac{35}{128}\,\pi f\left(\frac{\zeta_{MAX}}{R}\right)^{3/2}\left\{S^{6/5}F\left(\frac{6}{5},\frac{1}{2},\frac{11}{5};S\right) - S^{6/5}F\left(\frac{6}{5},\frac{1}{2},\frac{11}{5};S_G\right)\right\},$$

$$\beta = \beta_G + \dot{\beta}_G(t_N-t_G) + \frac{35\pi f}{8\cdot 64}\left(\frac{\zeta_{MAX}}{R}\right)^{3/2}\left\{-S^{8/5}{}_3F_2\left(1,\frac{8}{5},\frac{17}{10};\frac{11}{5},\frac{13}{5};1\right) + \right. \tag{10.49b}$$

$$\left. + S_G^{8/5}{}_3F_2\left(1,\frac{8}{5},\frac{17}{10};\frac{11}{5},\frac{13}{5};S_G\right) - S_G^{6/5}F\left(\frac{6}{5},\frac{1}{2},\frac{11}{5};S_G\right)\left(t_N-t_G\right)\right\}.$$

For very large $\dot{\beta}_A$ complete sliding starts at the beginning of impact, i.e.: $S_G \to 0$. In this case equation (10.48) becomes :

$$\frac{d\beta(T/2)}{dt_N} = \frac{d\beta_A}{dt_N} - \frac{35\pi}{128}\left(\frac{\zeta_{MAX}}{R}\right)^{3/2}F\left(\frac{6}{5},\frac{1}{2},\frac{11}{5};1\right). \tag{10.50}$$

If complete sliding continues in the period of relaxation, equation (10.49) yields :

$$\frac{d\beta(T)}{dt_N} = \frac{d\beta(T/2)}{dt_N} - \frac{35\pi}{128}\left(\frac{\zeta_{MAX}}{R}\right)^{3/2}F\left(\frac{6}{5},\frac{1}{2},\frac{11}{5};1\right). \tag{10.51}$$

Insertion of (9.3), (9.4) in (10.50), (10.51) yields :

$$\frac{d\beta(T)}{dt} = \frac{d\beta(0)}{dt} - \frac{f\dot{\zeta}_A}{R}\sqrt{\frac{\zeta_{MAX}}{R}}\frac{21\pi^{3/2}\Gamma(1.2)}{32\,\Gamma(1.7)}. \tag{10.52}$$

The necessary condition (10.7) for sliding shortly after the beginning of impact is :

$$\dot{\beta}_A > \frac{f\dot{\zeta}_A}{R}\sqrt{\frac{R}{\zeta_{MAX}}}\frac{3\pi}{16(1-\nu)}, \tag{10.53}$$

where we substituted ζ with ζ_{MAX}. Equations (10.52), (10.53) yield and inequality for the change $\Delta\dot{\beta}$ of the angular velocity:

$$|\Delta\dot{\beta}| = \left|\frac{d\beta(T)}{dt} - \frac{d\beta(0)}{dt}\right| < \dot{\beta}_A\frac{\zeta_{MAX}}{R}\frac{7\pi\Gamma(1.2)(1-\nu)}{2\,\Gamma(1.7)}. \tag{10.54}$$

10.5 The torsional impact for elliptical contact area

For complete adhesion the torsional impact can be calculated analogously to section 10.1 and 10.2. In the case of complete sliding Coulomb's law has the form:

$$\sigma_{Z\theta} = f\sigma_{ZZ} = \frac{3fF_z}{2\pi ab}\sqrt{1 - \frac{x^2}{a^2} - \frac{y^2}{b^2}}, \tag{10.55}$$

The stress distribution must be integrated to determine the torque :

$$M_Z = \frac{3fF_z}{2\pi ab}\int_0^{2\pi}\int_{r=0}^{r(\theta)}\sqrt{1 - \frac{r^2}{a^2}\sin^2\theta - \frac{r^2}{b^2}\cos^2\theta}\cdot r^2 dr d\theta \tag{10.56}$$

The result is :

$$M_Z = \frac{3}{8}fF_z a\,E(k), \tag{10.57}$$

with E(k) as elliptical integral of the second kind (5.13) and the modul k :

$$k = \sqrt{1 - b^2/a^2}. \tag{10.58}$$

There are two limits :

1.) Circle :
$$M_z = \frac{3\pi}{16}fF_z a. \tag{10.59}$$

2.) Ellipse with $b \rightarrow 0$: $\qquad M_z = \dfrac{3}{8} fF_z a$. $\qquad\qquad$ (10.60)

Equations (10.56), (10.57) can be inserted in (10.44) and integrated analogously to section 10.4.

10.6 The numerical procedure

The program consists of the following parts :

1.) At the beginning of the period of compression the spheres stick always and equation (10.10) can be applied.
2.) Partial slip starts when the condition for partial slip (10.7) is satisfied, such that equations (10.28) are valid.
3.) Complete sliding can be assumed, when e.g. $k' = 0.1$ in equation (5.37). Then the method of chapter (10.4) can be applied.
4.) At the end of impact the torsional coefficient of restitution can be calculated :

$$\varepsilon_{TOR} = - \dot{\beta}(T)/\dot{\beta}(0) \; .$$ $\qquad\qquad$ (10.61)

The coefficient of restitution depends on several parameters, like :

$$\dot{\beta}(0), \; \zeta_{MAX}/R, \; f, \; \nu, \; a/b \; .$$ $\qquad\qquad$ (10.62)

Equation (10.40) yields the asympote for small angular velocities $\dot{\beta}(0)$:

$$\frac{\dot{\beta}(T)}{\dot{\beta}(0)} = \left[\, 1 - \frac{5}{2} \frac{\zeta_{MAX}}{R} (1-\nu)(T-2) \, \right] \left[\, 1 - 5 \frac{\zeta_{MAX}}{R} (1-\nu)(T-2) \, \right] . \qquad (10.63)$$

The asymptote for complete adhesion defined by (10.52) has an inclination of 45° and intersects the x-axis at the distance d :

$$\dot{\beta}(T) = \dot{\beta}(0) - d \; ,$$

$$d = \frac{f \dot{\zeta}_A}{R} \sqrt{\frac{\zeta_{MAX}}{R}} \; \frac{21 \, \pi^{3/2} \, \Gamma(1.2)}{32 \; \Gamma(1.7)} \; . \qquad\qquad (10.64)$$

The asymptotes (10.63), (10.64) are plottet in fig. 10.2, for the impact of a steel

sphere and a rubber sphere. In the case of the steel sphere, the asymptote (10.64) is valid for very large angular velocities of several thousand rotations per second. The higher value of the asymptotes (10.63), (10.64) can be used as approximation for the coefficient of restitution, which is slightly smaller than the real value. Horák (1961) observed a change of sign of the torsional velocities before and after impact in his experiments, but he used very soft and possibly hollow rubber balls. Furthermore it seems, that the contact radius in his experiments was much larger than the allowable 10% of the ball radius in the frame of the Hertzian theory.
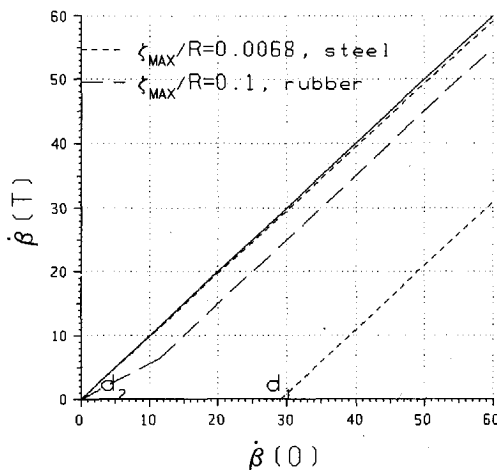

Fig. 10.2: Equations (10.63), (10.64).

11 Numerical solution of the contact problem by J. J. Kalker

The basic concept of the numerical solution of contact problems was worked out by J. J. Kalker. He published the first algorithm for frictional contact problems, especially rolling contact (1967). In that work the contact pressure and deformation was prescribed by polynomials. These polynomials are not useful for large contact areas with more than 50 points, because they become unstable for high orders. The first algorithm for a wide class of normal contact problems was published by Fridman and Chernina (1967). They used a variatonal formulation of the contact problem to reduce it to a so called quadratic programming problem. This formulation is necessary to prove existence and uniqueness of normal contact, which was done by Fichera (1964). Independent of Fridman and Chernina, Conry and Seirig (1971) and Kalker and Van Randen (1972) came up with optimization solutions for the normal contact problem. Kalker & Van Randen calculated influence coefficients for the normal deflexion of the surface due to a linear pressure distribution on a triangle. The contact area consists of a mesh of triangles.

In a paper dating from (1971) Kalker introduced a variational principle for the problem of friction. This principle appeared to be quite powerful in two- dimensional frictional contact in which there are only the normal and one tangential direction. Interesting results on steady-state and non-steady-state 2D rolling where obtained. The principle could be adapted to a 3D situation, but it was too slow to be of much practical use. An improved variational principle, due to Duvaut and Lions (1972) led to a much faster steady-state program called Duvorol (Kalker, 1979).

Although most of Kalkers work was dedicated to rolling problems, his algorithms can be applied to all types of contact problems on the base of the half-space approximation. This approximation was published by H.Hertz (1882), who used the half-space solutions of Boussinesq (1885) and Cerruti (1882) for the normal contact of ellipsoid bodies. Numerical algorithms on the base of this theory are much faster than FEM-methods. Kalker proved in his work, that the nonlinear frictional problem can be solved with successive algorithms. He used an equidistant rectangular mesh with a constant pressure distribution over each element. The form of the contact area and the slip area could be determined by a successive correction. The slip and stress directions

were calculated with a Newton-Raphson method. Furthermore he developed several algorithms which accelerated the calculation. These are already the essential parts of the numerical solution of the impact problem.

11.1 The load-displacement equations for a discrete pressure distribution

The use of a rectangular mesh with a constant pressure distribution over each element allows an easy programming of this problem. Indeed, polynomials or linear pressure distributions yield more difficult programs, which are difficult to correct even if the algorithm converges. This is the reason, why we used Kalker's method for our problem. We present his formulation here, because it differs slightly from our notation. His load displacement equations have the form :

$$
\begin{bmatrix} u_j \\ v_j \\ w_j \end{bmatrix} = \begin{bmatrix} \xi \\ \eta \\ \zeta - z \end{bmatrix} + \frac{1}{\pi G} \sum_{i=1}^{N} \begin{bmatrix} KI_5 & KI_6 & (1-\nu)I_1 \\ (1-\nu)I_1+\nu I_2 & \nu I_3 & -KI_5 \\ \nu I_3 & (1-\nu)I_1+\nu I_4 & -KI_6 \end{bmatrix} \begin{bmatrix} p_{i1} \\ p_{i2} \\ p_{i3} \end{bmatrix} , \quad (11.1)
$$

i = point of application , j = point of observation .

The material constants G, K and ν are :

$$
\frac{1}{G} = \frac{1}{2} \left(\frac{1}{G_1} + \frac{1}{G_2} \right) , \quad \frac{\nu}{G} = \frac{1}{2} \left(\frac{\nu_1}{G_1} + \frac{\nu_2}{G_2} \right) , \quad \frac{K}{G} = \frac{1}{2} \left(\frac{1-2\nu_1}{G_1} - \frac{1-2\nu_2}{G_2} \right) . \quad (11.2)
$$

Index 1 denotes the wheel and index 2 the rail, resp. the upper and the lower body. The orientation of the mesh is shown in figure 11.1.

$$
\left. \begin{array}{ll}
I_1 = \iint_M \dfrac{dx'dy'}{|x-x'|} , & I_3 = \iint_M \dfrac{(x-x')(y-y')}{|x-x'|} dx'dy' , \\[3mm]
I_2 = \iint_M \dfrac{(x-x')^2}{|x-x'|} dx'dy' , & I_4 = \iint_M \dfrac{(x-x')}{|x-x'|} dx'dy' , \\[3mm]
\multicolumn{2}{c}{I_j = I_j(x, x_p, \Delta x) , \quad j = 1 \ldots 4 ,} \\[2mm]
\multicolumn{2}{c}{M \text{ is the rectangle with the vertices } (x_p \pm \Delta x/2 , y_p \pm \Delta y/2) ,} \\[2mm]
\multicolumn{2}{c}{\Delta x, \Delta y : \text{ length of the sides of the discretization rectangles.}}
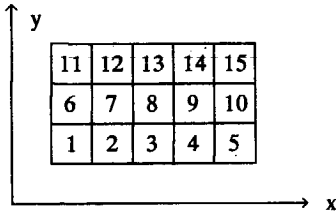\end{array} \right\} \quad (11.3)
$$

Fig. 11.1: Discretization of the
contact area.

Using the following abbreviated notations :

$$[\, \ldots \,]_x = [\, \ldots \,]_{x-x_p-\Delta x/2}^{x-x_p+\Delta x/2}, \quad (11.4)$$

we have that :

$$\iint_M \frac{\partial^2 f}{\partial x' \partial y'} \, dx'dy' = [\, [f(x',y')]_x \,]_y, \quad (11.5)$$

and it may be verified, that with :

$$sh^{-1} z \equiv \ln(z+\sqrt{z^2+1}) , \quad (11.6)$$

the derivatives of the integrals I_j are :

$$\left.\begin{array}{r}
\dfrac{\partial^2}{\partial x' \partial y'} \left\{ \, y' \, sh^{-1}\left(\dfrac{x'}{|y'|}\right) + x' \, sh^{-1}\left(\dfrac{y'}{|x'|}\right) \, \right\} = \dfrac{1}{\sqrt{x'^2+y'^2}} \, , \\[2mm]
\dfrac{\partial^2}{\partial x' \partial y'} \left\{ \, y' \, sh^{-1}\left(\dfrac{x'}{|y'|}\right) \, \right\} = \dfrac{x'^2}{(x'^2+y'^2)^{3/2}} \, , \\[2mm]
\dfrac{\partial^2}{\partial x' \partial y'} \left\{ \, - \sqrt{x'^2+y'^2} \, \right\} = \dfrac{x'y'}{(x'^2+y'^2)^{3/2}} \, , \\[2mm]
\dfrac{\partial^2}{\partial x' \partial y'} \left\{ \, \dfrac{1}{2} \, y' \, \ln\left(x'^2+y'^2\right) + x' \, \tan^{-1}\left(\dfrac{y'}{x'}\right) \, \right\} = \dfrac{x'}{x'^2+y'^2} \, .
\end{array}\right\} \quad (11.7)$$

By means of (11.6) and (11.7) we can readily integrate the integrals in (11.3). Comparison with the formulation of chapter 4.3 shows, that both formulations are identical.

11.2 Contact algorithms for normal contact

In this section we discuss a very simple and effective algorithm, which was conceived by Johnson in the late sixties, early seventies; it was rediscovered by Ahmadi, Keer and Mura (published 1983), while Kalker removed a restriction and gave a new proof of it (1982). Fig. 11.2 shows the module NORM with the logical variable ContactChanged and the deformed distance d_i (Kalker, 1990).
The characteristics of this algorithm are :

1.) The loops are nested and not sequential. It follows that the contact area first decreases until it remains constant. The following step belongs to the outer loop and the contact area may increase again. The inner loop is again repeated until no further decrease of the contact area occurs. The outer loop is repeated if necessary.

2.) The contact area K is initialized at the beginning. It may be zero or all elements of the area of integration may belong to K. Another possibility would be an approximation with Hertz's solution (see chapter 5.1).

3.) The most time consuming part of the program is the matrix inversion which is necessary to solve the linear equation system.

$\sigma_i = 0$, for $1 \leq i \leq n+1$;   ContactChanged = True;
For $i=1$ to $n+1$ do
yes $d_i \leq 0$?   no
$i \in$ Contact $i \notin$ Contact
While ContactChanged do
While ContactChanged do
ContactChanged = False;
For $i=1$ to $n+1$ do
yes $i \in$ Contact ?   no
$d_i = 0$; $\sigma_i = 0$;
Solve the linear equation system;
For $i=1$ to $n+1$ do
yes $i \in$ Contact ?   no
yes $\sigma_i \leq 0$?   no
$i \notin$ Contact; ContactChanged = True;
For $i=1$ to $n+1$ do
yes $i \notin$ Contact ?   no
yes $d_i \geq 0$?   no
$i \in$ Contact; ContactChanged = True;
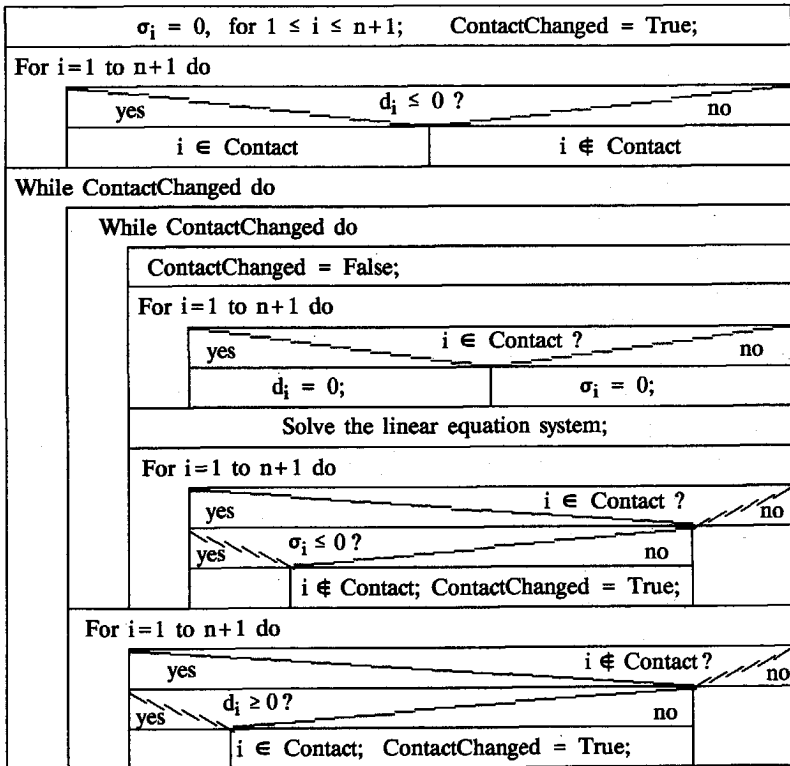
Fig. 11.2: The module Norm.

A proof of the validity of this algorithm is given in Kalker (1983). There are other algorithms, which presuppose special forms of the normal pressure, like the Line Contact Theory (1971). It presupposes that the contact area is slender and the tips are not blunt. The last restriction was removed by Reusner (1977), who assumed that the pressure distribution in the narrow direction is semi-elliptical.

In fig. 11.2 the Nassi-Shneiderman diagram of the module Norm is drawn, where the variable σ_i denotes the normal stress, d_i the normal distance of the surfaces, i is the index of the element and 'ContactChanged' denotes a boolean variable.

11.3 Algorithms for frictional contact

This algorithm solves the frictional contact problem when the normal pressure, the creepage, and the previous traction distibution are given. From the Nassi-Shneiderman diagram of the module TANG (Kalker 1986) in fig. 11.3, we see that this algorithm is very similar to the algorithm for the normal problem. The arrangement of the loops is sequentiel again and instead of the contact area K the stick area A is determined. The initialized values are arbitrary. Some questions must be answered before this algorithm can be programmed: There are several ways of linearization and my opinion is that a third inner loop would be necessary to solve the nonlinear equation system, until the error of the linearized solution is small enough. There are three algorithms proposed by J.J Kalker (1986) for frictional contact:

1.) The Johnson process.

Calculate the normal problem N, and then the tangential problem T. In this manner the influence of N on T is taken into account, but not vice versa. In the case of bodies of similar material this solution is exact. Otherwise the Johnson process offers an approximation.

2.) The Panagiotopoulos process.

This is a chain of Johnson processes, viz. NT NT NT . . . . until convergence occurs, or the iteration bound is reached.

3.) The Kombi process.

This is an alternative of the Panagiotopoulos process. In it, N and T are combined. Kombi reduces to the Johnson process when the materials are similar, but then it costs roughly three times as much computer time as the Johnson

process. On the other hand for dissimilar materials Kombi takes the interrelation of N and T into account at every step of the algorithm. Neither the Panagiotopoulos nor the Kombi process converge in all possible cases.

The convergence of this algorithm depends also on the linearized equations, because the Newton-Raphson formula converges only for small corrections $\Delta \tau$. Furthermore the approximation for the slip area must be good enough, because otherwise slip is assumed in the potential area of adhesion, with too high values for the stress.

$\tau_i = 0$, for $1 \leq i \leq n+1$; SlipAreaChanged = True; Initialize Sliparea;
While SlipAreaChanged do

While SlipAreaChanged do

SlipAreaChanged = False;

For i=1 to n+1 do

i ∈ SlipArea?   yes / no

$\sigma_{ti} = -f|\sigma_i| s_i/|s_i|$; $s_i = 0$;

Solve the nonlinear equation system;

For i=1 to n+1 do

i ∉ SlipArea?   yes / no

$|\sigma_{ti}| > |f\sigma_{ni}|$?   yes / no

i ∈ SlipArea; SlipAreaChanged = True;

For i=1 to n+1 do

i ∈ SlipArea?   yes / no

$(\sigma_{ti} s_i) < 0$?   yes / no

i ∉ SlipArea; SlipAreaChanged = True;

Fig. 11.3: The module Tang with the slip s_i and the tangential stress σ_{ti}.

The Nassi-Shneiderman diagram of module Tang is drawn in fig. 11.3, with the tangential stress σ_{ti}, the normal stress σ_{ni}, the slip s_i of element i and the boolean variable 'SlipAreaChanged'.

12 The Gauss-Seidel solution for frictional contact problems

The Gauss-Seidel Method makes it possible to solve contact problems with more than 1000 points in the contact area, on IBM-compatible personal computers under the operating system MS-DOS, without memory swapping on the hard disk and without protected mode. The two basic advantages, compared with the ordinary Gauss elimination, are the savings of computer memory and execution time. Earlier programs, like Kalker's program Contact, installed on a standard IBM-AT/286, were able to calculate about $n = 50$ points in the contact area, with an execution time of n^3. The execution time of our program increases proportional to n^2, and a typical load-history in 10 steps, for a flat punch with 1000 points, was running two days on an IBM386/33MHz. We store only $3n$ coefficients of the periodic load-displacement matrix, instead of the complete set of coefficients, which amounts to 29 kilobytes memory compared with 11 megabytes for 400 points. Kalker used a similar formulation in his program 'Contact' (Kalker 1990), but he still stores the inverse matrix, which is not necessary for the Gauss-Seidel method.

Contact calculations with modern Finite Element programs require a three-dimensional mesh with approximately n^2 nodes, and load displacement matrices of the magnitude of n^4, which yields long execution times and makes large hard disks necessary. Besides, the nonlinear iteration process with varying slip directions, stick areas and contact areas, is very difficult to progam with Finite Element Methods.

Our program consists of four basic modules: The first module solves the linear equation system, the second tests the contact area, the third determines the slip area and the last one calculates the approximated slip directions. Two modules for the Hertz problem were copied from the program 'Contact' by J.J. Kalker. Other modules of our program perform graphical operations. All modules were written in Turbo-Pascal with the typical Structured Programming Techniqes. The four basic modules can be concatenated sequentially or nested coherently, but not every arrangement will converge.

Some computational difficulties arise through the fact, that the contact area, the slip area and the slip directions must be known, in order to establish the linear equation system for the stresses and deformations. On the other hand, the stresses and

deformations must be known in order to test the contact conditions. Therefore we use a first estimation and solve the linear equation system recursively, until the solution is found. The test of the contact conditions and the correction of the slip directions has to be arranged consistently for each solution, to avoid divergence of the process.

The contact conditions and sign conventions are formulated in chapter 12.1, and in chap. 12.2 we describe some contact algorithms and the modules. In chapter 12.3 we reformulate the linear equation system, in order to reveal the internal symmetries in the matrices. These symmetries are due to the homogeneity of the half-space, because a constant pressure distribution on any rectangle produces always the same deformation field relative to the loaded rectangle, i. e.: The solution is a combination of point loads, which produce the same deformation on different positions. This idea can even be used to solve problems with arbitrary bodies, when the solution for a point load is known, possibly by Finite Element Methods. In chapter 12.4 we describe the Gauss-Seidel algorithm, which solves the linear equation system for the stresses with given displacements in the stick area on the condition, that the contact area, the stick area and the stress directions are fixed.

A considerable theoretical and numerical work, done by J.J. Kalker (1988, 1990), proved that the contact and the slip area can be determined by recursive routines, which correct the shape and size of these areas successively, on the points where the contact conditions are violated. However, a first guess has to be made and the slip directions must be constant. A similar, recursive procedure can be created for the stress directions, such that the stress direction is oriented opposite to the current slip directions in the first step, and the linear equation system is solved in the next step, repeatedly, but this algorithm diverges after a few cycles. In chapter 12.5 we develop an algorithm of the 'Regula Falsi' Type, which solves the nonlinear equation system approximately by linearization and repeats the Gauss-Seidel procedure for the new slip directions. This algorithm requires little computer storage and converges rapidly, but the condition for the linearization is a relatively exact solution. If the initial values of the stress σ are to incorrect, the linearization does not converge. Nevertheless, our program solves this problem anyway by trial and error, because we interrupt the slip direction loop after some cycles and the points with wrong slip directions are added to the stick area in the last loop. In the case of complete adhesion, we have relatively correct stress directions, which are the first estimation for the slip directions when slip starts in some points in the next loop. The convergence depends also on the numbers for the maximal iterations of each cycle. Small numbers make the program faster, but the solution of each loop becomes more inaccurate, such that divergence can take

place.

The Gauss-Seidel algorithm is a version of the 'Successive Over Relaxation' method (SOR) with an 'Over Relaxation Factor' of the amount of one. In the case of complete adhesion without slip in the contact area, the load-displacement matrix is symmetric and positive definite and so the SOR method converges always (Engeln-Muellges 1987). The proof of convergence for partial slip is more complicated. In chapter 13 we will prove convergence for complete slip in x-direction and a contact area in the form af a small strip, parallel to the x-axis, which is the extreme form for maximal interaction between normal and tangential stresses. We continue with the derivation of a formula for the limit of convergence, which is never violated in real contact problems. Since the influence of the slip stresses on the process of convergence is much smaller for other forms of contact areas and for smaller slip areas, the SOR method converges always in cases, where the limit of convergence is not reached.

An estimation for the optimal 'Over Relaxation Factor' is possible, but we have to calculate the eigenvalues of different matrices, which depend on the contact area, the stick area, the coefficitents of friction and on the material. We do not investigate this eigenvalue problem any further, because the solution is more complicated than the solution of our contact problem and the 'Over Relaxation Factor' changes through the iteration process.

12.1 Contact conditions and sign conventions

The surface of the two bodies can be given in discrete form for a set of points x_k, y_k or as a mathematical function. To simplify matters, we assume Hertzian surfaces (Hertz 1882), which can be approximated by elliptical paraboloids. The undeformed distance is given by equation (5.2) :

$$z = Ax^2 + By^2 . \qquad (12.1)$$

The formulae for A and B can be found in chapter 5.1 of this work. Now we move the upper body 2 relative to the lower body 1 in x,y,z-direction over the distances ξ, η, ζ and twist body 2 by the amount Ω. The combined displacements of the two surfaces are :

$$U[1,m,n] = u_1 - u_2 = u = \xi + y\Omega \ , \quad \left.\right\} \ \text{in the stick area} \ ,$$
$$U[2,m,n] = v_1 - v_2 = v = \eta - x\Omega \ , \quad$$
$$U[3,m,n] = w_1 + w_2 = w = \zeta - Ax^2 - By^2 \ , \text{ in the contact area} \ ,$$
$$\xi = \xi_2 - \xi_1 \ , \quad \eta = \eta_2 - \eta_1 \ , \quad \zeta = \zeta_2 - \zeta_1 \ . \tag{12.2}$$

with ξ, η, ζ from (5.19). We illustrate the sign convention for the displacements in fig. 5.4, where the coordinate system is fixed on the lower body 1 and body 2 is shifted in x-direction by the amount ξ. In the following sections we regard the contact area, looking from a point above body 1 in z-direction. It is important to remember this sign convention, because Kalker (1990) defines body 1 as the upper body and shifts body 1 relative to body 2, which produces negative deformations on body 1. Compared to our sign conventions, left and right and top and bottom of Kalkers stick area are reverse, looking on body 1.

The normal contact stress p_z (4.4a) must be positive inside of the contact area and zero outside. The contact stress is positive for compression, because contact stresses are mostly compressive :

$$\sigma[3,m,n] > 0 \ , \text{ in the contact area} \ ,$$
$$\sigma[i,m,n] = 0 \ , \ i=1,2,3, \text{ outside of the contact area} \ . \tag{12.3}$$

We assume Coulomb friction :

$$|\sigma_t| < f_{stat} \, \sigma_n \ , \text{ in the stick area} \ , \quad \left.\right\} \ f_{stat} \geq f_{kin} \ ,$$
$$\sigma_t = - f_{kin} \frac{s}{|s|} \, \sigma_n \ , \text{ in the slip area} \ , \quad$$
$$\sigma_t = (\ \sigma[1,m,n], \ \sigma[2,m,n]\ )^T \ , \quad \sigma_n = \sigma[3,m,n] \ , \tag{12.4}$$
$$s = (\ s_x[m,n], \ s_y[m,n]\ ) \ ,$$

where the variables f_{kin}, f_{stat} denote the kinetical and statical coefficient of friction. The direction of the frictional stress σ_t, which body 2 excerts on body 1, is opposite to the direction of the velocity s of body 1 relative to body 2. We call this relative velocity *slip*. Coulomb's law measures the force on one body, and attaches the laboratory system for the relative velocity on the other body (fig. 12.1).

The slip directions change in the course of the load history and must be calculated for each increment. We introduce the 'rigid shift increments' $\Delta\xi$, $\Delta\eta$ in x, y- direction, the increment of the 'rigid rotation' $\Delta\Omega$, and the slip s_x, s_y to formulate Coulomb's law in the slip area :

$$s_x[m,n] = -\Delta\xi + \Delta U[1,m,n] + y[m,n]\,\Delta\Omega,$$

$$s_y[m,n] = -\Delta\eta + \Delta U[2,m,n] - x[m,n]\,\Delta\Omega,$$

$$\Delta\xi = \Delta\xi_2 - \Delta\xi_1,\ \Delta\eta = \Delta\eta_2 - \Delta\eta_1,\ \Delta\zeta = \Delta\zeta_2 - \Delta\zeta_1,\ \Delta\Omega = \Delta\Omega_2 - \Delta\Omega_1,$$

$$\Delta U[l,m,n] = \Delta U_1[l,m,n] - \Delta U_2[l,m,n], \tag{12.5}$$
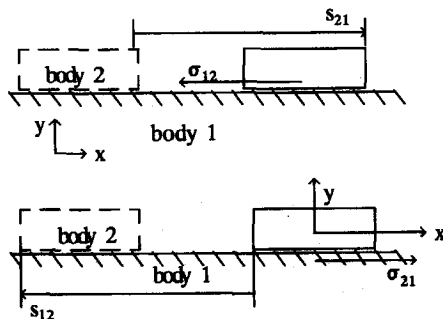
where the low indices denote body 1 or body 2.

Fig. 12.1: The slip s_{ik} of body i relative to body k and
the stress σ_{ki}, which body k excerts on body i.

The next condition avoids penetration outside of the contact area :

$$U[3,m,n] > \zeta - Ax^2 - By^2 \text{ , outside of the contact area ,} \tag{12.6}$$

where ζ designates the approach of distant reference points of the two bodies. The stresses of correspoinding points on the surface of the two bodies must be opposite in the contact area :

$$\sigma[l,m,n]\,|_{\text{body 1}} = -\sigma[l,m,n]\,|_{\text{body 2}} \text{ , in the contact area , } 1 \leq l \leq 3 \text{ ,} \tag{12.7}$$

where the normal stress $\sigma[3,m,n]$ on body 2 is measured in the common coordinate system, with z_2 pointing into body 1. The summation of all stresses yield the forces F[i]:

$$F[i] = \sum_{m=0}^{\text{rows-1}} \sum_{n=0}^{\text{cols-1}} \sigma[i,m,n]\,\Delta x\,\Delta y \text{ , } i = 1, 2, 3 \text{ .} \tag{12.8}$$

12.2 Vector formulation of the load-displacement equations

The arrangement of the stress and displacement components in two dimensional arrays in equations (4.13), (4.23) is very useful for programming, but it obstructs the recognition of the symmetry of the matrix A of the load displacement coefficients. Thus we rearrange the displacement array U line by line in the one column vector u, starting with the displacement components in x-direction :

$$u^T = (u_1^T, u_2^T, u_3^T) , \qquad (12.9)$$

$$u_i^T = (U[i;0,0], U[i;0,1], U[i;0,2], \dots , U[i;rows-1,cols-2], U[i;rows-1,cols-1]),$$

where the letter T indicates transposition. The vector u is decomposed in the partitions u_1, u_2, u_3 of the displacement components in x-, y- and z-direction. We rearrange the stress array σ and the array A :

$$\begin{bmatrix} u_1 \\ u_2 \\ u_3 \end{bmatrix} = \begin{bmatrix} A_{11} & A_{12} & A_{13} \\ A_{21} & A_{22} & A_{23} \\ A_{31} & A_{32} & A_{33} \end{bmatrix} \begin{bmatrix} \sigma_1 \\ \sigma_2 \\ \sigma_3 \end{bmatrix} . \qquad (12.10)$$

Above and in the following bold capitals denote matrices. The submatrices A_{ij} are two dimensional square arrays forming the partitioned matrix A, which is a square matrix containing $3n \cdot 3n$ elements, $n = cols \cdot rows$. From (4.23) follows, that the diagonal submatrices A_{ii} and A_{12}, A_{21} are symmetric while the other matrices are skewsymmetric. To understand the structure of the matrices A_{ij} we have to analyse the interaction between the rows of the contact area. Therefore we decompose matrix A_{11} into the submatrices B_j, which describe the deformation of first row due to a pressure distribution acting on the elements of row j :

$$A_{11} = \begin{bmatrix} B_0 & B_1 & B_2 & B_3 & \dots & B_{rows-1} \\ B_1 & B_0 & B_1 & B_2 & \dots & B_{rows-2} \\ B_2 & B_1 & B_0 & B_1 & \dots & B_{rows-3} \\ \dots & \dots & \dots & \dots & \dots & \dots \\ B_{rows-1} & \dots & \dots & \dots & \dots & B_0 \end{bmatrix} . \qquad (12.11)$$

The submatrices B_j are quadratic with $cols \cdot cols$ Elements. Equation (4.23) yields :

$$B_{|m-j|}[k,n] = A[1,0,0;1,|m-j|,|n-k|], \quad 0 \le k,n \le cols-1, \quad 0 \le j,m \le rows-1. \quad (12.12)$$

A_{11} is called a symmetric Block Toeplitz Matrix (Horn/Johnson 1985), because the submatrices B_j are arranged in a cyclic form. Every submatrix B_j is a symmetric

Toeplitz Matrix again :

$$
\mathbf{B_j} = \begin{bmatrix} b_{j0} & b_{j1} & b_{j2} & \ldots & b_{j,cols-1} \\ b_{j1} & b_{j0} & b_{j1} & \ldots & b_{j,cols-2} \\ b_{j2} & b_{j1} & b_{j0} & \ldots & b_{j,cols-3} \\ \cdots & \cdots & \cdots & \cdots & \cdots \\ b_{j,cols-1} & \cdots & \cdots & \cdots & b_{j0} \end{bmatrix} \, .
$$
(12.13)

Now we set $j=0$ and the component b_{0i} describes the deformation $u_1[i]$ in x-direction of element $[0,i]$ of the first line of the contact area in fig 4.1, due to a constant stress distribution in x-direction, of the amount of one, acting on the first rectangle $[0,0]$ of the contact area. The components b_{0i} form the first line of matrix $\mathbf{B_0}$. The second line describes the deformations of the same elements due to a constant pressure distribution, of the amount of one, on the second rectangle $[0,1]$ of the contact area (fig. 12.2). Since the pressure distribution of element $[0,1]$ is identical to the former distribution on element $[0,0]$, the deformation of the second element $[0,1]$ must now be identical to the former deformation of the first element. Application of the same pressure distribution on the third element yields a deformation of this element which is identical to the former deformation of the second element etc. Thus we get the symmetric Toeplitz stucture of $\mathbf{B_0}$, where the matrix components are constant on diagonals. From the symmetry of A in (4.23) follows the symmetry of $\mathbf{B_0}$.

A similar interpretation shows, that matrix $\mathbf{B_1}$ contains the deformations $u_1[i]$ of the first line of rectangles of the contact area, resulting from a constant pressure distribution in one of the rectangles in line two. Since a unit pressure distribution on a rectangle on line 3 produces the same deformations in line 2 and a unit pressure distribution in any line deforms the foregoing line equally, all the blockmatrices in the neighbouring line parallel to the diagonal in $\mathbf{A_{11}}$ must be identical to the blockmatrix $\mathbf{B_1}$.

All matrices $\mathbf{A_{ii}}$ have the same structure. The arrangement of the blockmatrices of $\mathbf{C_j}$ in matrix $\mathbf{A_{12}}$ is skewsymmetric, while all blockmatrices are skewsymmetric. It follows that $\mathbf{A_{12}}$ is symmetric in its elements $\mathbf{A_{12}}[i,j]$. We show this in the following equations, where we use the letter $\mathbf{C_j}$ for the blockmatrices :

$$
\mathbf{A_{12}} = \begin{bmatrix} \mathbf{C_0} & \mathbf{C_1} & \mathbf{C_2} & \ldots & \mathbf{C_{rows-1}} \\ -\mathbf{C_1} & \mathbf{C_0} & \mathbf{C_1} & \ldots & \mathbf{C_{rows-2}} \\ -\mathbf{C_2} & -\mathbf{C_1} & \mathbf{C_0} & \ldots & \mathbf{C_{rows-3}} \\ \cdots & \cdots & \cdots & \cdots & \cdots \\ -\mathbf{C_{rows-1}} & \cdots & \cdots & \cdots & \mathbf{C_0} \end{bmatrix} \, .
$$
(12.14a)

$$
\mathbf{C_j}[k,n] \, , \quad 0 \le k,n \le cols-1 \, , \quad 0 \le j \le rows-1 \, .
$$

$$\mathbf{C_j} = \begin{bmatrix} c_{j0} & c_{j1} & c_{j2} & \cdots & c_{j,cols-1} \\ -c_{j1} & c_{j0} & c_{j1} & \cdots & c_{j,cols-2} \\ -c_{j2} & -c_{j1} & c_{j0} & \cdots & c_{j,cols-3} \\ \cdots & \cdots & \cdots & \cdots & \cdots \\ -c_{j,cols-1} & \cdots & \cdots & \cdots & c_{j0} \end{bmatrix}.$$ (12.14b)

Matrix $\mathbf{A_{13}}$ contains blockmatrices $\mathbf{D_j}$ which are symmeric, but the arrangement of blockmatrices is skewsymmetric, while matrix $\mathbf{A_{23}}$ contains skewsymmetric blockmatrices $\mathbf{E_j}$, with a symmetric arrangement of the blockmatrices. If follows that the matrices. $\mathbf{A_{13}}$ and $\mathbf{A_{23}}$ are skewsymmetric in its elements. Using (4.23) and the results above, we can rewrite (12.10) to :

$$\begin{bmatrix} \mathbf{u_1} \\ \mathbf{u_2} \\ \mathbf{u_3} \end{bmatrix} = \begin{bmatrix} \mathbf{A_{11}} & \mathbf{A_{12}} & \mathbf{A_{13}} \\ \mathbf{A_{12}^T} & \mathbf{A_{22}} & \mathbf{A_{23}} \\ \mathbf{A_{13}^T} & \mathbf{A_{23}^T} & \mathbf{A_{33}} \end{bmatrix} \begin{bmatrix} \boldsymbol{\sigma_1} \\ \boldsymbol{\sigma_2} \\ \boldsymbol{\sigma_3} \end{bmatrix},$$ (12.15)

where we used the fact that the transposed of a skewsymmetric matrix is identical to its negative. From (12.15) we see, that the complete matrix $\mathbf{A}$ is symmetric.
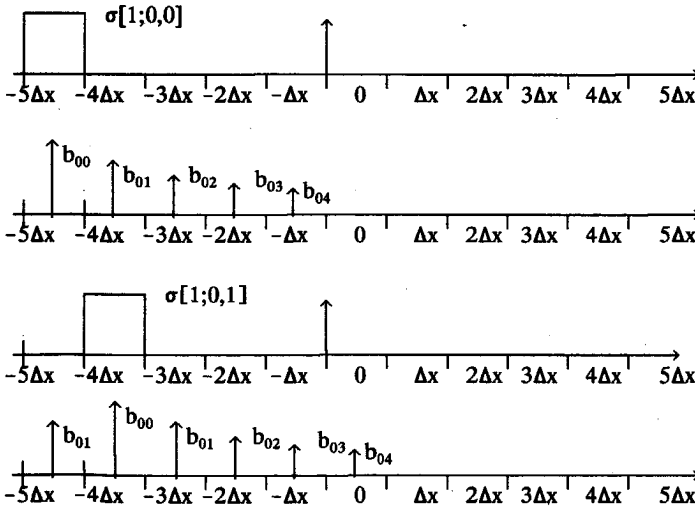
Fig. 12.2: The stress distribution on element 1 and 2 and the resulting deformations for the first row.

12.3 The Gauss-Seidel procedure

To simplify matters, we use the formulation of (12.15) in this chapter, by sorting the displacements in one column of the vector **u**, which has the form (12.9) and repeat this rearrangement for the stresses σ and the load displacement matrix **A**. Now we get for (12.15) :

$$\mathbf{A}\sigma = \mathbf{u} \ , \quad \mathbf{u}[l] = U[i;j,k] \ , \quad \sigma[l] = \sigma[i;j,k] \ ,$$

$$l = (i-1)N + j \cdot \text{cols} + k \ , \quad N = \text{cols} \cdot \text{rows} \ , \qquad (12.16)$$

$$1 \le i \le 3 \ , \quad 0 \le j < \text{rows} \ , \quad 0 \le k < \text{cols} \ , \quad 0 \le l < 3N \ ,$$

where the displacements **u** are given and the stresses σ are the unknown components. The arrangement of σ and **u** in (12.16) is identical to the arrangement in (12.9). The elements [0 .. N-1] denote the x-components, [N .. 2N-1] signify the y-components and [2N .. 3N-1] indicate the z-components of the stresses and displacements.

We modified the Gauss-Seidel procedure (Engeln-Muellges 1987), because the tangential displacements are prescribed in the stick area only and Coulomb's law holds in the slip area, while the normal displacements are prescribed in the whole contact area :

$$\left. \begin{array}{l} \sigma_{m+1}[j] = \dfrac{1}{A[j,j]} \left\{ u[j] - \displaystyle\sum_{k=j+1}^{3N-1} A[j,k]\,\sigma_m[k] - \displaystyle\sum_{k=0}^{j-1} A[j,k]\,\sigma_{m+1}[k] \right\} , \\[4pt] \qquad \text{for } 2N \le j < 3N, \text{ or } j \text{ in the stick area} , \\[6pt] \sigma_{m+1}[j] = \cos \alpha_j \, \sigma_{m+1}[2N+j] \ , \ 0 \le j < N \ , \\ \sigma_{m+1}[j] = \sin \alpha_j \, \sigma_{m+1}[N+j] \ , \ N \le j < 2N, \end{array} \right\} \begin{array}{l} \\ \\ \text{for } j \text{ in the slip area,} \end{array} \qquad (12.17)$$

where σ_m indicates the solution of step m and α_j denotes the angle between the x-axis and the fixed stress direction. The first equation determines the tangential stress in the stick area and the normal stress in the contact area. The second equation determines the tangential stress in the slip area, following Coulomb's law. The second equation can be performed at the end of each iteration or directly after the determination of a normal stress component. We prove the convergence of this method for some examples in chapter 13.

The Gauss-Seidel algorithm converges for positive definite and symmetric matrices (Engeln/Muellges). **A** is positive definite, because :

$$\sum_j \sum_i A[i,j] \ \sigma[i] \ \sigma[j] \ = \ \sum_j u[j] \ \sigma[j] \ = \ E \ > \ 0 \ , \qquad (12.18)$$

where E is the work performed by the surface stresses $\sigma[j]$, which must be positive.

The programming of (12.17) can be simplified by moving the rows and columns of (12.17) symmetrically, which does not affect the symmetry and the positive definiteness in the case of complete adhesion. In our program we used the formulation (4.13), (4.23) for the matrix A and perform a double sum, to save computer memory. The change of sign in (4.23) can be formulated without multiplication to accelerate the program.

12.4 Linearization of the frictional law

We mentioned earlier, that a direct successive iteration method for the slip directions is unstable. Because equations (12.4), (12.5) are nonlinear, we choose the Regula Falsi procedure (Engeln-Muellges/Reuter 1987) and linearize these equations. The resulting linear equation system can be solved by matrix inversion.

The purpose of the Gauss-Seidel procedure, however, was to avoid the matrix inversion. The complete matrix of the linearized frictional law for the slip direction is still too large and the matrix inversion too slow for a useful program. We establish a compact linear equation system and solve it by a Gaussian Block Iteration Method. These corrections will be inserted in the Gauss-Seidel procedure to determine the correct solution σ_{10}, σ_{20} for the new slip directions. Now we calculate a new correction $D\sigma_1$, $D\sigma_2$ for the slip stress and repeat this procedure until the error between the slip direction and the direction of the stress becomes small enough.

We use the formulation (12.10), where the arrays U and σ of (4.13) are rearranged as vectors and the matrix A is a two dimensional array. The indices 1, 2, 3 denote the cartesian coordinates x,y,z. We repeat Coulomb's law (12.4), (12.5) for sliding friction in the slip area :

$$s_x[i] \ / \ s_y[i] \ = \ \sigma_1[i] \ / \ \sigma_2[i] \ ,$$
$$\sqrt{ \ \sigma_1{}^2[i] \ + \ \sigma_2{}^2[i]} \ = \ f_{kin}\sigma_3[i] \ , \quad \text{for } 0 \leq i < \ N \ , \qquad (12.19)$$

where N = rows · cols denotes the number of elements in the area of integration.

In the next step we linearize these equations in the slip area and fix the stresses in

the stick area and the normal stresses, because they change the slip directions indirectly only. We emphasize that a correct solution is not necessary in this part of the algorithm. We supply the correction with the letter D in (12.15), (12.19) and get the following equation system :

$$\begin{bmatrix} Du_1 \\ Du_2 \end{bmatrix} = \begin{bmatrix} Ds_x \\ Ds_y \end{bmatrix} = \begin{bmatrix} A_{11} & A_{12} \\ A_{21} & A_{22} \end{bmatrix} \begin{bmatrix} D\sigma_1 \\ D\sigma_2 \end{bmatrix} \, ,$$

$$\sigma_{10}[i] \, D\sigma_1[i] + \sigma_{20}[i] \, D\sigma_2[i] = 0 \, ,$$

(12.20)

$$\sigma_{20}[i] \, Ds_x[i] - \sigma_{10}[i] \, Ds_y[i] = s_{y0}[i] \, D\sigma_1[i] - s_{x0}[i] \, D\sigma_2[i] + s_{y0}[i] \, \sigma_{10}[i] - s_{x0}[i] \, \sigma_{20}[i] \, ,$$

where the index 0 denotes the solution of the step before. In (12.20) we assume, that $\sigma_3[i]$ is constant, because the influence of the slip stress on the normal stress is relatively small, and the equations are much simpler. The correction for $\sigma_3[i] = \sigma[3;m,n]$ will be determined automatically in the Gauss-Seidel procedure, where the correct solution for the new slip direction is generated. We rearrange the system (12.20) to a linear equation system for the vector $D\sigma_2$:

$$(-A_{21}E_1 + A_{22} + E_1A_{11}E_1 - E_1A_{12} - E_2E_1 - E_3) \, D\sigma_2 = -s_{y0} + E_1s_{x0} \, ,$$

(12.21)

where E_j are diagonal matrices with the elements :

$$E_1[i,i] = \sigma_{20}[i] / \sigma_{10}[i] \, , \quad E_2[i,i] = s_{y0}[i] / \sigma_{10}[i] \, , \quad E_3[i,i] = s_{x0}[i] / \sigma_{10}[i] \, . \quad (12.22)$$

Now we determine the correction of the slip stress $D\sigma_2$ from (12.21), (12.22) and calculate $D\sigma_1$ using (12.20). The matrix in parenthesis in (12.21) has the maximal dimension of N, where N denotes the number of elements in the slip area. We can use the Gauss-Seidel Block Iteration Method to invert the matrix in (12.22), because we need only an approximation. Since this algorithm is still in development, we can not give estimations of the minimal size of the Block Matrices, but we know, that this procedure diverges for a one-dimensional Block Matrix.

The stress $\sigma_{10}[i]$ is the denominator of the fractions in (12.22) and must not be zero. In the case of zero $\sigma_{10}[i]$, we have to determine the correction of $D\sigma_1[i]$ instead of $D\sigma_2[i]$, which is zero here. The equation for $D\sigma_1[i]$ is easily evaluated from (12.21), (12.22) by substitution of x for y and y for x and reversing the indices of A_{ij}, to :

$$(-A_{12}F_1 + A_{11} + F_1A_{22}F_1 - F_1A_{21} - F_2F_1 - F_3) \, D\sigma_1 = -s_{x0} + F_1s_{y0} \, , \quad (12.23)$$

$$F_1[i,i] = \sigma_{10}[i] / \sigma_{20}[i] \, , \quad F_2[i,i] = s_{x0}[i] / \sigma_{20}[i] \, , \quad F_3[i,i] = s_{y0}[i] / \sigma_{20}[i] \, . \quad (12.24)$$

In our program we add a small value, e.g. 1.0E−10, to the stress $\sigma_{10}[i]$, such that this value practically never becomes zero, and (12.21) can be used for all cases.

12.5 Contact algorithms

The equations (4.13) and (12.1)−(12.8) describe a nonlinear mixed boundary value problem with boundary and auxiliary conditions. On the condition that the contact area, the stick area and the slip directions area known, a linear equation system can be formulated, which can be solved by a modified Gauss-Seidel algorithm. Since we do not know these quantities at the beginning, we have to estimate them to get a first solution, which can be tested on the contact conditions. These tests determine the new contact area and the slip area, which we use to calculate a new solution. Repetition yields a recursive iteration method, which ends when the contact area and the slip area remain constant.

A direct, successive type of iteration does not work for the slip directions, because the slip at the border of the stick area is very small, while the stresses are big. Thus a small variation of the displacements at the border of the stick area has almost no effect on the stress distribution, but the slip directions can change very much. If the stresses are adapted to the new slip directions, the displacements can become very large in the next step and a successive algorithm of this type diverges. We bypass this problem by assuming 'Rigid slip' at the beginning and linearize (12.4), (12.5) around the current solution in one step of the slip algorithm. Now we solve the resulting linear equation system for the slip stresses approximately, which leads to an algorithm with good convergence and small memory requirements.

Our program consists of several inner and outer loops, in which the form of the contact area, the slip area and the slip directions are corrected. These loops can be executed in an arbitratry order, but not every arrangement will converge. It may be necessary to find out the best arrangement for special problems such as large contact areas or fast programs. In our program, we check the contact conditions in the deepest inner loop and proceed to the outer loop for the slip directions when the contact area is found. The next outer loop determines the new stick area. Since every step of one outer loop repeats all inner loops, this algorithm is not as fast as a sequential arrangement, but it converges safely.

We used structured programming techniques in the programming language Turbo Pascal for our modules. Several contact algorithms can be realized, by only moving a few lines in the main part of the program. The unit 'UNISLIP.pas' contains all the variable definitions, the input and output procedures, the procedures 'Hertz' and 'Hertzin' by J. J. Kalker, the procedure 'Coeff' to determine the load displacement coefficients and the procedure 'Displacements' to calculate the displacements. The file 'SLIP.pas' contains the rest of the procedures and the main part of the program. Some procedures are not used in the main part of the program.

The Nassi-Shneiderman diagram of the main part is shown in figure 12.3. The most important module is the function 'SeidTang', which performs the Gauss-Seidel procedure, described in Engeln-Muellges/Reuter (1987). The input of this function is the coefficient matrix, the constants which define the displacements of the stick area and some subordinate variables. The output are the stresses in the contact area. The basic formula is explained in chapter (12.5). 'Seidel' determines the stresses in the stick area by an iterative matrix inversion, and calculates the stresses in the slip area by Coulomb's law during each cycle of the Gauss-Seidel iteration.

The function 'SeidTang' is nested in the deepest loop of our program. The module 'Displacements' follows. It calculates the displacements (12.10), which are the input of the next module 'TestContact', where the contact conditions (12.3), (12.6) are tested. If one of these conditions is violated, the contact area will be corrected and the contact loop will be repeated, until the contact area remains constant.

The next loop for the slip directions contains the basic module 'SlipAlgorithm', which corrects the slip directions. 'SlipAlgorithm' calls the procedure 'DefineSlip-Matrix', which calculates the matrix of section 12.4 and 'SimEqu' to solve the linearized equation system for the stress directions. This equation system contains only a few rows of the contact area. The variable SMColMax, which has the amount of 80 here, denotes the maximal number of columns for the slip matrix, while a random procedure determines the number of rows in the contact area for the first cycle of this procedure. The procedure 'SlipAlgorithm' ends when all lines of the contact area have been calculated.

The module 'DefineStickArea' in the next loop testes Coulomb's law (12.4) in the stick area and corrects the stick area if necessary. The module 'Testsign' tests whether all stress directions are opposite or if some are equal to the slip directions. It happens sometimes, that the stresses are in the same direction and not opposite. 'Testsign' adds points with equal stress directions to the stick area and the contact loop will be repeated, until all stress directions are correct.

Initialize; InputWindow;		
SetImpact = True ?		
Yes		No
DefineImpactParameters		
DetermineCoefficients;		
For LoadCase := FirstCase to LastCase do Begin		
	For Increment: = FirstIncrement to LastInc[LoadCase] do Begin	

For LoadCase := FirstCase to LastCase do Begin
  For Increment: = FirstIncrement to LastInc[LoadCase] do Begin
    InitIncrement; TestContact; DefineConstants;
    Repeat | IterStick := 0;
      Repeat | IterStick := IterStick + 1; IterStressDir := 0;
        Repeat | IterStressDir := IterStressDir + 1;
                 IterContact := 0;
          Repeat | IterContact := IterContact + 1;
                   DefineConstants; SeidTang;
                   Displacements; TestContact;
          Until not(ContactChanged) or
               (IterContact > MaxContact);
          SlipAlgorithm;   Displacements;
          DefineStressDir;
        Until (StressDirFound) or (IterStressDir ≥ MaxStressDir)
        DefineStickArea;
      Until not(StickAreaChanged) or (IterStick > = MaxStick);
      TestSign;
    Until not(ContactChanged or StickAreaChanged) and StressDirFound and
          SeidelFound;
    CalculateForces;

Fig. 12.3: The structural diagram.

'DefineSlipStress' calculates the slip stresses in the new slip area and 'DefineConstants' defines the displacements in the new stick area. If the stick area changes, the contact loop will be repeated before the loop for the stick area continues.

The last part of this program tests the contact and the slip area again and repeats all loops if necessary. Now the end of the program is reached and a new increment of the load history may be calculated.

13 Contribution to the mathematical proof of

convergence

Much work was done to proof the existence and uniqueness of the contact mechanical field, using the principle of virtual work (Kalker 1990). In this chapter we will analyse the convergence of our algorithm of chapter 12 and the Gaussian Block Iteration resp. Panagiotopoulos process of chapter 11. We will regard this problem from a phenomenological point of view, rather than establishing a strong mathematical proof. It should enable the user of our program to enter the correct input values to achieve convergence.

Our program consists of four nested loops: The Gauss-Seidel loop, the contact loop, the slip direction loop and the stick area loop. Accordingly four levels of convergence must be considered. Instead of proving convergence for all types of load-histories, we will describe what to do to avoid divergence.

In the first part of the load-history the bodies are brought together and a contact area forms. Subsequently global displacements and forces are applied. We approximate the contact area by a rectangular mesh, while the load-history is replaced by a number of discrete displacement increments. Now we take step number i of this load-history, where a contact area C_i exists. In the next step we superpose a small displacement increment. The first solution in the contact loop is calculated on the old stick area and the contact conditions are tested. If the contact conditions are violated, the contact area changes and a new solution is calculated on the new area. If the increments are small enough, the contact area changes in a few points only, lets say one point, and the contact area is already found. If the contact area changes in a few points, a few combinations of this points must be checked, to determine the new contact area. As long as the variation of the contact area is small enough, the number of combinations is very small and the solution should be found after a few steps. We conclude that the contact loop converges always, as long as the increments are small enough. The same consideration holds for the calculation of the stick area in the stick area loop, but it does not hold for the first step of a flat punch problem were contact is initiated, because the contact area and the stick area change very much. In chapter 14.5 we discuss a flat punch with 1000 points and show that this example converges.

The slip directions in the slip direction loop are calculated using the linearized

equations (12.21), (12.23). We used the slip directions as the variables of the linearization, because we can always find a relatively correct estimation for the slip directions, assumming complete adhesion at the beginning of the stick area loop. The stress values in the slip area vary much more than the slip directions. Similar to the contact area, the slip directions change very little, if the increments are small enough. It follows, that the slip direction loop converges, and that convergence is save for all loops, except the Gauss Seidel loop, if the increments are small enough. The necessary size of the increments for convergence of a load-history can be determined mathematically, but numerical expirience shows, that the algorithm converges for all sizes of the increments.

The rest of this chapter is dedicated to the investigation of the convergence of the Gauss-Seidel procedure for some special examples. This method is characterized by the iteration formula:

$$\sigma_{n+1} = T \sigma_n + c , \qquad (13.1)$$

with the iteration matrix T, the vector c and the solution σ_n of step n. Decomposition of the vector σ_n into a linear combination of the eigenvectors of T proves, that this procedure converges, if the spectral radius of T is smaller than one. In the following sections we will analyse some simple examples, where convergence can be proved without determination of the eigenvalues.

We mentioned earlier, that the Gauss-Seidel method and the 'Successive Over Relaxation' method converge for positive definite and symmetric matrices. In the case of complete adhesion our matrix is always positive definite and symmetric and so the procedure converges. In the mixed case, however, where a slip area forms, we have to determine the tangential stresses in the slip area by Coulomb's law (12.4), (12.5) and the matrix of the linear equation system is indefinite and not symmetric. In this case, we know the tangential deformations in the stick area, the tangential stress in the slip area and the normal deformations in the whole contact area. Now we perform the Gauss-Seidel procedure for the area of adhesion and replace the slip stresses by Coulomb's law at the end of each iteration.

A small slip area should not disturb the process of convergence in the remaining area of adhesion, where the matrix is still symmetric and positive definite. We expect the worst case of convergence for full sliding in the whole contact area. To simplify the problem, we investigate 'Rigid Slip' only, where the slip direction is constant in the whole slip area. The difference between the correct solution for the slip directions and the 'Rigid Slip' solution is usually small and the proof of convergence for 'Rigid Slip'

should be enough for many problems.

13.1 Convergence of the Gauss-Seidel procedure for 'Rigid Shift'

In the case of 'Rigid Slip' with uni-directional local slip, we can orient one axis of the contact area opposite to the slip direction. The normal displacement u_3 is given and we use the normal component of (12.15) to determine σ_3 :

$$u_3 = f_{kin} A_{31} \sigma_3 + A_{33} \sigma_3 , \qquad (13.2)$$

with $\sigma_2 = 0$ and $\sigma_1 = f_{kin}\sigma_3$, according to Coulomb's law (12.4). After the calculation of the stress σ_3, we use (12.15) for the deformations u_1 and u_2.

Equation (13.2) shows, that the Gauss-Seidel procedure converges if A_{31} or f_{kin} vanish, because A_{33} is symmetric. For large r we can replace the integral in (4.8), (4.14) by the integrand and get with (4.9) and (4.23) :

$$A_{31}[i,k] = -A_{13}[i,k] \approx \frac{1}{4\pi} \left(\frac{1-2\nu_1}{G_1} - \frac{1-2\nu_2}{G_2} \right) \frac{(x_i-x_k)}{r^2} , \text{ for } i \neq k ,$$

$$0 \le i, k \le \text{cols} \cdot \text{rows} - 1 . \qquad (13.3)$$

We have to keep in mind that the definition of i, k in (13.3) differs from (4.14). The rectangles of the contact area in (13.3) are arranged in a vector of the form (12.9) and all rectangles are numbered continously from left to right and up and down. Thus the element numbers i and k range between 0 and cols $\cdot$ rows-1 and the number k in (13.3) defines the rectangle, where the stress $\sigma_1[k]$ acts, while the number i defines the place, where the deformation $u_1[i]$ is measured.

The elements of A_{31} vanish for similar materials or $x[k] = x[i]$, which is the case for a contact area in form of a small stripe parallel to the y-axis. To study the worst case with maximal values for $A_{31}[i,k]$, we take a contact area in form of a stripe parallel to the x-axis. Again we replace the integral (4.14) with the integrand :

$$A_{33}[i,k] \approx \frac{1}{\sqrt{(x_i-x_k)^2 + (y_i-y_k)^2}} \frac{1}{2\pi} \left(\frac{1-\nu_1}{G_1} + \frac{1-\nu_2}{G_2} \right) , \text{ for } i \neq k . \qquad (13.4)$$

The equations (13.3), (13.4) yield :

$$|A_{31}[i,k]| \approx |\gamma| \, A_{33}[i,k], \text{ for a stripe in x-direction and } i \neq k,$$

$$\gamma = \frac{\dfrac{1-2\nu_1}{2G_1} - \dfrac{1-2\nu_2}{2G_2}}{\dfrac{1-\nu_1}{G_1} + \dfrac{1-\nu_2}{G_2}} , \qquad (13.5)$$

where we used the relation $y[i] = y[k]$ for a stripe parallel to the x-axis. In the general problem we have several lines parallel to the x-axis and the matrix A_{31} has a stucture similar to A_{11} in (12.11), with a skewsymmetric arrangement of the blockmatrices. Formula (13.5) holds for a contact area in the form of a line parallel to the x-axis and for the partition B_0 of the general case. Comparison between (13.4) and (13.5) shows, that the blockmatrices B_j for $j > 0$ contain elements with smaller values than the elements of B_0 :

$$|B_j[i,k]| < |B_0[i,k]| , \text{ for all matrices } A_{kl} ,$$
$$0 \leq j \leq \text{rows}-1 , \quad 0 \leq i,k \leq \text{cols}-1 . \qquad (13.6)$$

Equation (13.6) holds for B_j , C_j of (12.14) etc. For complete slip in x-direction the asymmetric components in (13.2) become maximal, which is the worst case for convergence. The assumption of infinitely small rectangles in (13.4) and (13.5) yields an error, which can be determined using the correct values for the integrals from (4.14) :

$$A_{31}[i,k] = \frac{1}{4\pi} \left(\frac{1-2\nu_1}{G_1} - \frac{1-2\nu_2}{G_2} \right) \int \frac{\partial}{\partial x} \ln r \, dS ,$$
$$A_{33}[i,k] = \frac{1}{2\pi} \left(\frac{1-\nu_1}{G_1} + \frac{1-\nu_2}{G_2} \right) \int \frac{dS}{r} . \qquad (13.7)$$

The integrals in (13.7) can be determined with (4.29), using a mesh consisting of squares:

$$a_1 = (2k+1)\Delta x, \quad a_2 = (2k-1)\Delta x, \quad b_1 = \Delta x, \quad b_2 = -\Delta x, \text{ for } j=m=0, \quad (13.8)$$

with the result :

$$\int \frac{dS}{r} = (2k+1)\,\Delta x \ln \frac{1+\sqrt{(2k+1)^2+1}}{-1+\sqrt{(2k+1)^2+1}} - (2k+1)\,\Delta x \ln \frac{1+\sqrt{(2k-1)^2+1}}{-1+\sqrt{(2k-1)^2+1}} +$$

$$+ \; 2 \, \Delta x \ln \frac{(2k+1)+\sqrt{(2k+1)^2+1}}{(2k-1)+\sqrt{(2k-1)^2+1}} , \qquad (13.9a)$$

$$\int \frac{\partial}{\partial x} \ln r \, dS = -\Delta x \ln \frac{(2k+1)^2+1}{(2k-1)^2+1} - (4k+2)\,\Delta x \tan^{-1} \frac{1}{2k+1} + (4k-2)\,\Delta x \tan^{-1} \frac{1}{2k-1} \,. \tag{13.9b}$$

In the table below some values for the integrals in (13.9) are listed :

k	0	1	2	3	4	5	6	7	8
e	7.051	2.0761	1.0102	0.6697	0.5013	0.4007	0.3372	0.2860	0.2502
f	0	-1.9692	-0.9990	-0.6653	-0.5000	-0.4000	-0.3333	-0.2857	-0.2500
g	∞	2	1	0.6667	0.5000	0.4000	0.3333	0.2857	0.2500

Table 13.1 : The integrals (13.7), (13.9) .

The values e,f,g are defined as :

$$e = \int \frac{dS}{r} \,, \quad f = \int \frac{\partial}{\partial x} \ln r \, dS \,, \quad g = \frac{4a^2}{r} \,. \tag{13.10}$$

The error for $k=1$ in (13.5) is smaller than 6% for this contact area. Since this error decreases for larger values of k, we can use (13.5) as an approximation in the following calculation.

We derive the proof of convergence according to a paper of W. Niethammer (1970). The application of the iteration procedure (12.17) to complete slip in (13.2) and the introduction of some abbreviations yields :

$$D \, \sigma_{3,n+1} = L \, \sigma_{3,n+1} + u_3 - f_{kin} A_{31} \sigma_{3,n} + R \, \sigma_{3,n} \,, \tag{13.11a}$$

$$A_{33} = D - R - L \,, \quad R = L^T \tag{13.11b}$$

where we decomposed the matrix A_{33} into the diagonal matrix D, the right triangle matrix R and the left triangle matrix L. The upper index T denotes transposition. Usually (13.11a) is multiplied by the inverse diagonal matrix D^{-1}, to reduce rounding errors in the computation. Equation (13.11a) can be evaluated line by line by inserting the new left hand side into the product with the left hand matrix L. The procedure converges, if the matrix T :

$$T = (D-L)^{-1}(R - f_{kin} A_{31}) \,, \tag{13.12}$$

has eigenvalues λ less than 1. The eigenvalue equation has the form :

$$T z = \lambda z \,, \quad z^{CT} z = 1 \,, \quad |\lambda| < 1 \text{ for convergence} \,, \tag{13.13}$$

where z is an eigenvector associated with the eigenvalue of T (Horn/Johnson 1985).

We use the upper index C for componentwise, complex conjugation. (13.12) and (13.13) yield:

$$(R-f_{kin}A_{31})z = \lambda(D-L)z .$$ (13.14)

Insertion of (13.11b) in (13.14) proves the identity :

$$z^{CT}(D-A_{33}+R-2f_{kin}A_{31}-L)z = \lambda z^{CT}(D+A_{33}+R-L)z.$$ (13.15)

We reformulate (13.15) to :

$$\lambda = \frac{d-a+s-2b}{d+a+s}, \quad a = z^{CT}A_{33}z, \quad b = z^{CT}f_{kin}A_{31}z,$$
$$s = z^{CT}(R-L)z, \quad d = z^{CT}Dz.$$ (13.16)

The variables a,b,d,s denote complex scalars. The quadratic forms a,d of the symmetric and positive definite matrices A_{33} and D are positive, while $(R-L)$ and A_{31} are skewsymmetric and so the variables b and s are imaginary. Now we neglect the small error in (13.5), which is correct for infinitely small squares, and write :

$$A_{31} \approx \gamma(L^T-L), \quad \gamma > 0 ,$$ (13.17)

where we used the definition (13.11b) for A_{33}. We insert (13.17) in (13.16) and get the result :

$$s = i\alpha, \quad b = if_{kin}\gamma\alpha, \quad \alpha \text{ real.}$$ (13.18)

Equation (13.18) and (13.16) yield :

$$\lambda = \frac{d-a+i(1-2f_{kin}\gamma)\alpha}{d+a+i\alpha} .$$ (13.19)

The absolute value of λ must be less than 1 for convergence of the SOR method. We calculate the square of the absolute value of (13.19) :

$$(d-a)^2 + (1-2f_{kin}\gamma)^2\alpha^2 < (d+a)^2 + a^2,$$ (13.20)

which can be reformulated :

$$da > f_{kin}\gamma(f_{kin}\gamma-1)\alpha^2 .$$ (13.21)

and get the condition for convergence :

$$0 < f_{kin}\gamma < 1 , \quad \text{sufficient for convergence} .$$ (13.22)

Elastic Impact with friction, by J. Jaeger

Experience shows, that the frictional coefficient f_{kin} is always less than one. The maximal value of γ is 0.5, but for most material pairings its value is much smaller. Aluminum/steel for instance has a value of $\gamma = 0.1$. Thus the condition (13.22) is always satisfied, if γ is greater than zero. For negative frictional stresses equation (13.21) is satisfied, if the absolute value $|f_{kin}\gamma|$ is small enough. Equation (13.22) is exact for infinite small rectangles only, but there is still a large margin in (13.22) and (13.19) before the limit of convergence is exceeded. In the case of several lines of rectangles in the contact area, the values of A_{31} become smaller than in (13.17) and we expect smaller values of b in (13.16). Consequently the eigenvalues of the matrix T in (13.13) decrease and the process should converge better. From (13.22) we draw the conclusion, that the convergence deteriorates for increasing values of f_{kin} or γ, which is confirmed by empirical results, even if the contact area consists of a large number of stripes. The empirical limit of convergence for $|f_{kin}\gamma|$ in our program was between 5 and 10 for circular contact areas.

In the mixed case we can formulate a recursion formula similar to (13.11) with a decomposed matrix for the stick and slip area. The sum of the two matrices should have eigenvalues less than 1. A rough estimation of the eigenvalues of these matrices and empirical results show convergence. The formulation of the conditions of convergence for the Block Iteration Method in the next chapter clarify this problem.

In this chapter we considered equally directed local slip only. Usually the 'Rigid Slip' solution is a good approximation, but difficulties may arise for involved load-histories. The conditions of convergence for the torsional impact are still under investigation. Empirical tests show convergence for all types of load- histories.

In the case of negative slip stresses in (13.2) f_{kin} changes its sign. It follows, that we have to perform the Gauss-Seidel iteration backwards, resp. reverse the direction of the x-axis, to obtain the same condition of convergence (13.22) again. Numerical experience shows, that the number of iterations for negative and positive slip stresses is almost identical. That suggests the conjecture, that α is very small compared to d and a.

13.2 The Block Iteration Method for shift with complete adhesion

The Block Iteration Method corrects the vectors σ_1, σ_2, σ_3, while the Gauss-

Seidel procedure corrects every element $\sigma[i]$. The algorithm of the Block Iteration method is similar to the Gauss-Seidel method, formulated in block matrices. We write (12.15) in the form :

$$u = A \sigma .$$ (13.23)

Now we apply the SOR method (13.11) to (13.23) and get the iteration formula :

$$D \sigma_{n+1} = u + L \sigma_{n+1} + R \sigma_n , \quad \sigma_n^T = (\sigma_{1,n}^T , \sigma_{2,n}^T , \sigma_{3,n}^T) , \quad n = 1 ... \infty ,$$

$$D = \begin{bmatrix} A_{11} & 0 & 0 \\ 0 & A_{22} & 0 \\ 0 & 0 & A_{33} \end{bmatrix} , \quad L = \begin{bmatrix} 0 & 0 & 0 \\ -A_{12}^T & 0 & 0 \\ -A_{13}^T & -A_{23}^T & 0 \end{bmatrix} , \quad R = \begin{bmatrix} 0 & -A_{12} & -A_{13} \\ 0 & 0 & -A_{23} \\ 0 & 0 & 0 \end{bmatrix} .$$ (13.24)

where σ_{n+1} denotes the solution of (13.24) in step $n+1$. The vector-components of this solution $\sigma_{1,n+1}$, $\sigma_{2,n+1}$, $\sigma_{3,n+1}$ can be inserted successively into the right hand side of (13.24). It is important to realize, that this iteration is performed for the vectors σ_1, σ_2, σ_3 of σ instead of the elements $\sigma[i]$ in formula (13.11) of the Gauss-Seidel procedure. The procedure (13.24) converges, if the matrix T :

$$T = (D-L)^{-1}R$$ (13.25)

has eigenvalues λ_1 with an absolute value less than one. Again we get the eigenvalue equation $Tz = \lambda_1 z$ with the eigenvector z, which can be transformed to :

$$\lambda_1(D-L)z = Rz .$$ (13.26)

Insertion of (13.24) proves the next equation :

$$z^{CT}(D-A+R-L)z = \lambda_1 z^{CT}(D+A+R-L)z ,$$ (13.27)

where λ_1 can be evaluated :

$$\lambda_1 = \frac{d-a+s}{d+a+s} , \quad d = z^{CT}Dz, \quad a = z^{CT}Az, \quad s = z^{CT}(R-L)z.$$ (13.28)

The matrices D and A are symmetric and positive definite and so the scalars d and a are positive, while $(R-L)$ is skewsymmetric and $s = i\alpha$, with real α, is imaginary. It follows from (13.28) that the absolute value of λ_1 is smaller than one and the procedure converges :

$$|\lambda_1| < 1 .$$ (13.29)

To elucidate (13.23), (13.24) with an example, we set $\sigma_{2,n}=0$ and get the result :

$$A_{11}\,\sigma_{1,n+1} = u_1 - A_{13}\,\sigma_{3,n} \, ,$$
$$A_{33}\,\sigma_{3,n+1} = u_3 - A_{13}^T\,\sigma_{1,n+1} \, , \qquad (13.30)$$

we eliminate $\sigma_{1,n+1}$ in (13.30) :

$$\sigma_{3,n+1} = A_{33}^{-1}(u_3 - A_{13}^T A_{11}^{-1} u_1) + A_{33}^{-1} A_{13}^T A_{11}^{-1} A_{13}\,\sigma_{3,n} \, . \qquad (13.31)$$

From (13.29) we know, that the absolute values of the eigenvalues, i.e. the spectral radius, of the matrix M_1 :

$$M_1 = A_{33}^{-1}\, A_{13}^T\, A_{11}^{-1}\, A_{13} \, . \qquad (13.32)$$

must be less than one. We will use this result in the next chapter.

13.3 The Block Iteration Method for shift with 'Rigid Slip'

The Panagiotopoulos process (Kalker 1990) is similar to the Block Iteration Method. We use the term 'Rigid Slip' for the slip directions of rigid bodies. Again we orient one axis parallel to the slip directions and start with formula (13.2). Now we apply the Block Iteration Method :

$$\sigma_{3,n+1} = A_{33}^{-1}\, u_3 - f_{kin} A_{33}^{-1} A_{13}^T\,\sigma_{3,n} \, . \qquad (13.33)$$

This algorithm converges on the condition, that the absolute values of the eigenvalues of the matrix :

$$M_2 = f_{kin}\, A_{33}^{-1}\, A_{13}^T \qquad (13.34)$$

are less than one. We have the eigenvalue-equation :

$$\det(\,\lambda_2 I - M_2\,) = 0 \, , \qquad (13.35)$$

where det denotes the symbol for the determinant and λ_2 the eigenvalue. I is the unit matrix. A transformation yields :

$$\det A_{33}^{-1/2}\det (\,\lambda_2\, I - f_{kin}\, A_{33}^{-1/2} A_{13}^T\, A_{33}^{-1/2}\,) \det A_{33}^{1/2} = 0 \, . \qquad (13.36)$$

All eigenvalues λ_2 of (13.36) must be imaginary, because A_{13} is skewsymmetric and the congruence transformation with the symmetric matrix A_{33} yields a new skew symmetric matrix (Horn/Johnson 1985). We rewrite formula (13.35) :

$$\det (\lambda_2 A_{33} - f_{kin} A_{13}^{T}) = 0 . \tag{13.37}$$

For a small stripe of rectangles parallel to the x-axis (4.9) yields :

$$\partial^2 r / \partial x^2 \approx 0. \tag{13.38}$$

We use (4.14) and obtain :

$$A_{11}[i,k] \approx \frac{1}{2\pi} \left(\frac{1}{G_1} + \frac{1}{G_2} \right) \int \frac{dS}{r} . \tag{13.39}$$

Comparison of (13.39) with $A_{33}[i,k]$ of (4.14) yields :

$$A_{11}[i,k] \approx \varepsilon_1 A_{33}[i,k] , \quad \varepsilon_1 = \frac{1/G_1 + 1/G_2}{(1-\nu_1)/G_1+(1-\nu_2)/G_2} . \tag{13.40}$$

Insertion of (13.40) in M_1 from (13.32) and the skewsymmetry yields the matrix :

$$M_1 \approx -(A_{33}^{-1} A_{13})^2 / \varepsilon_1 , \tag{13.41}$$

which has eigenvalues $|\lambda_1| < 1$ from (13.29). Now we compare (13.41) with (13.34) and obtain :

$$M_2 \approx -f_{kin} \sqrt{\varepsilon_1 M_1} . \tag{13.42}$$

From (13.42) follows :

$$|\lambda_2| \approx f_{kin} \sqrt{\varepsilon_1 \lambda_1} . \tag{13.43}$$

The definition (13.40) of ε_1 shows that $\varepsilon_1 \leq 2$, while f_{kin} and $|\lambda_1|$ are less than one. It follows, that the eigenvalues $|\lambda_2|$ are less than one for $f_{kin} < 1/\sqrt{2}$. This condition assures convergence in most contact problems. The Block Iteration Method should converge for greater values of f_{kin} also, because we calculated the worst case in this chapter.

14 Numerical results for incremental load-histories

We performed several numerical calculations to analyse the restrictions of the analytical solutions of Mindlin, Cattaneo and the approximation of chapter 7. The largest difference between the analytical and the theoretical solution occurs for the theory of chapter 7. The correct solution depends on a large number of parameters, like the material constants, the frictional law and the size of the increments. If a high accuracy is necessary, the numerical theory must be used. The numerical calculation is very time consuming, because the contact area, the slip area and the slip directions must be calculated with a recursive procedure. Therefore the analytical solutions are important as approximation for the stress values and the size of the stick area.

Mindlin's theory is correct for similar materials with Poisson's number $\nu = 0$. For nonzero values of ν the stress direction differs about 5° from the theoretical value. In the case of varying forces, analysed by Mindlin & Deresiewicz (1953), the stress direction rotates about 180° for points which belong to the slip area and not to the x- or y-axis. The stress angle is a step function for $\nu = 0$ and becomes a S-function for $\nu \neq 0$. The same restrictions hold for Cattaneo's theory. In the case of slender elliptical contact areas, the stress direction varies for Poisson numbers different from zero, because the stiffnesses in x- and y-direction are different. This effect is only important for large slip areas and very slender ellipses. The comparison of the theory of chapter 7 and the numerical solution shows that the slip direction is not constant in the slip area. The value of the tangential stress and the size of the stick area are fairly correct, however. If follows that the analytical theory is very good for small slip areas or if the slip direction reverses. The numerical calculations show, that for $\nu = 0$ and in the absence of torsion the absolute value of the tangential stress is constant on elliptical rings which are similar and concentric to the form of the contact area. The effect of dissimilar materials or torsion on the tangential stress can only be calculated with the numerical theory. This is the reason, why we do not present any further analytical results with restricted validity in this thesis.

This chapter consists of five sections: 14.1 analyses the stress for spherical bodies of similar material; 14.2 is dedicated to elliptical bodies; 14.3 contains a load-history for dissimilar materials; 14.4 discusses torsion and the combination of torsion and shift and 14.5 presents some results for a flat punch.

14.1 Spheres

In fig 14.1 the forces and the displacements of the centers of the spheres are plotted for a load-history with $\nu_1 = \nu_2 = 0$. The displacement was applied in 36 steps and the contact area consists of 25 elements. In fig. 14.2 the theoretical and numerical load-displacement curve is plotted. The difference between both solutions is very small, even for 25 elements, such that 25 elements are enough for the determination of the force. The stress distribution of fig. 14.3 agrees very well with the analytical solution.

$$\nu_1 = \nu_2 = 0.0,$$
$$G_1 = G_2 = 82\ 000\ \text{N/mm}^2,$$
$$f_{stat} = f_{kin} = 1,$$
$$a = b = 1,$$
columns = 10,
rows = 7,
$\zeta = 0.1$ mm (penetration),
$\eta = 0$ (lateral shift),
$\phi = 0$ (no torsion).
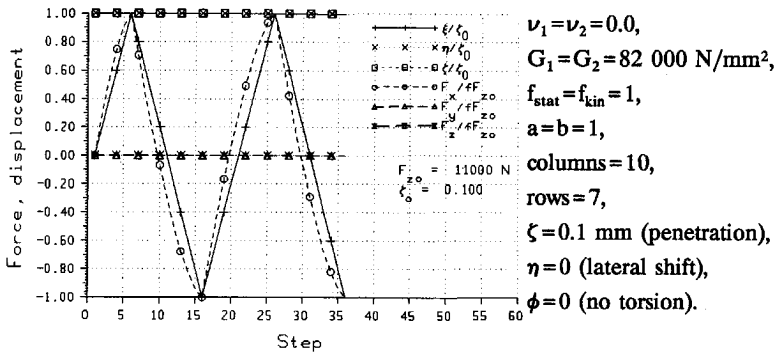
Fig. 14.1: Forces and displacements for a load-history.
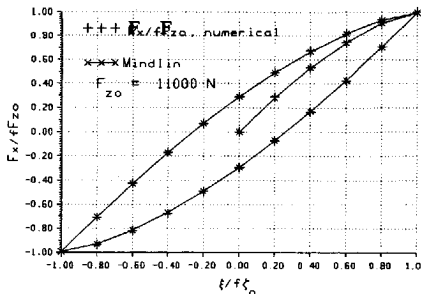
Fig. 14.2: The load-displacement curve for the load-history above.

On figures 14.4, 14.5 the same load-history with $\nu = 0.5$ was investigated. Fig. 14.5 shows, that the value of the stress angle is no more constant on circles. The stress angle rotates about 180° for a point besides the x- and y-axis, which belongs to the slip area.
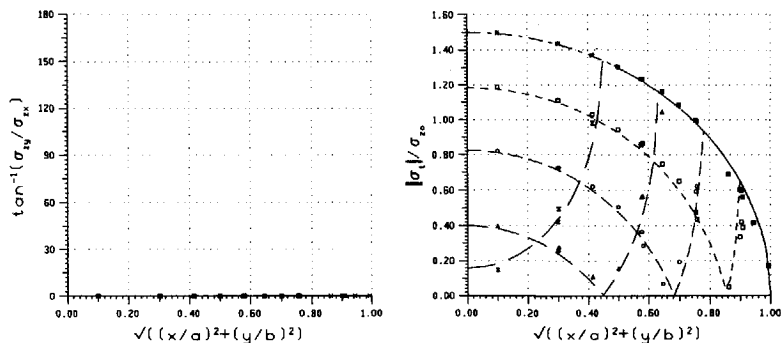
Figs. 14.3: The angle $\tan^{-1}(\sigma_{zy}/\sigma_{zx})$ and the tangential stress $|\sigma_t|/\sigma_{z0}$ for the steps 6,8 ... 16 of the load-history above.
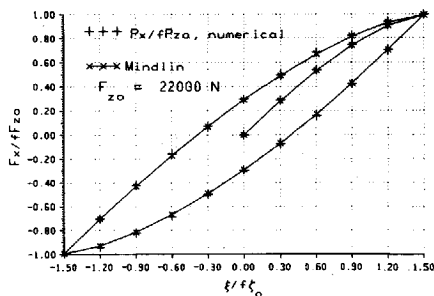
Fig. 14.4: Load-displacement curve

$\nu_1 = \nu_2 = 0.5$,

$G_1 = G_2 = 82\ 000\ \text{N/mm}^2$,

$f_{stat} = f_{kin} = 1$,

$a = b = 1$,

columns $= 10$,

rows $= 7$,

$\zeta = 0.1$ mm (penetration),

$\Delta\xi = 0.03$ mm (tang. increment),

$\eta = 0$ (lateral shift),

$\phi = 0$ (no torsion).
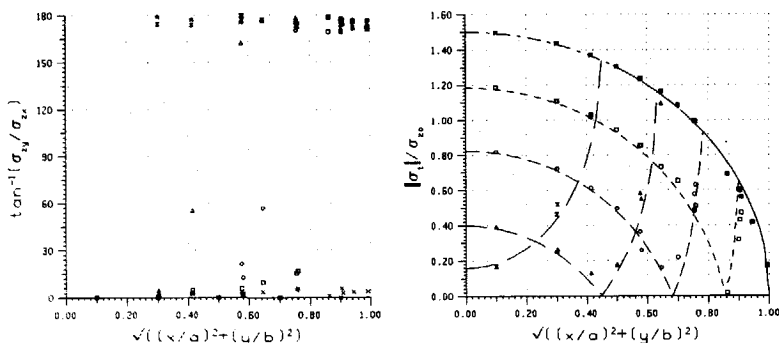
Fig. 14.5: The angle $\tan^{-1}(\sigma_{zy}/\sigma_{zx})$ and stress $|\sigma_{zt}|/\sigma_{z0}$

The next pictures show the tangential stress $\sqrt{\sigma_{zx}^2 + \sigma_{zy}^2}/\sigma_{z0}$ and the angle $\tan^{-1}(\sigma_{zy}/\sigma_{zx})$ for some 2-directional load-histories with $\nu_1 = \nu_2 = 0$. In fig. 14.6 the displacement-vectors are plotted for a set of load-histories. The first step 0-1 in fig. 14.6, which consists of a normal compression of the amount $f\kappa\Delta\zeta = 0.1$ and a tangential displacement $\Delta\xi = 0.1$, is applied in all load-histories. At the end of the first step the slip area covers the entire contact area. Subsequently a set of 5 displacement increments in another direction is superposed, until complete sliding occurs. The difference between the numerical and the analytical theory of chapter 7.2 becomes maximal for complete sliding, such that we study the worst case in these examples. For the load cases 1-6 and 1-7 complete sliding takes place, and the analytical approximation for this case is the Cattaneo-theory of chapter 7.1, with the current value of the displacement.

$\nu_1 = \nu_2 = 0$,
$G_1 = G_2 = 82\ 000\ \text{N/mm}^2$,
$f_{stat} = f_{kin} = 1$,
rows $= 15$,
columns $= 20$.
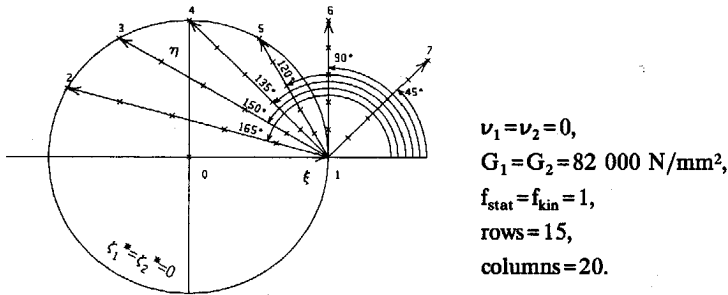
Fig. 14.6: The displacement vectors for some selected load histories.
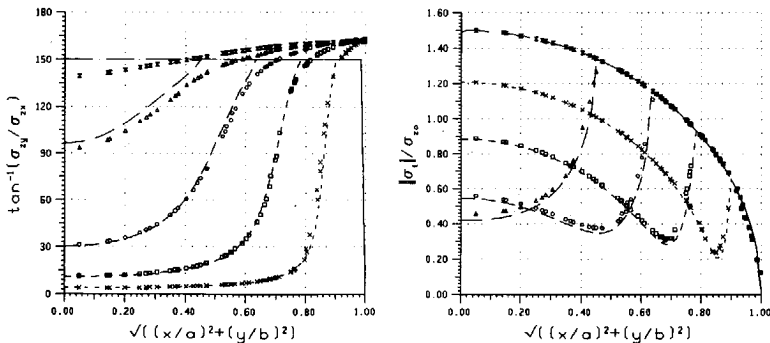
Fig. 14.7: Load-history 1-2 of fig. 14.6.
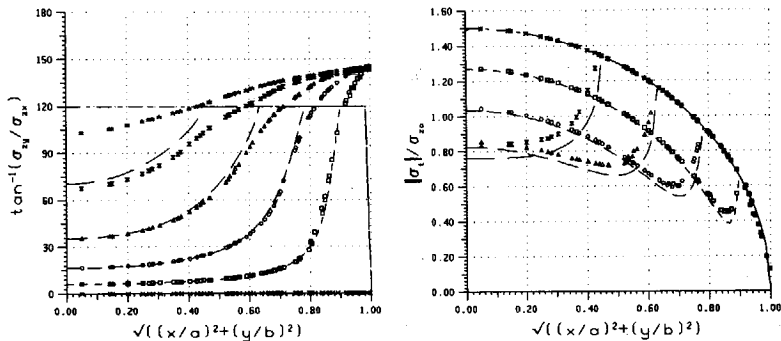
Fig. 14.8: Load-history 1-3 of fig. 14.6.
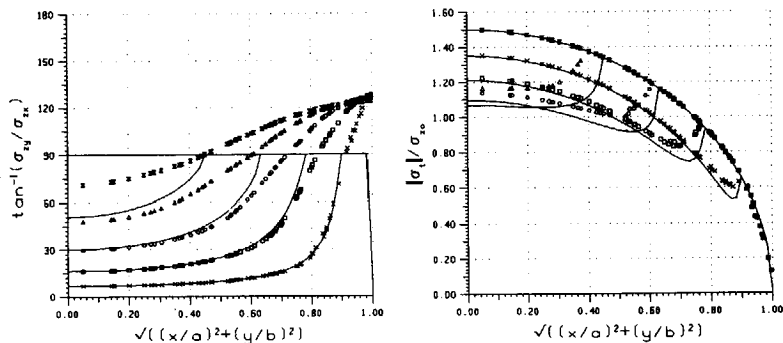
Figs. 14.9: Load-history 1-4 of fig. 14.6.
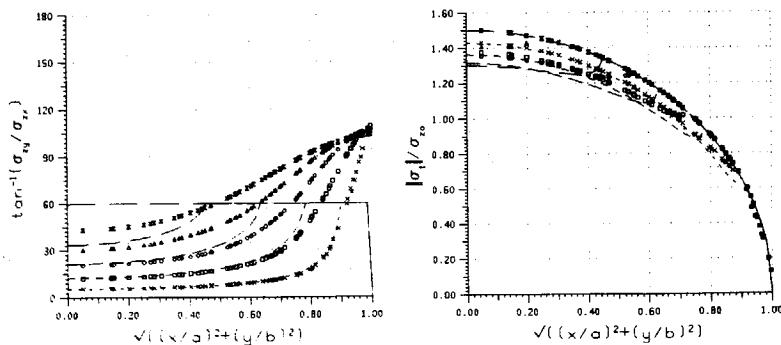
Fig. 14.10: Load history 1-5 of fig. 14.6.
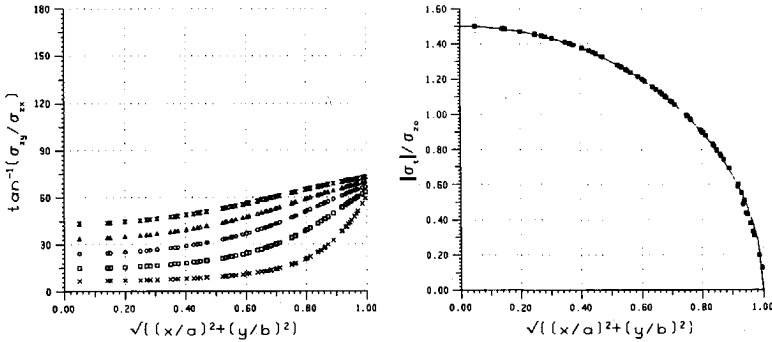
Fig. 14.11: Load-history 1-6 of fig. 14.6.
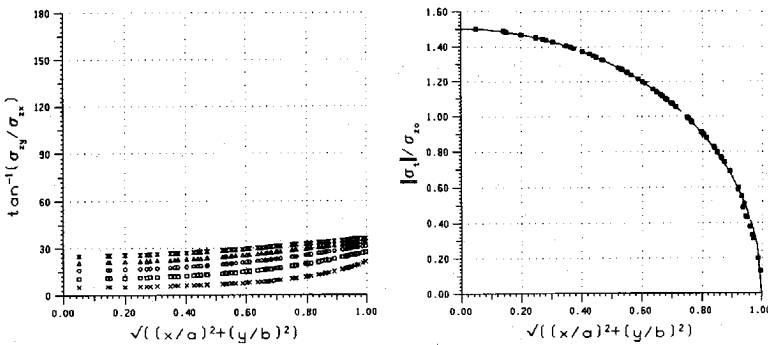
Fig. 14.12: Load-history 1-7 of fig. 14.6.

Figs. 14.7-14.12 show, that the tangential stress of the numerical solution, which is drawn with markers, corresponds very well with the analytical solution, drawn with full lines. The angle $\tan^{-1}(\sigma_{zy}/\sigma_{zx})$ differs up to $50°$ between the two theories at the border of the contact area. This difference becomes small in the stick area for small slip areas.

Poisson's number was zero for the examples above, such that the stress directions are constant on circles. The next figure 14.13 shows load-history 1-2 of fig 14.6 with $\nu_1 = \nu_2 = 0.5$, in which the values are no more constant on circles, because the markers can not be connected by a smooth line.
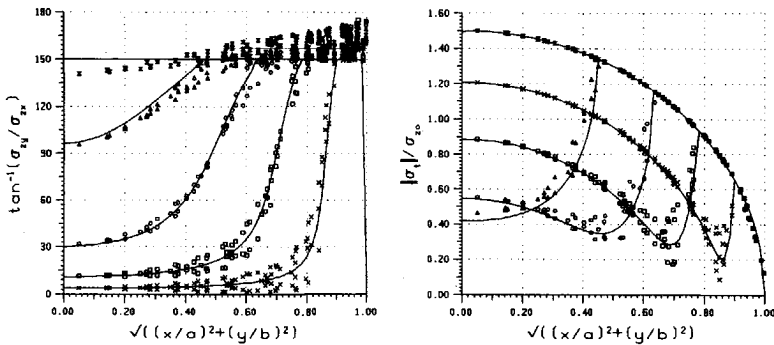
Fig. 14.13: Load-history 1-2 of fig. 14.6 with $\nu_1 = \nu_2 = 0.5$.

14.2 Elliptical contact areas
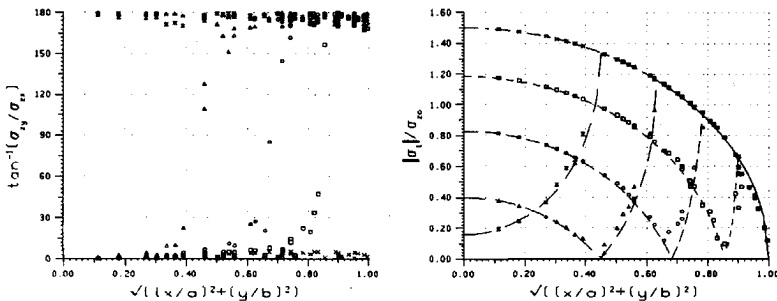
Fig. 14.14: Tang. stress for steps 6, 8 ... 16 of the load-history from fig. 14.1, with: $\nu_1 = \nu_2 = 0.5$, $c_x/c_z = 1.585$, $c_y/c_z = 1.415$, $G_1 = G_2 = 82\ 000$ N/mm^2, $f_{stat} = f_{kin} = 1$, $a = 2$, $b = 1$, columns = 20, rows = 10, $\zeta_0 = 0.1$ mm, $\Delta\xi = 0.0317$, $\phi = 0$.

The stress distribution for elliptical contact areas is very similar to the distribution for circular contact areas, as long as the ellipses are not very slender. In the case $\nu_1 = \nu_2 = 0$ the stress components σ_{zx} and σ_{zy} are constant on elliptical rings and the stiffnesses c_x, c_y, c_z are identical. Figures 14.14 show the absolute value and the angle of

the tangential stress for a load-history similar to fig. 14.1, with $\nu_1 = \nu_2 = 0.5$. After application of the normal compression $\zeta = 0.1$, the tangential displacement was increased by 5 increments of $\Delta\xi = 0.0317$ until full slip takes place. Afterwards ξ was decreased by the same increment until full slip occurs in the opposite direction. For a lateral displacement η the stress distribution is almost identical to the figure 14.14, while the stress angle moves about $90°$.

14.3 Dissimilar materials

In the case of different materials the normal compression produces tangential stress. A load-history in normal direction with periods of loading and unloading was analysed in the next figures. The period of loading is similar to a paper of Spence (1975). During unloading annular elliptical areas of slip and adhesion form, similar to the result of Turner (1979). The coefficient of friction was so small that full slip takes place ($f_{stat} = f_{kin} = 0.1$, $a/b = 4$). We found empirically that the stress angle has the form:

$$\sigma_{zy}/\sigma_{zx} = k \cdot y/x, \quad k = 2 \quad \text{for } a/b = 4. \tag{14.1}$$

with an empirical factor k.
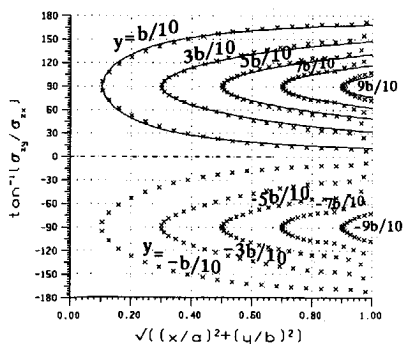
a/b = 4,
$\nu_1 = 0$, $\nu_2 = 0.5$,
$G_1 = G_2 = 82\,000$ N/mm^2,
$f_{stat} = f_{kin} = 0.1$,
columns = 40,
rows = 10,
$\zeta_0 = 0.1$, $\Delta\zeta = 0.01$ mm,
$\xi = \phi = 0$.

Fig. 14.15: Stress angle numerically.

In fig. 14.15 the numerical values (cross symbols) and the theoretical values (full line, y positive) are plotted. The ellipses represent constant values of y. The absolute value of the tangential stress is shown in fig. 14.16. The normal stress differs slightly from the Hertz solution.
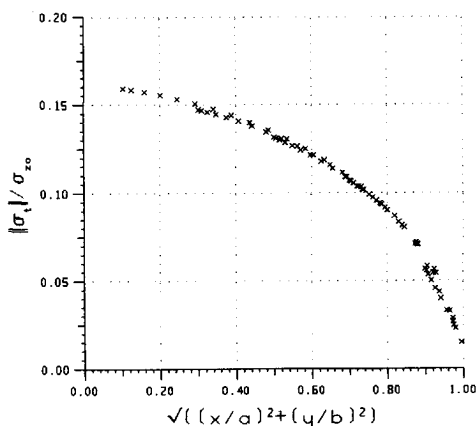
Fig. 14.16: Abs. value of the tangential stress.
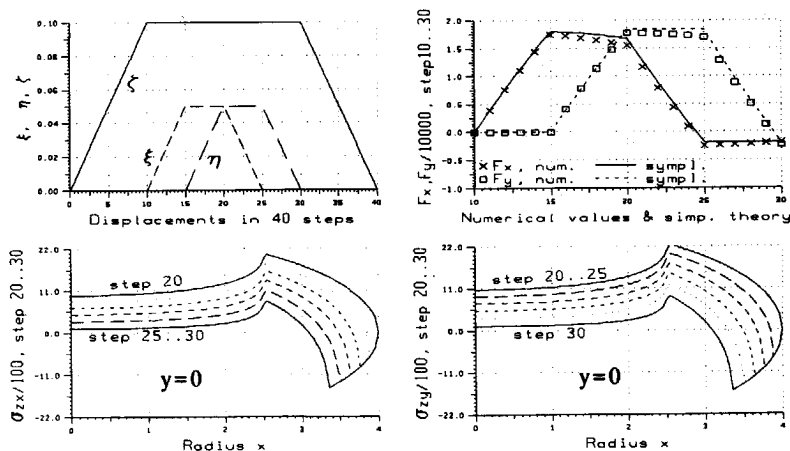
Fig. 14.17: Load-history Euromech90: $\nu_1 = 0.1$, $\nu_2 = 0.3$, $G_1 = G_2 = 82\ 000$ N/mm², $a/b = 4$, rows $= 10$, columns $= 40$, $f_{stat} = f_{kin} = 1.0\ \phi = 0$.

In the next example a load-history with 40 steps, $\nu_1 = 0.1$, $\nu_2 = 0.3$, $f_{stat} = f_{kin} = 0.1$ (fig.14.17) was calculated. In the steps 1..10 the normal displacement was continuously increased, followed by a tangential loading in x-direction in step 11..15. Afterwards, in step 16..20 the bodies are shifted in y-direction while ζ remains constant. Between step 21 and 25 the displacement was reduced in x-direction, which produced a point of instantaneous adhesion in step 21, as described in chapter 7.2. In step 26 the tangential shift was reduced in y-direction, and a 2-nd point of instantaneous adhesion

occurs, as described chapter 7.3. The 2-nd point of instantaneous adhesion was not recognized in the report at EUROMECH (Jaeger, 1990), where the steps 21..30 where approximated by the theory of chapter 7.2. The size of the stick area is plotted in fig. 14.18, in which the points of instantaneous adhesion come out very clear.
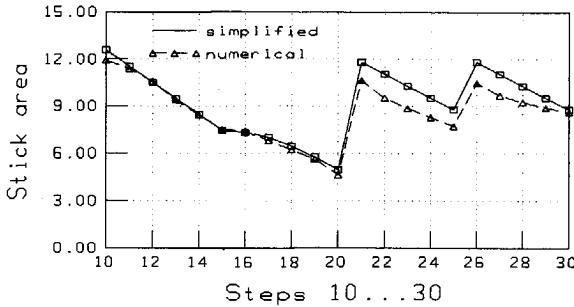
Fig. 14.18: The size of the stick area.

The stress angle for steps 2,3 and 10, plotted in fig. 14.19, is similar to fig. 14.15. During the tangential loading of steps 11..15 the tangential displacement ξ in x-direction is increased while η is constant; now the ellipses become smaller and change their form (fig. 14.20). The angle of step 25 is plotted fig. 14.21. Due to the normal load-history with dissimilar materials, the stress angle varies very much and is no longer constant on elliptical rings. The ellipses of fig. 14.19 become very slender and curved. The distribution of the normal stress is slightly different from the Hertz solution (not shown).
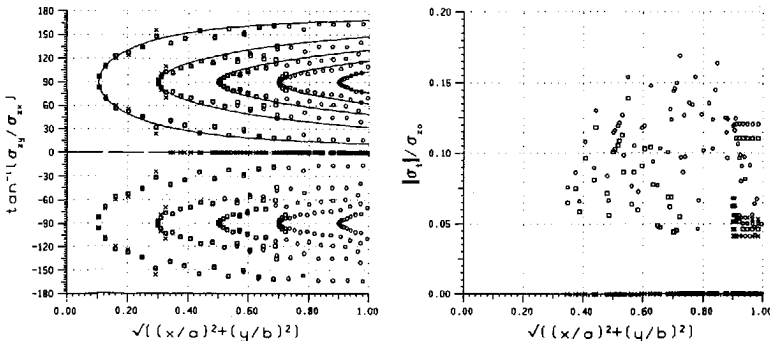
Fig. 14.19: Step 2 (cross), step 3 (square), step 10 (circle) and eq. (14.1) (full line).
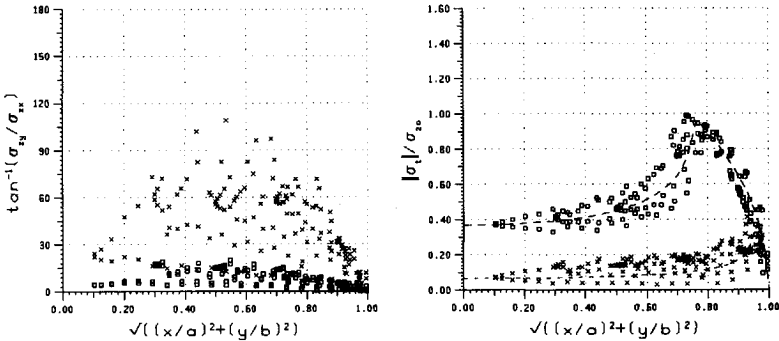
Fig. 14.20: Step 11 (cross), step 15 (square) of fig. 14.17.
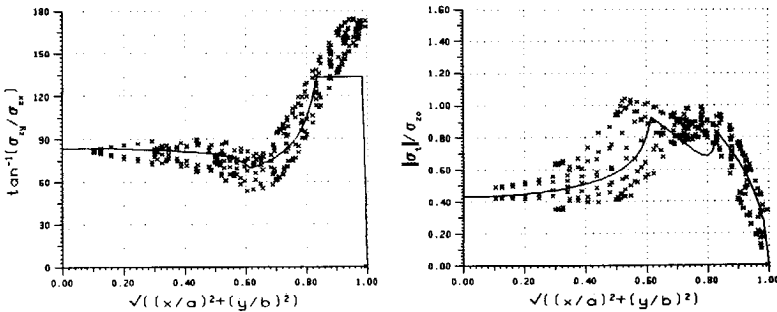
Fig. 14.21: Step 25 of fig. 14.17. The peaks in the theoretical solution (full line) mark the border of the old and new stick area.

14.4 Torsion with shift

In section 7.6 an approximation for pure torsion of elliptical bodies was discussed. Fig. 14.21 shows the torque of the numerical (marker) and the theoretical solution (7.65), which is drawn with a full line, for $a/b = 1$ and $a/b = 10$. The approximation (7.65) corresponds very well with the numerical solution, even in the case of dissimilar materials. Furthermore it turns out, that the numerical results for an area of integration with 50 points differ only slightly from the results with 400 points. Fig. 14.23 shows the contour of the stick area for the steps 2,3 .. 8 of the numerical solution with

400 points in fig. 14.22. In Fig. 14.24 the numerical solution for varying torques, drawn with markers, is compared with formula (7.66), drawn with a broken line.
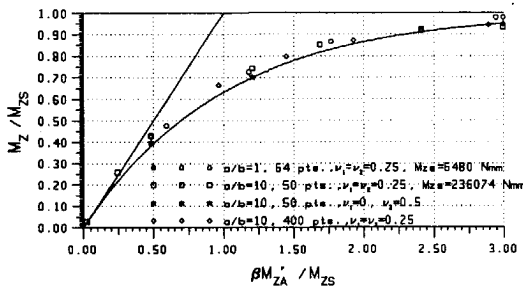
Fig. 14.22: The torque M_z as function of the twisting angle β (dimensionless).
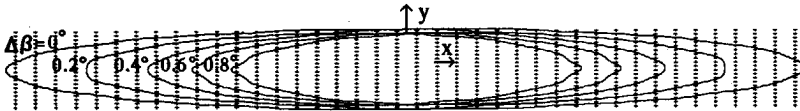
Fig. 14.23: The contour of the stick area $\Delta\beta = 0$, $0.2°$, $0.4°$.., $40*20$pts., $a/b = 10$.
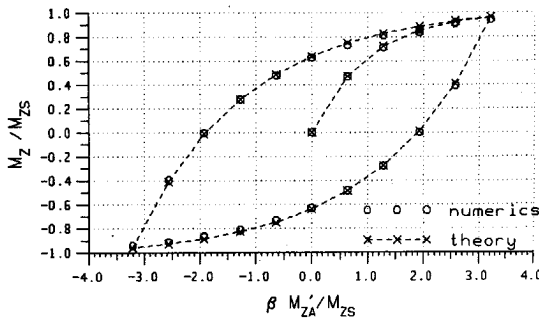
Fig. 14.24: Varying torque with $a/b = 1/10$, $\nu_1 = \nu_2 = 0$.

The next example consists of a normal compression of $\zeta = 0.1$ in the first step, superposed by 10 increments of $\Delta\xi = 0.02$ and $\Delta\beta = 0.2°$. The other values are: $\nu_1 = \nu_2 = 0$, $G_1 = G_2 = 82\ 000$ N/mm², $a = 10$, $b = 1$. Fig. 14.25 shows the angle and the absolute value of the stress (numerics: markers) for step 2. The stress angle for a rigid body movement (full lines in fig. 14.25) differ only by $10°...20°$ from the numerical solution of this step. Fig. 14.26 shows the similar result for the last step of this load-

history, in which the stress directions are identical with the rigid-slip directions.
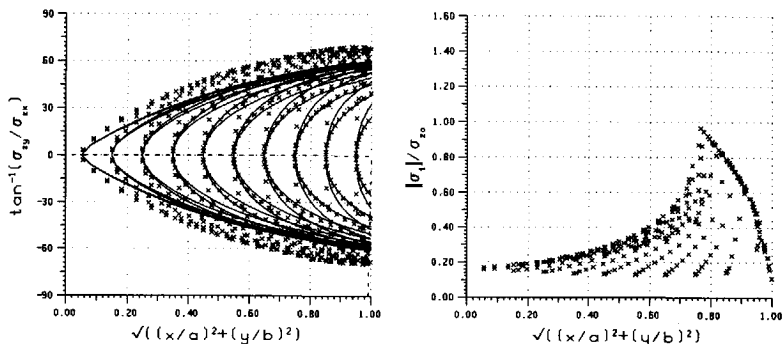
Fig. 14.25: Step 2, $\zeta=0.1$, $\xi=0.02$, $\beta=0.2°$.
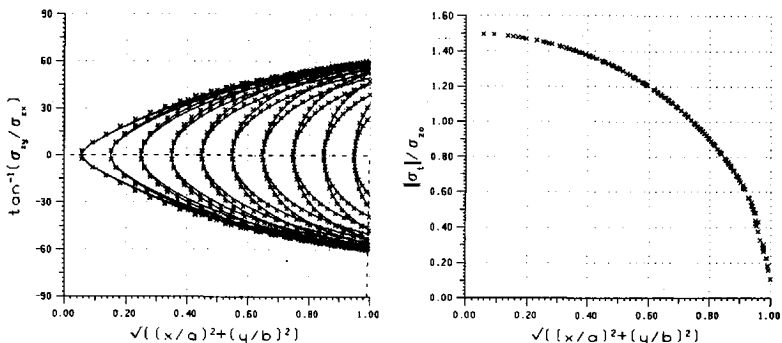
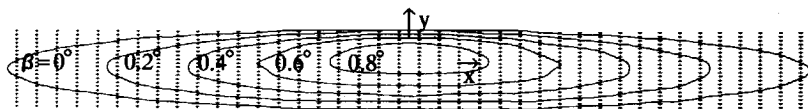Fig. 14.26: Step 11, $\zeta=0.1$, $\xi=0.2$, $\beta=2.0°$.

Fig. 14.27: Contour of the stick area for the load-history above, 40*20 pts.

The stick area in fig. 14.27 is dislocated in y-direction and has a non-elliptical form. For increasing values of β the stick area becomes rounder. The absolute value of the stress for each row of the contact area appear as lines of markers in fig. 14.25. The tangential stress on a section y=constant has a peak at the border of the stick area, which becomes maximal for y=0. The stress angles for each row of the contact area form also lines of markers in fig. 14.25. Instead of the simultaneous application of

shift and torsion in this example, the shift could be applied first and the torsion in the next steps. The stress direction of rigid slip-solution could be a first approximation of the stress direction in this case.
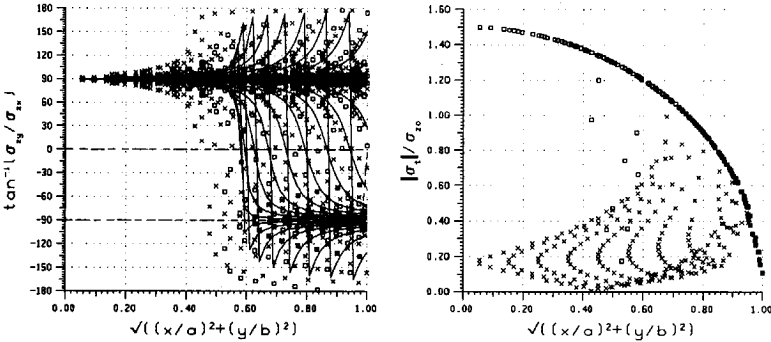

Fig. 14.28: Step 2 (cross) and step 11 (square), $\zeta = 0.1$, $\Delta\eta = 0.02$, $\Delta\beta = 0.2°$.
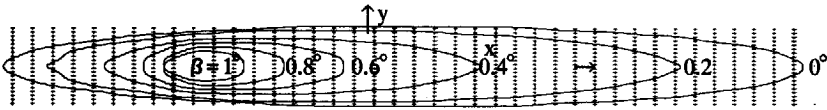

Fig. 14.29: Contour of the stick area for the load-history above.

Superposition of an incremental shift in y-direction $\Delta\eta = 0.02$ and torsion $\Delta\beta = 0.2$ dislocates the stick area in x-direction (fig. 14.29). The stress angle of each row for a rigid body movement is plotted as a full line in fig. 14.28. The difference between rigid-slip and the numerical solution becomes larger as in fig. 14.25. For increasing values of β the stick area becomes more circular.

Following Kalker (1967), we can regard the slip as a pure rigid body rotation about the spin pole (x',y'), in the case of large creepage and spin :

$$x' = -\eta/\beta, \quad y' = \xi/\beta , \tag{14.2}$$

with dimensionless β. The formulae for the force and the moment are:

$$f_x = \frac{F_x}{f_{stat}F_z} , \quad f_y = \frac{F_y}{f_{stat}F_z} , \quad m_z = \frac{M_z}{f_{stat}F_z\sqrt{ab}} ,$$

$$\tag{14.3a}$$

$$f_x = \frac{3\,\mathrm{sign}(\beta)}{2\pi ab} \int\!\!\int_C \sqrt{1 - \frac{x^2}{a^2} - \frac{y^2}{b^2}} \, \frac{(y'-y)\,dx\,dy}{\sqrt{(x-x')^2+(y-y')^2}} ,$$

$$f_y = -\frac{3\text{sign}(\beta)}{2\pi ab} \int\!\!\int_C \sqrt{1 - \frac{x^2}{a^2} - \frac{y^2}{b^2}} \frac{(x'-x)\ dx\ dy}{\sqrt{(x-x')^2+(y-y')^2}} \ ,$$

$$(14.3b)$$

$$m_z = \frac{3\text{sign}(\beta)}{2\pi(ab)^{3/2}} \int\!\!\int_C \sqrt{1 - \frac{x^2}{a^2} - \frac{y^2}{b^2}} \sqrt{(x-x')^2+(y-y')^2}\ dxdy + x'f_y - y'f_x \ .$$

Kalker (1967) also found some analyical formulae, when the spin pole lies inside of the contact area. He introduced the variables:

$$\alpha = \tan^{-1}(-x'/y'), \quad v_K = \sqrt{x'^2+y'^2} / \sqrt{ab} \ . \tag{14.4}$$
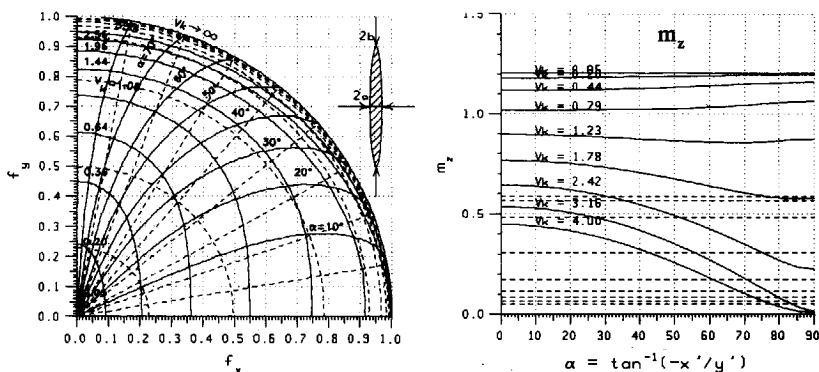
Fig. 14.30: The force and the moment for large creepage
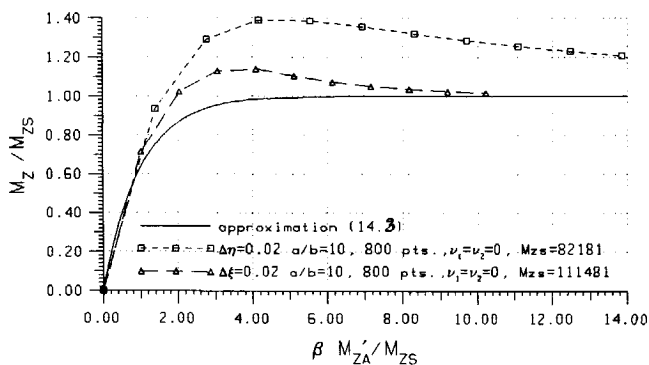(full line: $a/b = 1/10$, broken line: circle).

Fig. 14.31 : The normalized torque for torsion with shift.

We integrated (14.3), using a double Romberg integral (Engeln-Muellges 1987), and obtained the results for fig. 14.30 in a few minutes. The values of the elliptical contact area (full lines) differs very much from the result for a circle (broken line).

Fig. 14.31 shows the numerical result for the torque of the two load-histories above with torsion and shift. The torque for complete sliding M_{ZS} from (14.3) is smaller than the corresponding value without shift. Furthermore the torque is larger for shift along the long axis. The initial slope is identical with or without shift, because in the case of complete adhesion the superposition of shift does not change the torque. Fig. 14.32 shows the result for the forces.
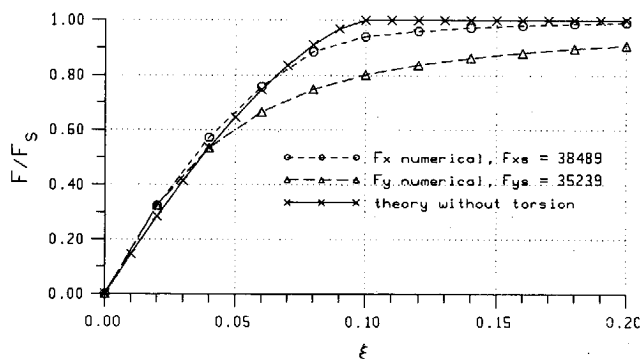

Fig. 14.32: The forces for shift in x- resp. y-direction with torsion.

In this chapter we considered some rather simple load cases, to get an idea of the complexity of some contact problems. A detailed analysis of some special load cases is not difficult with our numerical program.

14.5 Flat punch

Equations (4.14) show, that for $\nu_1 = \nu_2 = 0$ the tangential and normal stress of a flat punch differ only by a constant factor. The load displacement coefficients A_{ii} in (12.10) of the normal and tangential equations are identical:

$$A_{11} = A_{22} = A_{33}, \text{ for } \nu_1 = \nu_2 = 0. \tag{14.5}$$

It follows, that in this case complete sliding starts at the point $\xi = \zeta$. In the case $\nu_1 = \nu_2 = 0.5$ the normal and tangential solutions differ slightly, such that a slip area forms at a value of $\xi \approx 1.5 \cdot \zeta$, which is the value for complete sliding of two similar spheres. This period of partial slip is always very short for flat punches and preceeds the period of complete sliding.
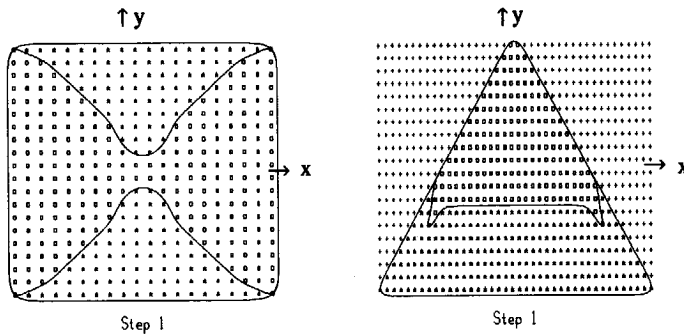

Fig. 14.33: rectangle ($\xi = 0.145$) and triangle ($\xi = 0.14$), $\zeta = 0.1$, $\nu_1 = \nu_2 = 0.5$, squares = slip area, stars = stick area.
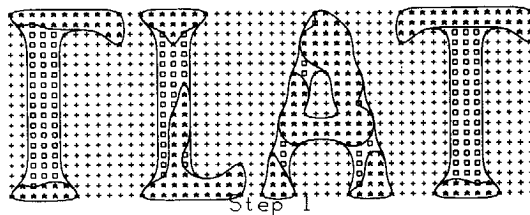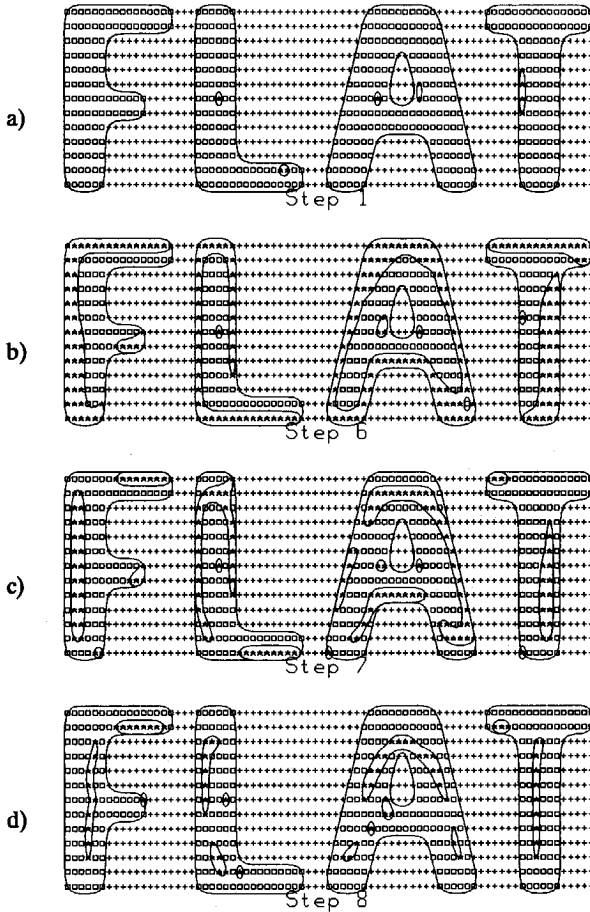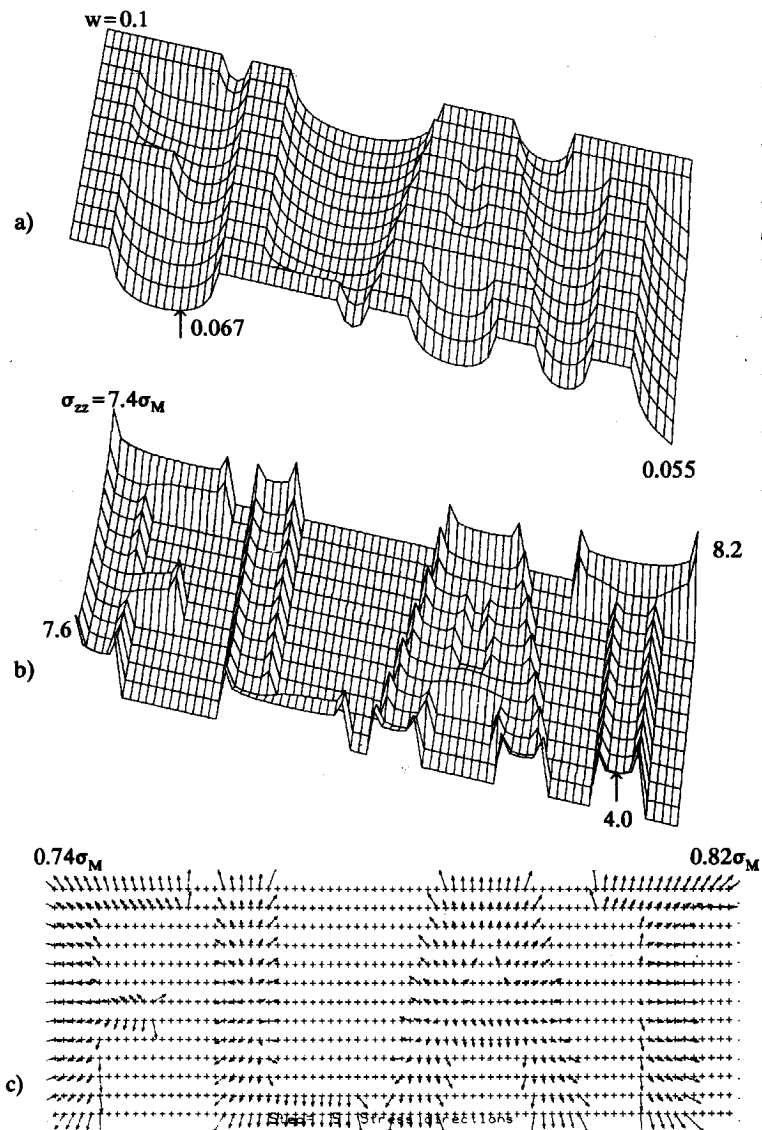

Fig. 14.34: cross = no contact, squares = slip area, stars = stick area, $\xi = 0.15$, $\zeta = 0.1$, $\nu_1 = \nu_2 = 0.5$.

The stick area for a rectangular resp. a triangular punch, shifted in x-direction is plotted in fig. 14.33. In fig. 14.34 the relatively complex slip area for a flat punch in form of four letters is plotted. This problem could be interesting for printing. Large normal pressure at the border of the stick area could improve the contrast, small pressures reduce the wear. Similarly to flat punches non-Hertzian punches of arbitrary shapes can be created and calculated.

Figs. 14.35: Stick area (stars), slip area (squares), no contact (cross);
a) step 1; b) step 6; c) step 7; d) step 8.
1000 points, $\nu_1 = 0$, $\nu_2 = 0.5$, $G_1 = G_2 = 82\ 000$ N/mm^2,
a=1, b=0.3, f=0.1, $\zeta = 0.1$.

w=0.1

a)

↑0.067

$\sigma_{zz}=7.4\sigma_M$

0.055

8.2

7.6

b)

4.0

$0.74\sigma_M$

$0.82\sigma_M$

c)

Figs. 14.36: step 5; a) Normal displacement w; b) Normal stress σ_{zz} divided by the Hertzian mean stress $F_z/\pi ab = 9246$ N/mm², F_z from (5.14); c) Tangential stress σ_t.

0.015.   0.014
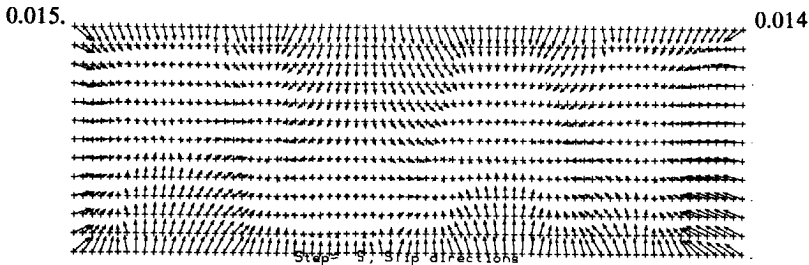

Fig. 14.37: Tangential slip of step 5.

Figs. 14.35 show a normal load history with 1000 points in 10 steps, with $\Delta\zeta = 0.02$ for steps 1..5, and $\Delta\zeta = -0.02$ for steps 6..10. In the period of compression, between steps 1 and 5, the slip area of fig. 14.35a) remains unchanged. At the beginning of the unloading process a stick area forms at the border of the contact area, because the stresses at the borders decrease more than in the centers, at the beginning. Later, in step 8 (fig. 14.35d), the stick area moves inward, similar to the unloading process of dissimilar Hertzian bodies (Turner 1979). This problem was solved on an 80386/33MHz computer in 2 days. The control parameters influence the convergence very much in this case. We selected following control parameters: MaxSeidel = 30, MaxStick = 1. The number of Gauss-Seidel iterations should be: MaxSeidel $\approx$ $\sqrt{\text{cols*rows}}$ for a good convergence. It is interesting, that a small number of stick area loops improves the convergence in this case, because the stick area could increase after each iteration of the stick area loop. With a large value for MaxStick the stick area decreases until complete sliding takes place and the linearized slip directions are so wrong, that a chaotic stick area is selected in the next step.

Fig. 14.36a) shows the normal displacement and 14.36b) the normal stress as in form of 3-dimensional functions. Some values for w and σ_{zz} are given, with σ_M as the Hertzian mean stress for an elliptical contact area with the dimensions of the area of integration. The values for the displacements are always better than the stresses, because the stresses are the derivatives of the displacements. Fig. 14.36c) shows the tangential stress σ_t of step 5 in form of arrows and fig. 14.37 the tangential slip, which must be opposite.

15 Numerical results for the coefficient of restitution

The coefficient of restitution R_x is defined by equation (9.31) as the ratio of the tangential velocities in the contact point before impact to after impact. The torsional coefficient of restitution is similarly defined as the ratio of the torsional velocity before to after impact. In the case of the tangential impact of two spheres of similar material the coefficient of restitution depends on two parameters κ and λ only (Maw, Barber, Fawcett, 1981). κ is the combined material parameter and λ the fraction of the tangential velocity $\dot{\xi}$ divided by the normal velocity $\dot{\zeta}$ and the coefficient of friction f:

$$\kappa = \left(\frac{2-\nu_1}{2G_1} + \frac{2-\nu_2}{2G_2} \right) \bigg/ \left(\frac{1-\nu_1}{G_1} + \frac{1-\nu_2}{G_2} \right) , \quad \lambda = \frac{\dot{\xi}}{f\,\dot{\zeta}} , \quad 1 \leq \kappa \leq 1.5. \quad (15.1)$$

For different materials the coefficient of restitution depends also on the difference parameter of the materials γ, which some authors call Dundurs constant and on the coefficient of friction.

$$\gamma = \left(\frac{1-2\nu_1}{2G_1} - \frac{1-2\nu_2}{2G_2} \right) \bigg/ \left(\frac{1-\nu_1}{G_1} + \frac{1-\nu_2}{G_2} \right) , \quad -0.5 \leq \gamma \leq 0.5. \quad (15.2)$$

The torsional coefficient of restitution depends on κ, γ and the angular velocity. If a tangential velocity is superposed, the tangential and torsional coefficients depend on all the parameters mentioned above. For ellipsoid bodies the situation becomes more complex, because the coefficient of restitution depends on the inertial properties of the bodies and the form of the contact ellipse. The solution for complete adhesion was discussed in section 9.4. In the case of partial slip the impact must be calculated numerically.

Equations (15.1), (15.2) and the limits for Poisson's number yield the following limits for γ, which are plotted in fig. 15.1:

$$
\begin{aligned}
\nu_1 < 0.5: \quad & \gamma > \kappa - 1.5 , \\
\nu_1 > 0: \quad & \gamma(1+\delta) < \kappa(1+3\delta) - 1.5 - 2.5\delta , \; \delta = G_2/G_1 , \\
\nu_2 < 0.5: \quad & \gamma < 1.5 - \kappa , \\
\nu_2 > 0: \quad & \gamma(1+\delta) > 2.5 + 1.5\delta - \kappa(3+\delta),
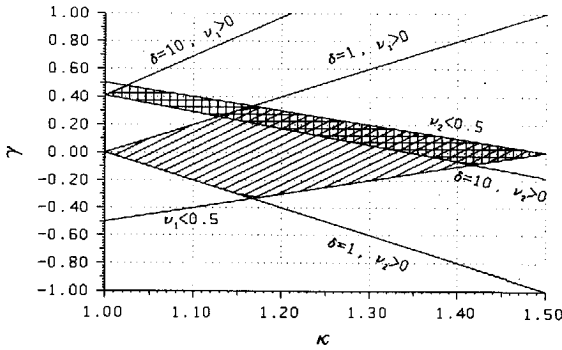\end{aligned}
\qquad (15.3)
$$

Fig. 15.1: The limits of γ (15.3) for $\delta = 1$ (hatched) and $\delta = 10$ (cross-hatched), $\delta = G_2/G_1$.

15.1 Verification of the Cattaneo-Mindlin theory

We found a very good correspondence between the numerical solution for similar materials and the Cattaneo-Mindlin theory. This is not trivial because the Cattaneo-Mindlin theory is an approximation. In Fig. 15.2 the coefficient of restitution is plotted as a function of κ and λ defined by equation (15.1). For $\lambda \geq 7$ complete slip occurs and the coefficient of restitution is defined by equation (9.31) with:

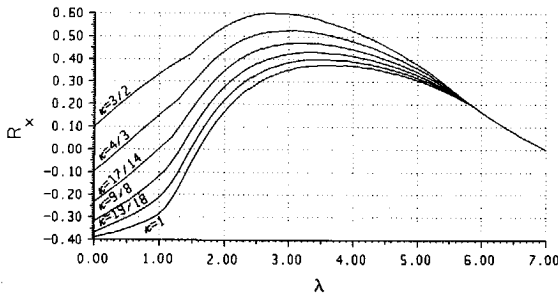$$D_{xx}/D_{zz} = 7/2, \quad \text{for spheres.} \tag{15.3}$$

Fig. 15.2 : R_x as function of κ and λ for $\nu_1 = \nu_2 = 0.0, 0.1, ..0.5$, resp. $\kappa = 1, 19/18 ...$

Fig. 15.2 shows the coefficient of restitution for different values of Poisson's number $\nu_1=\nu_2=0$, 0.1 .. 0.5 resp. the corresponding values of κ from (15.1). Fig 15.3 shows the stress distribution for $\kappa=3/2$ and $\lambda=1$ for an impact with 50 steps and 600 points.
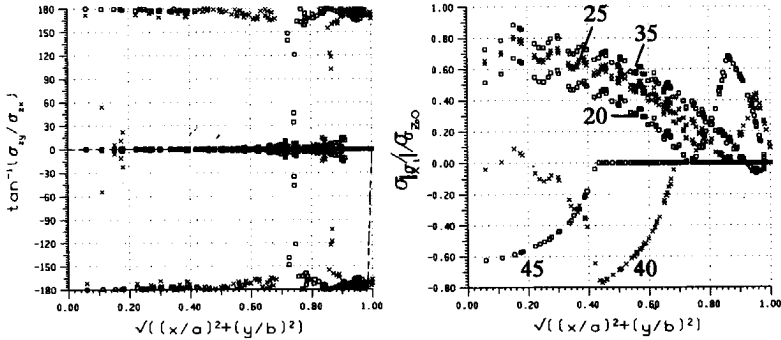

Fig. 15.3 Stress distribution, step 10, 25, 35, 40, 45.
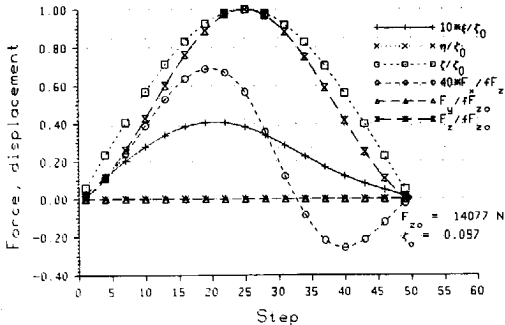
15.2 Dissimilar materials

$\nu_1=0$, $\nu_2=0.5$,
$G_1=G_2=82000 \text{ N/mm}^2$,
$f_{stat}=f_{kin}=0.1$,
$m_1=m_2=2188$ g,
$20*20$ points,
$\dot{\xi}_0=0.05$ m/s,
$\dot{\zeta}_0=1$ m/s.

Fig. 15.4: Forces and displacements.

A large number of calculations with the numerical method of chapter 12 showed, that the coefficient of restitution for dissimilar materials depends on γ, defined by

equation (15.2) and f. The most important parameter seems to be the fraction f/γ, similar to the work of Spence (1975). Only values of $f/\gamma < 1$ produce a significant change of the coefficient of restitution, as fig. 15.6 shows. The difference increases when the coefficient of friction decreases. Fig. 15.4 shows the forces and displacements for a tangential impact of two spheres.

Step 20   Step 28

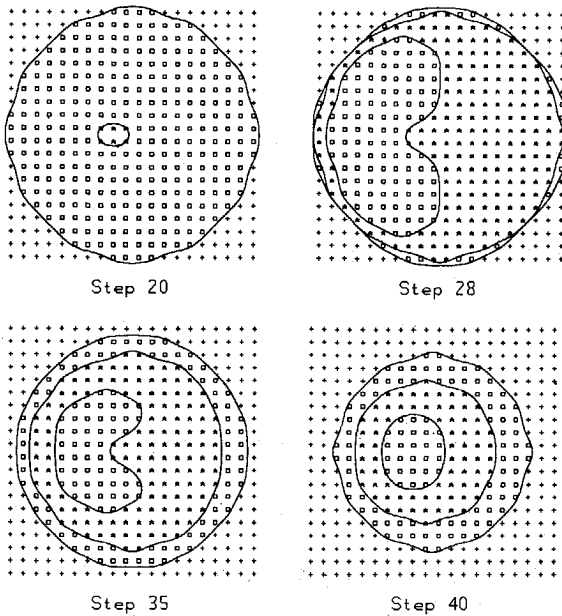Step 35   Step 40

Fig. 15.5: The smoothed stick area (stars) and the slip area (squares) for fig. 15.4.

Similar to a publication of Turner (1979) asymmetric rings of slip and adhesion appear during impact in the period of restitution. An example is plotted in fig. 15.5, where the slip area is small during the period of compression (step 20). In step 28 the period of restitution starts, in which a slip area forms inside of the stick area and at the border of the contact area. The slip area inside of the stick area decreases while the slip area at the border increases in the following steps. The contours in fig. 15.5 are smoothed by a standard procedure, so that the undulations, which are produced by the mesh size, are still visible and the form becomes evident. In the case of similar materials, there is a period of complete adhesion for $\lambda < 1$ in the state of compression, which raises the tangential stiffness, because the stiffness becomes larger for large stick

areas. This period of complete adhesion dissappears for dissimilar materials and thus the coefficient of restitution increases considerably for small coefficients of friction ($\lambda < 4$). A large number of calculations showed, that negative and positive values of γ produce the same coefficient of restitution. Some results for $\kappa = 1$ and different values of δ defined by equation (15.3) are plotted in figure 15.6. It turns out, that a number of 50 points in the contact area is already accurate enough for most problems. A 80386/33MHz personal computer needs about 6 minutes to calculate an impact with 50 points and 50 increments.
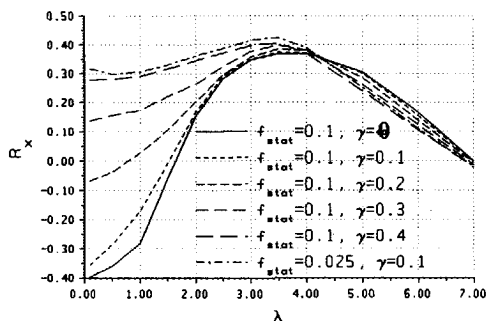

Fig. 15.6: The coefficient of restitution for different materials, $\kappa = 1$.

15.3 Torsion

Torsion reduces the stick area, which raises the coefficient of restitution for small λ, similar to the effect of dissimilar materials. We introduce a dimensionless rotation ω_N:

$$\omega_N = \frac{2a_{max}}{f \zeta_0} \, \omega \, , \quad f = f_{stat} = f_{kin}, \tag{15.4}$$

which is the most important parameter for torsion. The coefficient of restitution depends on λ, κ and γ again. Empirical experience indicates, that the other parameters, like ζ_0 and f, do not alter the coefficient of restitution very much. The rotation must be very high and the normal velocity small to affect the coefficient of restitution.
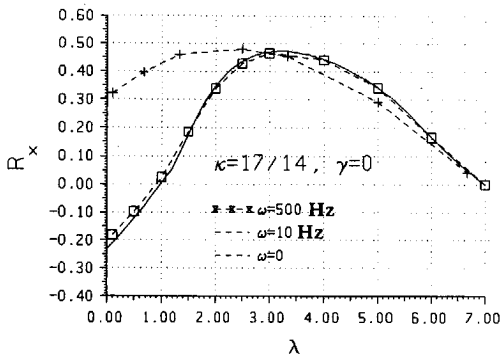
Fig. 15.7: The coefficient of restitution with spin

Figure 5 shows the coefficient of restitution for the impact of two steel spheres with $\omega = 10\text{Hz} = 600/\text{min}$ and $\omega = 500\text{Hz} = 30000/\text{min}$. The impact velocity in normal direction was $7.16\text{m/s} = 23.5\text{feet/s}$. It is obvious that for 600 rotations per minute the rotational effect can almost be neglected.

15.4 Ellipsoid bodies
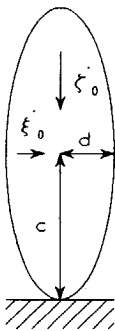
Fig. 15.8: Ellipsoid.

The impact of an ellipsoid body with the axis d, c in x- resp. z-direction on a rigid plane is a good example for the impact. The components a and b of **R** defined in (6.6) may be zero and the moment of inertia around the y- axis becomes:

$$\theta_{yy} = \theta_b = \frac{m}{5} (c^2 + d^2) . \qquad (15.5)$$

The components D_{xx}, D_{zz}, defined by equations (8.29), (8.31) become:

$$D_{xx} = \frac{5c^2}{m(c^2 + d^2)} + \frac{1}{m} \frac{1}{m}, \quad D_{zz} = \frac{1}{m} . \qquad (15.6)$$

The fraction D_{xx}/D_{zz} in equation (9.44) for complete adhesion has a minimum for $c \ll d$ and a maximum for $c \gg d$:

$$1 \leq D_{xx}/D_{zz} \leq 6. \tag{15.7}$$

The fraction c_x/c_z (5.25) reaches its minimum of 0.5 for infinitely small ellipses shifted along the long axis with $\nu = 0.5$ and its maximum of 1 for $\nu = 0$:

$$0.5 \leq c_x/c_z \leq 1.0. \tag{15.8}$$

Insertion of (15.7), (15.8) in (9.44) yields:

$$7.81 \leq \phi \leq 26.85, \text{ for ellipsoids.} \tag{15.9}$$

In figure 9.1 these values are marked by ellipses.

16 Conclusion

In the first section 16.1 of this chapter we summarize the achievements of this thesis and in chapter 16.2 further research is discussed.

16.1 Results of this thesis

In this thesis we investigate quasistatic, transient load-histories without rolling, of elastic bodies, which can be approximated by half-spaces. We created a new analytical theory for the contact of two bodies, and we found some analytical results for the tangential and the torsional impact. We also developed a program, which can solve frictional contact problems with contact areas of one thousand points, on small personal computers. The user of this program has the possibility to control the convergence, by changing several parameters, like the size of the increments and the maximal number of iterations of each loop. We also made some contributions to the proof of convergence of our algorithm. We calculated several load-histories and presented the results graphically, such that the reader gets a deaper insight in contact mechanics. Finally we plotted the tangential coefficient of restitution for the impact of two spheres of dissimilar materials, which defines the velocities after the impact.

In this section we will discuss the new results in detail. The base of our work are the load-displacement equations, which are stated in chapter 4, and some well known load-histories in contact mechanics, which are discussed in chapter 5. A generalization of Mindlin&Deresiewicz's theory, under a new point of view, is presented in chapter 6. Introducing so-called Cattaneo-Mindlin functions, we found that the system depends only on the moments of instantaneous adhesion, which occured during the previous load-history. This consideration simplifies their theory considerably and allows a generalization for elliptical contact areas and arbitrary load-histories. The generalization holds also for load-histories under varying tangential directions, as we showed in chapter 7. In chapter 7.6 an approximation for the torsion of elliptical contact areas under varying torque is presented and compared with numerical results. This

Elastic Impact with Friction, by J. Jaeger.

approximation appears to be very good.

The equations of motion and the contact law for impact problems without torsion is stated in chapter 8. In Chapter 9 we calculate some analytical solutions for the impact of two spheres. A tangential coefficient of restitution is introduced and an analytical solution for complete adhesion is presented. This tangential coefficient of restitution is very powerfull in impact theories, because it allows an easy calculation of the global impact parameters and it can be tabulated for many problems. In chapter 10 we analyse the purely torsional impact, similar to the tangential impact, and discuss some analytical results.

The numerical theory of J. J. Kalker is discussed in chapter 11. He published several papers about the numerics of contact problems. Our algorithm is based on his experience. In chapter 12 we apply the Gauss-Seidel theory to the contact problem, state the contact conditions and linearize the frictional law. A contact algorithm is also presented, where several parameters can be chosen, to accelerate the program and to avoid divergence. In chapter 13 a contribution to the mathematical proof of convergence is made, on the base of sufficiently small increments, where the variation of the stick area and the stress direction is very small. In the case of a flat punch, however, the stick area changes very much at the beginning of contact, independent of the size of the increments, and the convergence is bad, but we could always achieve convergence in our calculations. The parameters allow the control of convergence on different levels: the contact area loop, the stress direction loop, the stick area loop and the most outer loop. If divergence occurs, any loop can be interrupted after an adequate number of iterations, such that the calculation is correct enough on one hand, and a swinging between two solutions is avoided on the other hand. We proof only the convergence of the Gauss-Seidel algorithm for some simple examples.

In chapter 14 we compare our theory with some numerical results. It turns out, that our approximation of chapter 7, for load-histories without torsion, can not describe the stress directions exactly, but the absolute value of the stress, the size of the stick area and the global forces and displacements are accurate enough. Especially the points of instantaneous adhesion appear very clearly in our numerical results. Concerning the stress directions, it must be kept in mind that no analytical theory can predict them exactly. We also found, that for $\nu_1 = \nu_2 = 0$ and no torsion the stress is always constant on ellipses, which are similar to the contact area. We also studied a load-history with dissimilar materials and presented the results graphically. In section 14.4 the combination of shift and torsion is analysed and the torque and the force are plotted for an example. The asymptotes for complete adhesion and for full sliding

were already calculated by Mindlin (1949) and Kalker (1967), while a general approximation turns out to be very difficult. A flat punch with 1000 points and different materials is presented in section 14.5.

Finally, in chapter 15, some numerical results for the impact are presented. We calculated the coefficient of restitution for the impact of spheres of similar materials, and found that the coefficient of restitution of the Cattaneo-Mindlin theory and the numerical solution correspond very well. For different materials the coefficient of restitution increases considerably in the range $\lambda < 4$. For a special example, the forces, displacements and the stick area are plotted. The stick area was smoothed with a Bezier function, which gives a realistic view of the form of this area, but the contour is still undulating. Here we benefit from the Gauss-Seidel procedure, which allows large areas of integration, containing many points. The influence of torsion is also calculated with the result, that the coefficient of restitution increases for $\lambda < 3$, if the torsional velocity is high enough or the normal velocity is very small. Finally, a special example of the impact of ellipsoid bodies is analysed.

At the beginning of the programming typical programming errors, like wrong boundary conditions etc., led to divergence of the algorithm. Later we limited the number of contact iterations by the variable MaxContact, to accelerate the program, which also produced divergence in some examples. Other limits for the Gauss-Seidel iteration (MaxSeidel etc.) influence convergence too. The reliability of convergence increases, when these parameters increase, but the calculation time increases too. It was therefore necessary to allow the user to change these variables. Furthermore it was necessary to use assembler code for the Gauss-Seidel part, where the largest amount of time is consumed, and to install a numerical coprozessor.

We tested several possibilities of the graphical representation of the stresses, the slip directions, the deformations of the bodies and the contour of the areas. The stress was plotted with arrows, which shows the spin pole very well, but the variation in the course of the load-history is not easy to see. A representation in form of a three-dimensional surface is very paper consuming and the variation in the time is not visible either. Therefore we plotted the stress angle and the absolute value of the tangential stress on a two-dimensional diagram. Furthermore the displacements and the forces had to be plotted. It was also necessary to smooth the contour of the stick area and the contact area. All the graphics mentioned above where included in a graphical program.

16.2 Further research

Further research in contact mechanics depends on the problems which arise in practice and theory. One practical aspect is e.g., the design of the surfaces of contacting bodies, in order to reduce the stress. The study of non-Hertzian surfaces is very important here. An example for the theoretical research is the tabulation of parameters, like the tangential coefficient of restitution for the frictional impact. Large contact areas are necessary to study the local stress distribution in the contact area of different materials. With a memory of 640 kBytes the maximal size of the area of integration was 1000 points in our program, but it is possible to calculate larger contact areas, using the non-protected mode of MS-DOS or UNIX and faster computers.

It could be of interest to tabulate characteristical parameters for other load-histories, which arise in mechanical supports and foundations. A more theoretical question is the convergence of the Gauss-Seidel method for special contact areas and load-histories. This can be done by the explicit calculation of the eigenvalues of the matrix T in equation (13.1), for some special problems. A further acceleration of the algorithm can be achieved, using the Multi-Grid method for the matrix vector product, but great importance must be set on a clear programming and the control of the accuracy of the Multi Grid Method.

Our program allows also the study of different coefficients of friction $f_{kin} \neq f_{stat}$ and non-Hertzian contact surfaces. An investigation of such problems should consider, which coefficients and which surfaces are most important, before parameter tables can be listed. The theory of impact could be extended by the calculation of coefficients of restitution for non-spherical bodies and non-hertzian surfaces. It would also be of interest to apply the Gauss-Seidel method to transient rolling. It is not clear, however, if variational methods allow the use of the Gauss-Seidel method. A complete theory for varying torques can be created, on the base of Lubkin's formulae, similar to the theory of chapter 7. An analytical approximation for load-histories with shift and spin may also be possible, although numerical methods can replace analytical methods. In this work we analysed load-histories with prescribed displacements only. If the forces are prescribed, another equation must be added to the load-displacement equations and the convergence of the Gauss-Seidel method becomes uncertain. Since the global values of the forces and displacements can be calculated with small contact areas, it is possible to solve the linear equation system by direct inversion of the load-

displacement equations and the additional equations for the sum of the stresses, which must be equal to the forces (Kalker's method).

If the surfaces and the displacements are symmetric, the equations can be evaluated on only half or a quarter of the surface, which accelerates the program by the factor 4 resp. 16. Our program could be generalized for arbitrary surfaces, such that a user-friendly input of the undeformed distance is possible, in form of a formula or discrete values. The stresses under the surface are of interest also. They can be calulated on the assumption of discrete forces on each element or with Kalker's integrals (1986b).

Very interesting is a generalization of the point-load solution of the half-space, using FEM-solutions for a point load on a hollow sphere or cylinder etc. The load-displacement coefficients A, of equation (4.13), could be determined for a special mesh size, and used in our program. This works only for homogeneous bodies, where the deformation field is independent of the position of the point-load. Contact problems for a flat punch of soft material can not be calculated with this method, because a point-load on the center produces another deformation field as a point load on the edge.

Finally the use of parallel computers would accelerate the calculation very much. To that end a mixture of the single-step and the multi-step Gauss-Seidel method could be used, such that a set of parallel processors calculates the new solution simultaneously for a set of points. In fact there are several ways to parallelize the code, and the best way must be found empirically.

17 References

Numbers in square brackets refer to sections where the reference is cited.

Abramowitz, M., Stegun, I., 1964, Handbook of mathematical functions, Dover Publications, New York, [5.1].

Ahmadi, N., Keer, L. M., Mura, T., 1983, Non-Hertzian stress analysis for an elastic half- space in normal and sliding contact, International Journal of Solids and Structures, **19**, 357-377, [11].

Barber, J. R., 1979, Adhesive contact during the oblique impact of elastic spheres, J. Appl. Math. and Phys., ZAMP, Vol. **30**, 468-476, [3.2].

Boussinesq, J., 1885, Application des potentiels à l'étude de l'équilibre et du mouvement des solides élastiques, Paris, Gauthier-Villars, [1].

Cattaneo, C., 1938, Sul contatto die due corpi elastici: distributione locale degli sforzi, Academia Nazionale dei Lincei, Rendiconti, Serie 6, Vol. **27**, 342-348, 434-436, 474-478, [3.1].

Cerruti, V., 1882, Accademia Nazionale dei Lincei, Roma, Mem. fis. math. [1].

Conry, T. F., Seirig, A., 1971, A mathematical programming method for the design of elastic bodies in contact, Journal of Applied Mechanics, **38**, 387-392, [11].

Deresiewicz, H. J., 1957, J. Appl. Mech., Oblique contact of non-spherical elastic elastic bodies, Vol. 24, 623-624 [3.2].

Duvaut, G., Lions, J. L., 1972, Les inéquations en mécanique et en physique, Dunod, Paris, [11].

Eason, G., 1966, The displacements produced in an elastic half-space by a suddenly applied surface force, Journal of the Institute of Mathematics and its Applications, Vol. 2, 299-326, [3.1].

Engeln-Muellges, G., Reutter, F., 1987, Numerische Mathematik für Ingenieure, Bibliographisches Institut, Zürich, ISBN 3-411-03151-4, [12.1].

Engeln-Muellges, G., Reutter, F., 1987, Formelsammlung zur Numerischen Mathematik mit Turbo-Pascal-Programmen, Bibliographisches Institut, Zürich, ISBN 3-411-03156-5, [12.1].

Euler, L., 1746, De la force de percussion et de sa véritable mesure, Memoires de L'Academie Royale des Sciences de Berlin, 1, 21-53, [3.1].

Fichera, G. 1964, Problemi elastostatici con vincoli unilaterale: il probleme di Signorini con ambigue condizioni al contorno, Memorie Accademia Nazionale dei Lincei, Ser. 8, Vol. 7, p. 91-140, [11].

Flamant, 1892, Comptes Rendues, Vol 114, 1465, Paris [3.2].

Fridman, V. M., Chernina, V. S., 1967, The solution of the contact problem of elastic bodies by means of an iteration method, (in Russian), Mekhanika Tverdogo Tela, Akademia Nauk SSSR, 1, 116-120, [11].

Galileo, G., 1638, Discorsi e dimostrazioni matematiche [3.1].

Gladwell, G. M. L., 1980, Contact problems in the classical theory of elasticity, Sijthoff& Noordhoff, Alphen an den Rijn, [4.1].

Gradstein - Ryshik, 1981, Tables Tafeln, Verlag Harri Deutsch, Thun - Frankfurt / M., ISBN 3 87144 350 6,

Hertz, H., 1882, Über die Berührung fester elastischer Körper, Journal für die reine und angewandte Mathematik (Crelle), 92, 156-171, [1].

Horák, Z., 1931, Théorie generale du choc dans les systèmes matérials, J. école polytech, Ser. 2, Vol. 28, 15, [3.2].

Horák, Z., 1961, The theory of the spinning impact of imperfectly elastic bodies, Czechoslovakian Journal of physics, B11, 46-65, [3.2].

Horn, A. R., Johnson, C. R., 1985, Matrix analysis, Cambridge University Press, Cambridge, ISBN 0-521-305861, [12.3].

Hunter, S. C. 1957, Energy absorbed by elastic waves during impact, Journal of Mechanics and Physics of Solids, 5, 162-171, [3.1].

Hunter, S. C., The Hertz problem for a rigid spherical half-space, Trans. ASME, Series E, Journal of Applied Mechanics, Vol. 28, pp. 611, [3.2].

Huygens, 1703, De motu corporum ex percussione, reprinted in: Oeuvres complètes de Christian Huygens, publiées par la société hollandaise des sciences, vol. 16, La Haye, Martinus Nijhoff, 1929, [3.1].

Jaeger, J., 1990, An incremental load history, Colloquium Euromech 273: Unilateral contact and dry friction, La Grande Motte, May 29th - June 1st, Université Montpellier II, 77-80, [7].

Johnson, K. L., 1985, Contact Mechanics, Cambridge University Press, Cambridge (UK), [3.2].

Kalker, J. J., 1991, Viscoelastic multilayered Cylinders rolling with dry friction, J. Appl. Mech., Vol. 58, 666-679, [11.2].

Kalker, J. J., 1990, Three-dimensional elastic bodies in rolling contact, Kluwer Academic Publishers, ISBN 0-7923-0712-7, [3.2].

Kalker, J. J., 1988, Contact mechanical algorithms, Communications of Applied Numerical Methods, 4, 25-32, [3.2].

Kalker, J. J., 1986a, The principle of virtual work and its dual for contact problems, Ingenieur-Archiv, 56, 453-467, [3.2].

Kalker, J. J., 1986b, Numerical calculation of the elastic field in a half-space, Communications of Applied Numerical Methods, 2, 401-410, [3.2].

Kalker, J. J., 1979, The computation of three-dimesional rolling contact with dry friction, International Journal of Numerical Methods in Engineering, 14, p. 1293-1307, [11].

Kalker, J. J., van Randen, Y., 1972, A minimum principle for frictionless elastic contact with application to non-Hertzion half-space contact problems, Journal of Engineering Mathematics, 88, 193-206, [11].

Kalker, J. J., 1971, A minimum principle for the law of dry friction with application to elastic cylinders in rolling contact, Journal of Applied Mechanics, 38, 875-880, 881-887, [3.2].

Kalker, J. J., 1967, On the rolling contact of two elastic bodies in the presence of dry friction, Thesis Delft, [3.2].

Keller, J. B., 1986, Impact with friction, Journal of Applied Mechanics, Vol. 53, 1-4, [8.2].

Klarbring, A., 1990, (Non-)uniqueness and (non-)existence of frictinonal rate problems, Colloquium Euromech 273: Unilateral contact and dry friction, La Grande Motte, May 29th - June 1st, Université Montpellier II, 89-92, [6].

Love, A. E. H., 1927, A treatise on the mechanical theory of elasticity, Cambridge University Press, [3.2].

Lubkin, J. L., 1951, The torsion of elastic spheres in contact, Journal of Applied Mechanics, Vol. 18, 183-187, [5.4].

Mach, E., 1960, The science of mechanics by Ernst Mach, Chicago, The Open Court Publishing Co., Library of Congress Catalog, Card Number: 60-10179 (Translation of: E. Mach, 1912, Die Mechanik in ihrer Entwicklung, Leipzig, Brockhaus), [3.1].

Machalický, J., 1973, Šikmý nedokonale drsný ráz nedokonale pružné koule na tuhou desku, Acta Poytechnica, (The oblique, imperfect rough impct of an imperfect elastic sphere on a rigid plane), Práce, ČVUT, Praze, H, 1, 1973, 37-57, [3.2].

Marci, M., 1639, De proportione motus, Prag [3.1].

Maw, N., Barber, J. R., Fawcett, J. N., 1976, The oblique impact of elastic spheres, Wear, 38, 101, [3.2].

Maw, N., Barber, J. R. & Fawcett, J. N., 1981, The role of tangential compliance in oblique impact. Journal of Lubrication Technology, Trans. ASME, Series F, 103, 74-80, [3.2].

Mindlin, R. D., 1949, Compliance of elastic bodies in contact, J. Appl. Mech., Vol. 16, 259-268, [3.2].

Mindlin, R. D., Deresiewicz, H., 1953, Elastic spheres in contact under varying oblique forces, Journal of Applied Mechanics, Vol. 20, 327-344, [3.2].

Neuber, H., 1937, Kerbspannungslehre, Julius Springer, Berlin, Germany, pp. 85-90, [5.3].

Neumann, F., 1885, Vorlesungen über die Theorie der Elastizität, Kap. 20, Leipzig, [3.1].

Newton, Isaac, 1686, Philosophiae naturalis principia mathematica (Translated by A.Motte), New York, D.Adee, 1848. [3.1].

Niethammer, W., 1970, Ueber- und Unterrelaxation bei linearen Gleichungssystemen, Computing, 5, 303-311, [13.1].

Panagiotopoulos, P. D., 1975, A nonlinear programming approach to the unilateral contact and friction-boundary value problem in the theroy of elasticity, Ingenieur-Archiv, 44, 421-432, [13.3].

Raoof, M., Hobbs, R. E., 1989, Tangential compliance of rough elastic bodies in contact, Journal of Tribology, Vol 111, 726-729, [5.2].

Reusner, H., 1977, Druckflächenbelastung und Oberflächenverschiebung im Wälzkontakt von Rotationskörpern, thesis Karlsruhe, SKF Schweinfurt, (in German), [11.2].

Spence, D. A., 1975, The Hertz problem with finite friction, Journal of Elasticity, 5, 297-319, [14.3].

Szabo, I., 1979, Geschichte der mechanischen Prinzipien und ihre wichtigsten Anwendungen, Stuttgart, Birkhäuser, [3.1].

Turner, J. R. 1979, The frictional unloading problem on a linear elastic half-space, J. Inst. Maths. Applics., Vol. 24, 439-469, [14.3].

de St. Venant, B., 1867, Journ. de Math. (2), Vol. 12, 237-376, [3.1].

Vermeulen, P. J., Johnson, K. L., 1964, Contact of nonspherical bodies transmitting tangential forces, Journal of Applied Mechanics, 31, 338-340, [7.1].

Wittenburg, J., 1977, Dynamics of systems of rigid bodies, Teubner, Stuttgart, ISBN 3-519-02337-7, [8.1].

Curriculum Vitae

On the 31st December 1955 I was born in Laufenburg/Baden, Germany, as son of Klaus Jäger and Hildegart Jäger.

From 1962 to 1966 I visited the primary school in Bad Säckingen, Germany. The next five years, from 1966 to 1971, I attended the modern secondary school in Bad Säckingen. From 1971 to 1974 I visited the classical secondary school in Lörrach, Germany, and finished it with my "Abitur".

From 1974 to 1979 I studied Machine Construction at the Technical University of Karlsruhe, where I received the Engineering Diploma for Machine-Construction.

From 1980 to 1985 I worked as a scientific member of the staff at the Institute of Theoretical Mechanics of the TU Karlsruhe. In this time I developed the basic concept of the elastic impact.

From 1986 to 1990 I worked at the Department for Compensators of the factory IWKA in Karlsruhe / Blankenloch, and developed the numerical part of the thesis in my free time. I worked at the analytical calculation of compensators with Prof. Axelrad from the Bundeswehrhochschule München, and at the numerical calculation of structural details with a Finite Element program.

From 1990 to 1991 I configured hard- and software for modern Computer Aided Engineering methods at the engineering office Ergometric Hartman in Karlsruhe. I spent the rest of the time for the completion of this doctorate.